frontiers | Research Topics

Application of next-generation sequencing for cancer drug repositioning

Edited by
Zhi Li, Fengfeng Zhou, Chi Zhang and Huidan Zhang

Published in
Frontiers in Oncology
Frontiers in Pharmacology

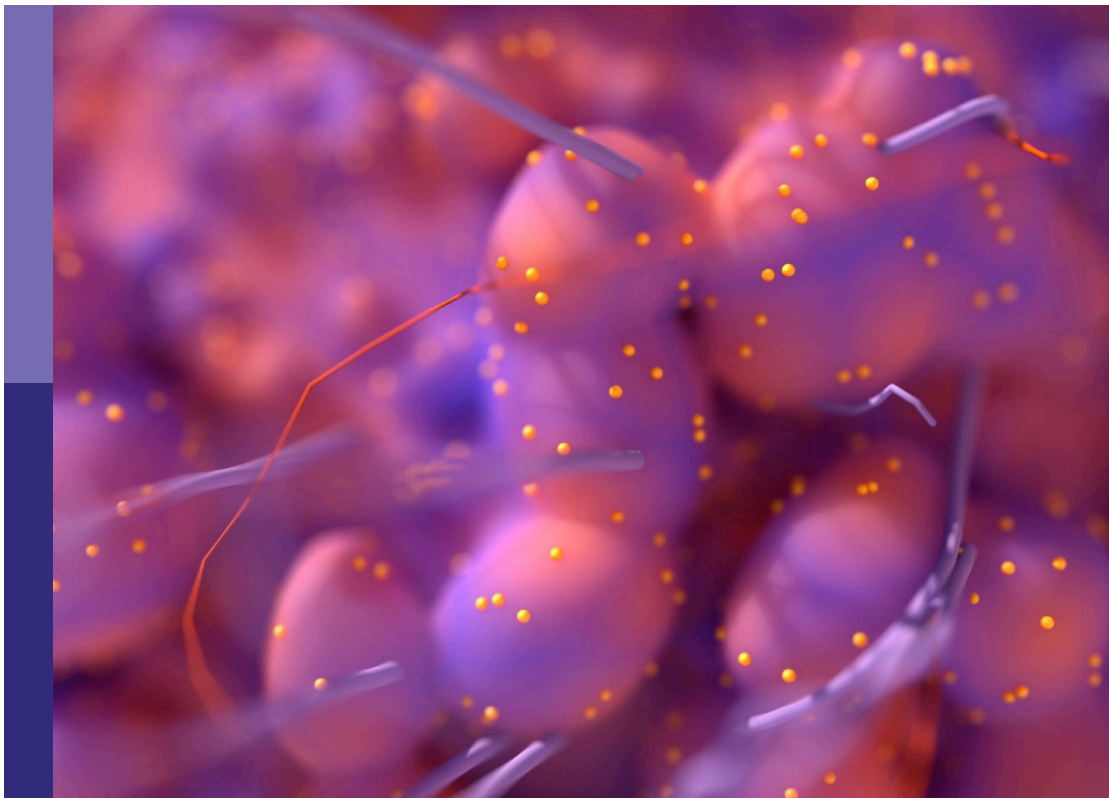

ISSN 1664-8714
ISBN 978-2-83251-002-5
DOI 10.3389/978-2-83251-002-5

About Frontiers

Frontiers is more than just an open access publisher of scholarly articles: it is a pioneering approach to the world of academia, radically improving the way scholarly research is managed. The grand vision of Frontiers is a world where all people have an equal opportunity to seek, share and generate knowledge. Frontiers provides immediate and permanent online open access to all its publications, but this alone is not enough to realize our grand goals.

Frontiers journal series

The Frontiers journal series is a multi-tier and interdisciplinary set of open-access, online journals, promising a paradigm shift from the current review, selection and dissemination processes in academic publishing. All Frontiers journals are driven by researchers for researchers; therefore, they constitute a service to the scholarly community. At the same time, the *Frontiers journal series* operates on a revolutionary invention, the tiered publishing system, initially addressing specific communities of scholars, and gradually climbing up to broader public understanding, thus serving the interests of the lay society, too.

Dedication to quality

Each Frontiers article is a landmark of the highest quality, thanks to genuinely collaborative interactions between authors and review editors, who include some of the world's best academicians. Research must be certified by peers before entering a stream of knowledge that may eventually reach the public - and shape society; therefore, Frontiers only applies the most rigorous and unbiased reviews. Frontiers revolutionizes research publishing by freely delivering the most outstanding research, evaluated with no bias from both the academic and social point of view. By applying the most advanced information technologies, Frontiers is catapulting scholarly publishing into a new generation.

What are Frontiers Research Topics?

Frontiers Research Topics are very popular trademarks of the *Frontiers journals series*: they are collections of at least ten articles, all centered on a particular subject. With their unique mix of varied contributions from Original Research to Review Articles, Frontiers Research Topics unify the most influential researchers, the latest key findings and historical advances in a hot research area.

Find out more on how to host your own Frontiers Research Topic or contribute to one as an author by contacting the Frontiers editorial office: frontiersin.org/about/contact

Application of next-generation sequencing for cancer drug repositioning

Topic editors

Zhi Li — The First Affiliated Hospital of China Medical University, China
Fengfeng Zhou — Jilin University, China
Chi Zhang — Indiana University Bloomington, United States
Huidan Zhang — Harvard University, United States

Citation

Li, Z., Zhou, F., Zhang, C., Zhang, H., eds. (2022). *Application of next-generation sequencing for cancer drug repositioning*. Lausanne: Frontiers Media SA.
doi: 10.3389/978-2-83251-002-5

Table of contents

frontiers in Oncology

CASE REPORT
published: 11 June 2021
doi: 10.3389/fonc.2021.688200

Case Report: Vemurafenib Treatment in Brain Metastases of *BRAF*^{S365L}-Mutant Lung Papillary Cancer by Genetic Sequencing of Cerebrospinal Fluid Circulating Tumor DNA Detection

Jianing Jiang[1,2*], *Jinqi Gao*[3], *Gang Wang*[1], *Jinyan Lv*[1], *Wenting Chen*[1], *Jing Ben*[1] *and Ruoyu Wang*[1,2*]

[1] Department of Oncology Medicine, Affiliated Zhongshan Hospital of Dalian University, Dalian, China, [2] The Key Laboratory of Biomarker High Throughput Screening and Target Translation of Breast and Gastrointestinal Tumor, Dalian, China, [3] Department of Intervention, The Second Hospital Affiliated to Dalian Medical University, Dalian, China

OPEN ACCESS

Edited by:
Zhi Li,
The First Affiliated Hospital of China Medical University, China

Reviewed by:
Fei Zhnag,
Shanghai Jiaotong University, China
Hamed Barabadi,
Shahid Beheshti University of Medical Sciences, Iran
Zihang Xu,
Shanghai University of Traditional Chinese Medicine, China

***Correspondence:**
Ruoyu Wang
wangruoyu1963@163.com
Jianing Jiang
jing_jianing@126.com

Specialty section:
This article was submitted to Pharmacology of Anti-Cancer Drugs, a section of the journal Frontiers in Oncology

Received: *30 March 2021*
Accepted: *10 May 2021*
Published: *11 June 2021*

Citation:
Jiang J, Gao J, Wang G, Lv J, Chen W, Ben J and Wang R (2021) Case Report: Vemurafenib Treatment in Brain Metastases of BRAF^{S365L}*-Mutant Lung Papillary Cancer by Genetic Sequencing of Cerebrospinal Fluid Circulating Tumor DNA Detection. Front. Oncol. 11:688200. doi: 10.3389/fonc.2021.688200*

BRAF mutations, primarily sensitizing mutations, such as *BRAF*^{V600E}, have been proven to response to the *BRAF* inhibitor, Dabrafenib combined with trametinib therapy, but there have been no data demonstrating that it has activity against NSCLC-related brain metastases (BM). How patients harboring *BRAF*^{S365L} mutation (a rare mutation following *BRAF*^{V600E}-inhibitor treatment) in NSCLC is unknown. Vemurafenib, another *BRAF* inhibitor, can reverse the resistance that develops with the *BRAF*^{S365L} mutation following dabrafenib combined with trametentinib treatment in melanoma, but none has been reported in NSCLC. Lung papillary cancer, as a rare typing, occupies about 4% of NSCLC. Hence, we reported the first case of a patient with BM of lung papillary carcinoma harboring a *BRAF*^{V600E} mutation who benefited from dabrafenib combined with trametinib, and following the development of the *BRAF*^{S365L} mutation, vemurafenib remained an effective therapeutic option. Moreover, we found that the next-generation sequencing (NGS) of cerebrospinal fluid (CSF) circulating tumor DNA (ctDNA) may potentially provide more accurate information about intracranial lesions than ctDNA in the blood serum, which will be a better detection method.

Keywords: *BRAF*^{V600E} mutation, BM of NSCLC, *BRAF*^{S365L} mutation, CSF ctDNA, vemurafenib

INTRODUCTION

In recent years *BRAF*^{V600E} (v-Raf murine sarcoma viral oncogene homolog B) mutation occurring in 1% to 2% of patients with NSCLC, has become an important therapeutic target (1, 2). Dabrafenib combined with trametinib therapy has received full approval from the United States Food and Drug Administration (FDA) for the treatment of advanced *BRAF*^{V600E}-mutant NSCLC in 2017, but none has reported its activity against NSCLC with BM. Unfortunately, resistance inevitably develops in

BRAF^{V600E}-driven NSCLC patients, such as *BRAF*^{S365L} mutation. One study showed that the *BRAF*^{S365L} mutation can result in resistance to the MAPK inhibitor trametinib in melanoma with *BRAF*^{V600E} mutation, but the resistance can be reversed by vemurafenib (3). Vemurafenib, another selective oral inhibitor of *BRAF*^{V600E} kinase, is associated with a response rate of approximately 50% and improved survival among patients with *BRAF*^{V600E} mutation-positive metastatic melanoma. However, there is no such research in NSCLC, and a phase II trial of vemurafenib in *BRAF*^{V600E}-mutant NSCLC is currently ongoing (4). Lung papillary cancer, as a rare typing of lung adenocarcinoma, occupies about 4% of NSCLC, and provides a better prognosis than lung mucinous adenocarcinoma, but had a worse one than other types of lung adenocarcinoma. And *BRAF*^{V600E} may occur in 0.08% of lung papillary cancer, which is quite a small amount of it. Thus, we report, for the first time, the use of dabrafenib combined with trametinib for treating BM of lung papillary cancer carrying the *BRAF*^{V600E} mutation, and vemurafenib remained an effective therapeutic strategy for overcoming the resistance induced by the *BRAF*^{S365L} mutation, which was identified by genetic sequencing of CSF ctDNA in this patient.

CASE REPORT

The patient was a 40-year-old man who presented without any symptoms. But during the routine medical examination, chest X-ray ordered revealed a shadow in his right lung. A subsequent chest computed tomography (CT) scan revealed consolidation in the upper lobe of the right lung (**Figure 1A**). Palpation revealed a mass in the right supraclavicular lymph node. A pathological examination of the superficial lymph node biopsy was conducted, and lung papillary carcinoma was diagnosed (**Figures 2A–C**). The primary lesion was present in the right lung, with right supraclavicular lymph node metastases, and the disease was diagnosed as right lung papillary cancer cT2N3M0 (IIIB). The lymph node biopsy revealed the absence of EGFR mutation or ALK fusion by ARMS-PCR, so four cycles of chemotherapy with paclitaxel plus carboplatin were given, and the lesions remained stable, with the curative effect stable disease (SD) and the PFS 3 months. To achieve better results, radioactive seed implantation was performed in the lesion of the right lung, by percutaneous puncture under the guidance of CT scan, 28 seeds were implanted, with the radiation dose 140 Gy, seeds activity 0.6 and the half-life 2.5 months, and the lesions again remained stable, with the curative effect SD and the PFS 9 months (**Figures 1B1**, **2**). Then the patient returned with paroxysmal headache. Head magnetic resonance imaging (MRI) revealed lesions in the right parietal lobe, bilateral frontal lobes, and the right cerebellar hemisphere (**Figures 1C1, 2**). Whole brain radiotherapy was administered, with the whole brain (6MV X ray, Dt:3960cGy/180cGy/22F) and the metastases lesions (6MV X ray, Dt:5280cGy/240cGy/22F). After the radiotherapy, the lesions regressed with the curative effect evaluation was PR (partly response, PR) (**Figures 1D1, 2**). At that time, a chest CT showed that the lesion in the right lung remained stable, but new lesions were observed in the lower lobe of the left lung and the mediastinal lymph nodes, so intensity-modulated radiation therapy was administered to the mediastinal lesions. Three months later, chest CT again showed stable lesions, but an abdominal contrast-enhanced CT revealed multiple lesions in the liver, and a mass in the pancreas metastases (**Figures 1E1, 2**).

To identify further treatment options, targeted next-generation sequencing (NGS) using a cancer-relevant gene panel was performed on both the biopsy sample of the right lung and plasma ctDNA. A *BRAF*^{V600E} mutation was identified both in the tissue (allele fraction [AF], 11.8%) and the plasma (AF, 4.3%) ctDNA (**Figures 3A1, 2**). Dabrafenib and trametinib were given orally daily, and the lesions in chest, abdomen and brain all regressed within the first 6 months, with the curative effect evaluation regressed SD (**Figures 1F1–8**), but became enlarged 3 months later (**Figures 1G1–8**), with the curative effect enlarged SD and the PFS 6 months. No evident side effects occurred during the combination therapy. To explore potential resistance mechanisms, targeted NGS of both CSF ctDNA obtained by lumbar puncture and plasma ctDNA was conducted: NGS revealed the presence of the *BRAF*^{V600E} mutation in the CSF (AF, 37.8%) and in the plasma (AF, 0.4%) ctDNA (**Figures 3B1, 2**), as well as a newly acquired *BRAF*^{S365L} mutation in the CSF (AF, 25.5%) (**Figures 3B3**). The *BRAF*^{S365L} mutation indicates resistance to trametinib, so dabrafenib and bevacizumab were given as new therapy, but the lesions in the brain became enlarged, and evaluated as enlarged SD (**Figure 1H**). Therefore, vemurafenib was given with bevacizumab, and the lesions in brain regressed and others remained stable within the first 3 months, with the curative effect evaluation SD (**Figures 1I1–3**). Two months later, the patient experienced convulsions. The lesions in the brain remained stable. Targeted NGS of both the CSF cell-free DNA obtained by lumbar puncture and the plasma ctDNA revealed the presence of the *BRAF*^{V600E} mutation in the CSF (AF, 25.8%) and in the plasma (AF, 2.3%) ctDNA (**Figures 3C1, 2**), but the *BRAF*^{S365L} mutation in the CSF decreased substantially (AF, 0.5%) (**Figures 3C3**). Therefore, it may be the time of the tolerance of vemurafenib. The PFS of vemurafenib was 5 months, during that time, moderate rash was found in the upper limbs, no drug was given. And the rash disappeared soon after the drug's withdrawal. Therefore, dabrafenib, trametinib, and bevacizumab were administered again, the symptoms of dizzy, vomiting, and convulsions relieved in the first few months, and the patient died 8 months later.

DISCUSSION

BRAF mutation is important event in cancer development. Mutations in the BRAF gene are referred to as "activating mutations." *BRAF* proteins are part of a signaling pathway (RAF-MEK-ERK) that affects cell growth in several ways, to promote cell proliferation, cell survival, and aid in differentiation, migration, and inhibits apoptosis in several cancers, which has been proved to be a higher risk of recurrence and a bad prognostic factor of cancer. *BRAF*^{V600E} mutation, as the main

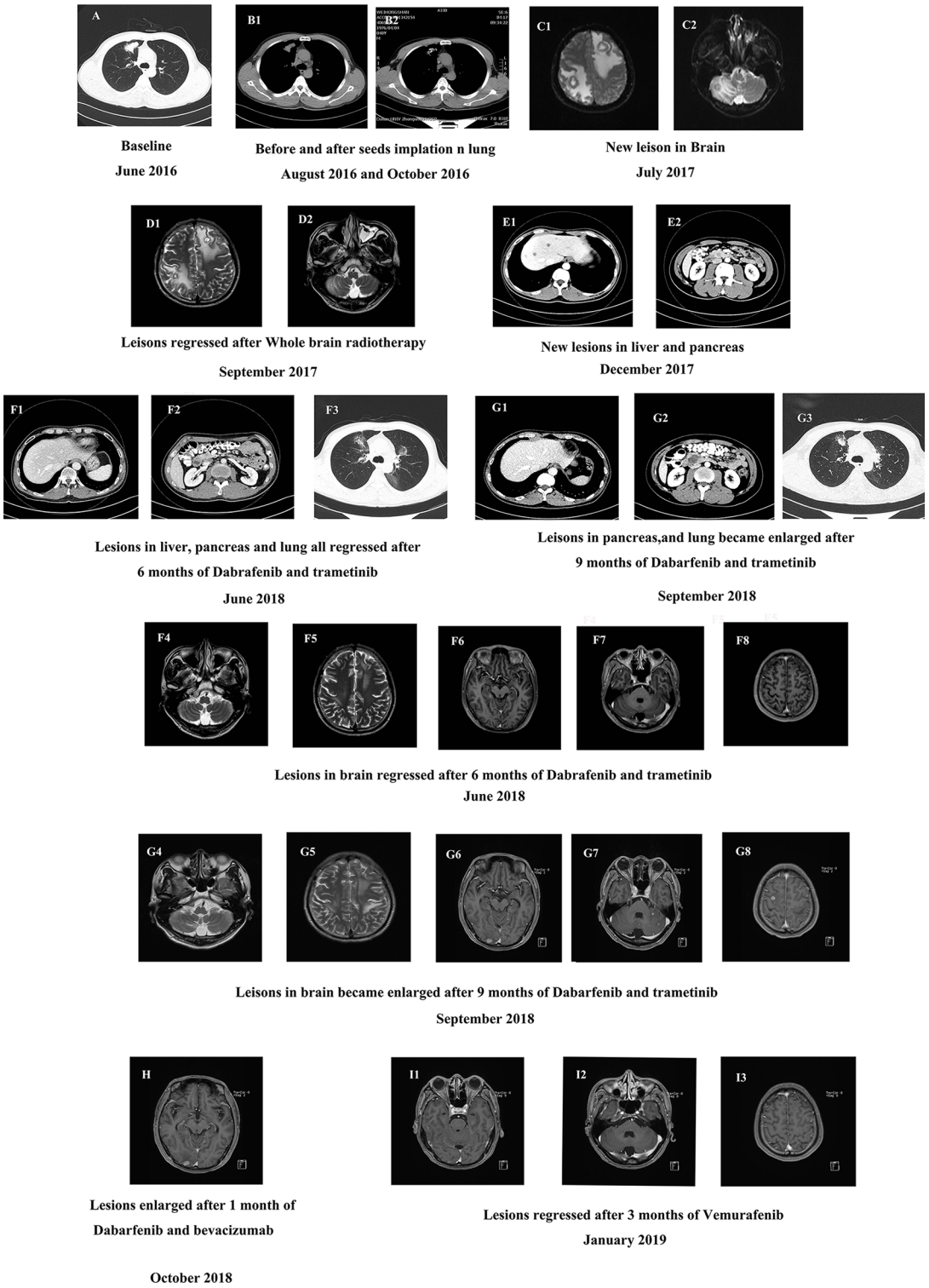

FIGURE 1 | **(A)** The baseline CT scan of the patient's chest in June 2016. **(B)** CT scan of the chest before and after the seeds implantation. **(C)** The baseline MRI scan of the patient's brain in July 2017. **(D)** MRI scan of the brain after 2 months of whole brain radiotherapy treatment in September 2017. **(E)** Contrast-enhanced CT scan of the new lesions in abdomen in December 2017. **(F1–8)** CT scan of the abdomen **(F1–2)**, chest **(F3)** and MRI scan of the brain **(F4–8)** after 6 months of dabrafenib combined with trametinib therapy in June 2018. **(G1–8)** CT scan of the patient's abdomen **(G1–2)**, chest **(G3)** and MRI scan of the brain **(G4–8)** after 9 months of dabrafenib combined with trametinib therapy in September 2018. **(H)** MRI scan of the brain after a month of dabrafenib with bevacizumab therapy in November 2018. **(I)** MRI scan of the brain after 3 months of vemurafenib with bevacizumab therapy in March 2019.

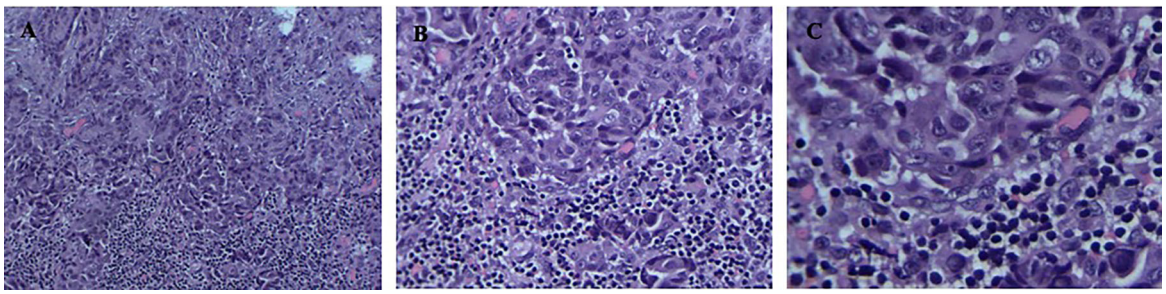

FIGURE 2 | **(A–C)** Positive detection of papillary carcinoma cells in needle biopsy sample of the superficial lymph node biopsy. Magnification; ×100, ×200, ×400.

type of *BRAF* mutations, has been proven to participate in several cancers, such as melanoma, NSCLC, colorectal cancer, and thyroid cancer. There have been three main *BRAF* inhibitors at present, dabrafenib, vemurafeinib, and encorafenib. Dabrafenib is a small molecule inhibitor of the *BRAF*-mutant kinase family, as a potent ATP-competitive inhibitor of *BRAF* kinase, it was approved for use in monotherapy or in combination with trametinib for the treatment of unresectable or metastatic $BRAF^{V600E}$ -mutated melanoma, advanced $BRAF^{V600E}$ -mutated NSCLC, and $BRAF^{V600E}$ -mutated locally advanced or metastatic ATC (anaplastic thyroid cancer, ATC). Vemurafenib, as another inhibitor of the *BRAF* mutant family, is known to promote the apoptosis of mutated cells in a dose-dependent manner. Specifically, it interrupts the BRAF/MEK step in the BRAF/MEK/ERK pathway. It was approved by the FDA in patients with $BRAF^{V600E}$ -mutated melanoma or the Erdheim-Chester disease containing the $BRAF^{V600E}$ mutation. In melanoma, BRAF monotherapy (vemurafenib) occurs drug resistance in a short time, and the combination therapy of dabrafenib and trametinib simultaneously inhibits the upstream and downstream pathway of MAPK, increases the efficacy and safety of monotherapy with *BRAF* inhibitor, and significantly improves the prognosis of patients with *BRAF* mutant melanoma.

In NSCLC, dabrafenib combined with trametinib therapy has received full FDA approval for the treatment of advanced $BRAF^{V600E}$-mutant NSCLC. The mPFS, OS, DCR, and ORR in first line of therapy by dabrafenib combined with trametinib may get 10.8 months, 17.3 months, 75%, and 63.9%. And the data will be 10.2 months, 18.2 months, 80.7% and 68.4% in subsequent lines of therapy. Compared with the Dabfrafenib monotherapy, the combination can inhibit the BRAF/MEK/ERK pathway completely. ORR rate for the combination had increased to 67% as did the median progression free survival, 10.2 months. Median overall survival was reported as 12.7 months in the Dabrafenib only cohort versus 18.2 months in the Dabrafenib and Trametinib cohort. Vemurafenib is another significant *BRAF* inhibitor, several clinical trials have indicated that it can be used in NSCLC harboring $BRAF^{V600E}$ mutation with the ORR 42% and median progression free survival was 7.3 months, which has been proved to be inferior to the combination. And it may be the reason for the failure to be approved by FDA in the NSCLC therapy. But there are no data that demonstrate that it has activity against NSCLC-related BM (5). The related clinical studies explored the patients with NSCLC harboring $BRAF^{V600E}$, to show that the combination therapy of dabrafenib and trametinib would be the first line therapy, but the studies didn't analyses the cases with brain metastases or not. However, in melanoma-related brain metastases, some clinical trials, such as the (COMBI-MB): a multi-cohort, open-label, phase 2 trial has showed dabrafenib and trametinib was active with a manageable safety profile in patients with $BRAF^{V600E}$ –mutation, but the median duration of response was relatively short (6). These results provide evidence of clinical benefit with dabrafenib and trametinib and support the need for additional research to further improve outcomes in patients with melanoma with brain metastases. Based on its effectiveness in the treatment of melanoma with BM, combination dabrafenib/trametinib therapy was given for this patient with lung papillary cancer with BM, and the lesions remained regressed for 6 months.

However, resistance developed, and the lesions became enlarged. Targeted NGS revealed the presence of the $BRAF^{V600E}$ mutation in the CSF (AF, 37.8%) and in the plasma (AF, 0.4%) ctDNA, and a newly acquired $BRAF^{S365L}$ mutation was revealed in the CSF (AF, 25.5%). The N-terminal, S365, is removed in BRAF V600E splice variants but its importance in full-length $BRAF^{V600E}$ mutants remains uncertain. $BRAF^{V600E}$ S365L displayed reduced sensitivity to RAF inhibitor at the level of MEK-ERK1/2 signaling, cell growth, and cell viability, suggesting that alteration or removal of the S365 14-3-3 binding site may contribute to RAF inhibitor resistance (7). To the best of our knowledge, there have been no studies of $BRAF^{S365L}$ mutation reported in NSCLC with BM. But one study suggested that $BRAF^{S365L}$ mutation indicates resistance to the MAPK inhibitor trametinib in melanoma with $BRAF^{V600E}$ mutation, but this resistance can be reversed by vemurafenib (3). Vemurafenib, another selective oral inhibitor of $BRAF^{V600E}$ kinase, is associated with a response rate of approximately 50% and improved survival among patients with $BRAF^{V600E}$ mutation-positive metastatic melanoma (8). Additionally, in a single-arm phase II study of vemurafenib for metastatic melanoma patients with BM, survival was extended to over 6 months, which is longer than the expected natural course of patients with BM (< 3 months) (9). However, there are no such reports in NSCLC, and a phase II trial of vemurafenib in $BRAF^{V600E}$-mutant NSCLC is currently ongoing (4). In theory, the CNS efficacy of these drugs is based

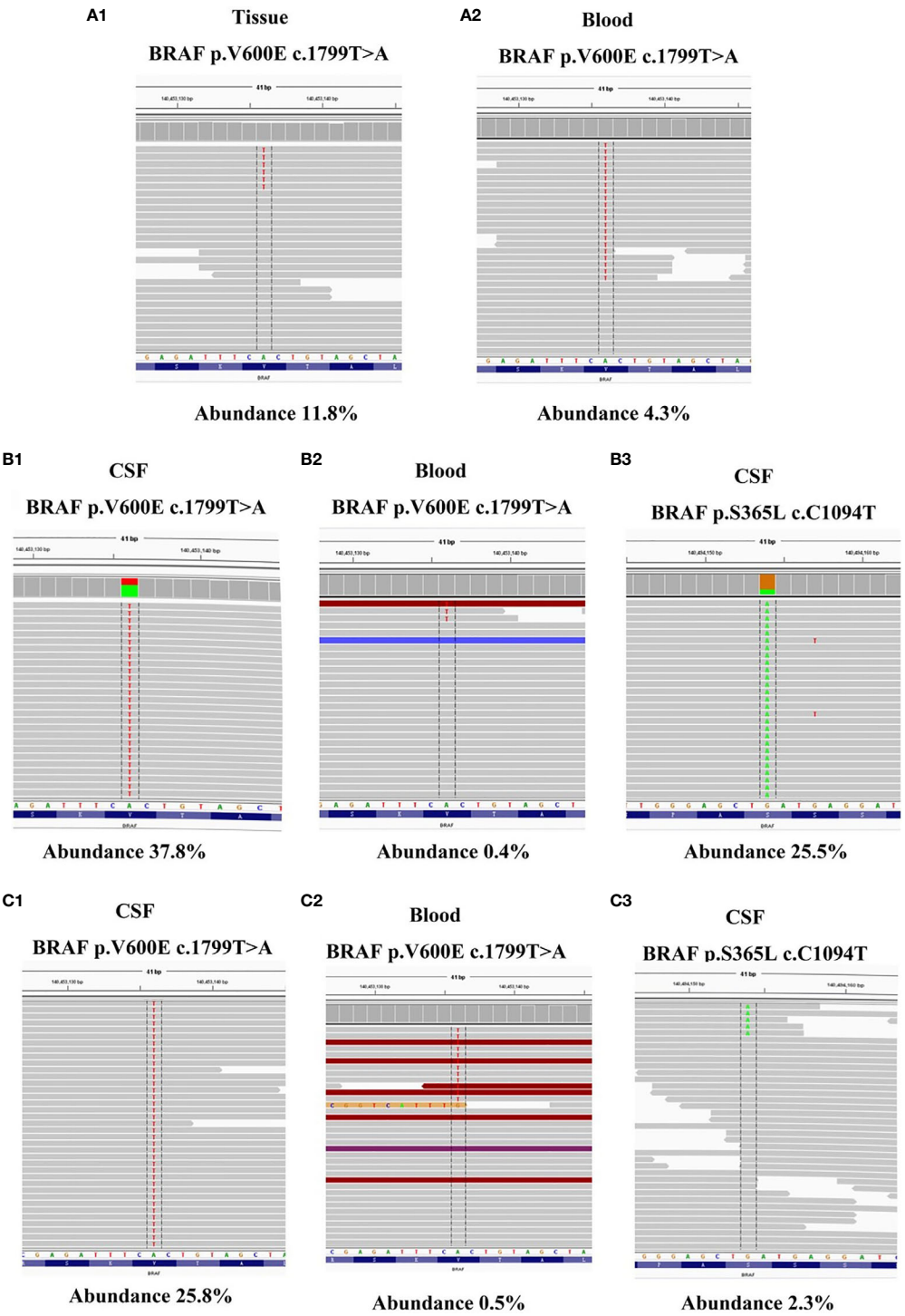

FIGURE 3 | **(A1–2)** NGS reads showing the *BRAF*^{V600E} mutation in both tumor tissue *BRAF*^{V600E} mutation in both tumor tissue and ctDNA from the plasma were visualized using the Integrated Genomics Viewer before dabrafenib combined with trametinib therapy. **(B1–3)** NGS reads showing the *BRAF*^{V600E} and *BRAF*^{S365L} mutation in both CSF and ctDNA from the plasma were visualized using the Integrated Genomics Viewer when the resistance of dabrafenib combined with trametinib therapy occurred. **(C1–3)** NGS reads showing the *BRAF*^{V600E} and *BRAF*^{S365L} mutation in both CSF and ctDNA from the plasma were visualized using the Integrated Genomics Viewer when the resistance of vemurafenib therapy occurred.

on the rationale that the blood-brain barrier is disrupted by tumor activity. In this case, with the patient's approval, vemurafenib was given, and the lesions regressed within the first 3 months and remained stable for the following 2 months. Then, the disappearance of the $BRAF^{S365L}$ mutation was noted, and dabrafenib and trametinib therapy was given, the symptoms of dizzy, vomiting and convulsions relieved in the first few months, to prove it benefit from the therapy.

It is worth mentioned that we confirmed that gene alterations detected in CSF ctDNA were superior to those of plasma ctDNA in *BRAF*-mutant NSCLC with BM. Owing to the blood-brain barrier, it is difficult for CSF ctDNA to circulate fully within the blood system, which results in a limited amount of ctDNA from the CNS being released to plasma. Therefore, plasma cannot accurately represent intracranial lesions clearly. From several papers of NSCLC-related brain metastases, the detection rate of CSF ctDNA varying from about 57.1% to 80.0%, and in blood ctDNA detection the rate was from 21.3% to 23.8% (10–12).When the resistance developed, targeted NGS revealed the presence of the $BRAF^{V600E}$ mutation in the CSF (AF, 37.8%) and in the plasmactDNA (AF, 0.4%). But the newly acquired $BRAF^{S365L}$ mutation was only revealed in the CSF (AF, 25.5%), suggesting the importance of CSF ctDNA as a liquid biopsy source for BM (10).

In addition, bevacizumab was used in this patient. As we know, anti-angiogenic therapy plays a major role in the management of brain metastases in NSCLC. Bevacizumab is widely used in combination with chemotherapy, radiotherapy, EGFR-TKI targeted therapy, and immunotherapy for NSCLC with BM. In a retrospective cohort study of bevacizumab for advanced NSCLC, analysis of the brain metastases subgroup showed that bevacizumab plus carboplatin paclitaxel significantly prolonged OS compared with carboplatin paclitaxel alone (11.3 months vs. 2.3 months). In this case, the benefit from bevacizumab seemed to be indistinct, several studies of bevacizumab combination therapy for NSCLC with BM are still in progress.

In summary, this is the first case report to describe a patient with $BRAF^{V600E}$-mutated lung papillary cancer with BM responding to dabrafenib combined with trametinib therapy; additionally, vemurafenib was effective against the newly evident $BRAF^{S365L}$ mutation. This case gives support for ongoing trials investigating the role of *BRAF* inhibitors in *BRAF*-mutated NSCLC with BM. And the findings also suggest that genome sequencing of the CSF is much more accurate than that of ctDNA in blood serum in NSCLC with BM. If ctDNA detection in blood serum yields negative results, CSF may be used to enhance detection.

DATA AVAILABILITY STATEMENT

The original contributions presented in the study are included in the article/supplementary material. Further inquiries can be directed to the corresponding authors.

ETHICS STATEMENT

The study involving human participants was reviewed and approved by the Affiliated Zhongshan Hospital of Dalian University Biomedical Research Ethics Committee. The patients/participants provided their written informed consent to participate in this study. Written informed consent was obtained from the individual(s) for the publication of any potentially identifiable images or data included in this article.

AUTHOR CONTRIBUTIONS

JG and GW performed the radiological analysis of MRI CT and PET-CT images. JJ wrote the first draft of the manuscript. RW wrote sections of the manuscript. All authors contributed to the article and approved the submitted version.

FUNDING

This work was supported by grants from the National Science Foundation of China (#81803109) and the Doctor Study-up Foundation of Liaoning Province (2019-BS-010).

ACKNOWLEDGMENTS

We thank the patient in this report and his family. Written informed consent was obtained from the patient for publication of this case report and any accompanying images.

REFERENCES

1. Planchard D, Smit EF, Groen HJM, Mazieres J, Besse B, Helland A, et al. Dabrafenib Plus Trametinib in Patients With Previously Treated *BRAF V600E* Mutant Metastatic Non-Small Cell Lung Cancer: An Open-Label, Multicentre Phase 2 Trial. *Lancet Oncol* (2016) 17:984–93. doi: 10.1016/S1470-2045(16)30146-2
2. Paik PK, Arcila ME, Fara M, Sima CS, Miller VA, Kris MG, et al. Clinical Characteristics of Patients With Lung Adenocarcinomas Harboring BRAF Mutations. *J Clin Oncol* (2011) 29:2046–51. doi: 10.1200/JCO.2010.33.1280
3. Hyman DM, Puzanov I, Subbiah V, Faris JE, Chau I, Blay J-Y, et al. Vemurafenib in Multiple Nonmelanoma Cancers With *BRAF* V600 Mutations. *N Engl J Med* (2015) 373(8):726–36. doi: 10.1056/NEJMoa1502309
4. Subbiah V, Gervais R, Riely G, Hollebecque A, Blay J-Y, Felip E, et al. Efficacy of Vemurafenib in Patients With Non–Small-Cell Lung Cancer With BRAF V600 Mutation: An Open-Label, Single-Arm Cohort of the Histology-Independent Ve-Baskets. *Am Soc Clin Oncol* (2020) 3:1–9.doi: 10.1200/PO.18.00266.
5. Planchard D, Maziers J, Riely GJ. Interim Results of Phase II Study BRF 113928 of Darafenib in BRAF V600E Mutation-Positive non-Small Cell Lung Cancer(NSCLC) Patients. *J Clin Oncol* (2013) 31:15–24. doi: 10.1200/jco.2013.31.15_suppl.8009
6. Davies MA, Saiag P, Robert C, Grob J-J, Flaherty KT, Arance A, et al. Dabrafenib Plus Trametinib in Patients With BRAF-mutant Melanoma Brain Metastases (COMBI-MB): A Multicentre, Multicohort, Open-Label, Phase 2 Trial. *Lancet Oncol* (2017) 18:863–73. doi: 10.1016/S1470-2045(17)30429-1

7. Vido Michael J, Justin R, Aplin Andrew E. Role of Serine 365 in BRAF V600E Sensitivity to RAF Inhibition. *Pigment Cell Melanoma Res* (2020) 1–7. doi: 10.1111/pcmr.12932
8. Robinson SD, Joyce A, O'Shaughnessy C, Cowey L, Konduri K. Braf V600E-Mutated Lung Adenocarcinoma With Metastases to the Brain Responding to Treatment With Vemurafenib. *Lung Cancer* (2014) 85(2):326–30. doi: 10.1016/j.lungcan.2014.05.009
9. Mcarthur G, Maio M, Arance A, Nathan P, Blank C, Avril MF, et al. Vemurafenib in Metastatic Melanoma Patients With Brain Metastases: an Open-Label, Single-arm, Phase 2, Multicenter Study. *Ann Oncol* (2017) 28 (3):634–641. doi: 10.1093/annonc/mdw641
10. De Mattos-Arruda L, Mayor R, Ng CKY, Weigelt B, Torrejon D, Oliveria M, et al. Cerebrospinal Fluid-Derived Circulating Tumour DNA Better Represents the Genomic Alterations of Brain Tumours Than Plasma. *Nat Commun* (2015) 6:8839–45. doi: 10.1038/ncomms9839
11. Ge M, Zhan Q, Ji X, Zhou X, Huang R, Liang X. Different Next-Generation Sequencing Pipelines Based Detection of Tumor DNA in Cerebrospinal Fluid of Lung Adenocarcinoma Cancer Patients With Leptomeningeal Metastases. *BMC Cancer* (2019) 19:143. doi: 10.1186/s12885-019-5348-3
12. Chunhua M, Xueling Y, Wenge X, Yu H. Detection of Circulating Tumor DNA From Non-Small Cell Lung Cancer Brain Metastasis in Cerebrospinal Fluid Samples. *Thorac Cancer* (2020) 11:588–93. doi: 10.1111/1759-7714.13300

Conflict of Interest: The authors declare that the research was conducted in the absence of any commercial or financial relationships that could be construed as a potential conflict of interest.

frontiers in Oncology

ORIGINAL RESEARCH
published: 21 October 2021
doi: 10.3389/fonc.2021.745590

Identification of Novel Drug Candidate for Epithelial Ovarian Cancer *via In Silico* Investigation and *In Vitro* Validation

Dan Zou[1,2†], Jin Bai[1,3†], Enting Lu[4], Chunjiao Yang[1], Jiaqing Liu[1], Zhenpeng Wen[1], Xuqin Liu[1], Zi Jin[5], Mengdan Xu[1], Lei Jiang[1], Ye Zhang[1] and Yi Zhang[4*]*

[1] The First Laboratory of Cancer Institute, The First Hospital of China Medical University, Shenyang, China, [2] Department of Medical Oncology, Cancer Hospital of China Medical University, Liaoning Cancer Hospital & Institute, Shenyang, China, [3] Department of Oncology, Shanghai East Hospital, Tongji University School of Medicine, Shanghai, China, [4] Department of Gynecology, First Hospital of China Medical University, Shenyang, China, [5] The First Department of Oncology, Shenyang Fifth People's Hospital, Shenyang, China

Epithelial ovarian cancer (EOC) has a poor prognosis and high mortality rate; patients are easy to relapse with standard therapies. So, there is an urgent need to develop novel drugs. In this study, differentially expressed genes (DEGs) of EOC were identified in The Cancer Genome Atlas (TCGA) and Gene Expression Omnibus (GEO) databases. Enrichment and protein–protein interaction (PPI) analyses were performed. The drug candidate which has the possibility to treat EOC was predicted by Connectivity Map (CMAP) databases. Moreover, molecular docking was selected to calculate the binding affinity between drug candidate and hub genes. The cytotoxicity of drug candidates was assessed by MTT and colony formation analysis, the proteins coded by hub genes were detected by Western blots, and apoptosis analysis was evaluated by flow cytometry. Finally, 296 overlapping DEGs (|log 2 fold change|>1; q-value <0.05), which were principally involved in the cell cycle ($p < 0.05$), and cyclin-dependent kinase 1 (CDK1) were screened as the significant hub gene from the PPI network. Furthermore, the 21 drugs were extracted from CMAPs; among them, piperlongumine (PL) showed a lower CMAP score (-0.80, -62.92) and was regarded as the drug candidate. Furthermore, molecular docking results between PL and CDK1 with a docking score of –8.121 kcal/mol were close to the known CDK1 inhibitor (–8.24 kcal/mol). Additionally, *in vitro* experiments showed that PL inhibited proliferation and induced apoptosis *via* targeting CDK1 in EOC SKOV3 cells. Our results reveal that PL may be a novel drug candidate for EOC by inhibiting cell cycle.

Keywords: epithelial ovarian cancer, CDK1, piperlongumine, molecular docking, cell cycle

OPEN ACCESS

Edited by:
Chi Zhang,
Indiana University Bloomington, United States

Reviewed by:
Zongyue Zeng,
First Affiliated Hospital of Chongqing Medical University, China
Enze Liu,
Indiana University, United States

***Correspondence:**
Yi Zhang
syzi@163.com
Ye Zhang
zhangyecmu@163.com

†These authors have contributed equally to this work and share first authorship

Specialty section:
This article was submitted to Pharmacology of Anti-Cancer Drugs, a section of the journal Frontiers in Oncology

Received: *22 July 2021*
Accepted: *28 September 2021*
Published: *21 October 2021*

Citation:
Zou D, Bai J, Lu E, Yang C, Liu J, Wen Z, Liu X, Jin Z, Xu M, Jiang L, Zhang Y and Zhang Y (2021) Identification of Novel Drug Candidate for Epithelial Ovarian Cancer via In Silico Investigation and In Vitro Validation. Front. Oncol. 11:745590. doi: 10.3389/fonc.2021.745590

INTRODUCTION

Epithelial ovarian cancer (EOC) is an aggressive malignancy and is most frequently diagnosed at an advanced disease stage (1). Currently, the most common treatment is surgery combined with platinum-based combination chemotherapy (2). However, 60% of patients relapsed after first-line therapy (3), and 50% showed resistance to chemotherapy. It is generally believed that EOC chemotherapy resistance is involved in the DNA damage response (DDR) process of the cell cycle (4, 5), in particular single-strand DNA break repair by poly ADP-ribose polymerase (PARP) and double-stranded repair through homologous recombination repair (HRR) of the BRCA1/2 genes. Therefore, it is the key to discovering drugs that affect the mechanism of drug resistance.

Currently, for the treatment of ovarian cancer, agents that target certain stages of the cell cycle, such as cyclin-dependent kinase inhibitors (CDKIs), have shown good efficacy in clinical trials. For example, ribociclib (6), a CDK4/6 inhibitor, which acts on the G1 phase of the cell cycle has been approved by the US Food and Drug Administration (FDA) for the treatment of breast cancer; it has also been used to treat ovarian cancer in phase II clinical trials (NCT02657928). Furthermore, AZD5438 (7, 8), a CDK1/2 inhibitor, enhances radiosensitivity of non-small cell lung cancer by impairing HRR of double-stranded breaks (DSBs) and has already been tested in the preclinical stage. Thus, it has been suggested that targeting the cell cycle is a novel and effective method to treat tumors. However, only a few CDKIs have so far been developed to treat ovarian cancer; thus, more chemotherapeutic agents, which are more efficacious and safe, need to be developed for treating ovarian cancer.

High costs necessitating strong financial support, long timelines, and requirement of substantial resources make development of a novel drug a difficult venture. Drug repurposing is an unconventional approach to identify novel indications of an approved or experimental drug (9). There are several successful examples. For instance, thalidomide was originally developed as an antiemetic in pregnancy but has currently garnered a huge market for the management of multiple myelomas (10). Metformin, widely used for first-line therapy of type 2 diabetes, has been found to possess an additional anticancer property (11). Therefore, repurposing of known drugs is a feasible drug development strategy.

In the present study, by focusing directly on EOC datasets, we aimed to develop a new drug to treat EOC by integrated bioinformatics and *in vitro* experiments. It was principally based on the Connectivity Map (CMAP) databases, which connect genes, drugs, and diseases by numerous cell line experiments. Then, molecular docking was used to matching potential drugs and screened proteins. Furthermore, *in vitro* experiments were used to validate our prediction. To a certain extent, our study may provide a basis for the treatment of EOC.

Abbreviations: CDK1, cyclin-dependent kinase 1; CMAP, Connectivity Map; DEGs, differentially expressed genes; EOC, epithelial ovarian cancer; GEO, Gene Expression Omnibus; GEPIA: the Gene Expression Profiling Interactive Analysis; GO, gene ontology; GTEx, the Genotype-Tissue Expression; KEGG, Kyoto Encyclopedia of Genes and Genomes; PPI, protein–protein interaction; PL, piperlongumine; TCGA, The Cancer Genome Atlas.

MATERIALS AND METHODS

Data Source and DEG Acquisition

Epithelial ovarian cancer-related mRNA data of cancer tissues and normal tissues were integrated from RNA-seq data and microarray expression datasets. First, the RNA-seq data were separately collected from The Cancer Genome Atlas (TCGA) database (http://cancergenome.nih.gov/) and the Genotype-Tissue Expression (GTEx) project (https://gtexportal.org/home/); the edition of the TCGA dataset on EOC was updated on July 20, 2019. The microarray expression datasets were obtained from the GEO database (https://www.ncbi.nlm.nih.gov/geo/), and the two gene expression profiles (GSE14407 and GSE54388) were both selected with the GPL590 platform. GSE14407 and GSE54388 were updated on March 25, 2019. Then, differential analyses of the two ways datasets were used by the R package Limma (https://bioconductor.org/packages/release/bioc/html/limma.html) (12) to determine differentially expressed genes (DEGs) with the criteria of $|\log2(FC)| > 1$ and adjusted p-value < 0.05. Furthermore, the differential analysis of RNA-seq data were log2(TPM+1) transformed and analyzed by the Gene Expression Profiling Interactive Analysis (GEPIA) (http://gepia.cancer-pku.cn/) (13).

Functional Enrichment Analyses

The potential mechanisms of the genes selected were studied, which were imported from the online bioinformatics database Metascape (http://metascape.org/) (14), including gene ontology (GO) Biological Processes and Kyoto Encyclopedia of Genes and Genomes (KEGG) pathway enrichment analyses as well as Protein Protein Interaction (PPI) establishment. In this study, significant terms met the criteria of a p value < 0.05 and the number of enriched genes ≥ 3.

PPI Network Module Analyses and Identification of Hub Genes

To visualize and analyze the PPI network, we used Cytoscape (version 3.7.0) software (http://www.cytoscape.org/) (15). First, molecular modules were analyzed by Molecular Complex Detection (MCODE) (16) plugin of Cytoscape. The parameter settings were set to default. The criteria were set as follows: MCODE scores > 3 and number of nodes > 4. Next, hub genes were screened from the PPI network using CytoHubba (17) plugin of Cytoscape with the recommended maximal clique centrality (MCC) ranking methods. The top 10 genes were noted as hub genes.

EOC-Associated Drug Prediction and Gene Set Enrichment Analysis (GSEA)

The connectivity map, which aims to connect the genes, drugs, and disease states by querying the gene lists of upregulated and downregulated genes, was employed. A so-called connectivity score was estimated to assess the priority of the prediction; a positive score denotes a stimulant effect of a drug on the query signatures, whereas a negative score implicates a repressed effect of a drug on the query signatures. This was based on different data and algorithms. CMAP (18), the first-generation connectivity map platform, using a microarray platform

(Affymatrix HT_HG_U133A with 22 283 probe sets), screened 1,309 FDA drugs treated in five cell lines, and the connectivity score was from –1 through 1. Then, LINCS (19), the next-generation connectivity map, including 476,251 genome-wide expression signature expression profiles gathered 27,927 perturbagens stimulated by 72 cell lines from 1.3M L1000 profiles. The connectivity score was from –100 through 100. In addition, to investigate the pathways affected by small molecule drugs, the raw data were selected from the CMAP database and analyzed using the function of GSEA from clusterProfiler package (20, 21) and the criteria of a p-value < 0.05, FDR <0.25.

Molecular Docking Between Drug Candidate and Hub Gene of EOC

The crystal structures of proteins coded by the hub gene were retrieved from the RCSB Protein Data Bank (PDB) (www.rcsb.org/pdb/home/home.do). Moreover, the three-dimensional structure of drugs was searched from PubChem (https://www.ncbi.nlm.nih.gov/pccompound). The molecular docking process involved preparing the proteins and ligands, setting up a grid, and docking the compounds; these were accomplished using the Schrodinger Glide docking protocol (Schrödinger, LLC, NY, USA) (22). The best pose was picked out by the docking score and the rationality of molecular conformation.

In Vitro Cell Lines and Chemicals

Human ovarian cancer cell lines SK-OV-3, CA-OV-3, and HO-8910 were obtained from the Cell Bank of Type Culture Collection of the Chinese Academy (Shanghai, China). SK-OV-3 was cultured in McCoy's 5A Complete Medium (Thermo Fisher, Belgium). CA-OV-3 was cultured in DMEM medium, and HO-8910 was cultured in RPMI-1640 medium. All the cell lines were cultured in medium supplemented with 10% fetal bovine serum (Greiner Bio-One, Belgium) and antibiotics (penicillin/streptomycin, 100 U/ml, Beyotime, Beijing, China) at 37°C in 5% CO_2.

PL was purchased from NeOnc Technologies, Inc. (Los Angeles, CA, USA) and diluted with DMSO to make stock solutions of 10 mM. In all cases of cell treatment, the final DMSO concentration in the culture medium never exceeded 0.5%. Stock solutions of all drugs were stored at −20°C.

Cell Viability Assay

The EOC cell lines were plated to 5 × 103 cells/well in 96-well plates for 24 h, then treated with the indicated concentrations of PL. Next, 50 μl of the MTT reagent (5 mg/ml) was added for 3 h, and then 150 μl of DMSO was admixed to dissolve the formazan crystals. Absorbance was measured at 570 nm using a spectrophotometer (Bio-Rad, Temse, Belgium). Cell viability was determined by dividing the absorbance values of treated cells with that of untreated cells.

Colony Formation Assay

Depending on the cell line, 200 cells were implanted in each well of a six-well plate and exposed to the indicated concentrations of PL for 24 h. Following this, drugs were withdrawn and cells were grown in normal culture for 14 days. Next, the cells were fixed with acetic acid-methanol (1:4) and stained with diluted crystal violet (1:30). Colonies that consisted of more than 50 cells were counted and calculated. The colony formation efficiency was calculated with the following formula: Survival Fraction = Colonies/Cell numbers × 100%. Three independent experiments were carried out.

Detection of Apoptotic Cells

Apoptosis was evaluated by using Annexin V-FITC Apoptosis Detection Kit (BD Biosciences Pharmingen, San Diego, CA, USA) according to the manufacturer's instructions. EOC cell lines (2.5–4.5 × 10^5 cells/well) were seeded in a six-well plate and grown to 70% confluence. After being treated with various concentrations of PL for 24 h and 48 h, the cells were trypsinized, collected, and washed twice with phosphate-buffered saline (PBS) and stained with FITC-Annexin V and propidium iodide (PI) for 15 min in the dark. The stained cell populations were determined using a FACSCalibur flow cytometer (Becton Dickinson, Bedford, MA, USA), and the data were analyzed using FlowJo Software 7.6 (TreeStar, Inc., San Car-los, CA, USA). Three independent experiments were carried out.

Western Blots

Cells were extracted, and protein was quantified as described previously (23). The cells were washed twice with PBS, lysed in lysis buffer (1% Triton X-100, 50 mM Tris–HCl pH 7.4, 150 mM NaCl, 10 mM EDTA, 100 mM NaF, 1 mM Na_3VO_4, 1 mM PMSF, 2 μg/ml aprotinin), and quantified using a BCA protein quantification kit (cat. no. ab102536; Abcam). The cell lysates were separated by 8% or 15% SDS-PAGE, and the samples were transferred onto a nitrocellulose membrane (Immobilon-P, Millipore; Merck KGaA). After blocking with 5% evaporated skimmed milk in Tris-buffered saline Tween-20 (TBST) buffer (10 mM Tris–HCl pH 7.4, 150 mM NaCl, 0.1% Tween-20) at room temperature for 1 h, primary antibodies were probed and incubated overnight at 4°C. Following three washes with TBST buffer, the membrane was incubated with secondary goat anti-rabbit and goat anti-mouse antibodies for 30 min at room temperature. Finally, the protein bands were detected with enhanced chemiluminescence reagent (SuperSignal™ Western Pico Chemiluminescent Substrate; Pierce; Thermo Fisher Scientific, Inc.) and scanned using the Electrophoresis Gel Imaging Analysis System (DNR Bio Imaging Systems, Neve Yamin, Israel).

Statistical Analysis

Statistical significance was evaluated with data from at least three independent experiments. GraphPad Prism 7.00 (GraphPad Software, San Diego, CA, USA) was used for data analysis. Statistical analysis was carried out using the Student's t-test for two groups, as well as one-way ANOVA for more than two groups. Data were presented as the mean ± SD. For all statistical tests, significance was established at $p < 0.05$. The number of asterisks in the figures indicates the level of statistical significance: *$p < 0.05$, **$p < 0.01$, ***$p < 0.001$, ****$p < 0.0001$.

RESULTS

Identification of Overlapping DEGs for EOC

In this study, DEGs and their significant biological characteristics were identified based on various GEO mRNA microarray datasets (GSE14407 and GSE54388) and the TCGA mRNA-seq dataset by integrated bioinformatics analysis of EOC (**Figure 1**). There were a total of 560 samples, including 454 EOC tissues and 106 normal tissues (GSE54388: 16T/6N; GSE14407: 12T/12N; RNA-seq: 426T(TCGA)/88GTEx, respectively). After gene expression assays and data processing and normalizing, we screened DEGs among each mRNA data set using the Limma with the criteria of $|\log2(FC)| > 1$ and an adjusted p-value < 0.05. Overall, a total of 1,188 DEGs were screened from the GSE54388 data set, including 518 upregulated and 670 downregulated genes (**Figure 1A**). There were 711 DEGs, including 255 upregulated and 456 downregulated genes in GSE14407 (**Figure 1B**). Additionally, 7,615 DEGs were selected from the TCGA data set, including 2,606 upregulated and 5,009 downregulated genes (**Figure 1C**). To confirm the reliability of DEGs in EOC, we obtained overlapping DEGs of the three datasets, including 115 common upregulated genes and 181 common downregulated genes (**Figures 1D, E** and **Supplementary Table 1**).

Functional Enrichment Analyses

We selected overlapping DEGs to investigate the enrichment of EOC in GO and KEGG pathways in Metascape. First, the KEGG pathways for DEGs were mainly cell cycle, oocyte meiosis, and p53 signaling pathway, which were found to be related to the development of multiple tumors and were involved in EOC tumorigenesis and pathogenesis (**Figure 2A**). For GO_BP enrichment analysis, they were enriched in cell cycle and apoptosis, such as cell division, mitotic nuclear division, and mitotic sister chromatid segregation (**Figure 2B**). For GO_MF analysis, they were enriched in DNA replication origine binding and microtubule binding (**Figure 2C**). For GO_CC analysis, they were enriched in spindle, chromosomal region, microtubule, and so on. These results indicated that DEGs might be related to the cell proliferation process (**Figure 2D**). In addition, the KEGG pathways of downregulated DEGs were enriched in tyrosine metabolism, drug metabolism-cytochrome P450, and retinol metabolism (**Figure 2A**).

PPI Network Module Analyses and Identification of Hub Genes

Furthermore, we constructed the PPI network presented in **Figures 3A, B**, and the whole network was clustered in three modules by MCODE plugin of Cytoscape. Module 1 included all

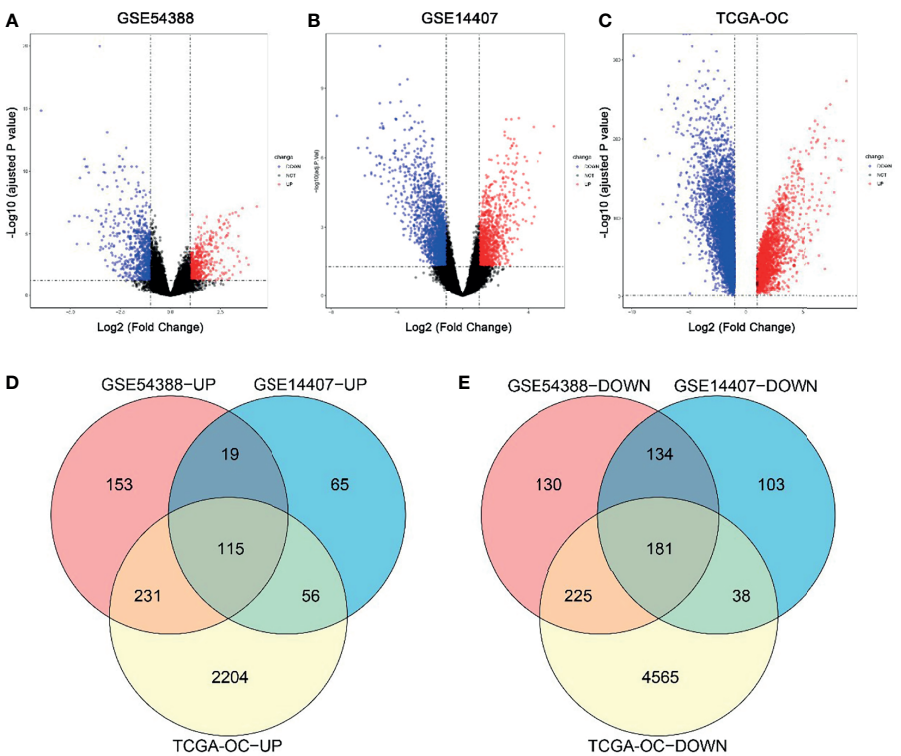

FIGURE 1 | Identification of common differentially expressed genes (DEGs) in three independent datasets. **(A–C)** Volcano plot for the DEGs in GSE54388 **(A)**, GSE14407 **(B)**, and TCGA-OC **(C)** datasets when comparing epithelial ovarian cancer (EOC) to normal ovarian subjects. The x-axis represents log2 (fold change), and y-axis represents significant difference expressed as –log10 (adjusted p-value). DEGs were determined using the limma package. The gene with the adjusted p-value < 0.05,$|\log2FC| \geq 2$ was considered significant. **(D, E)** A total of 115 common upregulated genes **(D)** and 181 common downregulated genes **(E)** were shared between these three independent datasets.

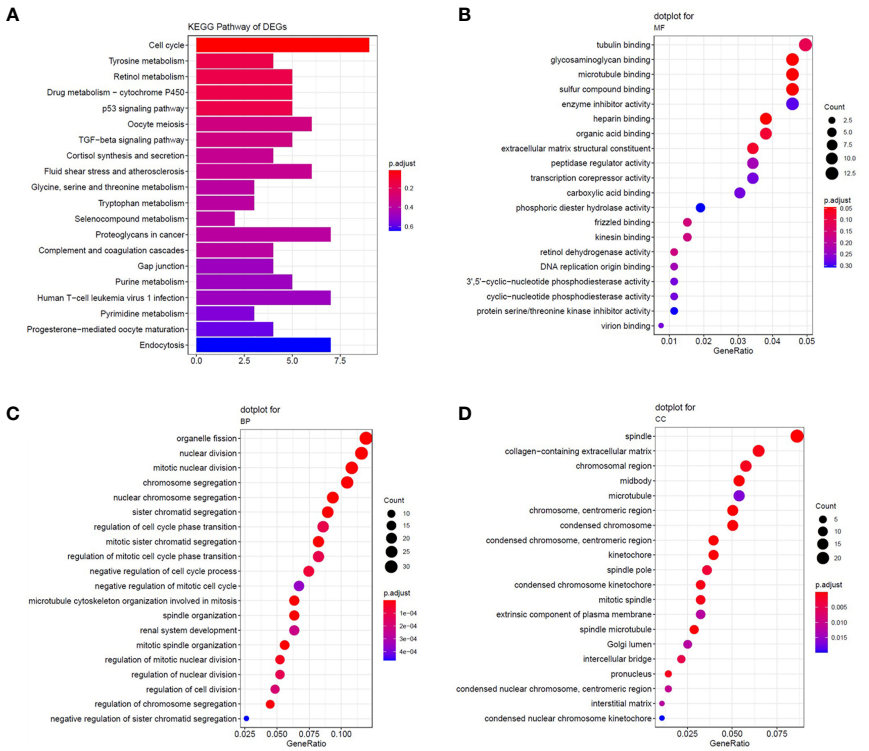

FIGURE 2 | The enrichment analysis of common DEGs. **(A)** Significantly enriched Kyoto Encyclopedia of Genes and Genomes (KEGG) pathways. **(B–D)** The results of GO enrichment for DEGs. Enrichment analysis of the common DEGs was assessed by the Metascape database separately. P-value < 0.05 was considered statistically significant.

common upregulated genes and were enriched in cell division, chromosome segregation, and mitotic sister chromatid segregation, which were G2/M related. Module 2 consisted of common upregulated genes and one common downregulated gene, enriched in the regulation of mitotic cell cycle, cell cycle process, and mitotic cell cycle phase transition. Module 3 included all common downregulated genes but had no exact analysis results.

Next, hub genes were selected among the overlapping DEGs by the CytoHubba plugin of the Cytoscape. The top 10 genes were screened as hub genes, including CDK1, CDC20, BUB1B, CCNB1, CDCA8, NUF2, SPC25, CENPF, CENPK, and ZWINT in descending order (**Figure 3C**). CDK1 received the maximum score among them, and it was selected as the significant hub gene. CDK1 expressed a significantly higher level in ovarian cancer tissues, compared with normal tissues (**Supplementary Table 1**). Further, a higher expression level of CDK1 was correlated with poor prognosis of ovarian cancer patients (**Figure 3D**).

EOC-Associated Drugs and GSEA

The overlapping DEGs generated for EOC were used to query CMAP and LINCS, respectively. By integrating the drugs from the two databases with score < 0, and p value < 0.05, we found that the 21 drugs were segregated into two clusters (**Figure 4A**); we selected the five drugs (piperlongumine, doxorubicin, vorinostat, methotrexate, and scriptaidin) in cluster 2, which had lower scores in both databases regarded as the potential drugs. Among them, four drugs (doxorubicin, vorinostat, methotrexate, and scriptaidin) have been used to treat EOC in clinical practice or clinical trials; PL received the lowest connectivity score, and there is litter evidence that it can treat EOC (23). Moreover, for piperlongumine, a total of 28 pathways were enriched (**Figure 4B**), including DNA replication, nucleotide excision repair, mismatch repair, and homologous recombination, which were closely related to the mechanism of EOC proliferation and drug resistance. Hence, we regarded PL as the candidate drug.

Interactions Between Drug Candidate and Hub Gene

To further predict whether PL could be a direct CDK1 inhibitor, we performed molecular docking using the Schrodinger Glide docking protocol. Surprisingly, we found that PL showed a good binding affinity for CDK1 protein with the docking glide score of –8.121 kcal/mol, which is close to that of the known CDK1 inhibitor, AZD5438 (–8.24 kcal/mol). Most of the drugs appeared to have an equivalent glide score range from –8.121 through –2.662 kcal/mol. As displayed in **Figure 5**, the top scoring ligands, such as PL, were observed to interact with three residues Leu-83, GLN-132, and GLN-49 through hydrogen bonding with their side chains. Taken together, our data indicated that PL can bind to a similar pocket on CDK1.

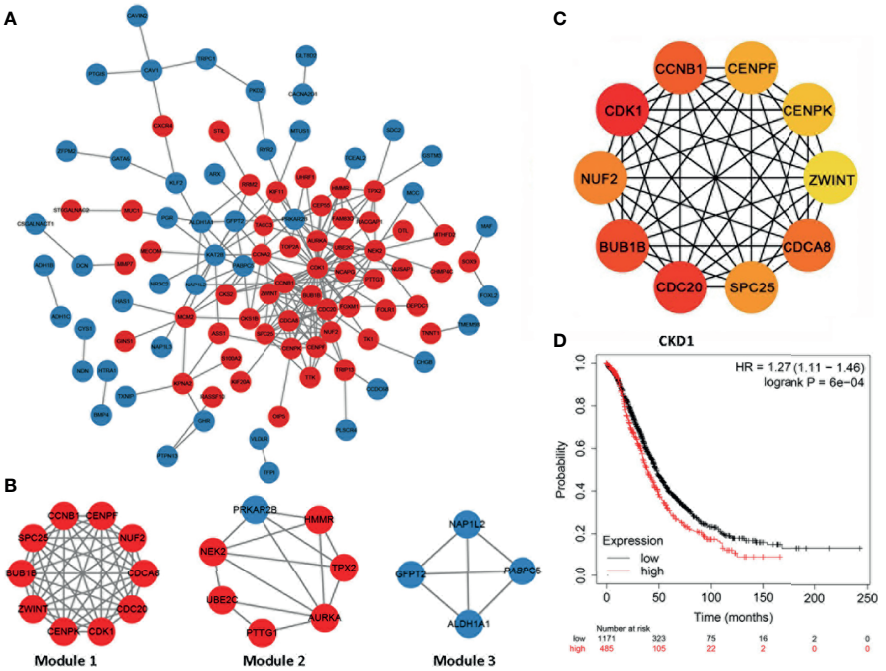

FIGURE 3 | The protein–protein interaction network and hub genes. **(A, B)** EOC-related network; red indicates common upregulated genes and blue represents and common downregulated genes. The internal interactions between common DEGs were mined by the Metascape database, and the network was visualized using Cytoscape software. **(C)** Top 10 EOC-related hub genes. The network was analyzed by the cytoHubba plugin of Cytoscape software with the method of MCC. All the hub genes were upregulated in EOC tissues. **(D)** High CDK1 expression was correlated with poor prognosis of ovarian cancer patients (hazard ratio = 1.27, 95% CI: 1.11–1.46, $p < 0.05$).

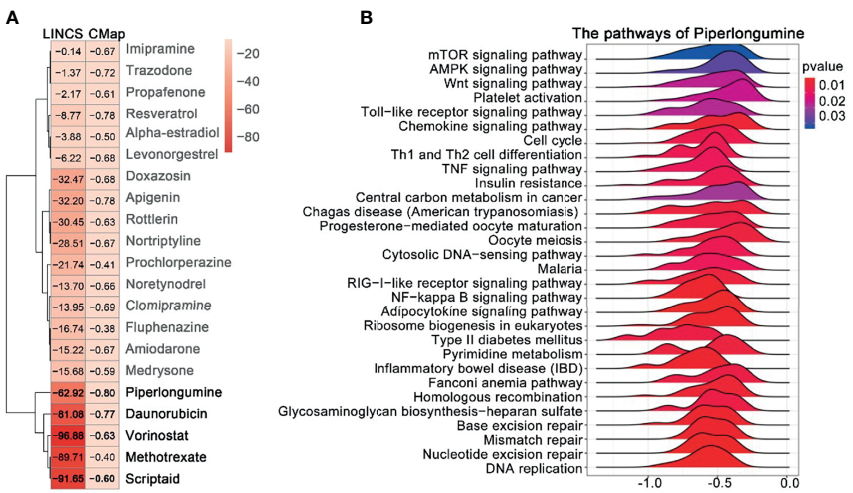

FIGURE 4 | Prediction of drug candidates and drug GSEA analysis. **(A)** Similarity score table for the drugs having at least one significant association with connectivity map databases. Each row corresponds to a drug, and columns correspond to two-generation connectivity map databases. The score labels with numbers indicate the significance of the results. The row labels written in bold indicate the drugs we selected for further analysis. **(B)** GSEA analysis of the piperlongumine was assessed by the clusterProfiler package; p-value < 0.05 was considered statistically significant.

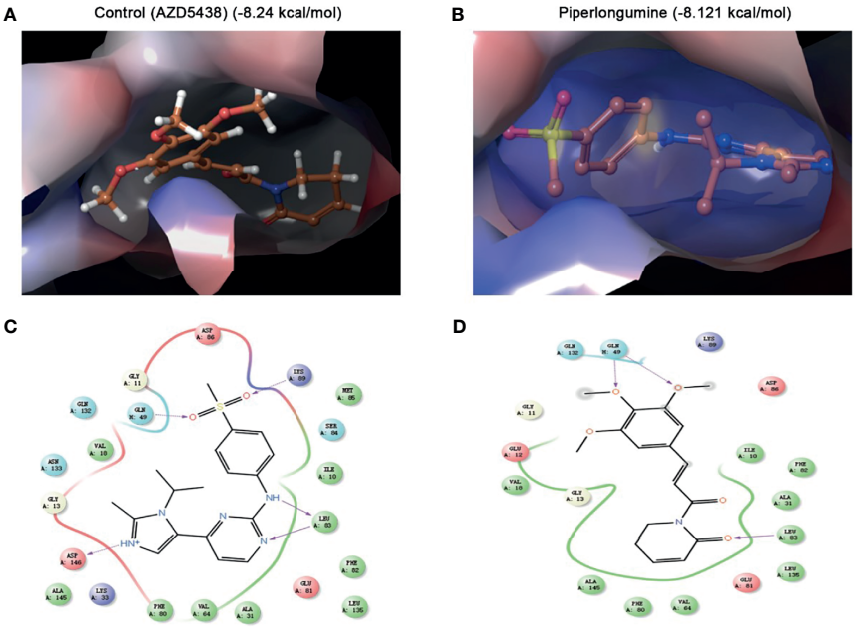

FIGURE 5 | Molecular docking simulation for piperlongumine and CDK1. **(A, B)** Docked structure and interactions of drugs [**(A)** AZD5438 (control), **(B)** piperlongumine] binding to CDK1. **(C, D)** 2D interaction diagrams of the residues of CDK1 involved in the binding of drugs [**(C)** AZD5438 (control), **(D)** piperlongumine]. The Schrodinger Glide docking protocol was used for this analysis.

In Vitro Studies

SKOV3, CA-OV-3, and HO-8910 cell cultures were exposed to different concentrations of PL for 24 h or 48 h, and cell viability was determined by MTT assay. As shown in **Figures 6A–C**, PL decreased cell viability in a concentration- and time-dependent manner. The IC50 value of SK-OV-3 was 49.32 and 16.28 μM in 24 and 48 h, respectively. For CA-OV-3, the IC50 in 24 and 48 h was 18.76 and 11.58 μM. For HO-8910, the IC50 in 24 and 48 h was 12.70 and 6.80 μM, respectively. Subsequently, a colony formation assay was also carried out; PL exposure caused a dose-dependent reduction in the number and size of colonies formed, compared with the control (**Figures 6D, E**). These data supported the inhibitory role of PL in ovarian cancer cell growth and colony formation. Additionally, PL induced lower levels of CDK1 and CCNB1 in a concentration-dependent manner, which is necessary for G2/M phase transitions of the cell cycle (**Figure 6F**). These results suggested that PL could inhibit EOC cell proliferation and affect the expression of CDK1.

Furthermore, to determine whether apoptosis was involved in PL-induced cytotoxicity, SKOV3 cells exposed to PL were stained with Annexin-V/FITC followed by flow cytometric analysis (**Figure 6G**). We observed an increase in apoptosis to 37.6% and 53.4% at 20 μM after 24 and 48 h, respectively.

DISCUSSION

In the current study, using gene expression data, a cluster of drugs that could potentially treat EOC was identified. Firstly, by merging TCGA mRNA-seq datasets and GEO mRNA microarray datasets, we generated overlapping DEGs as EOC signatures. Then, by integrating CMAP and LINCS databases, we identified potential drugs with lower negative connectivity scores that could evidently reverse EOC signatures. Based on the literature, four of these drugs were previously used clinically to treat EOC either as first-line treatment or as agents in clinical trials. This implies that we successfully predicted a group of known EOC drugs, without any hint of advanced drug information, suggesting that the remaining drug (piperlongumine) that we identified also has a high likelihood of treating EOC. Piperlongumine has been reported to inhibit several cancers, and only one study focused on ovarian cancer (24). In our study, the potential application of PL in EOC was further explored with a molecular docking test and *in vitro* experiments.

By merging EOC datasets from TCGA and GEO, 247 genes in total were considered as overlapping DEGs in EOC, including 103 common upregulated genes and 144 common downregulated genes. Then, common upregulated genes were mainly enriched in G2/M transition of the mitotic cell cycle, and the p53 signaling pathway, which are deemed to be a crucial pathway in the development and metastasis of EOC (25). Also, CDK1 was selected as the significant hub gene from the PPI network. It is well known that the abrogation of CDK1-CCNB1 activity blocks mitotic entry and arrests cells at the G2 phase (4).

We computed both CMAP and LINCS datasets to identify novel EOC drugs. Although CMAP has achieved remarkable success (26), some of its limitations cannot be ignored. For example, only five human cancer cell lines were used, and not

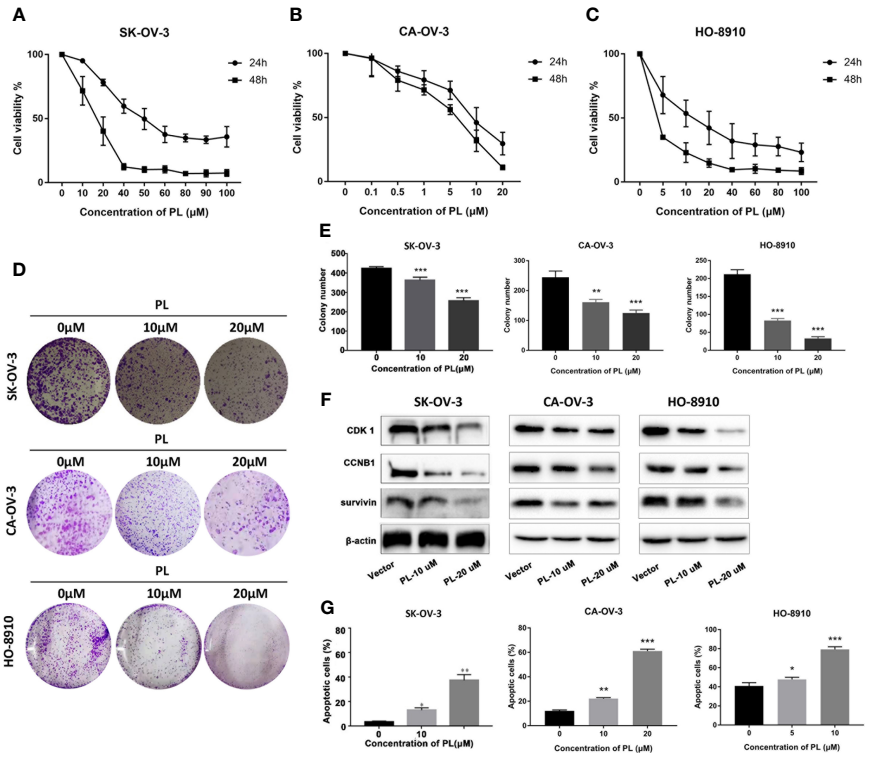

FIGURE 6 | PL inhibited growth and induced apoptosis *via* targeting CDK1 in EOC cells. **(A–C)** Cell viability was assessed by MTT assay at 24 h and 48 h after treatment, and IC50 was computed accordingly. **(D, E)** Cell proliferation capacity was evaluated by colony formation assay, where cells after treatment were plated with a density of 200 cells/well and grown for 7 days followed by staining. **(F)** Expression levels of CDK1, CCNB1, and survivin proteins after treatment of PL at 10 or 20 μM for 24 h in EOC cells by Western blot analysis. β-Actin was used as an equal loading control for normalization. **(G)** Apoptotic cells were evaluated by Annexin-V and PI staining and analyzed by flow cytometry. All data are shown as mean ± standard deviation (n = 3). One-way ANOVA with the multiple-comparison test was used to calculate statistics: *p < 0.05; **p < 0.01; ***p < 0.001.

all small molecules were tested on all these. The other drawbacks included limitations of dosages and time points and that several small molecules were tested using a 10-mM concentration with a 6-h perturbation time point. What is encouraging, LINCS covers 72 human cell lines and various cellular perturbations, including 15,000 small molecule compounds and 5,000 genes (gene silencing and overexpression). So we leveraged the LINCS dataset to increase the reliability of CMAP (27). In this study, the drugs with negative connectivity score were expected to be inversely correlated with EOC. Therefore, we focused on the five drugs with lower connectivity score from both CMAP and LINCS datasets. Among them, doxorubicin has been used clinically to treat ovarian cancer primarily by the mechanism of topoisomerase inhibition (28, 29). Vorinostat and scriptaid, two HDAC inhibitors, have been tested in ovarian cancer-associated clinical trials (30, 31). Methotrexate has been used as maintenance therapy in patients with advanced ovarian carcinoma (32). However, there is little evidence for PL treating ovarian cancer. Moreover, GSEA analysis showed that PL correlated with DNA replication, nucleotide excision repair, mismatch repair, and homologous recombination, which are important mechanisms for EOC drug resistance.

The molecular docking test, based on structure to design and understand the specific molecular mechanism, plays an important role in discovering drugs. There are a lot of successful examples in academia and industry. For instance, Mohamed et al. found that hesperidin formed a stable complex with a Polo-like kinase-1 active site by the approach of docking (33), Yu et al. used molecular docking to validate that Prestwick-685 and menadione may be the new esophageal carcinoma drugs (34). In our study, we selected the Schrodinger Glide docking protocol (35) to precisely simulate the interaction patterns and illustrate how PL acts on CDK1 proteins in the human body. Surprisingly, the results from docking tests demonstrated that PL could recognize and interact with CDK1 protein with a docking score of –8.121 kcal/mol, which was close to that of the known CDK1 inhibitor, AZD5438 (–8.24 kcal/mol). Therefore, it is suggested that PL has a considerable prospective role in the treatment of EOC by suppressing CDK1 proteins.

Piperlongumine, a biologically active alkaloid isolated from the roots of long pepper, is widely used as a traditional medicine in Ayurvedic medicine (36). It has been reported that PL selectively induces tumor cells death and delays tumor growth in hematologic tumors (37, 38) and diverse solid tumors (39–41). Furthermore, recent studies indicated that PL synergizes with cisplatin or

paclitaxel to inhibit the growth of both chemoresistant and chemosensitive ovarian cancer cells (24). Currently, the cytotoxic effect of PL depends on the increase in reactive oxygen species (24, 42) and induction of apoptosis and autophagy, restoration of mutant p53, and cell cycle arrest (43–45). However, the arrest of G2/M triggered by PL was only detected as a phenotype. Hence, it needs a precise study to uncover how PL influences the cell cycle.

Due to the central role of CDK1 in the regulation of the G2/M phase, targeting CDK1 has emerged as a highly promising therapeutic strategy. Currently, several CDKIs have been investigated in clinical trials for treatment of various types of malignancies. For example, AZD5438, a CDK1/2 inhibitor, preferentially targets proliferating cells and typical chemosensitivity or radiosensitivity modulators (7, 46). However, the lack of inhibitor specificity currently limits clinical development. In our study, we predicted the possibility of PL being a novel selective CDK1 inhibitor. Mechanistically, in our study, PL inhibited cell viability in a dose- and time-dependent manner and induced apoptosis in ovarian cancer cells. In addition, PL led to decreased levels of the proteins CDK1 and cyclin B. Therefore, our study defines the details of PL which may target CDK1 to inhibit EOC.

In summary, we screened the DEGs from both two sources (TCGA and GEO), repurposed drugs by the two-generation CMAP database (CMAP and LINCS). Then, molecular docking and *in vitro* experiments were performed to explore and validate the drug–target interactions. However, there are also certain limitations; we only selected one ovarian cancer cell line and had no *in vivo* test to validate the exact function of PL to ovarian cancer. Therefore, to some extent, we utilized both *in silico* and *in vitro* experiments to predict that PL could be a novel drug to treat EOC. Furthermore, the results need more further research, as well as *in vivo* experiments.

DATA AVAILABILITY STATEMENT

The original contributions presented in the study are included in the article/**Supplementary Material**. Further inquiries can be directed to the corresponding authors.

AUTHOR CONTRIBUTIONS

YiZ and YeZ designed research; JB and EL performed bioinformatics research; DZ, CY, and ZJ performed cell research; JL, ZW, and MX sorted data; DZ, and LJ wrote the paper and revised the manuscript. All authors contributed to the article and approved the submitted version.

FUNDING

This work was supported by the National Natural Science Foundation of China (Nos. 82073244, 81270036, 30901736), the Plan to Focus on Research and Development from the Science and Technology Project of Liaoning Province (No. 2017225029), and Shenyang Youth Science and Technology Innovation Talent Project (RC200267).

SUPPLEMENTARY MATERIAL

The Supplementary Material for this article can be found online at: https://www.frontiersin.org/articles/10.3389/fonc.2021.745590/full#supplementary-material

REFERENCES

1. Miller KD, Goding Sauer A, Ortiz AP, Fedewa SA, Pinheiro PS, Tortolero-Luna G, et al. Cancer Statistics for Hispanics/Latinos, 2018. *CA: Cancer J Clin* (2018) 68(6):425–45. doi: 10.3322/caac.21494
2. du Bois A, Quinn M, Thigpen T, Vermorken J, Avall-Lundqvist E, Bookman M, et al. 2004 Consensus Statements on the Management of Ovarian Cancer: Final Document of the 3rd International Gynecologic Cancer Intergroup Ovarian Cancer Consensus Conference (GCIG OCCC 2004). *Ann Oncol* (2005) 16 Suppl 8:viii7–viii12. doi: 10.1093/annonc/mdi961
3. du Bois A, Reuss A, Pujade-Lauraine E, Harter P, Ray-Coquard I, Pfisterer J. Role of Surgical Outcome as Prognostic Factor in Advanced Epithelial Ovarian Cancer: A Combined Exploratory Analysis of 3 Prospectively Randomized Phase 3 Multicenter Trials: By the Arbeitsgemeinschaft Gynaekologische Onkologie Studiengruppe Ovarialkarzinom (AGO-OVAR) and the Groupe D'investigateurs Nationaux Pour Les Etudes Des Cancers De L'ovaire (GINECO). *Cancer* (2009) 115(6):1234–44. doi: 10.1002/cncr.24149
4. Hosoya N, Miyagawa K. Targeting DNA Damage Response in Cancer Therapy. *Cancer Sci* (2014) 105(4):370–88. doi: 10.1111/cas.12366
5. Coleman RL, Oza AM, Lorusso D, Aghajanian C, Oaknin A, Dean A, et al. Rucaparib Maintenance Treatment for Recurrent Ovarian Carcinoma After Response to Platinum Therapy (ARIEL3): A Randomised, Double-Blind, Placebo-Controlled, Phase 3 Trial. *Lancet* (2017) 390(10106):1949–61. doi: 10.1016/S0140-6736(17)32440-6
6. Curigliano G, Gomez Pardo P, Meric-Bernstam F, Conte P, Lolkema MP, Beck JT, et al. Ribociclib Plus Letrozole in Early Breast Cancer: A Presurgical, Window-of-Opportunity Study. *Breast* (2016) 28:191–8. doi: 10.1016/j.breast.2016.06.008
7. Raghavan P, Tumati V, Yu L, Chan N, Tomimatsu N, Burma S, et al. AZD5438, an Inhibitor of Cdk1, 2, and 9, Enhances the Radiosensitivity of Non-Small Cell Lung Carcinoma Cells. *Int J Radiat Oncol Biol Phys* (2012) 84 (4):e507–14. doi: 10.1016/j.ijrobp.2012.05.035
8. Byth KF, Thomas A, Hughes G, Forder C, McGregor A, Geh C, et al. AZD5438, a Potent Oral Inhibitor of Cyclin-Dependent Kinases 1, 2, and 9, Leads to Pharmacodynamic Changes and Potent Antitumor Effects in Human Tumor Xenografts. *Mol Cancer Ther* (2009) 8(7):1856–66. doi: 10.1158/1535-7163.MCT-08-0836
9. Gupta SC, Sung B, Prasad S, Webb LJ, Aggarwal BB. Cancer Drug Discovery by Repurposing: Teaching New Tricks to Old Dogs. *Trends Pharmacol Sci* (2013) 34(9):508–17. doi: 10.1016/j.tips.2013.06.005
10. Moreau P, Attal M, Hulin C, Arnulf B, Belhadj K, Benboubker L, et al. Bortezomib, Thalidomide, and Dexamethasone With or Without Daratumumab Before and After Autologous Stem-Cell Transplantation for Newly Diagnosed Multiple Myeloma (CASSIOPEIA): A Randomised, Open-Label, Phase 3 Study. *Lancet* (2019) 394(10192):29–38. doi: 10.1016/S0140-6736(19)31240-1
11. Lee MS, Hsu CC, Wahlqvist ML, Tsai HN, Chang YH, Huang YC. Type 2 Diabetes Increases and Metformin Reduces Total, Colorectal, Liver and Pancreatic Cancer Incidences in Taiwanese: A Representative Population Prospective Cohort Study of 800,000 Individuals. *BMC Cancer* (2011) 11:20. doi: 10.1186/1471-2407-11-20
12. Smyth G. Limma: Linear Models for Microarray Data. In: R Gentleman, V Carey, S Dudoit, R Irizarry, W Huber, editors. *Bioinformatics and Computational Biology Solutions Using R and Bioconductor*. New York: Springer (2005). p. 397–420.

13. Tang Z, Li C, Kang B, Gao G, Li C, Zhang Z. GEPIA: A Web Server for Cancer and Normal Gene Expression Profiling and Interactive Analyses. *Nucleic Acids Res* (2017) 45(W1):W98–W102. doi: 10.1093/nar/gkx247
14. Tripathi S, Pohl MO, Zhou Y, Rodriguez-Frandsen A, Wang G, Stein DA, et al. Meta- and Orthogonal Integration of Influenza "OMICs" Data Defines a Role for UBR4 in Virus Budding. *Cell Host Microbe* (2015) 18(6):723–35. doi: 10.1016/j.chom.2015.11.002
15. Shannon P, Markiel A, Ozier O, Baliga NS, Wang JT, Ramage D, et al. Cytoscape: A Software Environment for Integrated Models of Biomolecular Interaction Networks. *Genome Res* (2003) 13(11):2498–504. doi: 10.1101/gr.1239303
16. Sun G, Li Y, Peng Y, Lu D, Zhang F, Cui X, et al. Identification of Differentially Expressed Genes and Biological Characteristics of Colorectal Cancer by Integrated Bioinformatics Analysis. *J Cell Physiol* (2019). doi: 10.1002/jcp.28163
17. Chin CH, Chen SH, Wu HH, Ho CW, Ko MT, Lin CY. cytoHubba: Identifying Hub Objects and Sub-Networks From Complex Interactome. *BMC Syst Biol* (2014) 8 Suppl 4:S11. doi: 10.1186/1752-0509-8-S4-S11
18. Lamb J, Crawford ED, Peck D, Modell JW, Blat IC, Wrobel MJ, et al. The Connectivity Map: Using Gene-Expression Signatures to Connect Small Molecules, Genes, and Disease. *Science* (2006) 313(5795):1929–35. doi: 10.1126/science.1132939
19. Subramanian A, Narayan R, Corsello SM, Peck DD, Natoli TE, Lu X, et al. A Next Generation Connectivity Map: L1000 Platform and the First 1,000,000 Profiles. *Cell* (2017) 171(6):1437–52.e17. doi: 10.1016/j.cell.2017.10.049
20. Wu T, Hu E, Xu S, Chen M, Guo P, Dai Z, et al. clusterProfiler 4.0: A Universal Enrichment Tool for Interpreting Omics Data. *Innovation* (2021) 2 (3):100141. doi: 10.1016/j.xinn.2021.100141
21. Yu G, Wang L, Han Y, He Q. clusterProfiler: An R Package for Comparing Biological Themes Among Gene Clusters. *OMICS: A J Integr Biol* (2012) 16 (5):284–7. doi: 10.1089/omi.2011.0118
22. Halgren TA, Murphy RB, Friesner RA, Beard HS, Frye LL, Pollard WT, et al. Glide: A New Approach for Rapid, Accurate Docking and Scoring. 2. Enrichment Factors in Database Screening. *J Med Chem* (2004) 47(7):1750–9. doi: 10.18632/oncotarget.3253
23. Zhang Y, Qu X, Teng Y, Li Z, Xu L, Liu J, et al. Cbl-B Inhibits P-Gp Transporter Function by Preventing Its Translocation Into Caveolae in Multiple Drug-Resistant Gastric and Breast Cancers. *Oncotarget* (2015) 6 (9):6737–48. doi: 10.18632/oncotarget.3253
24. Gong LH, Chen XX, Wang H, Jiang QW, Pan SS, Qiu JG, et al. Piperlongumine Induces Apoptosis and Synergizes With Cisplatin or Paclitaxel in Human Ovarian Cancer Cells. *Oxid Med Cell Longev* (2014) 2014:906804. doi: 10.1155/2014/906804
25. Lin ZP, Zhu YL, Ratner ES. Targeting Cyclin-Dependent Kinases for Treatment of Gynecologic Cancers. *Front Oncol* (2018) 8:303. doi: 10.3389/fonc.2018.00303
26. Kunkel SD, Suneja M, Ebert SM, Bongers KS, Fox DK, Malmberg SE, et al. mRNA Expression Signatures of Human Skeletal Muscle Atrophy Identify a Natural Compound That Increases Muscle Mass. *Cell Metab* (2011) 13 (6):627–38. doi: 10.1016/j.cmet.2011.03.020
27. Zador Z, King AT, Geifman N. New Drug Candidates for Treatment of Atypical Meningiomas: An Integrated Approach Using Gene Expression Signatures for Drug Repurposing. *PloS One* (2018) 13(3):e0194701. doi: 10.1371/journal.pone.0194701
28. Gabizon AA, Patil Y, La-Beck NM. New Insights and Evolving Role of Pegylated Liposomal Doxorubicin in Cancer Therapy. *Drug Resist Update* (2016) 29:90–106. doi: 10.1016/j.drup.2016.10.003
29. Coleman RL, Monk BJ, Sood AK, Herzog TJ. Latest Research and Treatment of Advanced-Stage Epithelial Ovarian Cancer. *Nat Rev Clin Oncol* (2013) 10 (4):211–24. doi: 10.1038/nrclinonc.2013.5
30. Matulonis U, Berlin S, Lee H, Whalen C, Obermayer E, Penson R, et al. Phase I Study of Combination of Vorinostat, Carboplatin, and Gemcitabine in Women With Recurrent, Platinum-Sensitive Epithelial Ovarian, Fallopian Tube, or Peritoneal Cancer. *Cancer Chemother Pharmacol* (2015) 76(2):417–23. doi: 10.1007/s00280-015-2813-9
31. Takai N, Ueda T, Nishida M, Nasu K, Narahara H. A Novel Histone Deacetylase Inhibitor, Scriptaid, Induces Growth Inhibition, Cell Cycle Arrest and Apoptosis in Human Endometrial Cancer and Ovarian Cancer Cells. *Int J Mol Med* (2006) 17(2):323–9. doi: 10.3892/ijmm.17.2.323
32. El-Husseiny K, Motawei H, Ali MS. Continuous Low-Dose Oral Cyclophosphamide and Methotrexate as Maintenance Therapy in Patients With Advanced Ovarian Carcinoma After Complete Clinical Response to Platinum and Paclitaxel Chemotherapy. *Int J Gynecol Cancer* (2016) 26 (3):437–42. doi: 10.1097/IGC.0000000000000647
33. AlAjmi MF, Rehman MT, Hussain A, Rather GM. Pharmacoinformatics Approach for the Identification of Polo-Like Kinase-1 Inhibitors From Natural Sources as Anti-Cancer Agents. *Int J Biol Macromol* (2018) 116:173–81. doi: 10.1016/j.ijbiomac.2018.05.023
34. Chen YT, Xie JY, Sun Q, Mo WJ. Novel Drug Candidates for Treating Esophageal Carcinoma: A Study on Differentially Expressed Genes, Using Connectivity Mapping and Molecular Docking. *Int J Oncol* (2019) 54(1):152–66. doi: 10.3892/ijo.2018.4618
35. Sastry GM, Adzhigirey M, Day T, Annabhimoju R, Sherman W. Protein and Ligand Preparation: Parameters, Protocols, and Influence on Virtual Screening Enrichments. *J Comput Aided Mol Des* (2013) 27(3):221–34. doi: 10.1007/s10822-013-9644-8
36. Bezerra DP, Pessoa C, de Moraes MO, Saker-Neto N, Silveira ER, Costa-Lotufo LV. Overview of the Therapeutic Potential of Piplartine (Piperlongumine). *Eur J Pharm Sci* (2013) 48(3):453–63. doi: 10.1016/j.ejps.2012.12.003
37. Han SS, Son DJ, Yun H, Kamberos NL, Janz S. Piperlongumine Inhibits Proliferation and Survival of Burkitt Lymphoma *in vitro*. *Leuk Res* (2013) 37 (2):146–54. doi: 10.1016/j.leukres.2012.11.009
38. Han SS, Han S, Kamberos NL. Piperlongumine Inhibits the Proliferation and Survival of B-Cell Acute Lymphoblastic Leukemia Cell Lines Irrespective of Glucocorticoid Resistance. *Biochem Biophys Res Commun* (2014) 452(3):669–75. doi: 10.1016/j.bbrc.2014.08.131
39. Wang F, Mao Y, You Q, Hua D, Cai D. Piperlongumine Induces Apoptosis and Autophagy in Human Lung Cancer Cells Through Inhibition of PI3K/Akt/mTOR Pathway. *Int J Immunopathol Pharmacol* (2015) 28(3):362–73. doi: 10.1177/0394632015598849
40. Bharadwaj U, Eckols TK, Kolosov M, Kasembeli MM, Adam A, Torres D, et al. Drug-Repositioning Screening Identified Piperlongumine as a Direct STAT3 Inhibitor With Potent Activity Against Breast Cancer. *Oncogene* (2015) 34(11):1341–53. doi: 10.1038/onc.2014.72
41. Wang Y, Wu X, Zhou Y, Jiang H, Pan S, Sun B. Piperlongumine Suppresses Growth and Sensitizes Pancreatic Tumors to Gemcitabine in a Xenograft Mouse Model by Modulating the NF-Kappa B Pathway. *Cancer Prev Res (Phila)* (2016) 9(3):234–44. doi: 10.1158/1940-6207.CAPR-15-0306
42. Han LC, Stanley PA, Wood PJ, Sharma P, Kuruppu AI, Bradshaw TD, et al. Horner-Wadsworth-Emmons Approach to Piperlongumine Analogues With Potent Anti-Cancer Activity. *Org Biomol Chem* (2016) 14(31):7585–93. doi: 10.1039/C6OB01160H
43. Basak D, Punganuru SR, Srivenugopal KS. Piperlongumine Exerts Cytotoxic Effects Against Cancer Cells With Mutant P53 Proteins at Least in Part by Restoring the Biological Functions of the Tumor Suppressor. *Int J Oncol* (2016) 48(4):1426–36. doi: 10.3892/ijo.2016.3372
44. Wang Y, Wang JW, Xiao X, Shan Y, Xue B, Jiang G, et al. Piperlongumine Induces Autophagy by Targeting P38 Signaling. *Cell Death Dis* (2013) 4:e824. doi: 10.1038/cddis.2013.358
45. Bezerra DP, Moura DJ, Rosa RM, de Vasconcellos MC, e Silva AC, de Moraes MO, et al. Evaluation of the Genotoxicity of Piplartine, an Alkamide of Piper Tuberculatum, in Yeast and Mammalian V79 Cells. *Mutat Res* (2008) 652 (2):164–74. doi: 10.1016/j.mrgentox.2008.02.001
46. Sorf A, Novotna E, Hofman J, Morell A, Staud F, Wsol V, et al. Cyclin-Dependent Kinase Inhibitors AZD5438 and R547 Show Potential for Enhancing Efficacy of Daunorubicin-Based Anticancer Therapy: Interaction With Carbonyl-Reducing Enzymes and ABC Transporters. *Biochem Pharmacol* (2019) 163:290–8. doi: 10.1016/j.bcp.2019.02.035

Conflict of Interest: The authors declare that the research was conducted in the absence of any commercial or financial relationships that could be construed as a potential conflict of interest.

this article, or claim that may be made by its manufacturer, is not guaranteed or endorsed by the publisher.

frontiers in Oncology

CASE REPORT
published: 13 January 2022
doi: 10.3389/fonc.2021.783158

Recurrent Gallbladder Carcinoma With pMMR/MSS Achieved a Complete Response Following Camrelizumab Combined With Apatinib: A Case Report

Liting Zhong[1], *Xiaoyu Liu*[2], *Zelei Li*[1], *Xuebing Zhang*[1], *Yuli Wang*[1] *and Weiwei Peng*[1]*

[1] Department of Oncology, Ganzhou People's Hospital (The Affiliated Ganzhou Hospital of Nanchang University), Ganzhou, China, [2] Department of Imaging, Ganzhou People's Hospital (The Affiliated Ganzhou Hospital of Nanchang University), Ganzhou, China

Gallbladder carcinoma (GBC) with proficient mismatch repair (pMMR)/microsatellite stable (MSS) is associated with limited response to programmed death-1 (PD-1) inhibitor monotherapy. Limited data of PD-1 blockade combined with anti-angiogenic therapy in GBC are reported. One recurrent GBC patient with pMMR/MSS was treated with camrelizumab plus apatinib. After 4 cycles of combination therapy, the patient achieved a durable complete response with manageable toxicity. The next-generation sequencing and immunohistochemistry analysis showed that tumor mutation burden (TMB) was 7.26 mutants/Mb and PD-L1 expression was 10% (tumor proportion score) and 20% (immune proportion score). This case suggests that camrelizumab in combination with apatinib may be an effective treatment option for GBC patients with pMMR/MSS status, who have moderate expression of TMB and PD-L1. Additionally, TMB and PD-L1 expression may serve as potential biomarkers for predicting PD-1 inhibitor response of GBC. Furthermore, this needs to be verified in future studies.

Keywords: gallbladder carcinoma, PD-1 blockade, anti-angiogenic therapy, pMMR/MSS, case report

OPEN ACCESS

Edited by:
Zhi Li,
The First Affiliated Hospital of China Medical University, China

Reviewed by:
Tommaso Stecca,
ULSS2 Marca Trevigiana, Italy
Li Zhou,
Peking University Cancer Hospital, China

***Correspondence:**
Weiwei Peng
pengweiwei2008@163.com

Specialty section:
This article was submitted to Pharmacology of Anti-Cancer Drugs, a section of the journal Frontiers in Oncology

Received: *25 September 2021*
Accepted: *21 December 2021*
Published: *13 January 2022*

Citation:
Zhong L, Liu X, Li Z, Zhang X, Wang Y and Peng W (2022) Recurrent Gallbladder Carcinoma With pMMR/MSS Achieved a Complete Response Following Camrelizumab Combined With Apatinib: A Case Report. Front. Oncol. 11:783158. doi: 10.3389/fonc.2021.783158

INTRODUCTION

Gallbladder carcinoma (GBC) is one of the most common primary malignancies of the biliary tract. Treatment protocols for advanced GBC are limited, and the prognosis is extremely poor, with a median overall survival of around 4–7 months (1). At present, combined chemotherapy is the main treatment for patients with advanced GBC; however, this therapy is highly toxic and provides patients limited survival benefit. Moreover, pembrolizumab was approved for advanced GBC patients with deficient mismatch repair (dMMR) or microsatellite instability-high (MSI-H). However, dMMR/MSI-high cancer is extremely rare. More effective and safe treatments are urgently needed for recurrent GBC, especially those with proficient mismatch repair (pMMR)/microsatellite stable (MSS) status.

Immunotherapy such as immune checkpoint inhibitors (ICIs) had become prospective therapeutic schemes in a variety of cancers. Several clinical trials were also conveyed in biliary

tract cancers (BTC), including the KEYNOTE-028 trial and KEYNOTE-158 trial. However, the objective response rate (ORR) of ICI monotherapy are only about 6%–13% in BTC (2). Therefore, a new scheme of treatment combination is needed to overcome ICI resistance. Camrelizumab, a high-affinity, humanized, IgG4-κ PD-1 monoclonal antibody, was widely applied for cancer therapy. Apatinib, a selective vascular endothelial growth factor receptor (VEGFR)-2 inhibitor, could modulate tumor microenvironment (TME) *via* relieved hypoxia, accelerated tumoral infiltration of CD8+ T cells, and decreased recruitment of tumor-associated macrophages (3). For advanced HCC, camrelizumab and apatinib combination therapy acquired a 34.3% ORR as the first-line and 22.5% as the second-line therapy (4). Moreover, several trials for osteosarcoma, gastric cancer, and advanced triple-negative breast cancer have shown that camrelizumab combined with apatinib was effective and tolerable (5–7). However, data of clinical trials of camrelizumab plus apatinib in GBC patients are insufficient.

Here, we report a recurrent metastatic GBC patient with pMMR/MSS who has obtained complete response to camrelizumab combined with apatinib treatment.

Case Presentation

The patient was a 60-year-old male with a medical history of hypertension and hepatitis B cirrhosis. He received regular anti-hypertension and antiviral treatment. In May 17, 2020, abdominal computed tomography (CT) revealed a gallbladder mass at the fundus (2.7 × 2.2 cm in size) at an annual medical examination. Enhanced scan showed that the mass was markedly enhanced. Enlarged lymph nodes were not found in the abdomen. He showed no obvious symptoms of discomfort, and physical examination was normal. Then, he received open cholecystectomy and regional lymphadenectomy in May 27, 2020. Surgeons found that the tumor directly invaded the liver. Therefore, hepatectomy with partial resection of segments 4 and 8 was performed. Postoperative pathology indicated a pT3N0M0 adenocarcinoma with poor differentiation, without lymph node metastasis and with a negative surgical margin. The abundance of ERBB2 mutation was 26.94%, which suggested the possible therapeutic potential of trastuzumab. Then, he was treated with 6 adjuvant treatments from July 18, 2020, to October 18, 2020. Gemcitabine (1,000 mg/m^2, d1, d8), albumin-bound paclitaxel (125 mg/m^2, d1, d8), and trastuzumab (6 mg/kg, d1) were administered every 3 weeks.

In November 6, 2020, abdominal magnetic resonance imaging (MRI) indicated multiple lesions in the right lobe of the liver, the largest measuring 1.1 cm × 1.1 cm adjacent to the surgical zone (**Figure 1A**). Moreover, the carbohydrate antigen 19-9 (CA-199) level was elevated at 29.03 U/ml (normal levels, <25 U/ml). This patient refused chemotherapy. Additionally, he received next-generation sequencing (NGS) analysis of tissue sample. NGS was performed on an Illumina HiSeq sequencer (Illumina, San Diego, CA) with a median unique exon coverage depth of 800× in a College of American Pathologists (CAP) and Clinical Laboratory Improvement Amendments (CLIA) certified laboratory (3D Medicine Inc., Shanghai, China). NGS results are presented in **Table 1**. The patient had tumor mutation burden (TMB) of 7.26 mutants/Mb, with pMMR/MSS status.

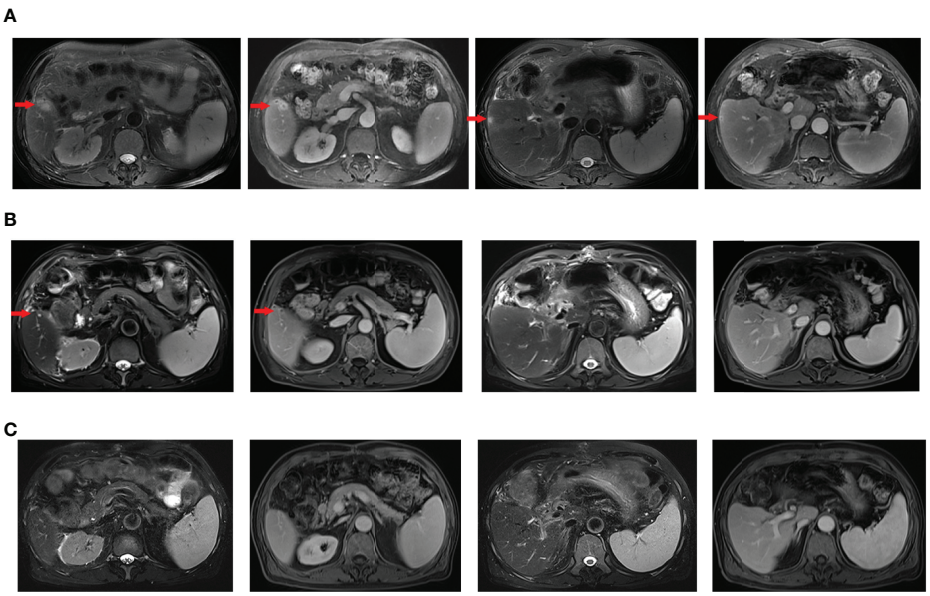

FIGURE 1 | Enhanced abdominal magnetic renounce imaging (MRI) of the reported case. **(A)** T2-weighted and arterial phase images of liver metastasis before camrelizumab combined with apatinib (November 6, 2020). The red arrows direct to the recurrent lesions in the liver. **(B)** MRI showed a partial response in liver metastasis from T2-weighted and arterial phase images after 2 cycles of combination therapy (December 22, 2020). The mass (arrow) adjacent to the surgical zone decreased to 0.6 cm in the maximum diameter (1.1 cm before treatment). The lesion under the liver capsule of S5 disappeared. **(C)** MRI showed that lesions in the liver completely disappeared after 4 cycles of combination therapy (February 1, 2021).

TABLE 1 | The results of next-generation sequencing (NGS) analysis.

Cohort	Value
Microsatellite	Microsatellite stable
MLH1, MSH2, MSH6, PMS2	No variants detected
Tumor mutation burden	7.26 Mutants/Mb
PD-L1 expression	Positive, 10% (tumor proportion score[a]), 20% (immune proportion score[b])
EBV	Negative
HLA Class I	Partial homozygous
Gene	Mutation (abundance/copy number)
ERBB2	p.V777L Exon 20 (26.94%)
AR	Increase in copy number (6)
TERT	c.-124C>T (7.42%)
ERBB3	p.G284R Exon 7 (11.72%)
KMT2C	p.I3493Pfs*13 Exon 43 (6.31%)
BTK	Increase in copy number (6)
TP53	p.R306*Exon 8 (11.21%), p.C135Ffs*15 Exon 5 (4.62%)

[a]*Tumor proportion score (TPS) was defined as the percentage of tumor cells showing a membranous PD-L1 expression with any intensity over all tumor cells.*
[b]*Immune proportion score (IPS) was defined as the percentage of PD-L1-positive immune cells of any intensity over all tumor-associated immune cells.*

Immunohistochemistry (IHC) results showed that programmed death ligand-1 (PD-L1) expression was 10% (tumor proportion score, TPS) and 20% (immune proportion score, IPS; **Figure 2**). The profile of genetic alterations included ERBB2, AR, TERT, ERBB3, KMT2C, BTK, and TP53. Consequently, and after obtaining the consent from the patient, camrelizumab combined with apatinib was initiated from November 16, 2020. He was administered 200 mg camrelizumab intravenously over 30 min every 3 weeks. The patient received apatinib orally at 500 mg per day. One month later, he developed grade 3 hypertension, which was attributed to apatinib. Then, the dose of apatinib was decreased to 250 mg per day. In the following treatment, no serious adverse event was observed except for grade 2 leukopenia and grade 2 thrombocytopenia, which may be attributed to both drugs and cirrhosis with splenomegaly.

On December 22, 2020, MRI showed exceptional shrinkage of the tumor and the lesion under the liver capsule of segment 5 (S5) disappeared, with a partial response after two cycles of treatment (**Figure 1B**). Furthermore, lesions in the liver completely disappeared (**Figure 1C**) and CA-199 was reduced to normal levels (22.93 U/ml) after four cycles of treatment. The therapeutic effect was determined to be a complete response, as assessed by the Response Evaluation Criteria in Solid Tumors RECIST Version 1.1. At the last follow-up (September 24, 2021), the patient was in good health and MRIs confirmed a sustained response. Since initiating camrelizumab and apatinib, he has obtained a progression-free survival (PFS) of 10 months. The patient is still on treatment with camrelizumab (200 mg, Q3 weeks) plus apatinib (250 mg QD) as of the submission date of this article. **Figure 3** outlines the patient's history.

DISCUSSION

There are limited treatment options for patients with recurrent GBC. Herein, we report a case in which camrelizumab combined with apatinib is effective and safe in a recurrent GBC patient with pMMR/MSS status. This is the first report demonstrating that recurrent GBC with pMMR/MSS has achieved a complete response following PD-1 inhibitor plus anti-angiogenic therapy.

Several studies have demonstrated that ICI and anti-angiogenic agent combination therapy has synergistic antitumor activity in solid tumors (8–10). The vascular endothelial growth factor (VEGF) has pleiotropic immunosuppressive effects including impairment of dendritic cell function, as well as mobilization of immunosuppressive cells such as myeloid-derived suppressor cells, regulatory T cells, and tumor associated macrophages (11). Currently, most trials combining anti-VEGF therapy with immunotherapy for GBC are in the recruitment period. In addition, few trials have reported detailed outcome. The initial result of combining camrelizumab with apatinib in 21 advanced BTC patients has shown that no patient achieved complete response, 4 patients obtained partial response, and 11 patients had stable disease with manageable toxicity (12). The synergistic effect of anti-angiogenic agents with immunotherapy may be largely attributed to the immunomodulatory function of anti-angiogenic agents on TME rather than their direct antitumor activity (13, 14),

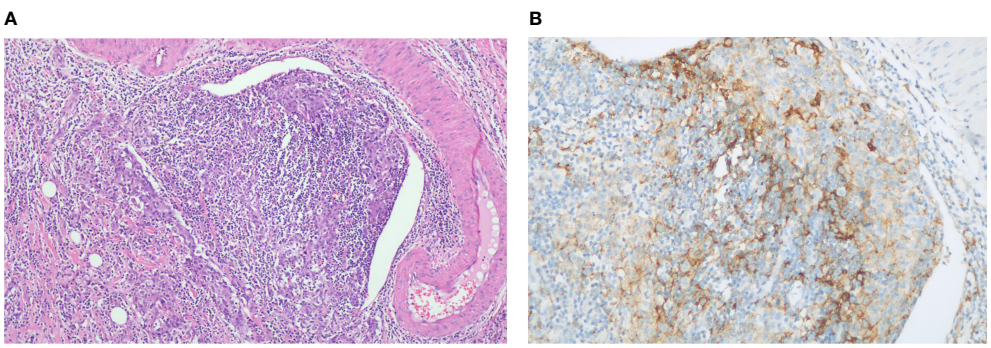

FIGURE 2 | Histopathology of gallbladder carcinoma. **(A)** H&E stain, original magnification ×100. **(B)** PD-L1 immunohistochemistry (antibody Ventana SP263), original magnification ×200.

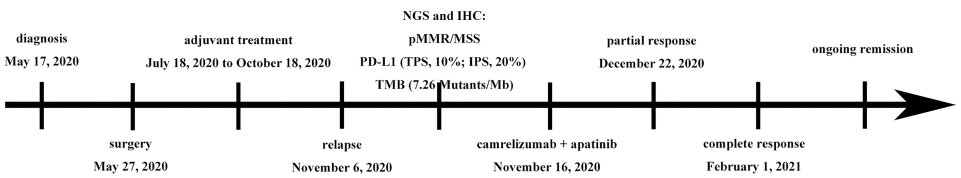

FIGURE 3 | Timeline of the clinical course in this patient.

as it was found that a low-dose anti-angiogenic agent was superior to higher doses in inhibiting tumor growth in animal models when combined with immunotherapy (3). In our case, the patient with reduced dose of apatinib (250 mg, QD) was effective. Hence, future clinical trials were needed to validate the optimal dosage of apatinib considering side effects and clinical response.

Recently, the U.S. Food and Drug Administration granted approval to pembrolizumab for BTC with dMMR/MSI-high. However, dMMR/MSI-high cancer is extremely rare, seen in only 1% to 3% of patients with BTC (15, 16), suggesting the necessity of identifying better predictive biomarkers for immunotherapy. Several studies have shown that PD-L1 expression is associated with the efficacy of PD-1 blockade (17, 18). Currently, a positive rate of PD-L1 expression of between 9% and 11.6% was reported in BTC patients receiving ICIs (19, 20). Kim et al. indicated that the PD-L1 expression rate of tumor cells (≥1%) is correlated with better ORR and prolonged PFS in a study focusing on nivolumab treatment for refractory BTC (21). In the KEYNOTE-158 trial, the patients with PD-L1-expressing BTC had an ORR 6.6%, and the ORR was 2.9% in patients with PD-L1 non-expressing tumors (2). PD-L1-expressing tumors were defined as a combined positive score of ≥1, which was calculated as the number of PD-L1–positive cells (tumor cells, lymphocytes, macrophages) divided by the total number of tumor cells and multiplied by 100. TMB may be the next predictor for PD-1 inhibitor therapy (22). It has been demonstrated that cancers with a high TMB express higher numbers of neoantigens, which can be identified by the immune system in response to ICI treatment (23–25). In our case, the patient with pMMR/MSS status had moderate expression of PD-L1 (TPS, 10%; IPS, 20%) and TMB (7.26 mutants/Mb). Camrelizumab combined with apatinib induced successful results in the recurrent GBC patient with pMMR/MSS. Therefore, it may be valuable to assess PD-L1 expression and TMB for the GBC patients, especially those with pMMR/MSS status, in order to direct the adjuvant treatment.

We reported that a recurrent GBC patient with pMMR/MSS achieved durable complete response from the combined treatment of camrelizumab and apatinib. PD-L1 expression and TMB may be the predictive markers for GBC patients who would profit from anti-PD-1 therapy. Future studies on combination therapy will reveal the true potential of combination ICIs and anti-angiogenic agents in GBC.

DATA AVAILABILITY STATEMENT

The datasets presented in this study can be found in online repositories. The names of the repository/repositories and accession number(s) can be found in the following: NCBI SRA BioProject, accession no: PRJNA786280.

ETHICS STATEMENT

Written informed consent was obtained from the individual(s) for the publication of any potentially identifiable images or data included in this article.

AUTHOR CONTRIBUTIONS

LZ: manuscript writing. XL and ZL: imaging analysis. XZ and YW: data collection. WP: manuscript revision. All authors contributed to the article and approved the submitted version.

FUNDING

This work was supported by the Health Science and Technology Project of Jiangxi Province (202140765).

REFERENCES

1. Cheng H, Zhou D, Wang S, Ding J, Ma F. The Immunological Characteristics of Gallbladder Carcinoma and Advances in Immunotherapy Practices. *Biosci Trends* (2021) 15(1):9–15. doi: 10.5582/bst.2020.01039
2. Piha-Paul SA, Oh DY, Ueno M, Malka D, Chung HC, Nagrial A, et al. Efficacy and Safety of Pembrolizumab for the Treatment of Advanced Biliary Cancer: Results From the KEYNOTE-158 and KEYNOTE-028 Studies. *Int J Cancer* (2020) 147(8):2190–8. doi: 10.1002/ijc.33013
3. Zhao S, Ren S, Jiang T, Zhu B, Li X, Zhao C, et al. Low-Dose Apatinib Optimizes Tumor Microenvironment and Potentiates Antitumor Effect of PD-1/PD-L1 Blockade in Lung Cancer. *Cancer Immunol Res* (2019) 7(4):630–43. doi: 10.1158/2326-6066.CIR-17-0640
4. Xu J, Shen J, Gu S, Zhang Y, Wu L, Wu J, et al. Camrelizumab in Combination With Apatinib in Patients With Advanced Hepatocellular Carcinoma (RESCUE): A Nonrandomized, Open-Label, Phase II Trial. *Clin Cancer Res: An Off J Am Assoc Cancer Res* (2021) 27(4):1003–11. doi: 10.1158/1078-0432.ccr-20-2571

5. Xie L, Xu J, Sun X, Guo W, Gu J, Liu K, et al. Apatinib Plus Camrelizumab (Anti-PD1 Therapy, SHR-1210) for Advanced Osteosarcoma (APFAO) Progressing After Chemotherapy: A Single-Arm, Open-Label, Phase 2 Trial. *J Immunother Cancer* (2020) 8(1):e000798. doi: 10.1136/jitc-2020-000798
6. Liang L, Wen Y, Hu R, Wang L, Xia Y, Hu C, et al. Safety and Efficacy of PD-1 Blockade-Activated Multiple Antigen-Specific Cellular Therapy Alone or in Combination With Apatinib in Patients With Advanced Solid Tumors: A Pooled Analysis of Two Prospective Trials. *Cancer Immunol Immunother: CII* (2019) 68(9):1467–77. doi: 10.1007/s00262-019-02375-z
7. Liu J, Liu Q, Li Y, Li Q, Su F, Yao H, et al. Efficacy and Safety of Camrelizumab Combined With Apatinib in Advanced Triple-Negative Breast Cancer: An Open-Label Phase II Trial. *J Immunother Cancer* (2020) 8(1):e000696. doi: 10.1136/jitc-2020-000696
8. Fan Y, Zhao J, Wang Q, Huang D, Li X, Chen J, et al. Camrelizumab Plus Apatinib in Extensive-Stage SCLC (PASSION): A Multicenter, Two-Stage, Phase 2 Trial. *J Thorac Oncol: Off Publ Int Assoc Study Lung Cancer* (2021) 16 (2):299–309. doi: 10.1016/j.jtho.2020.10.002
9. Nayak L, Molinaro AM, Peters K, Clarke JL, Jordan JT, de Groot J, et al. Randomized Phase II and Biomarker Study of Pembrolizumab Plus Bevacizumab Versus Pembrolizumab Alone for Patients With Recurrent Glioblastoma. *Clin Cancer Res: An Off J Am Assoc Cancer Res* (2021) 27 (4):1048–57. doi: 10.1158/1078-0432.CCR-20-2500
10. Raghav K, Liu S, Overman MJ, Willett AF, Knafl M, Fu SC, et al. Efficacy, Safety and Biomarker Analysis of Combined PD-L1 (Atezolizumab) and VEGF (Bevacizumab) Blockade in Advanced Malignant Peritoneal Mesothelioma. *Cancer Discov* (2021) 7(14):2230. doi: 10.1158/2159-8290.CD-21-0331
11. Yang J, Yan J, Liu B. Targeting VEGF/VEGFR to Modulate Antitumor Immunity. *Front Immunol* (2018) 9:978. doi: 10.3389/fimmu.2018.00978
12. Wang D, Yang X, Long J, Lin J, Mao J, Xie F, et al. The Efficacy and Safety of Apatinib Plus Camrelizumab in Patients With Previously Treated Advanced Biliary Tract Cancer: A Prospective Clinical Study. *Front Oncol* (2021) 11:646979. doi: 10.3389/fonc.2021.646979
13. Huang Y, Goel S, Duda D, Fukumura D, Jain R. Vascular Normalization as an Emerging Strategy to Enhance Cancer Immunotherapy. *Cancer Res* (2013) 73 (10):2943–8. doi: 10.1158/0008-5472.can-12-4354
14. Huang Y, Yuan J, Righi E, Kamoun W, Ancukiewicz M, Nezivar J, et al. Vascular Normalizing Doses of Antiangiogenic Treatment Reprogram the Immunosuppressive Tumor Microenvironment and Enhance Immunotherapy. *Proc Natl Acad Sci USA* (2012) 109(43):17561–6. doi: 10.1073/pnas.1215397109
15. Rashid A, Ueki T, Gao Y, Houlihan P, Wallace C, Wang B, et al. K-Ras Mutation, P53 Overexpression, and Microsatellite Instability in Biliary Tract Cancers: A Population-Based Study in China. *Clin Cancer Res: An Off J Am Assoc Cancer Res* (2002) 8(10):3156–63. doi: 10.1117/12.2051463
16. Winkelmann R, Schneider M, Hartmann S, Schnitzbauer AA, Zeuzem S, Peveling-Oberhag J, et al. Microsatellite Instability Occurs Rarely in Patients With Cholangiocarcinoma: A Retrospective Study From a German Tertiary Care Hospital. *Int J Mol Sci* (2018) 19(5):1–10. doi: 10.3390/ijms19051421
17. Wang D, Lin J, Yang X, Long J, Bai Y, Yang X, et al. Combination Regimens With PD-1/PD-L1 Immune Checkpoint Inhibitors for Gastrointestinal Malignancies. *J Hematol Oncol* (2019) 12(1):42. doi: 10.1186/s13045-019-0730-9
18. Blair A, Murphy A. Immunotherapy as a Treatment for Biliary Tract Cancers: A Review of Approaches With an Eye to the Future. *Curr Problems Cancer* (2018) 42(1):49–58. doi: 10.1016/j.currproblcancer.2017.10.004
19. Fontugne J, Augustin J, Pujals A, Compagnon P, Rousseau B, Luciani A, et al. PD-L1 Expression in Perihilar and Intrahepatic Cholangiocarcinoma. *Oncotarget* (2017) 8(15):24644–51. doi: 10.18632/oncotarget.15602
20. Walter D, Herrmann E, Schnitzbauer A, Zeuzem S, Hansmann M, Peveling-Oberhag J, et al. PD-L1 Expression in Extrahepatic Cholangiocarcinoma. *Histopathology* (2017) 71(3):383–92. doi: 10.1111/his.13238
21. Kim R, Chung V, Alese O, El-Rayes B, Li D, Al-Toubah T, et al. A Phase 2 Multi-Institutional Study of Nivolumab for Patients With Advanced Refractory Biliary Tract Cancer. *JAMA Oncol* (2020) 6(6):888–94. doi: 10.1001/jamaoncol.2020.0930
22. Sha D, Jin Z, Budczies J, Kluck K, Stenzinger A, Sinicrope FA. Tumor Mutational Burden as a Predictive Biomarker in Solid Tumors. *Cancer Discov* (2020) 10(12):1808–25. doi: 10.1158/2159-8290.CD-20-0522
23. Steuer C, Ramalingam S. Tumor Mutation Burden: Leading Immunotherapy to the Era of Precision Medicine? *J Clin Oncol: Off J Am Soc Clin Oncol* (2018) 36(7):631–2. doi: 10.1200/jco.2017.76.8770
24. Chan T, Yarchoan M, Jaffee E, Swanton C, Quezada S, Stenzinger A, et al. Development of Tumor Mutation Burden as an Immunotherapy Biomarker: Utility for the Oncology Clinic. *Ann Oncol: Off J Eur Soc Med Oncol* (2019) 30 (1):44–56. doi: 10.1093/annonc/mdy495
25. Li X, Song W, Shao C, Shi Y, Han W. Emerging Predictors of the Response to the Blockade of Immune Checkpoints in Cancer Therapy. *Cell Mol Immunol* (2019) 16(1):28–39. doi: 10.1038/s41423-018-0086-z

Conflict of Interest: The authors declare that the research was conducted in the absence of any commercial or financial relationships that could be construed as a potential conflict of interest.

frontiers in Pharmacology

ORIGINAL RESEARCH
published: 02 March 2022
doi: 10.3389/fphar.2022.863856

Immunotherapeutic Value of MAP1LC3C and Its Candidate FDA-Approved Drugs Identified by Pan-Cancer Analysis, Virtual Screening and Sensitivity Analysis

Xudong Zhang[1], *Kunhang Li*[1], *Shiyu Zhong*[1], *Shengyu Liu*[1], *Tao Liu*[1], *Lishuai Li*[1], *Shuo Han*[1], *Qingqing Zhai*[2], *Nan Bao*[3], *Xin Shi*[4,5]* and *Yijun Bao*[1]*

[1]Department of Neurosurgery, The Fourth Hospital of China Medical University, Shenyang, China, [2]School of Management, Shanghai University, Shanghai, China, [3]College of Medicine and Biological Information Engineering, Northeastern University, Shenyang, China, [4]School of Maths and Information Science, Shangdong Technology and Business University, Yantai, China, [5]Business School, All Saints Campus, Manchester Metropolitan University, Manchester, United Kingdom

OPEN ACCESS

Edited by:
Zhi Li,
The First Affiliated Hospital of China Medical University, China

Reviewed by:
Hongli Shan,
Harbin Medical University, China
Daling Ding,
The First Affiliated Hospital of Zhengzhou, China

***Correspondence:**
Yijun Bao
yjbao@cmu.edu.cn
Xin Shi
x.shi@mmu.ac.uk

Specialty section:
This article was submitted to Pharmacology of Anti-Cancer Drugs, a section of the journal Frontiers in Pharmacology

Received: *27 January 2022*
Accepted: *14 February 2022*
Published: *02 March 2022*

Citation:
Zhang X, Li K, Zhong S, Liu S, Liu T, Li L, Han S, Zhai Q, Bao N, Shi X and Bao Y (2022) Immunotherapeutic Value of MAP1LC3C and Its Candidate FDA-Approved Drugs Identified by Pan-Cancer Analysis, Virtual Screening and Sensitivity Analysis. Front. Pharmacol. 13:863856. doi: 10.3389/fphar.2022.863856

Background: The autophagy pathway within the tumour microenvironment can be regulated to inhibit or promote tumour development. In the fight against tumour growth, immunotherapy induces an anti-tumour immune response, whereas autophagy modulates this immune response. A key protein in the autophagy pathway, microtubule-associated protein 1 light chain 3 (MAP1LC3), has recently become a hotspot for tumour research. As a relatively novel member, the function of MAP1LC3C in tumours still need to be investigated. Therefore, the goal of this study was to look into the possible link between MAP1LC3C and immunotherapy for 33 kinds of human malignancies by using pan-cancer analysis.

Methods: High-throughput sequencing data from The Cancer Genome Atlas, Genotype-Tissue Expression Project and Cancer Cell Line Encyclopedia databases, combined with clinical data, were used to analyze the expression of MAP1LC3C in 33 types of cancer, as well as patient prognosis and neoplasm staging. Activity scores were calculated using ssGSEA to assess the MAP1LC3C activity in pan-cancer. Associations between MAP1LC3C and the tumour microenvironment, including immune cell infiltration and immunomodulators, were analyzed. Moreover, tumour tissue ImmuneScores and StromalScores were analyzed using the ESTIMATE algorithm. Additionally, associations between MAP1LC3C and tumour mutational burden/microsatellite instability, were investigated. Finally, based on the expression and structure of MAP1LC3C, the United States Food and Drug Administration (FDA)-approved drugs, were screened by virtual screening, molecular docking and NCI-60 drug sensitivity analysis.

Results: Our study found that MAP1LC3C was differentially expressed in tumour and normal tissues in 23 of 33 human cancer types, among which MAP1LC3C had prognostic effects in 12 cancer types, and MAP1LC3C expression was significantly correlated with tumour stage in four cancer types. In addition, MAP1LC3C activity in 14 cancer types was

consistent with changes in transcription levels. Moreover, MAP1LC3C strongly correlated with immune infiltration, immune modulators and immune markers. Finally, a number of FDA-approved drugs were identified via virtual screening and drug sensitivity analysis.

Conclusion: Our study investigated the prognostic and immunotherapeutic value of MAP1LC3C in 33 types of cancer, and several FDA-approved drugs were identified to be highly related to MAP1LC3C and can be potential cancer therapeutic candidates.

Keywords: pan-cancer analysis, prognosis, immunotherapy, tumor microenvironment, molecualr docking

INTRODUCTION

Autophagy is a process that occurs in all eukaryotes, involving in the capture by an autophagosome and transport to the lysosomes for decomposition and recycling (Ohsumi, 2012; Morishita and Mizushima, 2019). Autophagy has long been considered as a non-selective process that meets the needs of cell synthesis and metabolism; however, recent studies have proved the existence of selective autophagy pathways, specifically targeting damaged organelles, pathogens and unfolded proteins (Le Guerroué et al., 2017). To better cope with stresses in the tumour microenvironment, the autophagy pathways in various cell types can be regulated to inhibit or promote tumour development (Xia et al., 2021).

The immune system plays an important role in preventing tumour occurrence, development and metastasis and in tumour treatment. Immune surveillance is a function of the immune system that helps to recognise, kill and remove tumour cells; however, tumour cells can evade tumour immunity through immunosuppressive responses (Zou, 2005). Moreover, immunotherapy fights against tumours by arousing the anti-tumour immune response in the immune system (Zou et al., 2016). Recent studies have shown that autophagy is involved in the various biological processes of immune cells (Clarke and Simon, 2019) and can modulate tumour growth by regulating the immune response (Yang et al., 2018).

A common key factor in both selective and non-selective autophagy pathways is the ubiquitin-like protein binding system, including the ATG5-ATG12 binding system and ATG8-lipidation system (Tooze and Yoshimori, 2010). Human cells contain at least six ATG8 family members, which can be divided into two subfamilies: MAP1LC3A (LC3A), LC3B, LC3C and GABARAP, GABARAPL1, GABARAPL2 (Slobodkin and Elazar, 2013). Microtubule-associated protein 1 light chain 3 (MAP1LC3), a ubiquitinated protein of the ATG8-lipidation system, is involved in various pathophysiological processes of the body. The role and mechanism of MAP1LC3 subfamily in a tumour is complex, making it a hotspot for tumour research. However, research on MAP1LC3C, a relatively new member, is still lacking. There are few articles referring to MAP1LC3C and no articles that deeply investigate the function of this gene in tumours. Therefore, a pan-cancer study of MAP1LC3C is necessary.

This study is the first to analyse the prognostic and immunotherapeutic value of MAP1LC3C in various cancer types. The expression and activity of MAP1LC3C and its correlation with patient prognosis and tumour stage in 33 human cancer types, combined with clinical information, were analysed using online databases such as TCGA, GTEx and CCLE. The effects of MAP1LC3C on the immune microenvironment, tumour mutational burden (TMB), microsatellite instability (MSI) and two immunotherapy biomarkers were studied using CIBERSORT and ESTIMATE algorithms. Finally, based on the expression and structure of MAP1LC3C, virtual screening and drug sensitivity analysis of the FDA-approved drug library were conducted to identify therapeutic drugs. Therefore, this study aims to elucidate the role of MAP1LC3C in the immune system and its impact on cancer prognosis and immunotherapy, as well as to provide some references for therapeutic agents.

METHODS

Data Collection

Transcriptome expression profiles, clinical data and mutation data of 33 cancer types in the TCGA database were downloaded through Xena (Goldman et al., 2020). Control gene data of six cancer types (ACC, LGG, LAML, OV, TGCT and UCS) were obtained from the GTEx database (Consortium, 2020). Sequencing data of cell lines were obtained from the CCLE database (Nusinow et al., 2020). As this study used open data, ethical approval was not required.

Identification of MAP1LC3C Differential Expression and Its Association With Clinical Characteristics

MAP1LC3C expression data were extracted from the TCGA and GTEx databases, and the gene expression levels between 33 cancer and normal samples were compared using R-package LIMMA (Ritchie et al., 2015). Additionally, the correlation between MAP1LC3C expression and tumour stage was explored. Combined with clinical information, the relationship between gene expression level and patient survival was calculated using univariate Cox regression. When the hazard ratio (HR) was greater than 1 (HR > 1), MAP1LC3C expression was considered as a risk factor. Kaplan–Meier (KM) analysis was performed to compare the overall survival (OS), disease-specific survival (DSS), disease-free interval (DFI) and progression-free interval (PFI) of patients with cancer, which was stratified by median MAP1LC3C

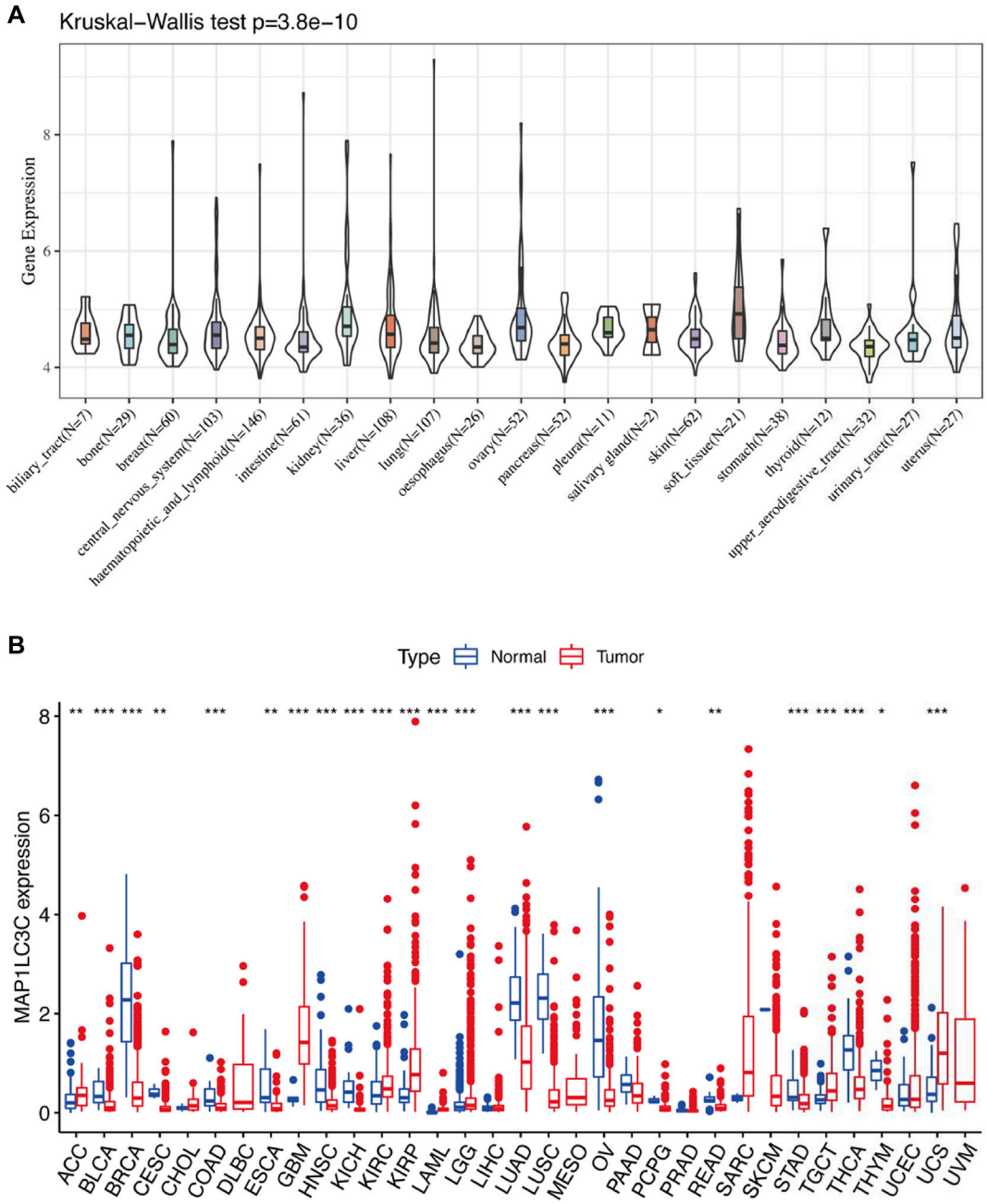

FIGURE 1 | Human pan-cancer analysis of MAP1LC3C expression level. **(A)** mRNA level of MAP1LC3C in the CCLE database. **(B)** mRNA level of MAP1LC3C in the TCGA and GTEx database (*p < 0.05; **p <0.01; ***p < 0.001).

expression. $p < 0.05$ was considered statistically significant for the analyses.

Study of MAP1LC3C Activity

To further study the activity of MAP1LC3C in pan-cancer, genes that are closely related to MAP1LC3C as relevant genes of MAP1LC3C through the co-expression method were found, and the MAP1LC3C activity score of each sample was obtained using R-package GSVA and ssGSEA method (Hänzelmann et al., 2013). The differences in MAP1LC3C activity between the normal and tumour groups were studied, and the scores of MAP1LC3C activity in 33 cancer types were obtained.

Correlation Analysis of MAP1LC3C Expression and Immune-Related Factors

The CIBERSORT algorithm was used to calculate the immune cell invasion level of each tumour sample (Newman et al., 2019). A total of 100 permutations were run using the LM22 signature. $p < 0.01$ and $|R| > 0.4$ indicated significant correlation. Immunoscores and

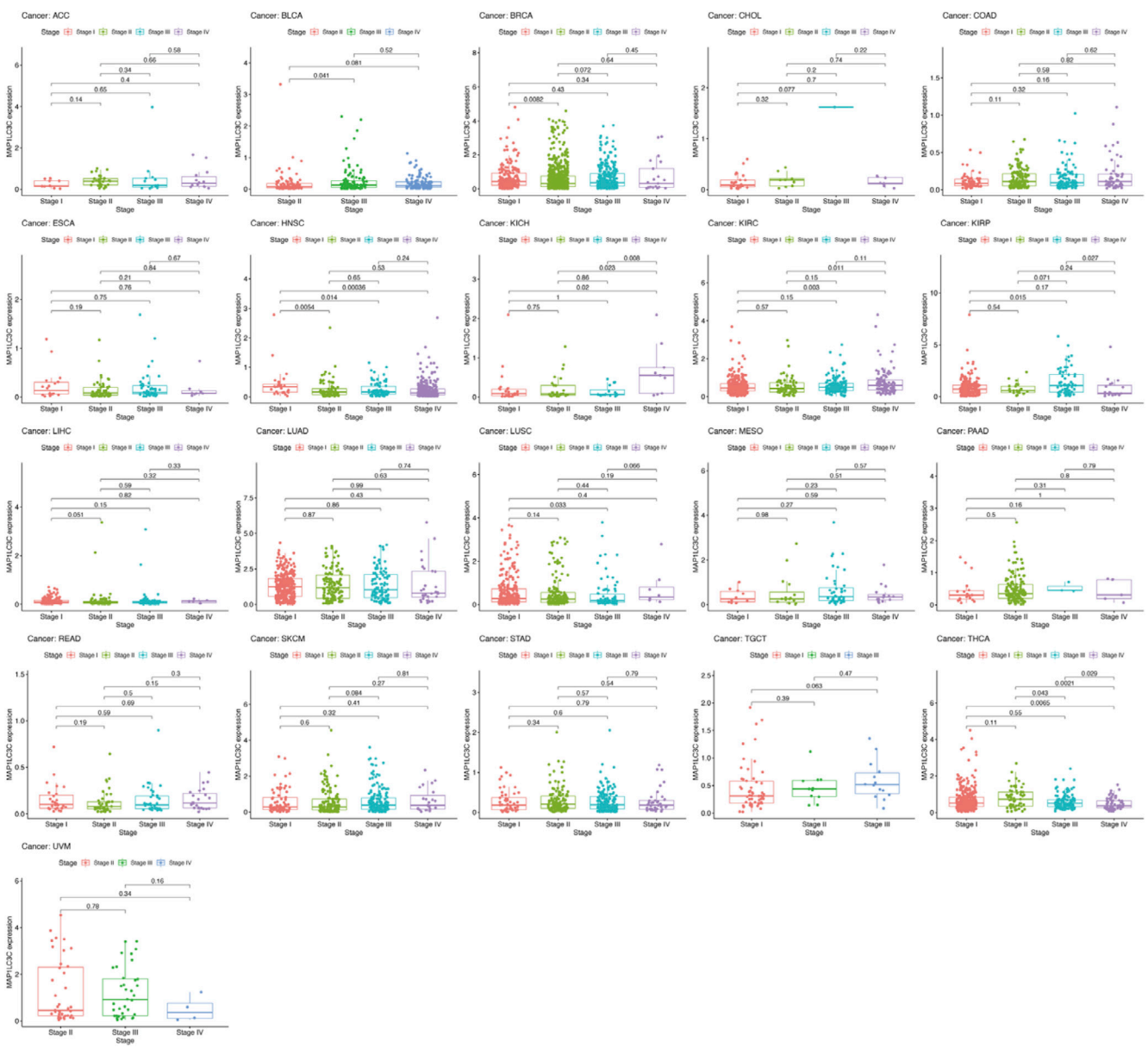

FIGURE 2 | Boxplot graph indicating the relationship between MAP1LC3C expression and pathological stage in 21 cancer types.

stromal scores were calculated for each sample using the ESTIMATE algorithm (Yoshihara et al., 2013). Additionally, the list of immune modulators (**Supplementary Table S1**), including immune inhibitors, stimulators and major histocompatibility complex (MHC) molecules, were downloaded from the TISIDB database (Ru et al., 2019).

VIRTUAL SCREENING AND MOLECULAR DOCKING

Structural information on 2858 FDA-approved and pharmacopeial drugs was downloaded from the TargetMol (Inc.A-Approved &, 2021). The spatial structure information of the MAP1LC3C protein (PDB 2NCN) was downloaded from the Protein Data Bank (PDB) database (Berman et al., 2000). The GHECOM algorithm was used to identify potential small molecule binding sites on the protein (Kawabata, 2010), and a docking pocket with volume 2,571 $Å^3$ was defined. UCSF DOCK 6.9 was used for virtual screening and molecular docking. Finally, PyMol was used to visualise the docked conformation, and Ligplus was used to analyse the interaction force (Wallace et al., 1995).

DRUG SENSITIVE ANALYSIS

The 23,808 identified RNA expression data and 23,255 analyzed drug data from the NCI-60 cell line were downloaded from the

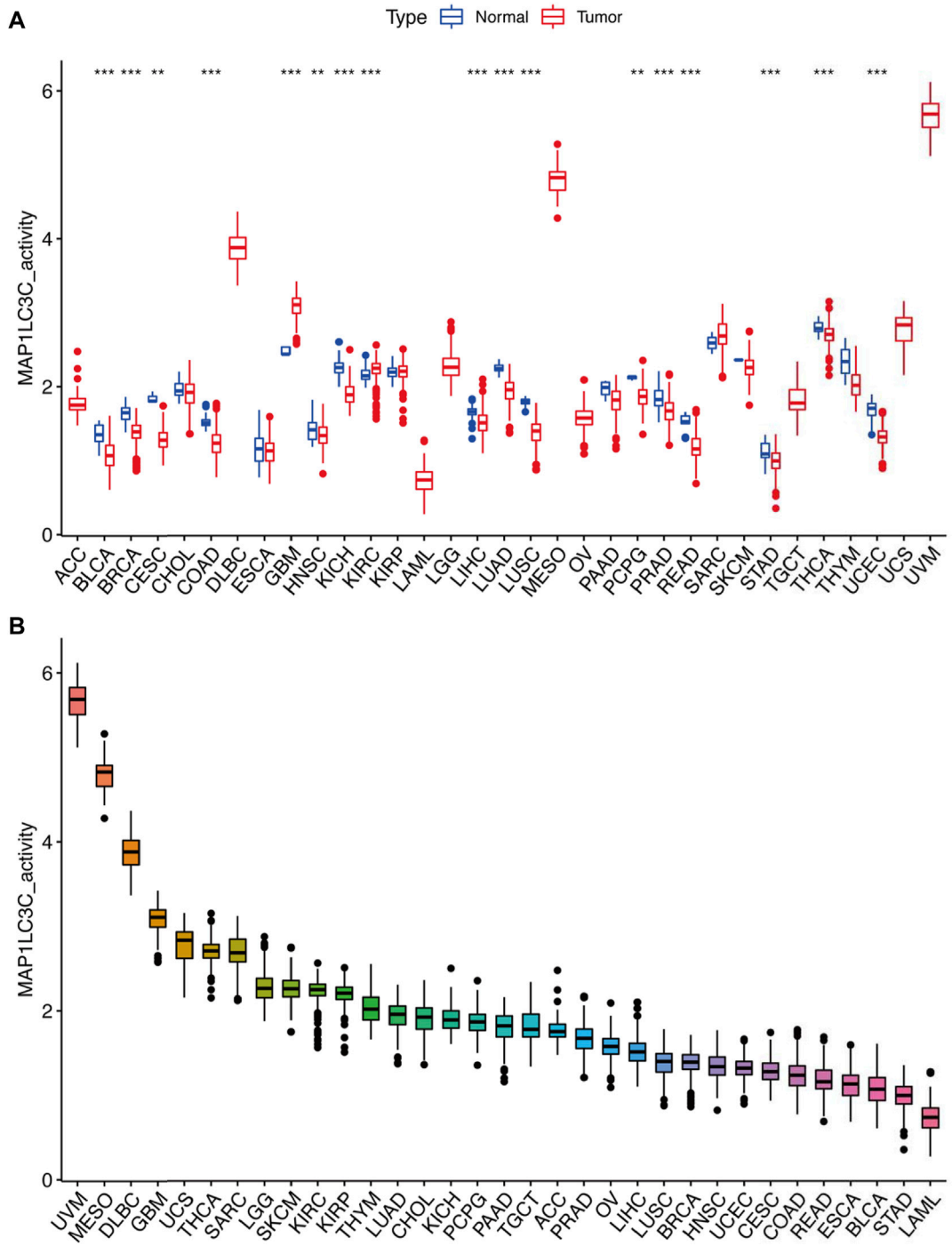

FIGURE 3 | Calculation and investigation of MAP1LC3C activity. **(A)** The activities of MAP1LC3C in normal and tumour tissues in 33 cancer types. **(B)** The average activity (from high to low) of MAP1LC3C (*$p < 0.05$; * *$p < 0.01$; * * *$p < 0.001$).

CellMiner database (Reinhold et al., 2012). To ensure the clinical practicality of the analysis results, FDA-approved drugs that had undergone clinical trial were selected to obtain a total of 792 drugs for the screening. MAP1LC3C expression was extracted and drug sensitivity (IC50) was calculated to obtain Pearson correlation coefficients between gene expression and different drugs, and the results were screened and visualized according to $p < 0.05$.

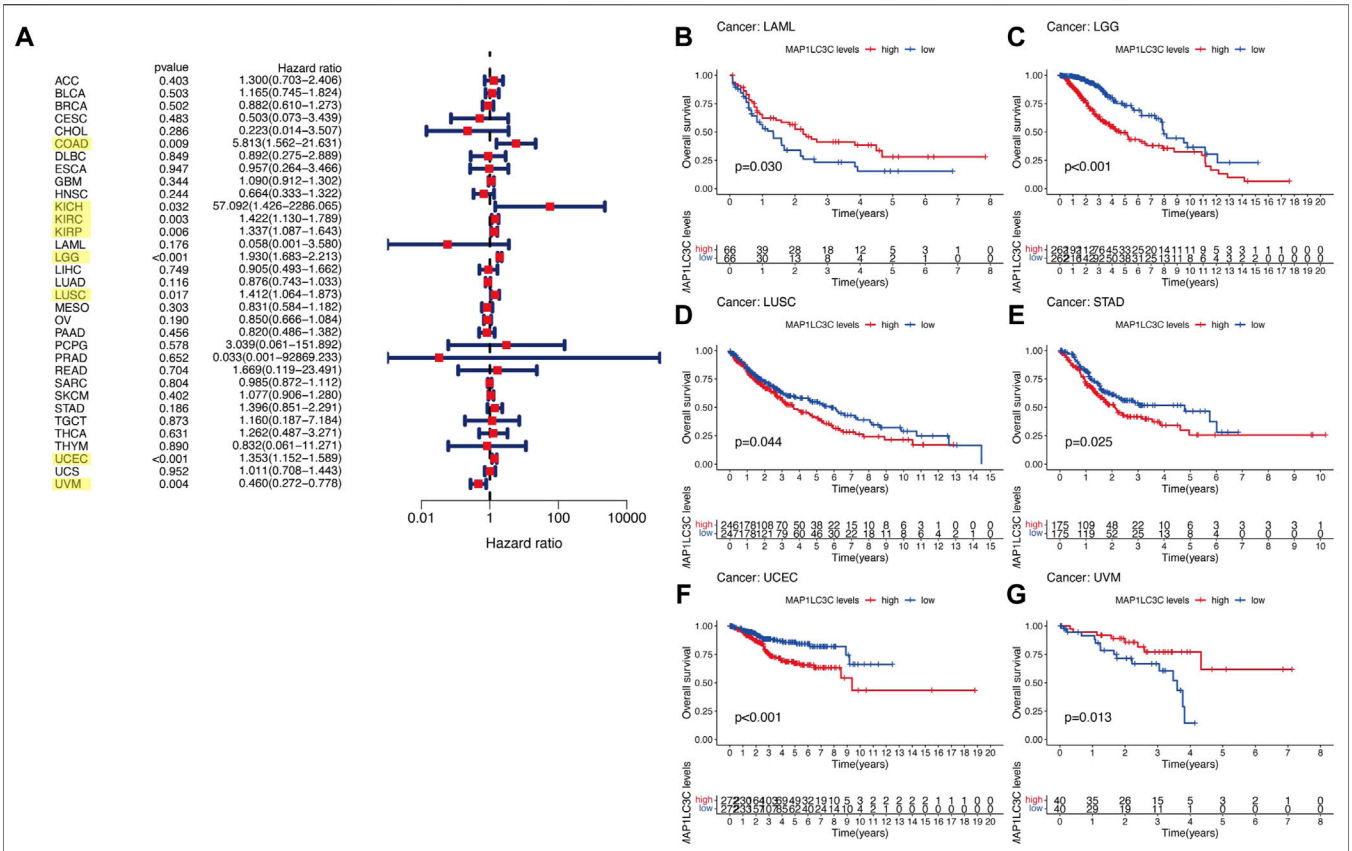

FIGURE 4 | Relationship between MAP1LC3C expression and patients' overall survival (OS) using **(A)** Forest map and **(B–G)** Kaplan-Meier analysis. The highlighted items mean that MAP1LC3C expression was significantly associated with the prognosis in these types of cancer ($p < 0.05$).

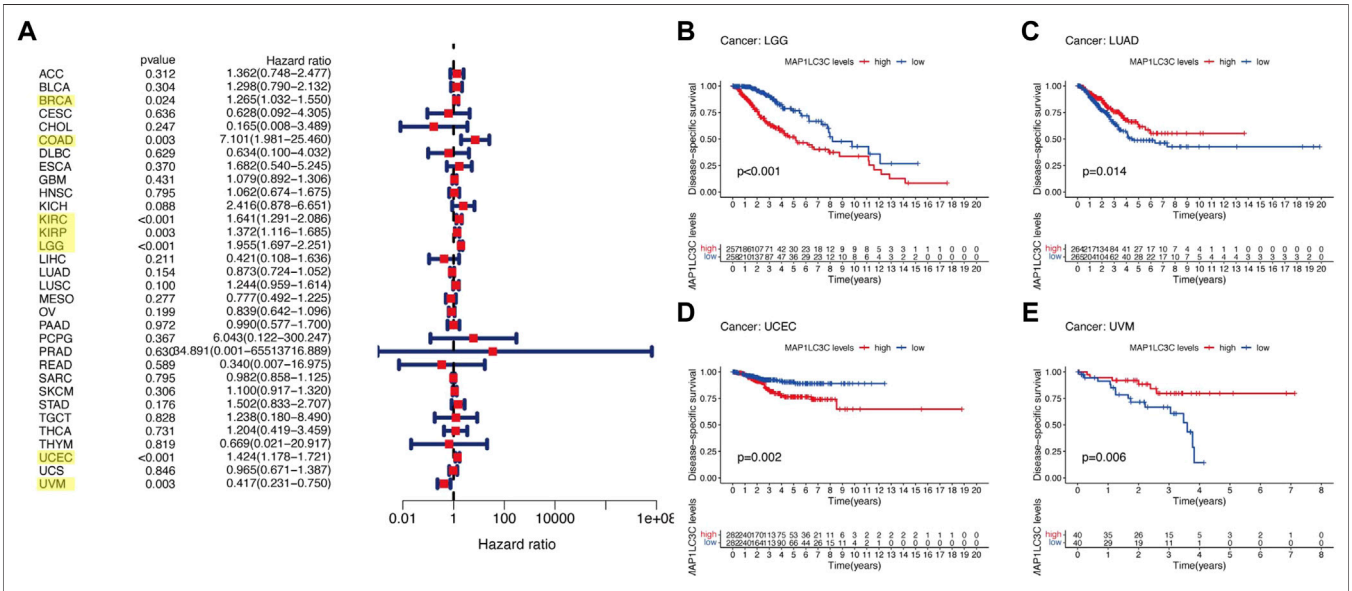

FIGURE 5 | Relationship between MAP1LC3C expression and patients' disease-specific survival (DSS) using **(A)** Forest map and **(B–E)** Kaplan-Meier analysis. The highlighted items mean that MAP1LC3C expression was significantly associated with the prognosis in these types of cancer ($p < 0.05$).

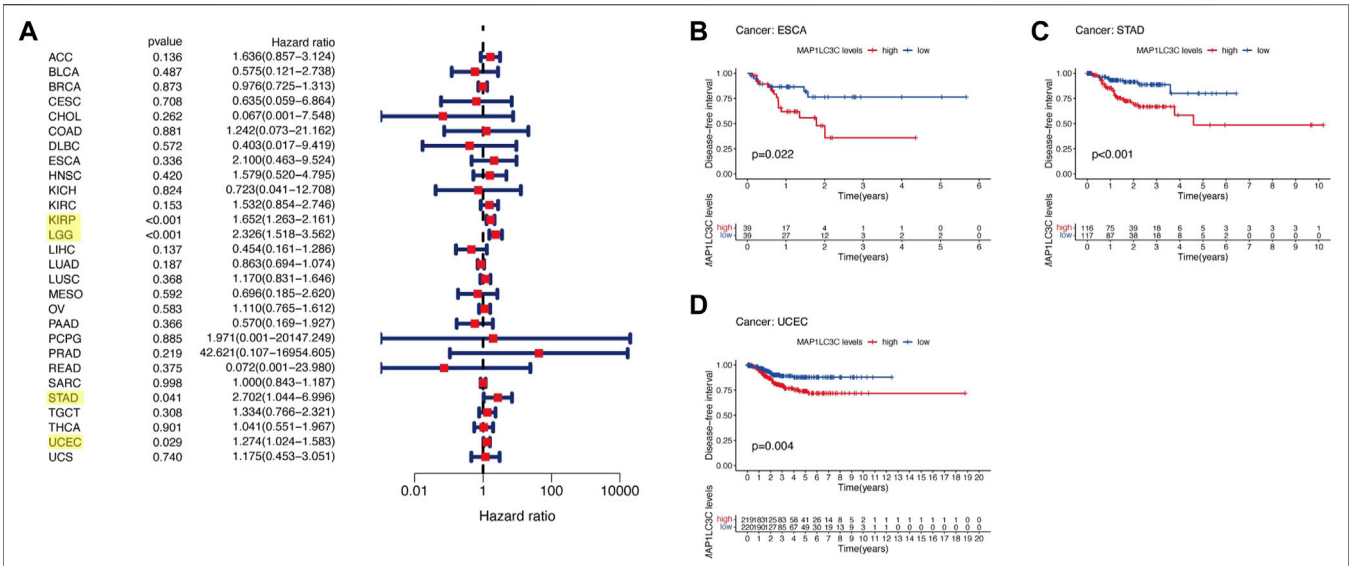

FIGURE 6 | Relationship between MAP1LC3C expression and patients' disease-free interval (DFI) using **(A)** Forest map and **(B–D)** Kaplan-Meier analysis. The highlighted items mean that MAP1LC3C expression was significantly associated with the prognosis in these types of cancer ($p < 0.05$).

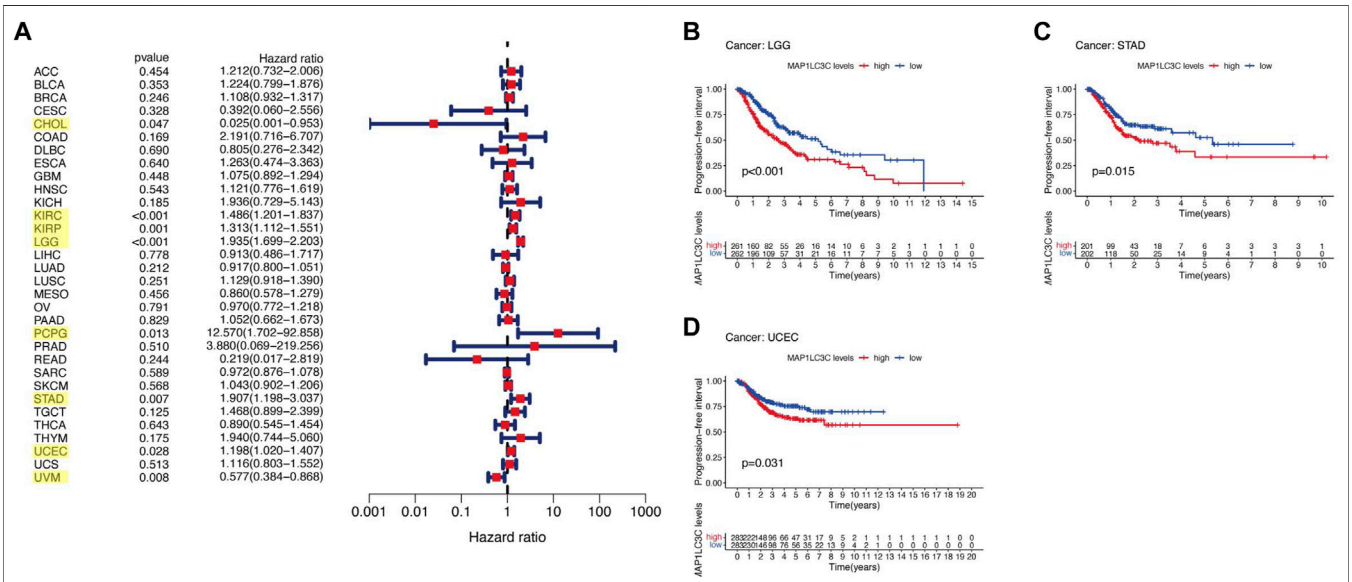

FIGURE 7 | Relationship between MAP1LC3C expression and patients' progression-free interval (PFI) using **(A)** Forest map and **(B–D)** Kaplan-Meier analysis. The highlighted items mean that MAP1LC3C expression was significantly associated with the prognosis in these types of cancer ($p < 0.05$).

RESULTS

Differential Expression of MAP1LC3C in 33 Cancer Types

Detailed information on the 33 types of cancer included in this study is shown in **Supplementary Table S2**. The gene expression profiles of various tumour cell lines downloaded from the CCLE database, and the MAP1LC3C expression levels of 21 tissues according to their tissue sources were analyzed. MAP1LC3C showed inconsistent expression levels in different cell lines (p = 3.8E-10, **Figure 1A**), but in soft tissue tumour cells showed the highest expression levels. Considering that several tumours in the TCGA database do not include normal sample data, normal sample data from the GTEx database were integrated with the tumour sample data from the TCGA database to analyse the expression differences of MAP1LC3C in 33 tumour types (**Figure 1B**). MAP1LC3C was significantly up-regulated in ACC, GBM, KIRC, KIRP, LAML, LGG, TGCT

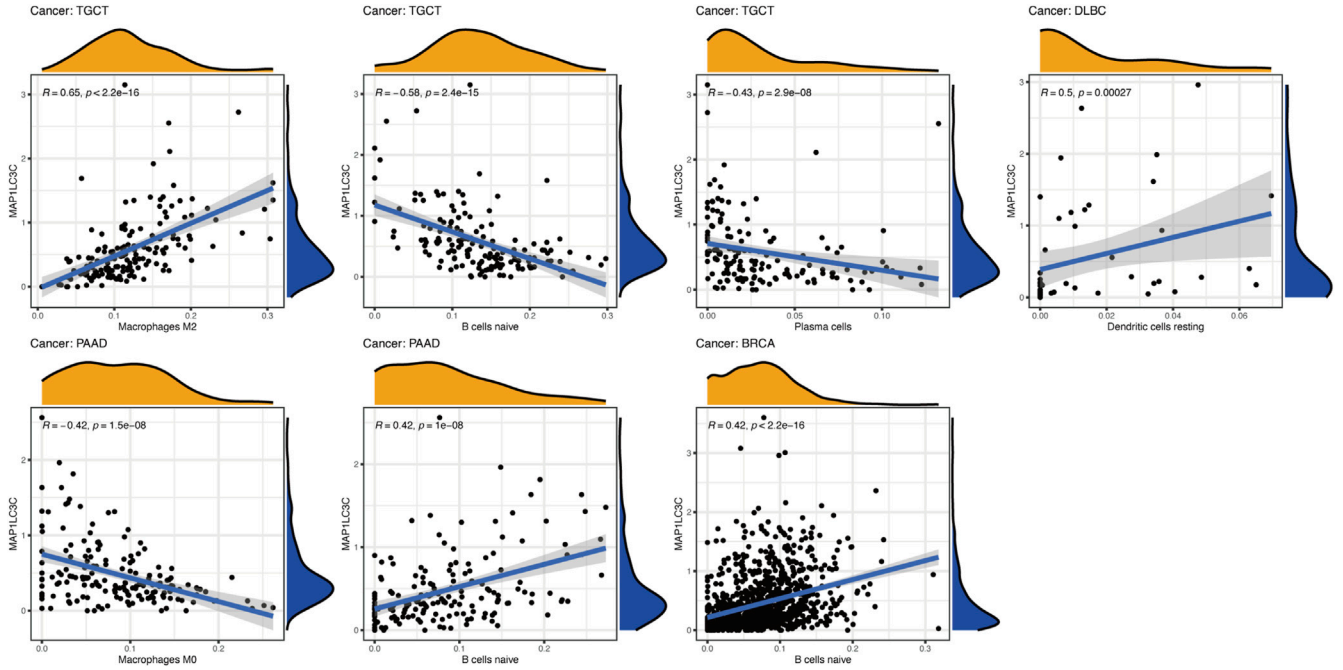

FIGURE 8 | Correlation analysis between MAP1LC3C expression and immune cell infiltration using CIBERSORT algorithm.

and UCS, but significantly down-regulated in BLCA, BRCA, CESC, COAD, ESCA, HNSC, KICH, LUAD, LUSC, OV, PCPG, READ, STAD, THCA and THYM. Meanwhile, MAP1LC3C expression was significantly correlated with the neoplasm staging of a few cancers, including HNSC, KICH, KIRC and THCA (**Figure 2**). As shown in **Figure 3**, TCGA data were used to analyse MAP1LC3C activity in 33 tumour types. The results showed that the transcription level was matched with MAP1LC3C activity. MAP1LC3C activity increased significantly in GBM, KIRC, BLCA, BRCA, CESC, COAD, HNSC, KICH, LIHC and LUAD tumour types, but decreased significantly in LUSC, PCPG, PRAD, READ, STAD, THCA and UCEC tumour types (**Figure 3A**). 4 tumour types including UVM, MESO, DLBC and GBM showed relatively high activity (**Figure 3B**).

PROGNOSTIC ROLE OF MAP1LC3C EXPRESSION

For the prognostic analysis, we selected clinical indicators, including overall survival (OS), disease-specific survival (DSS), disease-free interval (DFI) and progression-free interval (PFI). OS was defined as the time from the date of diagnosis to death, regardless of the cause. In OS analysis, Univariate Cox regression identified high MAP1LC3C expression as a risk factor for COAD, KICH, KIRC, KIRP, LGG, LUSC and UCEC, but as a protective factor for UVM (**Figure 4A**). KM analysis revealed that patients with high MAP1LC3C expression in LGG, LUSC, STAD and UCEC cancer types had lower OS rates than those with low MAP1LC3C expression. However, those with high MAP1LC3C expression in LAML and UVM had higher OS rates (**Figures 4B–G**). In DSS analysis, unlike OS, patients who died from causes other than the specified disease were not counted. Univariate Cox regression indicated high MAP1LC3C expression as a risk factor for BRCA, COAD, KIRC, KIRP, LGG and UCEC, but as a protective factor for UVM (**Figure 5A**). KM analysis demonstrated that patients with high MAP1LC3C expression in LGG and UCEC had lower DSS rates than those with low MAP1LC3C expression, while those with high MAP1LC3C expression in LUAD and UVM had higher DSS rates (**Figures 5B–E**). In DFI analysis, patients who died from causes other than the specified disease were not counted. Univariate Cox regression identified high MAP1LC3C expression as a risk factor for KIRP, LGG, STAD and UCEC (**Figure 6A**). KM analysis showed that patients with high MAP1LC3C expression in ESCA, STAD and UCEC had lower DFI rates than those with low MAP1LC3C expression (**Figures 6B–D**). Unlike DFI, PFI was defined as progression or death from disease, again from any cause. In PFI analysis, Univariate Cox regression identified high MAP1LC3C expression as a risk factor for KIRC, KIRP, LGG, PCPG, STAD and UCEC, but as a protective factor for CHOL and UVM (**Figure 7A**). KM analysis confirmed that patients with high MAP1LC3C expression in LGG, STAD and UCEC had lower PFI rates than those with low MAP1LC3C expression (**Figures 7B–D**). Notably, KIRP, LGG and UCEC showed significant differences in all four analyses above, and high MAP1LC3C expression suggested a poor prognosis in all three types of cancers.

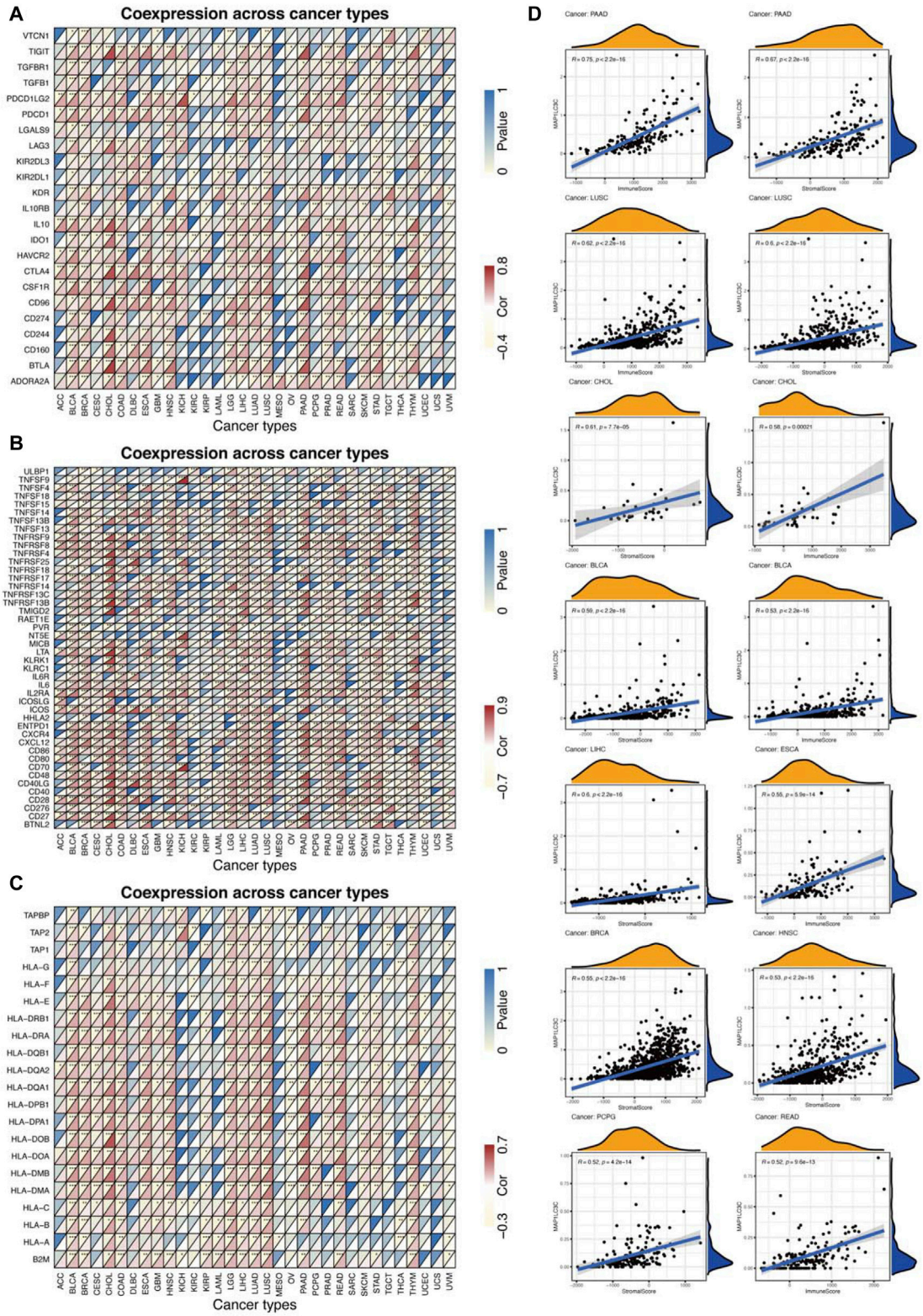

FIGURE 9 | Relationship between MAP1LC3C expression and cancer immunity. **(A)** Heat maps of the correlation between MAP1LC3C expression and immune inhibitors, **(B)** immune stimulators and **(C)** major histocompatibility complex (MHC) molecules in 33 cancer types. For each grid in Figures **(A–C)**, the colour of the upper left triangle represents the *p*-value, and the colour of the lower right triangle represents the Spearman correlation coefficient (*$p < 0.05$; **$p < 0.01$; ***$p < 0.001$). **(D)** Correlation analysis between MAP1LC3C expression and ESTIMATE scores in 33 cancer types.

Correlation Between MAP1LC3C Expression and Tumour Immunity

Using CIBERSORT, the detailed immune cell composition of all patients in the TCGA database was calculated, and the correlation between 22 immune cells in 33 cancer types and MAP1LC3C expression was determined (**Supplementary Table S3**). The results revealed that a majority of immune cells were significantly correlated with MAP1LC3C expression. As shown in **Figure 8**, three types of immune cells in TGCT, two types in PAAD and one type in DLBC and BRCA were correlated with the expression of MAP1LC3C, respectively ($p < 0.01$ and $|R| > 0.4$). As shown in **Figure 9A**, 23 immune inhibitors were analyzed, and the expression of MAP1LC3C was significantly correlated with the immune inhibitors of various cancer types, including CHOL, LGG and PAAD. Correlation analysis of 45 immune stimulators revealed a significantly positive correlation between MAP1LC3C expression in CHOL and PAAD and many immune stimulators in **Figure 9B**. Additionally, correlation analysis of 21 MHCs revealed a significantly positive correlation between MAP1LC3C expression in CHOL, LGG, LIHC and LUSC and multiple MHC molecules in **Figure 9C**.

ESTIMATE algorithm was used to calculate the tumour tissue's immuno/stromal-scores and evaluate the relationship between the immuno/stromal-scores and MAP1LC3C expression. **Figure 9D** showed a significantly positive correlation of MAP1LC3C expression in PAAD, LUSC, CHOL, BLCA, LIHC, ESCA, BRCA, HNSC, PCPG and READ with immuno/stromal-scores ($p < 0.01$ and $|R| > 0.5$). The detailed results of ESTIMATE scores are summarized in **Supplementary Table S4**.

The correlation between TMB/MSI and MAP1LC3C expression (**Supplementary Table S5**, **Figures 10A,B**) were evaluated. As shown in **Figure 10A**, only LGG showed a significantly positive correlation between MAP1LC3C expression and TMB, whereas STAD, SKCM, PAAD, LUSC, LUAD, LIHC, HNSC, DLBC, CESC and BRCA showed a significantly negative correlation. Moreover, MAP1LC3C levels were significantly positively correlated with MSI in ACC, COAD, MESO and TGCT, but significantly negatively correlated with DLBC, ESCA, HNSC, LIHC, LUAD, LUSC and STAD (**Figure 10B**). Therefore, MAP1LC3C expression is closely associated with the tumour immune microenvironment in a variety of cancers.

BIOLOGICAL FUNCTION OF MAP1LC3C

Given the differential expression of MAP1LC3C in many cancers, GSEA was used to assess the biological function of MAP1LC3C in 33 cancer types. In KIRC, MAP1LC3C shows enrichment in the following GO terms: GOBP_ENDOTHELIAL_CELL_MIGRATION, GOBP_REGULATION_OF_ENDOTHELIAL_CELL_MIGRATION, GOBP_RIBONUCLEOPROTEIN_COMPLEX_BIOGENESIS, GOBP_RIBONUCLEOPROTEIN_COMPLEX_BIOGENESIS and GOMF_RNA_BINDING_INVOLVED_IN_POSTTRANSCRIPTIONAL_GENE_SILENCING, and in the following KEGG terms: KEGG_AMINO_SUGAR_AND_NUCLEOTIDE_SUGAR_METABOLISM, KEGG_FRUCTOSE_AND_MANNOSE_METABOLISM, KEGG_GLYCINE_SERINE_AND_THREONINE_METABOLISM, KEGG_PEROXISOME and KEGG_TYPE_II_DIABETES_MELLITUS (**Figures 10C,E**). Additionally, in LGG, MAP1LC3C shows enrichment in the following GO terms: GOBP_IMMUNE_RESPONSE_REGULATING_SIGNALING_PATHWAY,GOBP_LEUKOCYTE_MIGRATION, GOBP_METAL_ION_TRANSPORT, GOBP_MUSCLE_SYSTEM_PROCESS and GOBP_POSITIVE_REGULATION_OF_RESPONSE_TO_EXTERNAL_STIMULUS, and in the following KEGG terms: KEGG_CHEMOKINE_SIGNALING_PATHWAY, KEGG_CYTOKINE_CYTOKINE_RECEPTOR_INTERACTION, KEGG_JAK_STAT_SIGNALING_PATHWAY, KEGG_NATURAL_KILLER_CELL_MEDIATED_CYTOTOXICITY and KEGG_NEUROACTIVE_LIGAND_RECEPTOR_INTERACTION (**Figures 10D**, **11F**).

VIRTUAL SCREENING AND MOLECULAR DOCKING BASED ON MAP1LC3C STRUCTURE

Using virtual screening and molecular docking of the FDA-Approved and Pharmacopeia Drug Library, the top 10 drugs with the best docking score were obtained (**Table 1**). The complete drug docking scores are shown in **Supplementary Table S6**, all drug IDs with drug names are listed in **Supplementary Table S7**. **Figure 11A** shows the MAP1LC3C protein, and **Figures 11B,C** show the binding sites and boxes of this protein, respectively. **Figures 11D–I** show the docking conformation and interaction force analysis of the top three best-combined drugs (T5584 [sodium phytate hydrate], T2971 [phytic acid] and T7387 [ceftaroline fosamil]). The function of sodium phytate is as a [PO4]3- storage depot and precursor for other inositol phosphates and pyrophosphates. While *in vitro*, it is an effective chelator of divalent and trivalent cations (Shears, 2001). Phytic acid is being investigated in clinical trials NCT01000233 for its value in the prevention of cardiovascular calcifications. Ceftaroline fosamil is a cephalosporin antibacterial agent for the treatment of the following infections caused by specified susceptible bacteria: Acute bacterial skin and skin structure infections and community-acquired bacterial pneumonia (Steed and Rybak, 2010). In summary, all of these drugs play an important role in the treatment of non-oncological diseases, but our studies suggest that they also have potential therapeutic value in oncology.

Correlation Between MAP1LC3C Expression and Drug Sensitivity

The examination of MAP1LC3C expression in NCI-60 cell lines showed a significant correlation between MAP1LC3C expression and drug sensitivity (**Table 2**). In particular, as MAP1LC3C expression increased, 6-Thioguanine, By-Product of CUDC-305, 8-Chloro- adenosine, DIGOXIN, AT-13387 and Volasertib had a lower IC50 against cancer cells (**Figures 12**, **13**). This implies that increased expression of MAP1LC3C

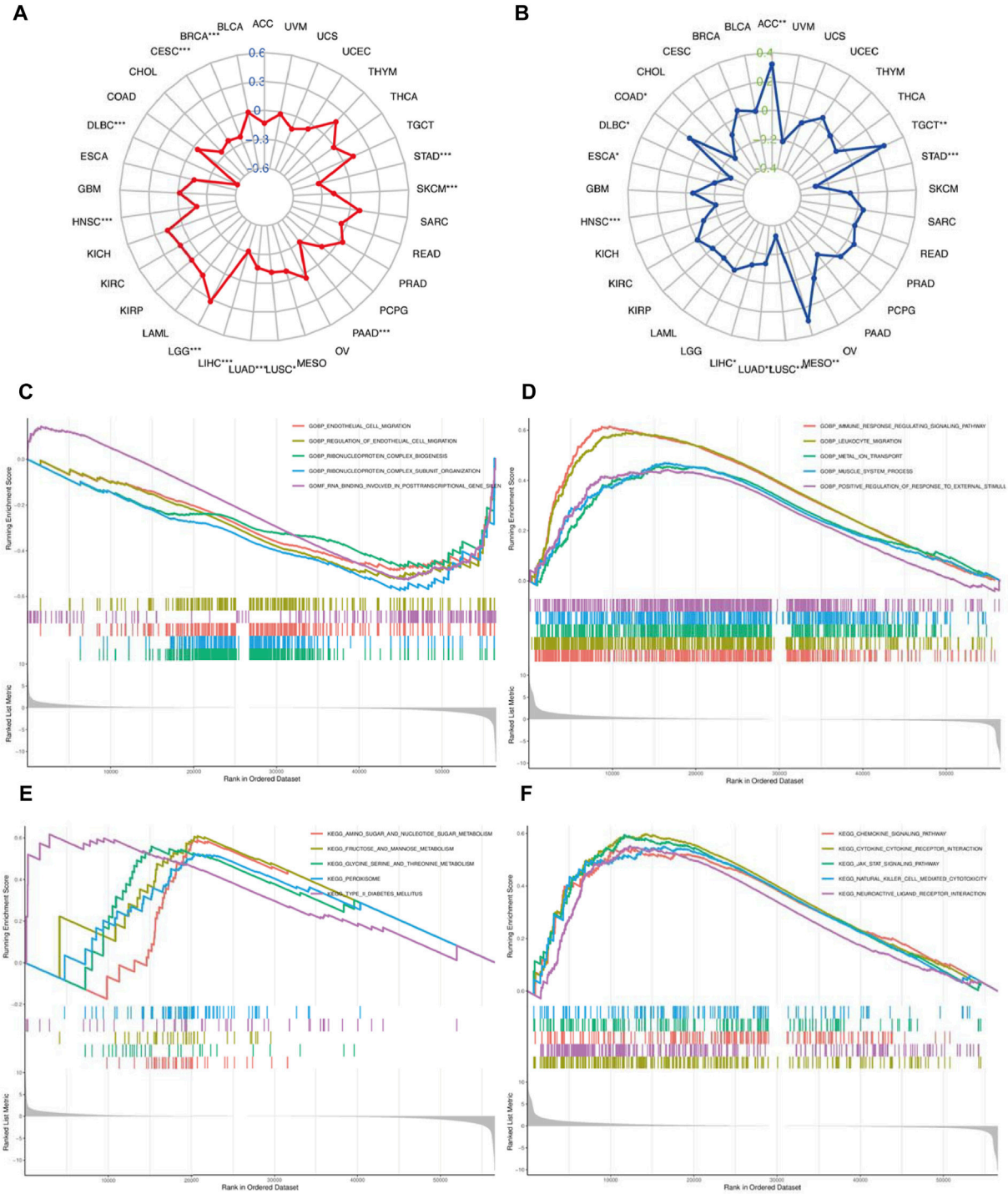

FIGURE 10 | (A) Correlation of MAP1LC3C expression with tumour mutational burden (TMB) and **(B)** microsatellite instability (MSI). The blue and green number represent Spearman's correlation coefficient for TMB and MSI, respectively (*p < 0.05; * *p < 0.01; ***p <0.001). GSEA analysis shows the GO terms related to MAP1LC3C expression in **(C)** KIRC and **(D)** LGG. GSEA analysis shows the KEGG pathways associated with MAP1LC3C expression in **(E)** KIRC and **(F)** LGG.

enhanced the sensitivity of cancer cells to these drugs. It is notable that Volasertib, which showed better results in the virtual screening, also obtained better results in the drug sensitivity analysis.

DISCUSSION

This study aimed to comprehensively investigate the differential expression of MAP1LC3C between the normal and tumour

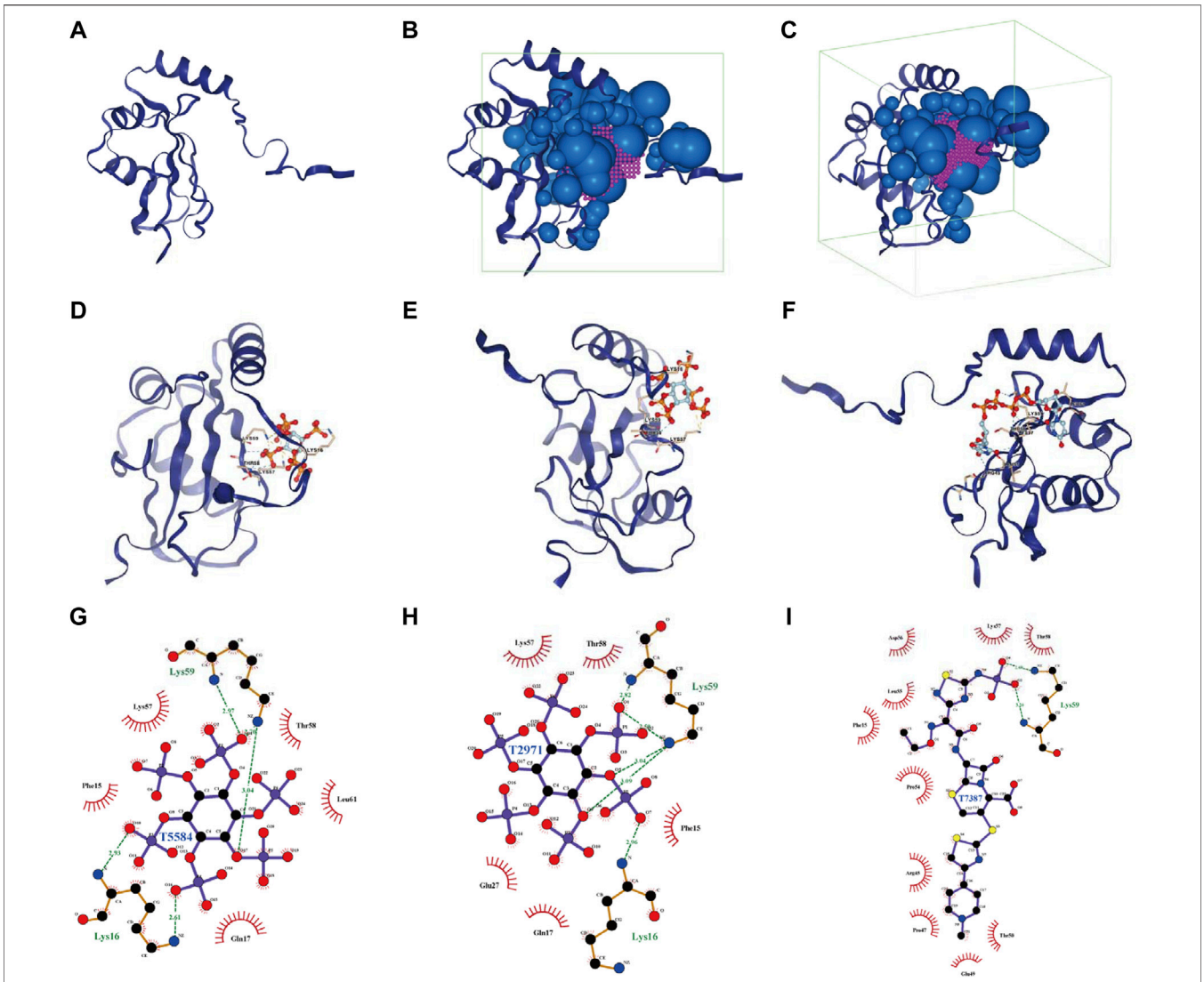

FIGURE 11 | Analysis of docking conformation and interaction force between MAP1LC3C and FDA-approved and pharmacopeia drugs obtained *via* virtual screening. **(A)** The three-dimensional structure of the MAP1LC3C protein. **(B, C)** The binding site and box of MAP1LC3C protein (purple, binding site; green, binding box; blue, little ball). **(D–F)** The three-dimensional docking conformations of T5584, T2971 and T7387 with MAP1LC3C visualised using PyMOL (Yellow dotted line, salt bridge (ionic bond); blue dotted line, hydrogen bond; residues are identified in the form of labels). **(G–I)** Ligplus shows a two-dimensional analysis of the drug molecule (middle)'s interaction forces with the associated amino acid residues (green dotted lines, hydrogen bonds; green amino acid names, amino acid residues forming the hydrogen bonds).

TABLE 1 | Top 10 drugs with the best docking score.

ID	Grid_Score	Grid_vdw_energy	Grid_es_energy	Internal_energy_repulsive
T5584	−138.6127	−37.7842	−100.8285	15.337
T2971	−138.3417	−32.2102	−106.1315	15.8525
T7423	−119.3529	−76.3458	−43.0071	19.8214
T7387	−107.2824	−61.3152	−45.9672	11.3924
T5036	−105.8314	−72.7612	−33.0702	9.9596
T5067	−101.6643	−76.9384	−24.726	19.2636
T2119	−99.7468	−80.3021	−19.4447	22.2605
T0313	−99.2818	−60.4463	−38.8356	44.4261
T5725	−98.9003	−73.7259	−25.1744	12.8408
T1352	−96.987	−54.7152	−42.2719	6.9319

TABLE 2 | Correlation of MAP1LC3C expression with FDA-approved/clinical trial drug sensitivity.

Gene	Drug	Cor	*p*-value
MAP1LC3C	6-Thioguanine	–0.3,852,155	0.00237,106
MAP1LC3C	By-Product of CUDC-305	–0.366,031	0.00402,544
MAP1LC3C	6-THIOGUANINE	–0.3,616,411	0.00452,394
MAP1LC3C	8-Chloro-adenosine	–0.3,187,263	0.01,306,425
MAP1LC3C	PENTOSTATIN	0.31,547,869	0.01,407,516
MAP1LC3C	Megestrol acetate	0.28,630,048	0.0265,773
MAP1LC3C	DIGOXIN	–0.2,790,328	0.03,085,066
MAP1LC3C	Tanespimycin	–0.2,772,625	0.03,197,435
MAP1LC3C	AT-13387	–0.2,762,148	0.03,265,537
MAP1LC3C	Silmitasertib	0.27,230,956	0.03,530,124
MAP1LC3C	Volasertib	–0.2,715,721	0.03,582,036
MAP1LC3C	Kahalide F	0.26,665,574	0.03,944,544
MAP1LC3C	Simvastatin	0.26,650,703	0.03,955,965
MAP1LC3C	AMG-900	–0.2,659,905	0.03,995,851
MAP1LC3C	Ixabepilone	–0.2,630,051	0.04,232,913
MAP1LC3C	SGX-523	0.25,809,477	0.04,647,964
MAP1LC3C	XAV-939	0.25,738,989	0.04,710,194

tissues and to study the prognostic effect and potential immunotherapeutic value of MAP1LC3C for various tumours. The results indicate that MAP1LC3C expression varies in different cancer types. Moreover, survival analysis revealed that abnormal MAP1LC3C expression plays a prognostic role in various types of cancer, including BRCA, COAD, ESCA, KICH, KIRC, KIRP, LAML, LGG, LUAD, LUSC, PCPG and STAD. Additionally, MAP1LC3C expression was correlated highly with the tumour microenvironment, immune cells, immune modulators, TMB and MSI. The biological functions and signalling pathways related to MAP1LC3C expression were also identified. Finally, FDA-approved drugs were screened through virtual screening and drug sensitivity analysis.

Immunotherapy represents a shift in treatment modalities for oncology, the goal is no longer to target the tumour itself, but to overcome the immune suppression caused by the tumour and its microenvironment, and then allow the immune system to target and kill the cancer cells (Billan et al., 2020). About 10 years ago, the first immune checkpoint inhibitor, ipilimumab, a monoclonal antibody targeting CTLA-4, was approved for the FDA and it marked the beginning of the immunotherapy era (Squibb, 2020a). Two additional immune checkpoint inhibitors targeting PD-1 (pembrolizumab and nivolumab) were subsequently approved, and all three were initially approved for unresectable or metastatic melanoma (Squibb, 2020b; Merck, 2020). More immune checkpoint inhibitors have subsequently been approved for a variety of cancers. As a result, immunotherapy is increasingly being used in the clinical management of tumours and our study also focuses on the analysis of the value of MAP1LC3C in immunotherapy to provide new insights into future immunotherapy regimens.

Identifying abnormally expressed genes and tumour-specific targets or features for personalized treatment in different cancers could increase the possibility of cure or remission for patients (Andre et al., 2014). Therefore, the use of TCGA and GTEx databases for pan-cancer analysis helps to determine the differential expression and role of MAP1LC3C in various types of cancer (Cao and Zhang, 2016; Cava et al., 2018). Furthermore, a thorough pan-cancer analysis can be performed in cell lines using the CCLE database to assess gene expression, which may have implications for future cell experiments. Consistent with previously reported results, differentially expressed MAP1LC3C has certain prognostic values in some cancers, especially COAD, LGG and LUAD. MAP1LC3C is a marker that indicates poor prognosis in patients with colon cancer, low-grade glioma and lung adenocarcinoma (Xu et al., 2020; Guo et al., 2021; Wang et al., 2021).

Generally, the protein expression level better reflects the tissue activity (Mo et al., 2021). Due to the lack of relevant data on protein expression levels in public databases, it is difficult to study MAP1LC3C protein expression level. However, MAP1LC3C activity score in various cancer types was obtained using the ssGSEA method. By comparing the transcription level and activity score, the transcription levels of some cancers (BLCA, BRCA, CESC, COAD, GBM, HNSC, KICH, KIRC, LUAD, LUSC, PCPG, READ, STAD and THCA) were matched with MAP1LC3C activity, indicating that the transcription levels represented activation or repression of MAP1LC3C. If the transcription levels could not be matched with MAP1LC3C activity in certain cancers, it indicates that it may be due to post-transcriptional protein level modifications or protein metabolism, which affect MAP1LC3C expression. In our study, there were no cancers with mismatches.

Tumour tissue contains not only tumour cells but also immune cells. Immune cells that infiltrate the tumours can profoundly influence tumour development and anti-cancer therapy (Dalton et al., 1993). Therefore, the quantification of immune cells has extraordinary significance. Recently, immunotherapy has shown an increased efficacy in the treatment of tumours (Finn, 2008). This study reports that the expression level of MAP1LC3C is related to cancer immunity. A strong correlation between MAP1LC3C and macrophages M2, B cells naive and plasma cells was observed in TGCT. In PAAD, a strong correlation was noted between MAP1LC3C and macrophages M0 and B cells naive. Correlation analysis of 23 immune inhibitors showed that MAP1LC3C expression was significantly correlated with various immune inhibitors agents of different cancer types, especially CHOL, LGG and PAAD. Correlation analysis of 45 immune activators showed a significantly positive correlation of MAP1LC3C expression in CHOL and PAAD with many immune activators. The correlation between MAP1LC3C expression and 21 MHCs was also analysed. Human leukocyte antigen (HLA) is the expression product of human MHC, which is the most complex polymorphic system in the human body (Norman et al., 2017). It is worth noting that MHC is closely related to human immune response, immune regulation and few pathological state generation (Xu et al., 2006; Wang et al., 2013). The results indicated that most cancers were positively correlated with HLA. ESTIMATE is a tool for analysing tumour purity and stromal and immune cells' presence in the tumour (Yoshihara et al., 2013). ESTIMATE algorithm generates four final scores: stromal score (indicating the presence of stromal cells in the tumour tissue), immune score (indicating the invasion

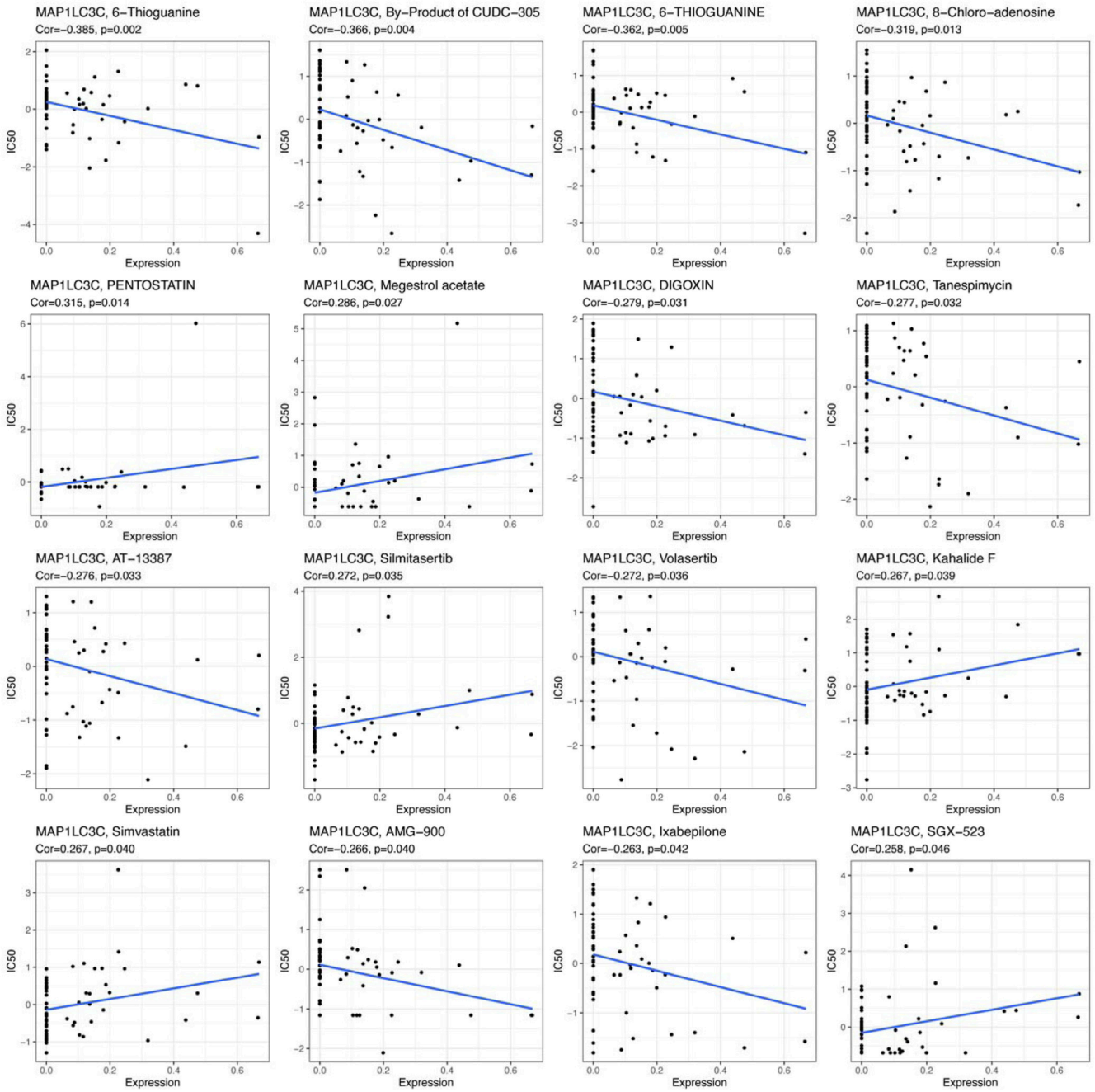

FIGURE 12 | Scatter plot of the relationship between MAP1LC3C expression and drug sensitivity.

of immune cells in the tumour tissue), ESTIMATE score and tumour purity score. Our results revealed that MAP1LC3C expression in PAAD, LUSC, CHOL and BLCA had a significantly positive correlation with matrix fraction and immune fraction. In ESCA and READ, MAP1LC3C expression was significantly positively correlated with immune score, and in LIHC, BRCA, HNSC and PCPG, MAP1LC3C expression was significantly positively correlated with stromal scores.

Gene mutation is the main cause of cancer (Martincorena and Campbell, 2015). Specific gene mutations can be used to predict patient prognosis and treatment outcome (Sanz-Garcia et al., 2017). There is a likelihood that more neoantigens are formed with more somatic mutations in a tumour, which can help the adaptive immune system in recognising and detecting cancer. TMB provides a useful estimate of the tumour-neoantigen load (Chan et al., 2019), and the level of TMB affects the production of

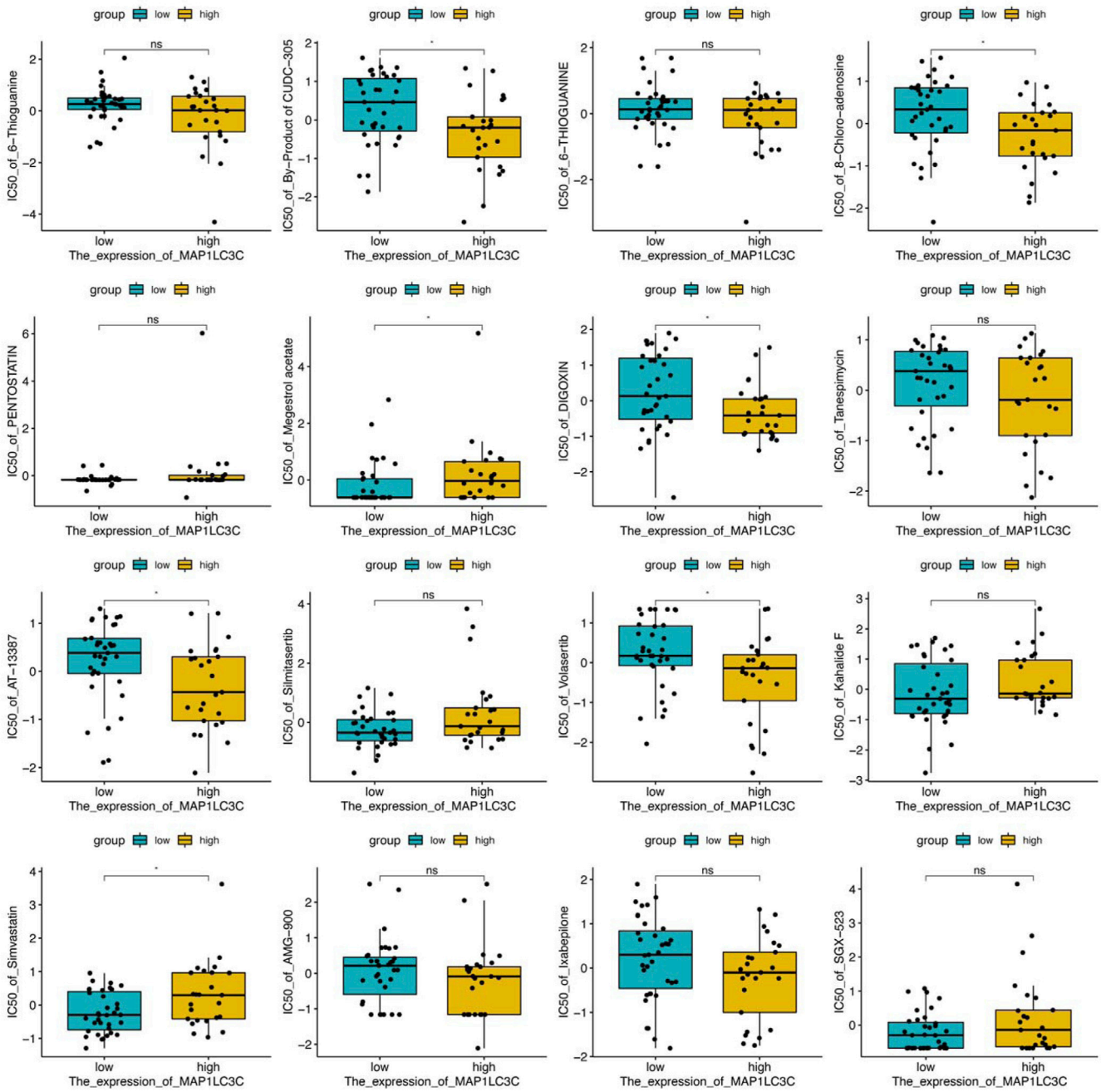

FIGURE 13 | Boxplot of drug sensitivity in high and low expression groups of MAP1LC3C (*$p < 0.05$).

immunogenic peptides, thereby influencing the response of patients to immune checkpoint inhibitors (Havel et al., 2019). Additionally, MSI is a powerful mutant phenotype caused by DNA mismatch repair defects (Yamamoto and Imai, 2019), and it is an important indicator for predicting tumour occurrence and development (Li et al., 2020). MSI is also used as an FDA-approved biomarker for immunotherapy (Lemery et al., 2017). Our study reports that MAP1LC3C is highly negatively correlated with these two immunotherapy biomarkers (TMB and MSI) in a few cancers, such as DLBC, HNSC, LIHC, LUAD, LUSC and STAD. These results suggest that MAP1LC3C may influence the immunotherapy response of these six cancer types.

Furthermore, virtual screening is a commonly used computational technique for drug designing. Virtual screening can be divided into two categories: structure-based virtual screening and ligand-based virtual screening (Lavecchia and Di Giovanni, 2013; Forli, 2015). Virtual screening based on the three-dimensional structure of the receptor (target protein)

was adopted to screen for drugs that had a good interaction with the MAP1LC3C protein from the FDA-Approved and Pharmacopeia Drug Library. Furthermore, a drug sensitivity analysis using data from the NCI-60 cell line was performed. On the one hand, these results demonstrate the feasibility of MAP1LC3C as a drug target and, on the other hand, provide a reference for the development of therapeutic drug regimens. Notably, the drug with better results in both the virtual screen and the drug sensitivity analysis is Volasertib, a Plk1 inhibitor, that has reached phase III clinical trials for adult acute myeloid leukaemia patients ineligible for intensive remission induction therapy (Döhner et al., 2016). Given the better results of Volasertib in both drug sensitivity analysis and molecular docking against MAP1LC3C, it is worth trying to explore its therapeutic value in other cancers. In general, all the screened drugs can be considered as potential therapeutic agents for various cancer types. However, further *in vivo* studies need to be conducted.

CONCLUSION

To the best of our knowledge, this study is the first report to investigate the prognostic and therapeutic value of MAP1LC3C in 33 types of cancer. Our results suggested that MAP1LC3C can be a valuable prognostic biomarker for certain types of cancer, and showed high correlation with important immunological indexes in certain cancers. This will facilitate us to understand the role of MAP1LC3C in the immune system and lay a solid theoretical foundation for future immunotherapy. The FDA-approved drugs identified using virtual screening and drug sensitivity analysis could be potential cancer therapeutic agents, thereby paving the way for future cancer treatment research. The bioinformatics method was used in this study to provide relatively preliminary results and in future in-depth studies are needed to clarify the association between MAP1LC3C and cancer treatment.

DATA AVAILABILITY STATEMENT

The datasets presented in this study can be found in online repositories. The names of the repository/repositories and accession number(s) can be found in the article/**Supplementary Material**.

AUTHOR CONTRIBUTIONS

Conceptualization, YB. and XZ methodology, XZ software, XZ validation, YB XS. and QZ formal analysis, XZ investigation, KL, SL, SZ, TL, LL, NB and SH; resources, XZ data curation, XZ original draft preparation, XZ review and editing, XZ, YB and XS visualization, XZ supervision, XZ, YB and XS project administration, XZ, YB and XS funding acquisition, YB and XS All authors have read and agreed to the published version of the manuscript.

FINDING

This project was sponsored by Liaoning Provincial Natural Science Foundation (2020-MS-155), China Medical University novel coronavirus pneumonia prevention and control research project (No. 2020-12-11), Scientific Research Foundation for the Returned Overseas Chinese Scholars, State Education Ministry (2013-1792), National Science Foundation of China (72074104), Shenyang Planning Foundation for Science and Technology (21-173-9-38), and the first batch of medical education scientific research project of China Medical University for the 14th Five-Year Plan (YDJK2021039). The researchers are grateful for the support of several organizations.

SUPPLEMENTARY MATERIAL

The Supplementary Material for this article can be found online at: https://www.frontiersin.org/articles/10.3389/fphar.2022.863856/full#supplementary-material

REFERENCES

Andre, F., Mardis, E., Salm, M., Soria, J. C., Siu, L. L., and Swanton, C. (2014). Prioritizing Targets for Precision Cancer Medicine. *Ann. Oncol.* 25 (12), 2295–2303. doi:10.1093/annonc/mdu478

Berman, H. M., Westbrook, J., Feng, Z., Gilliland, G., Bhat, T. N., Weissig, H., et al. (2000). The Protein Data Bank. *Nucleic Acids Res.* 28 (1), 235–242. doi:10.1093/nar/28.1.235

Billan, S., Kaidar-Person, O., and Gil, Z. (2020). Treatment after Progression in the Era of Immunotherapy. *Lancet Oncol.* 21 (10), e463. doi:10.1016/S1470-2045(20)30328-4

Cao, Z., and Zhang, S. (2016). An Integrative and Comparative Study of Pan-Cancer Transcriptomes Reveals Distinct Cancer Common and Specific Signatures. *Sci. Rep.* 6, 33398. doi:10.1038/srep33398

Cava, C., Bertoli, G., Colaprico, A., Olsen, C., Bontempi, G., and Castiglioni, I. (2018). Integration of Multiple Networks and Pathways Identifies Cancer Driver Genes in Pan-Cancer Analysis. *BMC Genomics* 19 (1), 25. doi:10.1186/s12864-017-4423-x

Chan, T. A., Yarchoan, M., Jaffee, E., Swanton, C., Quezada, S. A., Stenzinger, A., et al. (2019). Development of Tumor Mutation burden as an Immunotherapy Biomarker: Utility for the Oncology Clinic. *Ann. Oncol.* 30 (1), 44–56. doi:10.1093/annonc/mdy495

Clarke, A. J., and Simon, A. K. (2019). Autophagy in the Renewal, Differentiation and Homeostasis of Immune Cells. *Nat. Rev. Immunol.* 19 (3), 170–183. doi:10.1038/s41577-018-0095-2

Consortium, G. T. (2020). The GTEx Consortium Atlas of Genetic Regulatory Effects across Human Tissues. *Science* 369 (6509), 1318–1330. doi:10.1126/science.aaz1776

Dalton, D. K., Pitts-Meek, S., Keshav, S., Figari, I. S., Bradley, A., and Stewart, T. A. (1993). Multiple Defects of Immune Cell Function in Mice with Disrupted Interferon-Gamma Genes. *Science* 259 (5102), 1739–1742. doi:10.1126/science.8456300

Döhner, H., Miguel, A. S., Sanz, A., Deeren, D., Demeter, J., Anagnostopoulos, A., et al. (2016). Phase Iii Randomized Trial of Volasertib Plus Low-Dose Cytarabine (Ldac) versus Placebo Plus Ldac in Patients Aged?65 Years with Previously Untreated Aml, Ineligible for Intensive Therapy. Available from https://library.ehaweb.org/eha/2016/21st/135257/hartmut.dhner.phase.iii.randomized.trial.of.volasertib.plus.low-dose.html?f=m3.

Finn, O. J. (2008). Cancer Immunology. *N. Engl. J. Med.* 358 (25), 2704–2715. doi:10.1056/NEJMra072739

Forli, S. (2015). Charting a Path to Success in Virtual Screening. *Molecules* 20 (10), 18732–18758. doi:10.3390/molecules201018732

Goldman, M. J., Craft, B., Hastie, M., Repečka, K., McDade, F., Kamath, A., et al. (2020). Visualizing and Interpreting Cancer Genomics Data via the Xena Platform. *Nat. Biotechnol.* 38 (6), 675–678. doi:10.1038/s41587-020-0546-8

Guo, J. C., Wei, Q. S., Dong, L., Fang, S. S., Li, F., and Zhao, Y. (2021). Prognostic Value of an Autophagy-Related Five-Gene Signature for Lower-Grade Glioma Patients. *Front. Oncol.* 11, 644443. doi:10.3389/fonc.2021.644443

Hänzelmann, S., Castelo, R., and Guinney, J. (2013). GSVA: Gene Set Variation Analysis for Microarray and RNA-Seq Data. *BMC Bioinformatics* 14, 7. doi:10.1186/1471-2105-14-7

Havel, J. J., Chowell, D., and Chan, T. A. (2019). The Evolving Landscape of Biomarkers for Checkpoint Inhibitor Immunotherapy. *Nat. Rev. Cancer* 19 (3), 133–150. doi:10.1038/s41568-019-0116-x

Inc., T.C. FDA-Approved & Pharmacopeia Drug Library (2021). Available from https://www.targetmol.com/compound-library/FDA-Approved%20&%20Pharmacopeia%20Drug%20Library#.

Kawabata, T. (2010). Detection of Multiscale Pockets on Protein Surfaces Using Mathematical Morphology. *Proteins* 78 (5), 1195–1211. doi:10.1002/prot.22639

Lavecchia, A., and Di Giovanni, C. (2013). Virtual Screening Strategies in Drug Discovery: a Critical Review. *Curr. Med. Chem.* 20 (23), 2839–2860. doi:10.2174/09298673113209990001

Le Guerroué, F., Eck, F., Jung, J., Starzetz, T., Mittelbronn, M., Kaulich, M., et al. (2017). Autophagosomal Content Profiling Reveals an LC3C-dependent Piecemeal Mitophagy Pathway. *Mol. Cel* 68 (4), 786–e6. doi:10.1016/j.molcel.2017.10.029

Lemery, S., Keegan, P., and Pazdur, R. (2017). First FDA Approval Agnostic of Cancer Site - when a Biomarker Defines the Indication. *N. Engl. J. Med.* 377 (15), 1409–1412. doi:10.1056/NEJMp1709968

Li, K., Luo, H., Huang, L., Luo, H., and Zhu, X. (2020). Microsatellite Instability: a Review of what the Oncologist Should Know. *Cancer Cel Int* 20, 16. doi:10.1186/s12935-019-1091-8

Martincorena, I., and Campbell, P. J. (2015). Somatic Mutation in Cancer and normal Cells. *Science* 349 (6255), 1483–1489. doi:10.1126/science.aab4082

Merck, P. (2020). (package Insert). Available from https://www.merck.com/product/usa/pi_circulars/k/keytruda/keytruda_pi.pdf.

Mo, Z., Li, P., Cao, Z., and Zhang, S. (2021). A Comprehensive Pan-Cancer Analysis of 33 Human Cancers Reveals the Immunotherapeutic Value of Aryl Hydrocarbon Receptor. *Front. Immunol.* 12, 564948. doi:10.3389/fimmu.2021.564948

Morishita, H., and Mizushima, N. (2019). Diverse Cellular Roles of Autophagy. *Annu. Rev. Cel Dev Biol* 35, 453–475. doi:10.1146/annurev-cellbio-100818-125300

Newman, A. M., Steen, C. B., Liu, C. L., Gentles, A. J., Chaudhuri, A. A., Scherer, F., et al. (2019). Determining Cell Type Abundance and Expression from Bulk Tissues with Digital Cytometry. *Nat. Biotechnol.* 37 (7), 773–782. doi:10.1038/s41587-019-0114-2

Norman, P. J., Norberg, S. J., Guethlein, L. A., Nemat-Gorgani, N., Royce, T., Wroblewski, E. E., et al. (2017). Sequences of 95 Human MHC Haplotypes Reveal Extreme Coding Variation in Genes Other Than Highly Polymorphic HLA Class I and II. *Genome Res.* 27 (5), 813–823. doi:10.1101/gr.213538.116

Nusinow, D. P., Szpyt, J., Ghandi, M., Rose, C. M., McDonald, E. R., Kalocsay, M., et al. (2020). Quantitative Proteomics of the Cancer Cell Line Encyclopedia. *Cell* 180 (2), 387–e16. doi:10.1016/j.cell.2019.12.023

Ohsumi, Y. (2012). Yoshinori Ohsumi: Autophagy from Beginning to End. Interview by Caitlin Sedwick. *J. Cel Biol* 197 (2), 164–165. doi:10.1083/jcb.1972pi

Reinhold, W. C., Sunshine, M., Liu, H., Varma, S., Kohn, K. W., Morris, J., et al. (2012). CellMiner: a Web-Based Suite of Genomic and Pharmacologic Tools to Explore Transcript and Drug Patterns in the NCI-60 Cell Line Set. *Cancer Res.* 72 (14), 3499–3511. doi:10.1158/0008-5472.CAN-12-1370

Ritchie, M. E., Phipson, B., Wu, D., Hu, Y., Law, C. W., Shi, W., et al. (2015). Limma powers Differential Expression Analyses for RNA-Sequencing and Microarray Studies. *Nucleic Acids Res.* 43 (7), e47. doi:10.1093/nar/gkv007

Ru, B., Wong, C. N., Tong, Y., Zhong, J. Y., Zhong, S. S. W., Wu, W. C., et al. (2019). TISIDB: an Integrated Repository portal for Tumor-Immune System Interactions. *Bioinformatics* 35 (20), 4200–4202. doi:10.1093/bioinformatics/btz210

Sanz-Garcia, E., Argiles, G., Elez, E., and Tabernero, J. (2017). BRAF Mutant Colorectal Cancer: Prognosis, Treatment, and New Perspectives. *Ann. Oncol.* 28 (11), 2648–2657. doi:10.1093/annonc/mdx401

Shears, S. B. (2001). Assessing the Omnipotence of Inositol Hexakisphosphate. *Cell Signal* 13 (3), 151–158. doi:10.1016/s0898-6568(01)00129-2

Slobodkin, M. R., and Elazar, Z. (2013). The Atg8 Family: Multifunctional Ubiquitin-like Key Regulators of Autophagy. *Essays Biochem.* 55, 51–64. doi:10.1042/bse0550051

Squibb, B.-M. (2020). Ipilimumab (Package Insert). Available from https://packageinserts.bms.com/pi/pi_yervoy.pdf.

Squibb, B.-M. (2020). Nivolumab (Package Insert). Available from https://packageinserts.bms.com/pi/pi_opdivo.pdf.

Steed, M. E., and Rybak, M. J. (2010). Ceftaroline: a New Cephalosporin with Activity against Resistant Gram-Positive Pathogens. *Pharmacotherapy* 30 (4), 375–389. doi:10.1592/phco.30.4.375

Tooze, S. A., and Yoshimori, T. (2010). The Origin of the Autophagosomal Membrane. *Nat. Cel Biol* 12 (9), 831–835. doi:10.1038/ncb0910-831

Wallace, A. C., Laskowski, R. A., and Thornton, J. M. (1995). LIGPLOT: a Program to Generate Schematic Diagrams of Protein-Ligand Interactions. *Protein Eng.* 8 (2), 127–134. doi:10.1093/protein/8.2.127

Wang, B., Niu, D., Lai, L., and Ren, E. C. (2013). p53 Increases MHC Class I Expression by Upregulating the Endoplasmic Reticulum Aminopeptidase ERAP1. *Nat. Commun.* 4, 2359. doi:10.1038/ncomms3359

Wang, Y., Lin, K., Xu, T., Wang, L., Fu, L., Zhang, G., et al. (2021). Development and Validation of Prognostic Model Based on the Analysis of Autophagy-Related Genes in colon Cancer. *Aging (Albany NY)* 13 (14), 19028–19047. doi:10.18632/aging.203352

Xia, H., Green, D. R., and Zou, W. (2021). Autophagy in Tumour Immunity and Therapy. *Nat. Rev. Cancer* 21 (5), 281–297. doi:10.1038/s41568-021-00344-2

Xu, H., Chun, T., Choi, H. J., Wang, B., and Wang, C. R. (2006). Impaired Response to Listeria in H2-M3-Deficient Mice Reveals a Nonredundant Role of MHC Class Ib-specific T Cells in Host Defense. *J. Exp. Med.* 203 (2), 449–459. doi:10.1084/jem.20051866

Xu, Z., Wu, Z., Zhang, J., Zhou, R., Ye, L., Yang, P., et al. (2020). Development and Validation of an Oxidative Phosphorylation-Related Gene Signature in Lung Adenocarcinoma. *Epigenomics* 12 (15), 1333–1348. doi:10.2217/epi-2020-0217

Yamamoto, H., and Imai, K. (2019). An Updated Review of Microsatellite Instability in the Era of Next-Generation Sequencing and Precision Medicine. *Semin. Oncol.* 46 (3), 261–270. doi:10.1053/j.seminoncol.2019.08.003

Yang, A., Herter-Sprie, G., Zhang, H., Lin, E. Y., Biancur, D., Wang, X., et al. (2018). Autophagy Sustains Pancreatic Cancer Growth through Both Cell-Autonomous and Nonautonomous Mechanisms. *Cancer Discov.* 8 (3), 276–287. doi:10.1158/2159-8290.CD-17-0952

Yoshihara, K., Shahmoradgoli, M., Martínez, E., Vegesna, R., Kim, H., Torres-Garcia, W., et al. (2013). Inferring Tumour Purity and Stromal and Immune Cell Admixture from Expression Data. *Nat. Commun.* 4, 2612. doi:10.1038/ncomms3612

Zou, W. (2005). Immunosuppressive Networks in the Tumour Environment and Their Therapeutic Relevance. *Nat. Rev. Cancer* 5 (4), 263–274. doi:10.1038/nrc1586

Zou, W., Wolchok, J. D., and Chen, L. (2016). PD-L1 (B7-H1) and PD-1 Pathway Blockade for Cancer Therapy: Mechanisms, Response Biomarkers, and Combinations. *Sci. Transl Med.* 8 (328), 328rv4. doi:10.1126/scitranslmed.aad7118

Conflict of Interest: The authors declare that the research was conducted in the absence of any commercial or financial relationships that could be construed as a potential conflict of interest.

Publisher's Note: All claims expressed in this article are solely those of the authors and do not necessarily represent those of their affiliated organizations, or those of the publisher, the editors and the reviewers. Any product that may be evaluated in this article, or claim that may be made by its manufacturer, is not guaranteed or endorsed by the publisher.

frontiers | Frontiers in Pharmacology

ORIGINAL RESEARCH
published: 28 April 2022
doi: 10.3389/fphar.2022.898679

Modulation of Tumor Immune Microenvironment and Prognostic Value of Ferroptosis-Related Genes, and Candidate Target Drugs in Glioblastoma Multiforme

Xudong Zhang[1†], Shengnan Jin[2†], Xin Shi[3,4], Shengyu Liu[1], Kunhang Li[1], Guojun Liu[1], Shiyu Zhong[1], Tao Liu[1], Lishuai Li[1], Shanwei Tao[5], Qingqing Zhai[6], Nan Bao[7], Lijie Ren[8], Ying Wu[9] and Yijun Bao[1]**

[1]Department of Neurosurgery, The Fourth Hospital of China Medical University, Shenyang, China, [2]Department of Developmental Cell Biology, China Medical University, Shenyang, China, [3]School of Maths and Information Science, Shangdong Technology and Business University, Yantai, China, [4]Business School, All Saints Campus, Manchester Metropolitan University, Manchester, United Kingdom, [5]Department of Neurosurgery, Luoyang Central Hospital Affiliated to Zhengzhou University, Luoyang, China, [6]School of Management, Shanghai University, Baoshan, China, [7]College of Medicine and Biological Information Engineering, Northeastern University, Shenyang, China, [8]Health Science Center, Neurology Department of Shenzhen Second People's Hospital, The First Affiliated Hospital of Shenzhen University, Shenzhen, China, [9]Phase I Clinical Trails Center, The First Affiliated Hospital of China Medical University, Shenyang, China

OPEN ACCESS

Edited by:
Fengfeng Zhou,
Jilin University, China

Reviewed by:
Hirotomo Ten,
Teikyo Heisei University, Japan
Li Bie,
Jilin University, China

***Correspondence:**
Yijun Bao
yjbao@cmu.edu.cn
Ying Wu
wuying@cmu.edu.cn

†These authors have contributed equally to this work

Specialty section:
This article was submitted to Pharmacology of Anti-Cancer Drugs, a section of the journal Frontiers in Pharmacology

Received: 17 March 2022
Accepted: 13 April 2022
Published: 28 April 2022

Citation:
Zhang X, Jin S, Shi X, Liu S, Li K, Liu G, Zhong S, Liu T, Li L, Tao S, Zhai Q, Bao N, Ren L, Wu Y and Bao Y (2022) Modulation of Tumor Immune Microenvironment and Prognostic Value of Ferroptosis-Related Genes, and Candidate Target Drugs in Glioblastoma Multiforme. Front. Pharmacol. 13:898679. doi: 10.3389/fphar.2022.898679

Glioblastoma multiforme (GBM) is the most common type of malignant brain tumor, among which IDH1-wild type GBM has a poor prognosis. Recent studies have shown that ferroptosis-related genes (FRGs) are correlated with the development and progression of cancer. In GBM, the role of FRGs associated with IDH1 status as biological indicators and therapeutic targets remains to be clarified. Ten of FRGs (STEAP3, HSPB1, MAP1LC3A, SOCS1, LOX, CAPG, CP, GDF15, CDKN1A, and CD44) associated with IDH1 status in GBM were identified as key genes through screening by survival analysis and Random Forest using The Cancer Genome Atlas (TCGA) datasets, and the protein expressions of key genes were verified. Transwell and qPCR results showed that ferroptosis promoted the migration of glioblastoma cells and affected the expression of key genes. Our study established the ferroptosis-related prognostic model for GBM patients based on ten key genes by a different modeling method from previous study, the GSVA algorithm. Further, we took the methods of functional enrichment analysis, clinical characteristics, immune cell infiltration, immunomodulator, ESTIMATE and single nucleotide variant (SNV) analysis to study the molecular mechanisms of prognostic model and key genes. The results showed that ten key genes were strongly associated with immune-related factors and were significantly involved in the p53 signaling pathway, senescence and autophagy in cancer, and in the negative regulation of protein kinase activity. Moreover, potential therapeutic drugs were identified by Virtual Screening and Molecular Docking. Our study indicated that the novel ferrotosis-related prognostic model for GBM patients and key genes possessed the prognostic and therapeutic values.

Keywords: ferroptosis, glioblastoma multiforme, IDH1, prognosis, multi-omics analysis

1 INTRODUCTION

Glioblastoma multiforme (GBM) is the most common malignant primary intracranial tumor with a poor prognosis despite the existence of therapeutic modalities including surgery, radiotherapy, and chemotherapy. The median survival is only 14–16 months (Ricard et al., 2012; Cancer Genome Atlas Research et al., 2015; Jiang et al., 2016; Chai et al., 2019). According to the World Health Organization (WHO) central nervous system (CNS) cancer classification, GBM can be divided into isocitrate dehydrogenase (IDH)-wild and IDH-mutant types, and IDH-wild type GBM has a relatively poorer prognosis (Yan et al., 2009; Louis et al., 2016). IDH1 mutation is one of the most common and earliest detected genetic alterations in diffuse gliomas, and evidence supports this mutation as a driver of glioma development (Agnihotri et al., 2014).

Ferroptosis is a novel iron-dependent, non-apoptotic form of cell death that kills cells through lipid peroxidation injury occurring on the cell membrane. Although the physiological role of ferroptosis remains to be elucidated, there is ample evidence that ferroptosis plays a very important role in organic diseases such as heart, liver, kidney, and brain (Fang et al., 2019; Jiang et al., 2021), particularly in the treatment of cancer by targeted key ferroptosis-related genes (FRGs) and pathways (Jiang et al., 2021).

In recent years, high-throughput sequencing technologies and genetic databases have been widely used in cancer diagnosis and prognosis studies. Although the role of FRGs in GBM has been initially investigated, few prognosis-related genes have been screened in previous literature (Zhu et al., 2021). The prognostic effectiveness and therapeutic performance of differential expressions of FRGs in IDH1-wild and IDH1-mutant GBM have not been investigated.

Therefore, our study aimed to find FRGs associated with IDH1 status in GBM, which are promising prognostic indicators and therapeutic targets for GBM. We analyzed the sequencing data of GBM patients in TCGA databases by bioinformatics, machine learning algorithm and multi-omics to identify FRGs associated with prognosis in GBM patients as key genes, and the protein expression of the key genes was validated. Ferroptosis was identified by Transwell and qPCR experiments to be associated with the migration ability of glioblastoma cells and affected the expression of key genes. We then established and validated the ferroptosis-related prognostic model for GBM patients. We also studied the possible regulatory mechanisms in terms of the impacts of model and key genes on cancer immunity, biological function, gene mutation and clinical characteristics. Furthermore, we identified potential therapeutic compounds through Virtual screening and Molecular docking.

2 MATERIALS AND METHODS

2.1 Data Collection

TCGA-GBM transcriptome expression profile data and genomic mutation data were downloaded through xena (Goldman et al., 2020), 166 TCGA-GBM tumor samples and five normal tissue samples were obtained. 290 FRGs were obtained by merging the datasets from literature (Liang et al., 2020; Zhuo et al., 2020), FerrDb (Zhou and Bao, 2020), MSigDB (Liberzon et al., 2015), and genecards (Stelzer et al., 2016). In addition, immunomodulators, including immunoinhibitors, immunostimulators and MHC molecules, were downloaded from the TISIDB database (Ru et al., 2019).

2.2 Identification of Key Genes and Survival Analysis

PCA scatter plot was analyzed using the R package ggplot2 (Wickham, 2016) and screening of DEG using R package limma (Ritchie et al., 2015). Genes with $p < 0.05$ and |log2 fold change (FC)| > 0.5 were considered as DEGs. Further genes screening using the R package randomForest (Liaw and Wiener, 2002), and genes with negative horizontal coordinate values (% IncMSE <0) were filtered, and WIPI1 and SOCS1 were deleted, but SOCS1 was strongly associated with GBM and retained. Ten key genes were obtained finally. Kaplan-Meier curves were plotted, and p-value < 0.05 was deemed to be a significant difference between high- and low-risk groups. Immunohistochemical results for key genes were obtained from the Human Protein Atlas (HPA) database (Uhlén et al., 2005). The sample sizes for each group were much larger than three. Antibody staining in the annotated cell types in the current human tissue is reported as not detected, low, medium, or high. The score is based on the staining intensity and fraction of stained cells, therefore the staining scores in different groups are comparable.

2.3 Biological Functional Analysis and Correlation Analysis of Clinical Characteristics

GO and pathway functional enrichment analysis of ten key genes were performed using R package cluster profiler (Yu et al., 2012). The correlation between each gene expression with the GBM clinical characteristics (IDH1 status, gender, and risk level) were analyzed and visualized by drawing mosaic plots with the R package mosaic (Pruim et al., 2017).

2.4 Cell Culture and Migration Assay

The human glioblastoma cell line U87MG was obtained from the Cell Resource Centre of Peking Union Medical College and U251MG from American Type Culture Collection. Cells were cultured in DMEM medium supplemented with 10% FBS and placed in a standard constant temperature CO_2 incubator (5% CO_2, 37°C). The Transwell system (24-well, 8 μm pore size polycarbonate membrane) was for *in vitro* migration assays. U251MG and U87MG cells were pretreated with ferroptosis activator erastin (10 μM) or control solvent for 24 h. Finally the cells attached to the lower surface of the filter membrane were fixed with 4% PFA and then stained with crystal violet. The migrated cells were photographed with a light microscope and counted using ImageJ software. The qPCR primer sequences were all obtained from Primerbank and synthesized by Sangon Biotech (Spandidos et al., 2009), and PCR primer sequences was shown in **Supplementary Table S1**. All experiments were repeated more than three times.

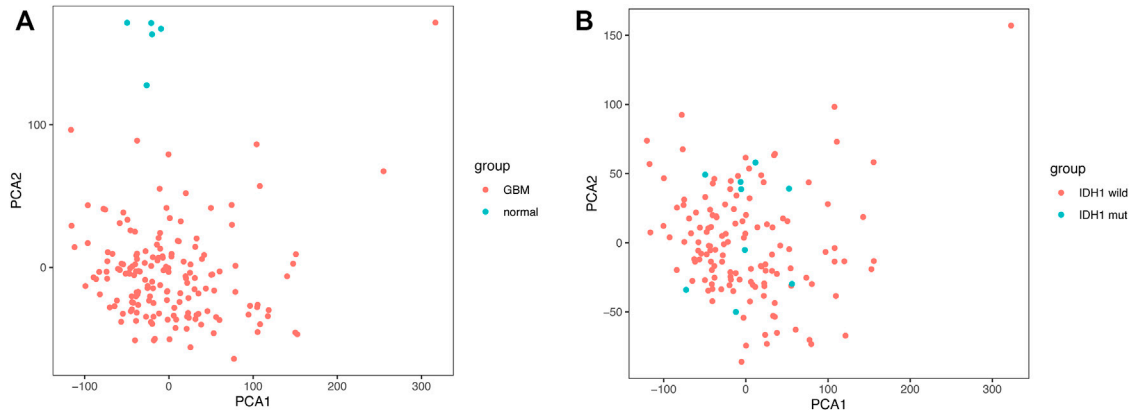

FIGURE 1 | Principal Component Analysis **(A)** GBM vs normal brain tissue **(B)** IDH1 wild vs. IDH1 mutant.

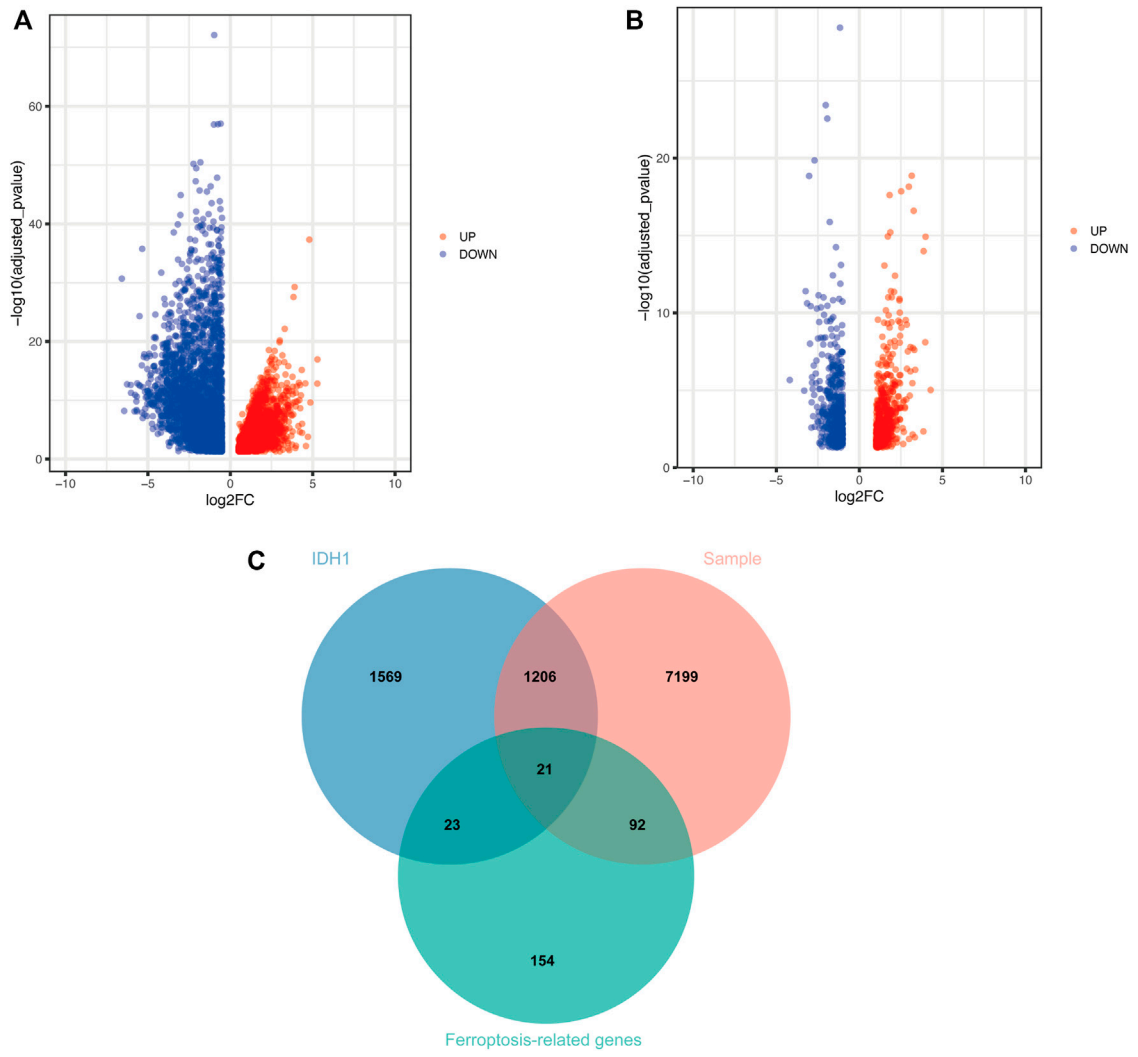

FIGURE 2 | Screening of DEGs **(A)** Volcano plot demonstrates DEGs of GBM vs. normal brain tissue **(B)** Volcano plot shows DEGs of IDH1 wild type vs. mutant type **(C)** Wayne plot indicates shared DEGs.

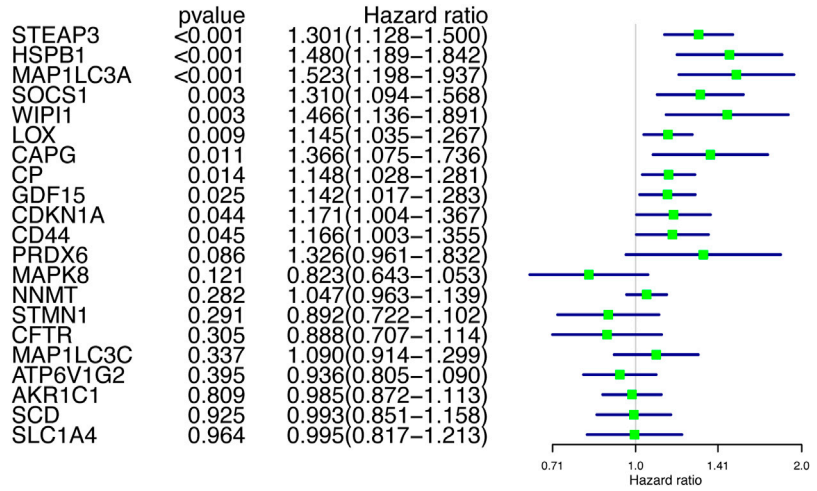

FIGURE 3 | Univariate Cox regression screening for prognosis-related genes.

2.5 Construction of Prognostic Model and Nomogram

Enrichment scores based on key gene sets were calculated for each sample using the GSVA algorithm (Hänzelmann et al., 2013) and KM curve was plotted. Survival scatterplot was analyzed using the R package ggplot2 and heatmap using the R package pheatmap, showing the expression of the key genes both in high- and low-risk groups. GSVA score was combined with the clinical indicators (age, sex, and radiation) for univariate and multifactor Cox regression analysis, respectively, and the nomogram and calibration curves were drawn.

2.6 Correlation Analysis of Immune Cell Infiltration, Immunomodulators and ESTIMATE Score

Calculation of immune cell infiltration levels for each sample of TCGA-GBM was performed using CIBERSORT website. Wilcox test was used to analyze the difference in immune cell infiltration between high- and low-risk groups and was considered significant with p-value < 0.001. Correlations between the gene expression and different immune cells were calculated and considered significant with p-value < 0.001 and $|r| > 0.2$. The stromal score and immune score were calculated for each sample using the ESTIMATE package (Yoshihara et al., 2013).

2.7 Single Nucleotide Variant Analysis of Key Genes

The maf data of varscan of TCGA-GBM were downloaded from the TCGA database. The key gene mutations were analyzed, and the SNV distribution was plotted using the R package maftools (Mayakonda et al., 2018).

2.8 Virtual Screening and Molecular Docking

The structural information of corresponding compounds was downloaded from DrugBank database (Wishart et al., 2018) and screened according to Lipinski's rule (hydrogen bond acceptor ≤10, hydrogen bond donor ≤5, rotatable bond ≤10, the logarithmic value of lipid-water partition coefficient ≤5, the molecular weight of 180–480, and polar surface area ≤140). Finally, 5,464 small molecule compounds were obtained. The spatial structure information of the key gene-encoded proteins was searched in the PDB database to find the relevant structural information of CAPG, CP and CD44 (Berman et al., 2000). The corresponding PDB files 6IGX, 4ENZ, and 4PZ3 were downloaded, and the approximate docking box range was determined based on the ligand information therein. We repaired the missing residues using modeller (Eswar et al., 2007). After setting other relevant parameters, we used autodock-vina to dock with the small molecule compounds separately and performed interaction force analysis using Ligplus. PyMol demonstrated docking conformations.

3 RESULTS

3.1 Identification of Key Genes

3.1.1 Differentially Expressed Ferroptosis-Related Genes associated with IDH1 Status

Given the importance of IDH1 status for the prognosis of GBM patients, we searched for genes related to IDH1 status in GBM patients. The PCA scatter plots of TCGA-GBM expression profile data combined with clinical data were divided into: A) GBM versus normal brain tissue, and B) IDH1 wild versus IDH1 mutant in **Figure 1**. Screening of differentially expressed genes (DEGs) using GBM versus normal brain tissue expression profile data identified 8,518 DEGs, of which 4,680 were down-regulated, and 3,838 up-regulated (**Figure 2A**). Similarly, 2,819 DEGs were found in the screening of IDH1 wild type versus mutant type, among 2,819 DEGs, 1771 were down-regulated and the rest of them were up-regulated (**Figure 2B**). The shared 1,227 DEGs (**Figure 2C**) were intersected with the collected 290 ferroptosis-related genes

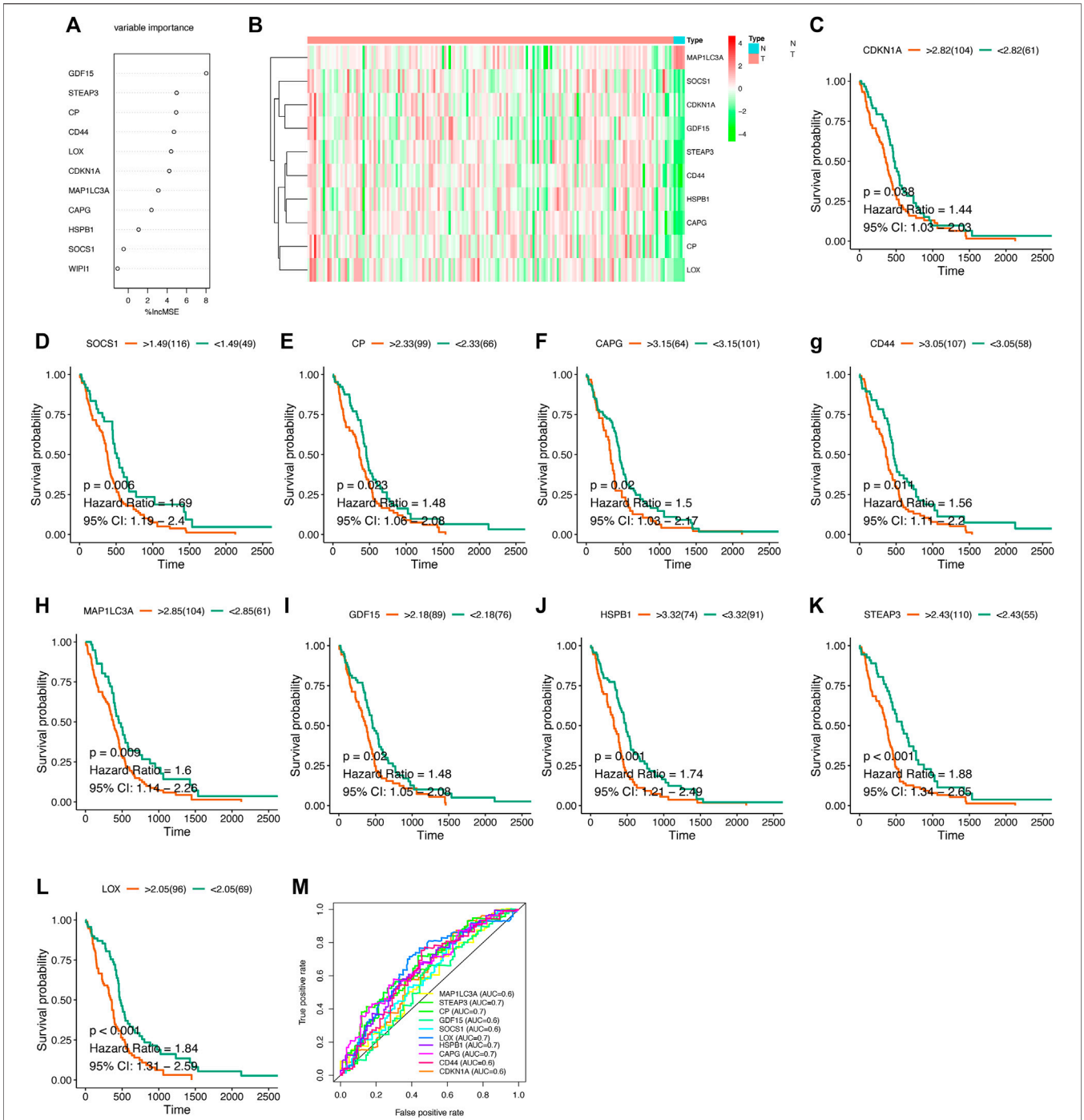

FIGURE 4 | Survival analysis of key genes **(A)** Random Forest screening for ten key genes **(B)** Heat map of expression of key genes in different groups **(C–M)** Kaplan-Meier survival curve and ROC curve.

(**Supplementary Table S2**). Consequently, 21 FRGs with significantly differential expressions were obtained.

3.1.2 Ferroptosis-Related Genes associated with Prognosis

After obtaining the differentially expressed FRGs, we wanted to verify whether these DEGs were associated with patient prognosis, which would have great clinical significance. So we further screened these FRGs for prognosis-related genes. Because the prognosis of GBM patients is usually poor, the identification of genes that indicate poor prognosis may facilitate the discovery of new therapeutic targets. Using Cox proportions for univariate survival analysis, 11 FRGs associated with prognosis ($p < 0.05$) were found and all of

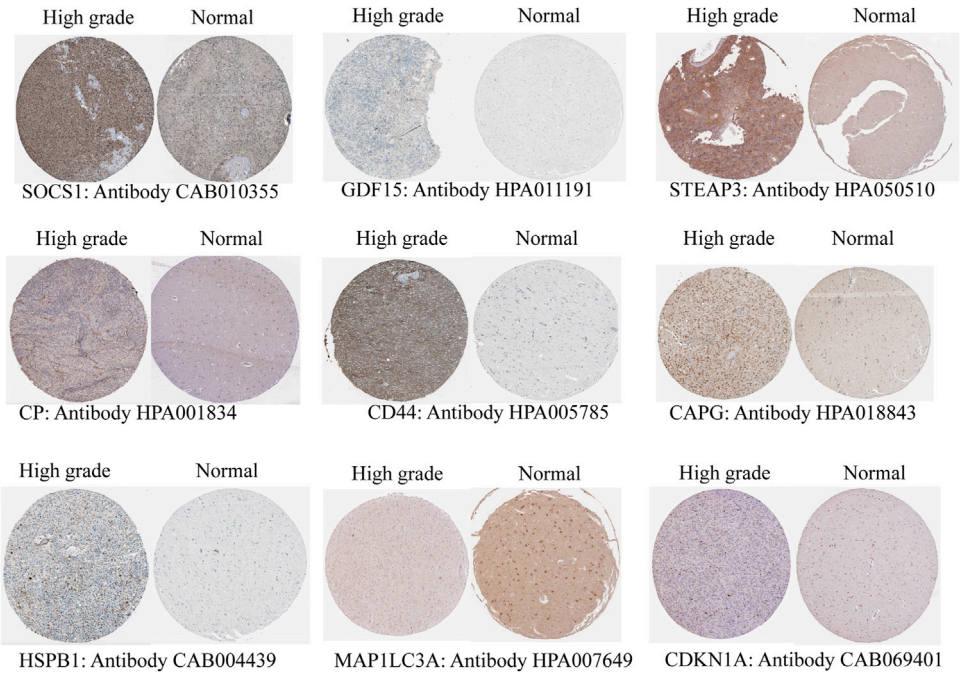

FIGURE 5 | Validation of protein expression by immunohistochemistry of the key genes from the Human Protein Atlas (HPA) database.

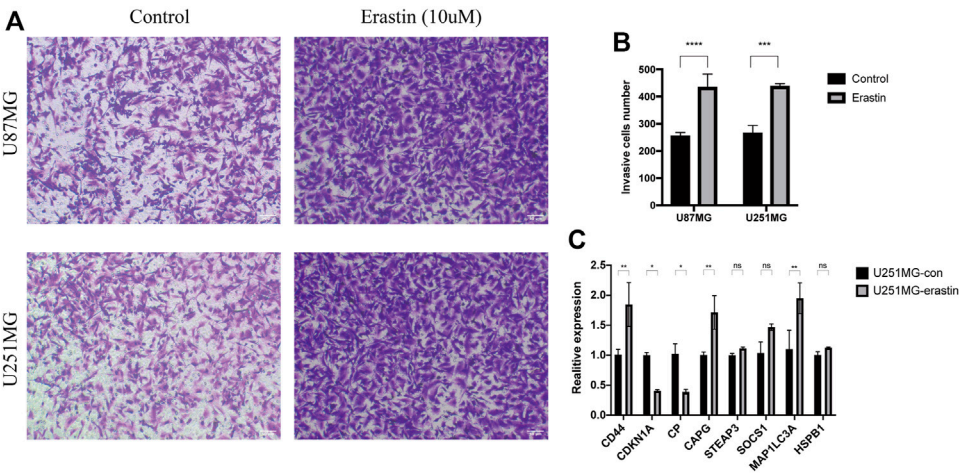

FIGURE 6 | Ferroptosis enhances glioblastoma cell migration **(A–B)** Light microscopic images and analysis of their data showed enhanced migratory ability of U251MG and U87MG cells treated with erastin (10 μm) compared to control **(C)** qPCR analysis showed that the expression of key genes is altered in the erastin (10 μm)-treated group compared to the control cells.

them indicated poor prognosis (HR > 1) (**Figure 3**). The gene WIPI1 was excluded by applying Random Forest to continue the screening (**Figure 4A**), then ten key genes (STEAP3, HSPB1, MAP1LC3A, SOCS1, LOX, CAPG, CP, GDF15, CDKN1A, and CD44) were screened and the heat map of expression was plotted in GBM versus normal brain tissue groups. MAP1LC3A was the only gene that high-expressed significantly in the normal brain tissue group (**Figure 4B**). According to genecards, the expression of MAP1LC3A was indeed suppressed in many tumor cell lines, suggesting that it may be involved in carcinogenesis (Stelzer et al., 2016). Subsequently, all ten key genes were divided into two groups based on the expression levels, and survival and prognosis were assessed by the Kaplan-Meier (KM) survival curves. All ten key genes (including MAP1LC3A) were identified to be at significant risk ($p < 0.05$), and higher

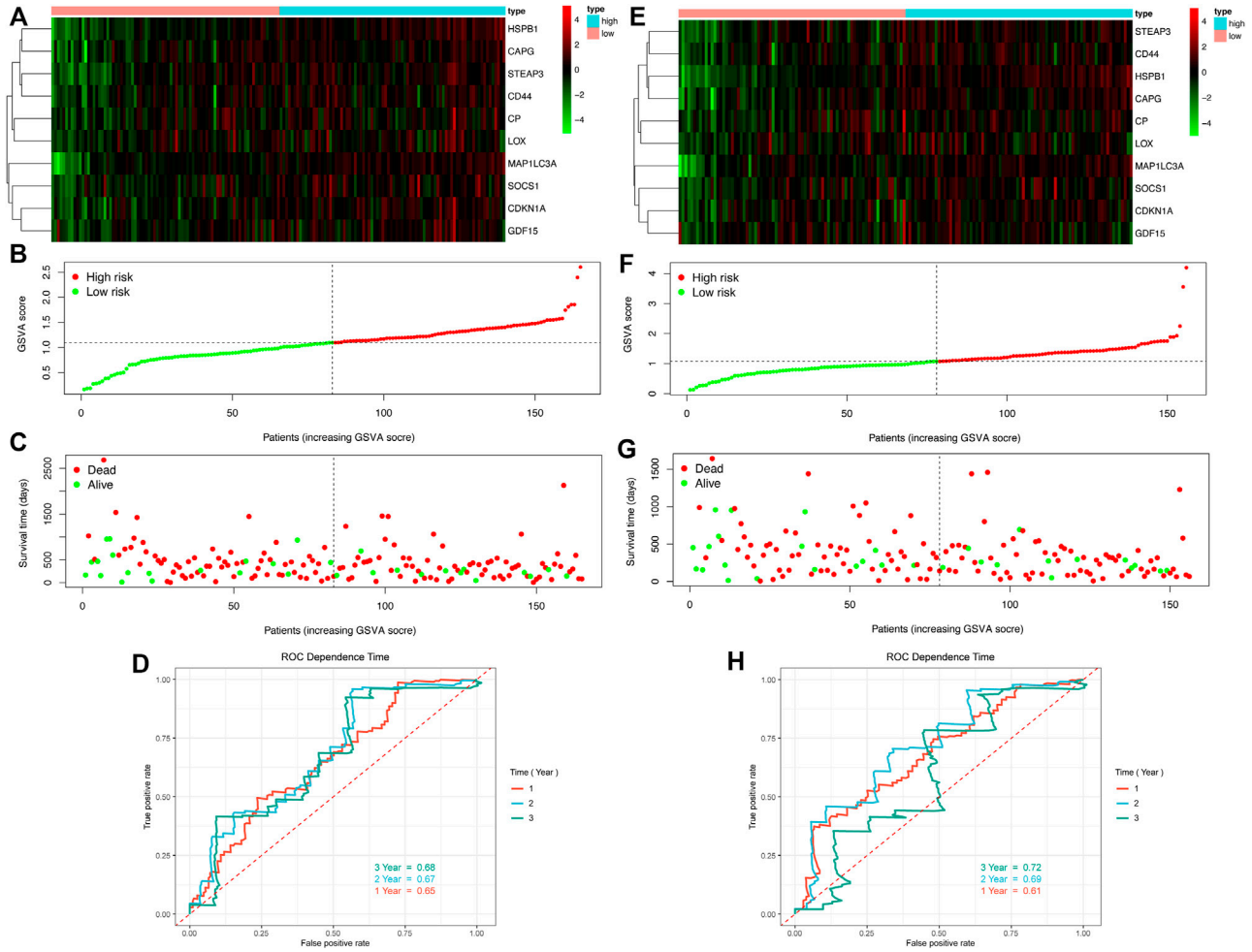

FIGURE 7 | Growth of GSVA score of GBM patients is associated with increased mortality and decreased survival time **(A–D)** OS **(E–H)** RFS **(A,E)** Heat maps of key genes expression profiles **(B–C,F–G)** Distribution of risk scores, patient survival times and status **(D,H)** ROC curves.

expression was associated with poorer prognosis (**Figure 4C** to 4L). The results of multi-gene ROC curve analysis showed that the area under the curve (AUC) is greater than 0.6 for all genes. The AUCs of STEAP3, CP, LOX, HSPB1, and CAPG were greater than 0.7. These results indicated that these ten key FRGs had good predictive performances (**Figure 4M**).

3.2 Protein Expression of Key Genes

To verify different protein expression encoded by the key genes in normal brain tissues and high-grade gliomas, immunohistochemistry analysis was obtained from the Human Protein Atlas (HPA) database (Uhlén et al., 2005). Nine of these key genes were included in the HPA database. STEAP3, HSPB1, SOCS1, CAPG, CP, GDF15, CDKN1A, and CD44 were highly expressed in high-grade gliomas compared with the normal brain tissue, and MAP1LC3A was highly expressed in the normal brain tissue (**Figure 5**). It was verified that the results of HPA are consistent with the results of our above transcriptome analysis.

3.3 Association of Ferroptosis With Cell Migration and Expression of Key Genes

To identify the relationship between ferroptosis and glioblastoma cell migration, we measured the migratory ability of glioblastoma cell lines (U251MG and U87MG) treated with the ferroptosis activator erastin using the transwell migration assay. The migratory ability of erastin-treated U251MG and U87MG cells was increased compared to control treatment (**Figures 6A,B**). The expression of several key genes was also examined by qPCR, which revealed significant changes in the expression of CD44, CDKN1A, CP, CAPG, and MAP1LC3A in erastin-treated U251MG and U87MG cells, with the upregulation expression of CD44, CAPG, and MAP1LC3A and the down-regulation of CDKN1A and CP (**Figure 6C**). These results suggest that ferroptosis enhances the migratory ability of glioblastoma cells and alters the expression of these key genes with poor prognosis.

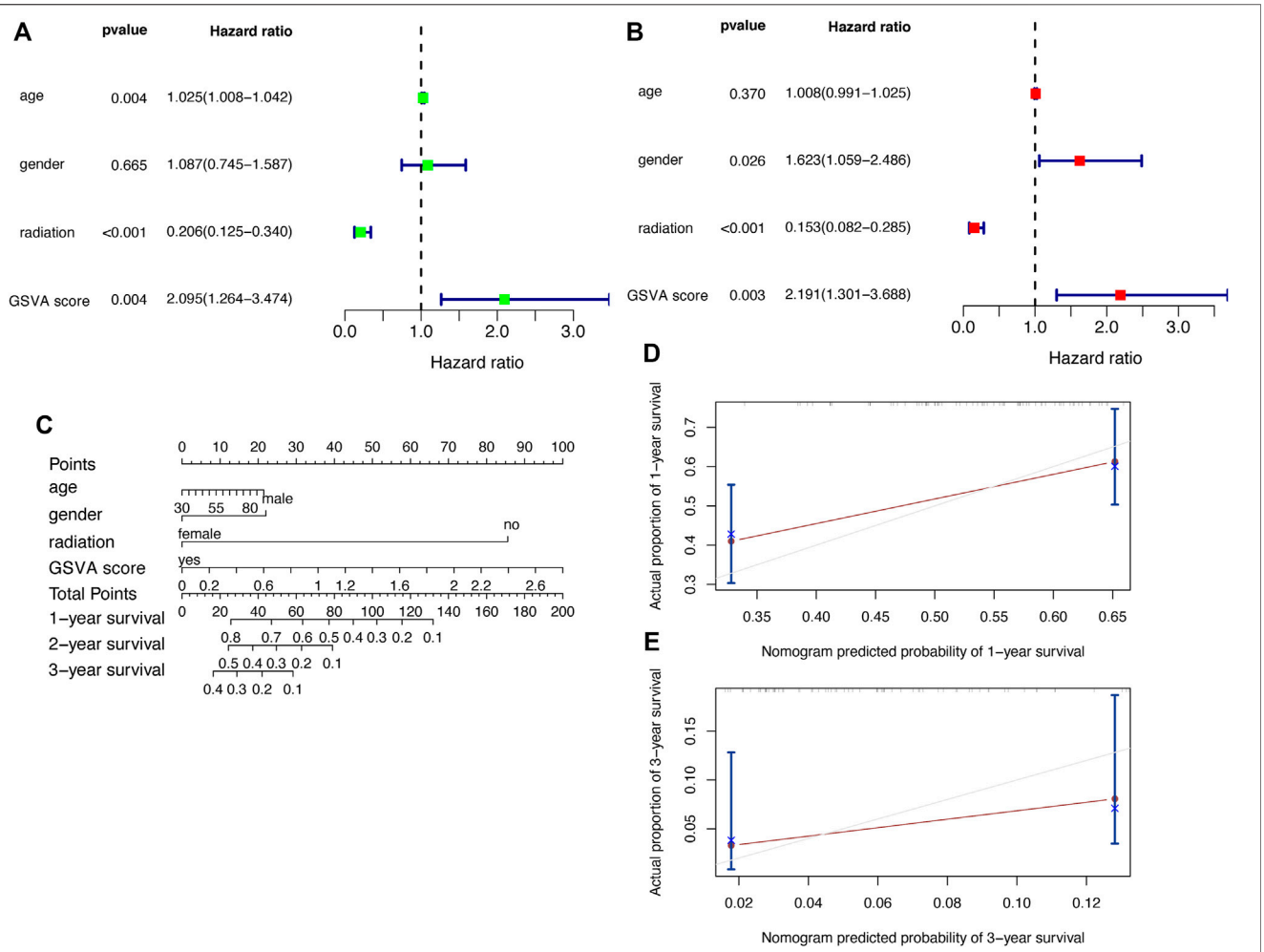

FIGURE 8 | Validation of the prognostic model with clinical factors **(A)** Univariate Cox regression analysis **(B)** Multivariate Cox regression analysis **(C)** Nomogram **(D,E)** Calibration curves.

3.4 Construction of Prognostic Model

3.4.1 Prognostic Modeling by GSVA

Following the confirmation of the prognosis-related single FRG, we constructed a prognostic model by integrating these ten genes, and the GSVA algorithm was used to calculate an enrichment score for each sample based on the key gene set, i.e., the GSVA score. Patients were divided into high- and low-risk groups based on the median GSVA score in overall survival (**Figures 7A–D**) and relapse-free survival (**Figures 7E–H**). Key gene heat maps were plotted separately (**Figures 7A,E**). Risk score, survival time and status of TCGA cohorts in OS were shown in **Figures 7B,C**, and those in RFS were illustrated in **Figures 7F,G**. The analysis showed that the mortality rose significantly with the increase of the GSVA score, and the ROC curve showed that the AUCs were all around 0.7, indicating good survival prediction of the model at one-, two- and three-year (**Figures 7D,H**).

3.4.2 Model Validation and Nomogram

After obtaining the above prognostic model, we need to verify its predictive power. We performed univariate (**Figure 8A**) and multivariate Cox analysis (**Figure 8B**), and the results showed that the GSVA score was an independent prognostic factor for GBM. To assist the clinicial decision-making process, we combined the GSVA score with clinical indicators (age, gender, and radiation) to construct a nomogram (**Figure 8C**), and the nomogram can predict the survival rate of GBM patients at one-, two- and three-year. The calibration curves (**Figures Figure8D,E**) indicate that this nomogram has strong predictive function.

3.5 Immune Microenvironment Analysis

3.5.1 Immune Cell Infiltration

We analysed the molecular mechanisms of these ten key genes from an immunological perspective. Tumor tissue contains not only tumor cells, but also immune cells. The immune cells that infiltrate tumors can profoundly affect the tumor development and anti-cancer therapy. Therefore, the quantification of immune cells is of extraordinary significance. We assessed the correlation between the prognostic model and the level of immune cell infiltration. The infiltration levels of 22 tumor immune cells in

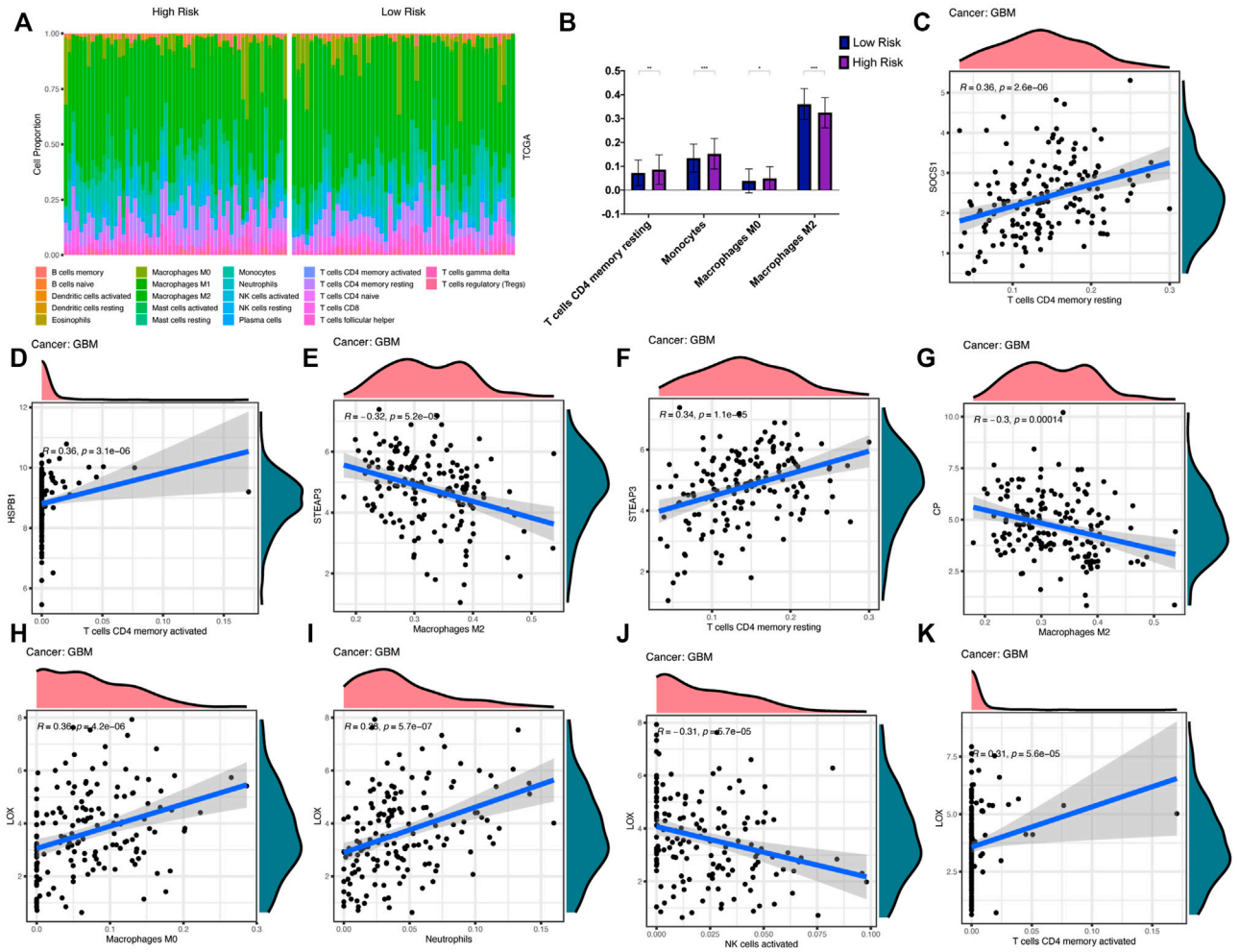

FIGURE 9 | Immune cell infiltration analysis **(A,B)** Infiltration differences of 22 immune cells in high- and low-risk groups in TCGA-GBM **(C–K)** Correlation curves show that infiltration levels of six immune cells are significantly correlated with key genes expression levels.

the TCGA-GBM datasets were calculated using the CIBERSORT website, and the differences of immune cell infiltration in the high- and low-risk groups in both datasets were demonstrated (**Figures 9A,B**). Correlation analysis showed that the infiltration levels of six immune cells were significantly correlated ($|r| > 0.3$, $p < 0.05$) with some key genes (**Figures 9C–K**). In particular, STEAP3 (R = −0.32, $p = 0.000052$) and CP (R = −0.3, $p = 0.00014$) were significantly negatively correlated with macrophages M2. LOX (R = −0.31, $p = 0.000057$) was significantly negatively correlated with NK cells activated. Therefore, these key genes were related to the development and prognosis of GBM.

3.5.2 Immunomodulation

In addition, the correlation between key gene expression and immunomodulators was also investigated. As shown in **Figure 10**, 23 types of immunoinhibitor have been analyzed (**Figure 10A**). Except for MAP1LC3A with a poor correlation, the remaining genes showed a strong correlation with immunoinhibitor, especially CAPG expression was significantly positively correlated with most of the immunoinhibitor. The correlation analysis of 42 immunostimulator (**Figure 10B**) showed that MAP1LC3A expression showed weak correlation with immunostimulator, while CAPG and CP showed significantly positive correlation. As shown in **Figure 10C**, 21 types of major histocompatibility complex (MHC) were analyzed. Human leukocyte antigen (HLA) is the expression product of the human MHC, which is the most complicated polymorphic system known in the human body (Norman et al., 2017). Notably, MHC is closely related to the immune response, immune regulation and the generation of certain pathological states in the body. CAPG unsurprisingly showed an extremely strong positive correlation. ESTIMATE is a tool for predicting tumor purity and the presence of infiltrating stromal and immune cells in the tumor (Yoshihara et al., 2013). The ESTIMATE algorithm generates four final scores: the stromal score (indicating the presence of stromal cells in the tumor tissue), the immune score (indicating the infiltration of immune cells in the tumor tissue), the ESTIMATE score, and

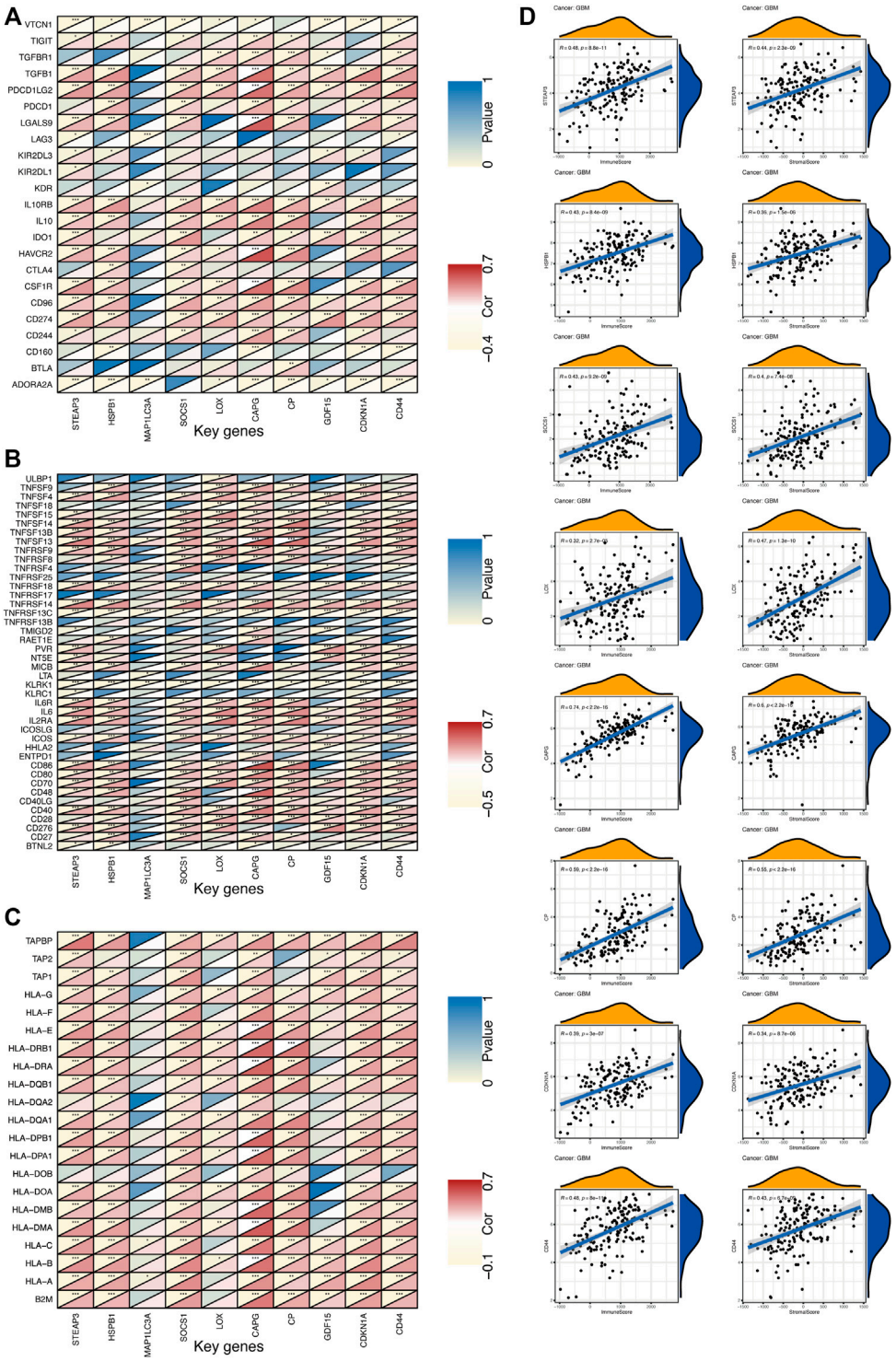

FIGURE 10 | The expression of key genes is correlated with GBM immunity **(A)** Heat map represents the correlation between immunoinhibitor and key gene expression in GBM. For each pair of genes, the triangles at the top left are colored to indicate the *p* values; the triangles at the bottom right are colored to indicate the Spearman correlation coefficients. $^{*}p < 0.05$; $^{**}p < 0.01$; $^{***}p < 0.001$ **(B)** Heat map represents the correlation between immunostimulator and key gene expression in GBM **(C)** Heat map represents the correlation between MHC molecules and key gene expression in GBM **(D)** The correlation between key genes and ESTIMATE scores in GBM.

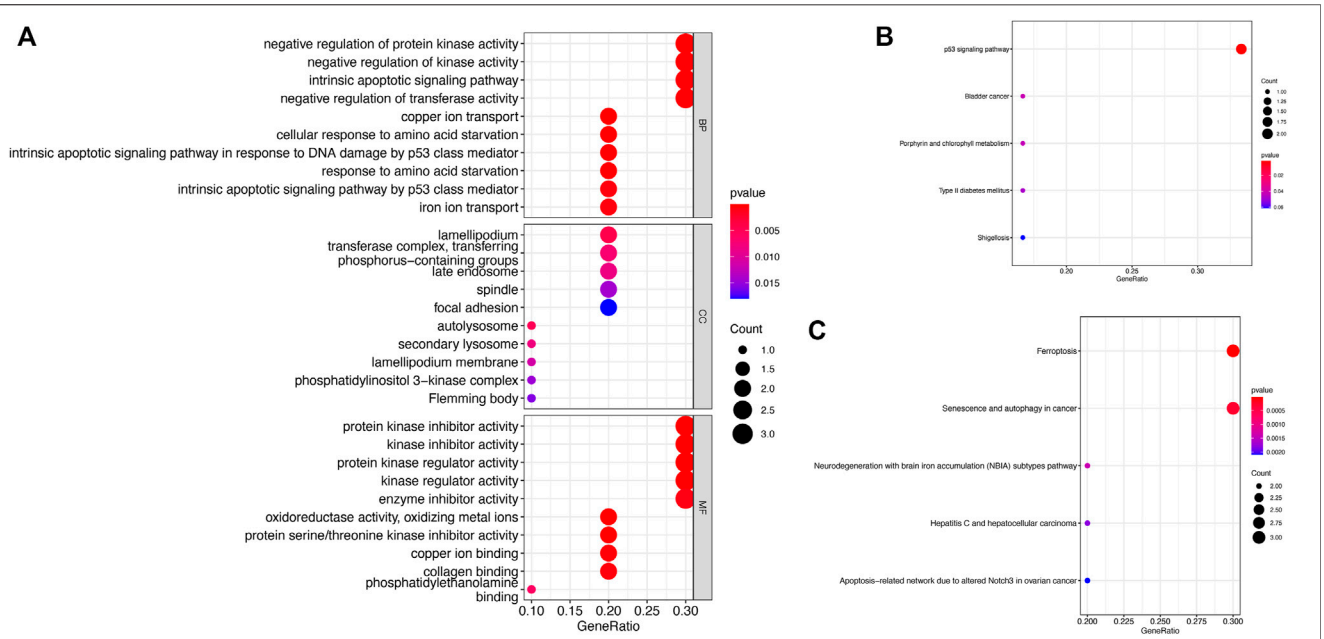

FIGURE 11 | Functional enrichment analysis of key genes **(A)** GO enrichment analysis **(B)** KEGG enrichment analysis **(C)** Wikipathway enrichment analysis.

the tumor purity. The results of ESTIMATE are summarized in **Figure 10D**. Remarkably, eight key genes (STEAP3, HSPB1, SOCS1, LOX, CAPG, CP, CDKN1A, and CD44) showed significant positive correlations with stromal score and immune score.

3.6 Functional Enrichment Analysis

We explored the molecular mechanisms of ten key genes in GBM from the perspective of biological function, and we performed GO, KEGG, and the wikipathway enrichment analysis (**Figure 11**). The GO enrichment analysis consisted of three parts (biological process, cellular components, molecular function), and the bubble plots for each gene showed the top 10 significantly enriched functional items (**Figure 11A**). The first four significant biological process (BP) items are 1) negative regulation of protein kinase activity, 2) negative regulation of kinase activity, 3) intrinsic apoptotic signaling pathway, and 4) negative regulation of transferase activity. We also found that the first three significant cellular components (CC) items are 1) lamellipodium, 2) transferase complex, transferring phosphorus-containing groups, and 3) late endosome. The enrichment analysis showed that the first three significant molecular function (MF) items are 1) protein kinase inhibitor activity, 2) kinase inhibitor activity, and 3) protein kinase regulator activity. The most significant pathway in the KEEG enrichment analysis is the p53 signaling pathway (**Figure 11B**), and the top two significant pathway items in the wikipathway enrichment analysis are 1) ferroptosis, and 2) senescence and autophagy in cancer (**Figure 11C**).

3.7 Single-Nucleotide Variant Analysis

We explored the molecular mechanisms of key genes from the perspective of gene mutations. The exploration of somatic mutations contributes to the understanding of tumor onset and development, and we can identify which mutations play an important role in the development of such kind of tumors, thus providing guidance on the pathogenesis and subsequent targeted treatment and prognosis of such tumors. We analyzed the SNV mutation data of ten key genes, among which six genes had different degrees of mutation (**Figure 12A**). Transition plots classified single-nucleotide variant (SNV) into six categories, and C > T mutations accounted for more than 50% of the total mutations among the six SNV mutations (**Figure 12B**). In a rainfall plot of the mutation distribution spectrum of the GBM samples, each dot indicated a mutation, and different colors of dots represented distinct SNV mutation types (**Figure 12C**). The mutation distribution and protein domain of key genes with higher mutation frequency were shown in **Figure 12D**. CP, CD44 and STEAP3 had the highest mutation frequency, and the most frequent mutation type was the missense mutation. The results showed that site mutations in these genes might play an important role in the prognosis of GBM. Mutations in these key genes are likely to make the gene replicate actively, which caused gene amplification.It is also possible that the gene will become more capable of synthesizing proteins, which will lead to high expression, resulting in a poor prognosis for the patient. Most importantly, gene amplification plays an important role in the activation of proto-oncogenes that cause cancer (George et al., 2008).

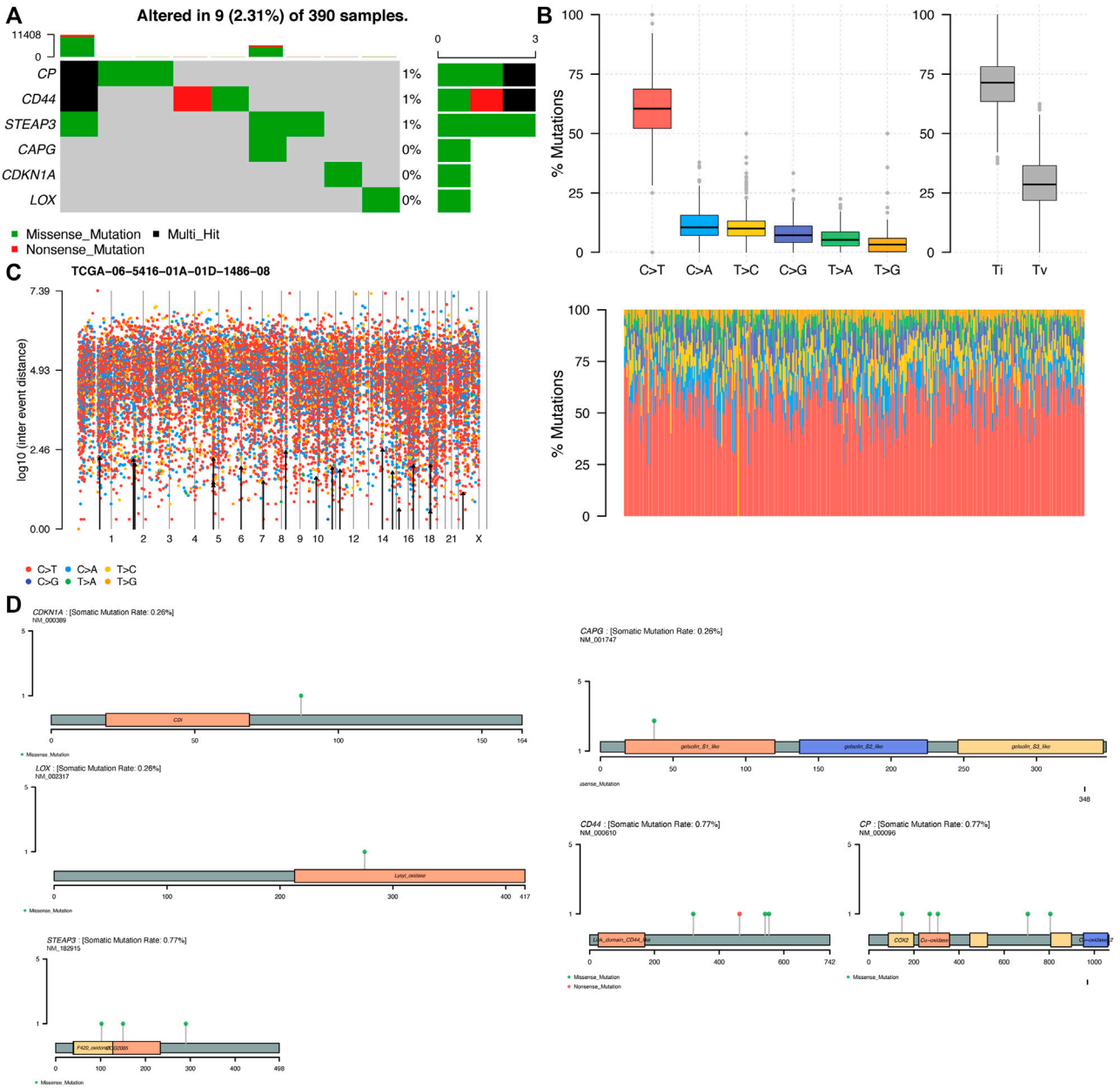

FIGURE 12 | Single-nucleotide variant (SNV) analysis **(A)** The key genes are sorted according to their mutation frequency, and different colors represent different mutation types **(B)** The transition plot shows the distribution of mutations in each sample in TCGA-GBM. The stacked bar plot (bottom) shows the mutation spectrum distribution **(C)** Rainfall plot of the mutation distribution spectrum of TCGA–06–5416–01A–01D–1486–08 **(D)** Distribution of mutations and protein domain of key genes with high mutation frequency. The main body of the image shows the protein structure with the structure name marked in the box and the lollipop indicates the mutation.

3.8 Correlation With Clinical Characteristics

We analysed the correlation between the expression of key genes and the risk levels of different patients from a clinical perspective, and we assessed the correlation of these key genes with clinical characteristics (IDH1, gender, and risk level). We divided the expression of key genes into high- and low-level groups according to their median values. The correlation between the gene expression and the clinical characteristics was analyzed, and a mosaic for each gene was plotted. Among these ten genes, GDF15 and LOX were significantly positively correlated with IDH1 and the risk level, and HSPB1 was negatively correlated with the gender ($p < 0.05$). CDKN1A, CAPG, and SOCS1 were weakly correlated with IDH1 and the risk level ($p > 0.05$, $|\text{residuals}| > 2$) (**Figure 13**), while the remaining genes had no correlation with any clinical characteristics (**Supplementary Figure S1**).

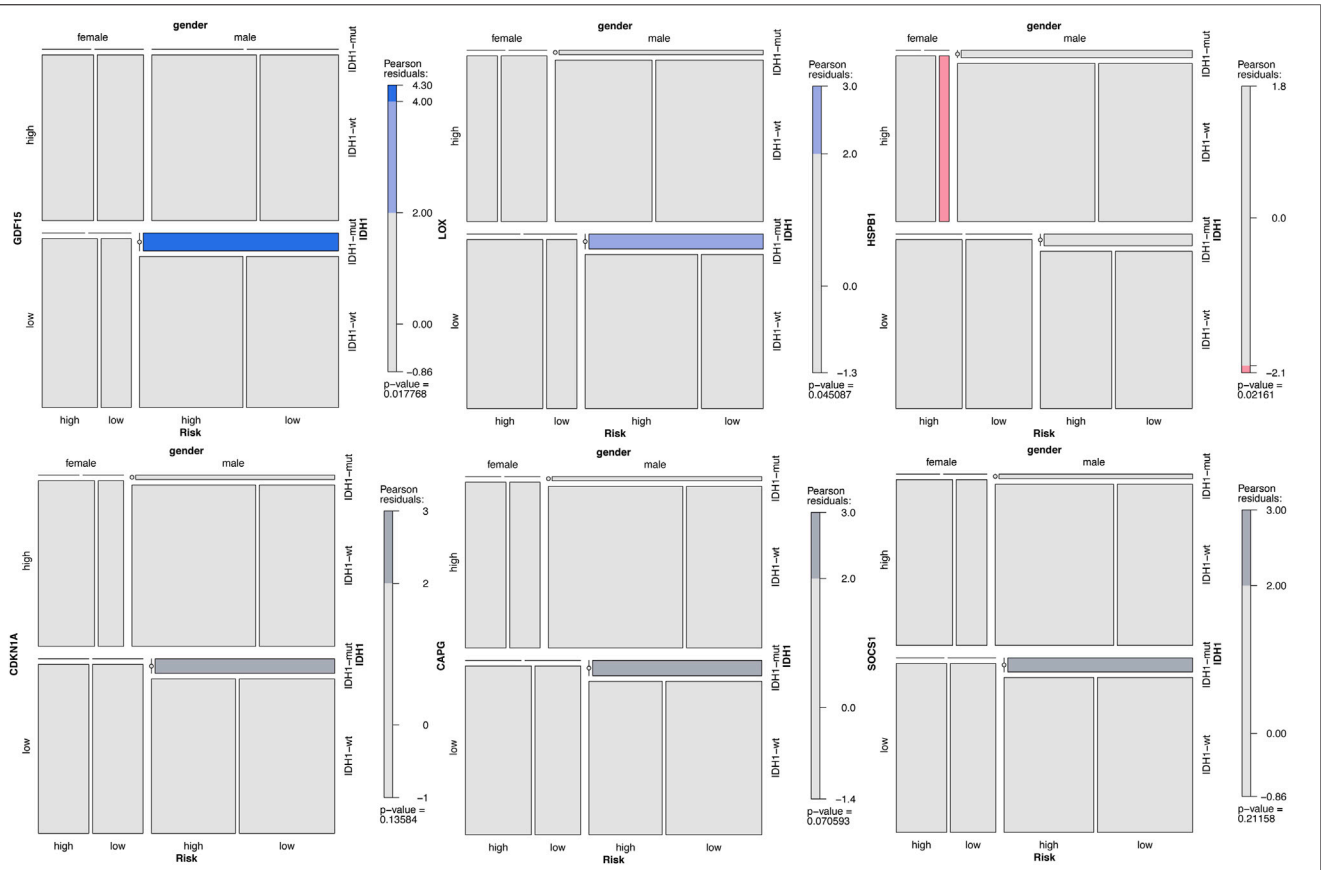

FIGURE 13 | Correlation analysis between the key genes and the GBM clinical characteristics. Note: The darker the color is, the stronger the correlation is. Blue indicates positive correlation, red expresses negative correlation, and grey has a weaker correlation.

3.9 Identification of Potential Therapeutic Drugs

To explore potential therapeutic drugs for GBM, three genes (CAPG, CP and CD44) with more significant results were selected from the key genes based on the above analysis, and performed Virtual Screening and Molecular Docking. The top ten small molecule compounds with the best docking scores to the three key genes were shown in **Table 1**, and the complete table of docking scores was shown in **Supplementary Table S3–S5**. The docking conformation and interaction force analysis of CAPG, CP, and CD44 with the better docking compounds were shown in **Figure 14**. According to the Drugbank (Berman et al., 2000), The drug DB09280, which has a good docking scores to both CAPG, CP, and CD44, is the FDA (Food and Drug Administration)-approved and commercialized drug Lumacaftor (brand name: Orkambi). In addition, DB14773 has a good binding affinity to both CAPG and CP (generic name: Lifirafenib).

4 DISCUSSION

In our study, 10 FRGs associated with IDH1 status and prognosis in GBM were identified using TCGA dataset, and their protein expression levels were validated. Transwell and qPCR results showed that ferroptosis promoted the migration of glioblastoma cells and affected the expression of key genes. Their biological functions were investigated by the GO, KEGG, and Wikipathway enrichment analysis. The results suggested that the key gene sets may be involved in the onset and development of GBM. These key genes with prognostic value were used to construct a prognostic model. The GSVA score was calculated for each sample using the GSVA algorithm, and the score was validated as an independent prognostic factor for GBM, and the nomogram constructed from this prognostic model had high predictive value. In addition, the analysis of immune infiltration, immunomodulators and ESTIMATE showed that the prognostic model and key genes were closely associated with immune-related factors and affected the development and prognosis of GBM. SNV analysis suggested that the mutations in the key genes might play an important role in the prognosis of GBM. Virtual Screening and Molecular Docking for potential therapeutic drugs were performed, which may provide assistance in the development of novel therapeutic chemicals for GBM.

GBM is one of the deadliest cancers worldwide. Although a great deal of research has been done in the last decade and current treatment modalities can extend the survival time and improve the quality of life to some extent, GBM remains an incurable and deadly

TABLE 1 | Top 10 compounds with the best docking score to CAPG, CP and CD44.

Gene Name	DrugBank_ID	Hydrogen acceptors	Hydrogen donors	Rotatable bonds	LogP	Molecular weight	TPSA	Affinity (kcal/mol)
CAPG	DB09280	8	2	5	4.4	.4	97.8	–8.3
	DB14773	8	2	3	3.7	478.4	89.1	–8.2
	DB01395	3	0	0	3.5	366.5	43.4	–8.2
	DB15345	8	1	5	1.1	451.5	79.8	–8.1
	DB08683	3	1	0	3.8	393.4	65.3	–8.1
	DB06925	7	2	3	4.9	422.4	80.9	–8
	DB04760	6	2	6	3.3	410.4	84	–7.9
	DB12012	8	1	4	3.3	455.4	80.2	–7.9
	DB03571	5	3	4	2.8	430.2	127	–7.8
	DB12886	5	2	5	4.9	402.4	53.6	–7.8
CP	DB06666	3	1	3	4.8	473.9	54.3	–10.1
	DB01940	7	4	7	4.1	474.5	125	–10.1
	DB09280	8	2	5	4.4	452.4	97.8	–10
	DB14773	8	2	3	3.7	478.4	89.1	–10
	DB06075	5	2	3	4.2	421.5	89.3	–9.7
	DB07514	5	2	2	3.7	397.5	84.1	–9.7
	DB12121	6	2	4	3.6	411.5	83.4	–9.6
	DB15308	4	2	3	3.9	388.4	83.1	–9.6
	DB07794	5	2	2	1.9	327.3	97.8	–9.5
	DB00820	4	1	1	2.3	389.4	74.9	–9.5
CD44	DB03583	7	4	3	1.8	441.5	135	–8.9
	DB02354	4	3	6	3.4	423.5	97.5	–8.8
	DB09280	8	2	5	4.4	452.4	97.8	–8.4
	DB00685	10	2	3	0.3	416.4	99.8	–8.3
	DB06850	4	4	7	1.5	385.5	111	–8.2
	DB07142	5	2	4	4.9	386.5	87	–8.2
	DB05470	7	2	4	2.5	404.3	102	–8.1
	DB05608	4	1	2	2.6	400.4	102	–8.1
	DB06858	4	4	7	2.5	413.6	111	–8.1
	DB08674	5	1	0	2.8	435.5	83.2	–8.1

disease, and patient survival rates are difficult to be improved (Daisy Precilla et al., 2021). Therefore, it is important to find new prognostic biomarkers and therapeutic targets for GBM.

The term ferroptosis was first coined in 2012 (Dixon et al., 2012), which means an iron-dependent regulatory cell death caused by excessive lipid peroxidation and subsequent cell membrane injury (Stockwell et al., 2017). Ferroptosis can be caused by exogenous or endogenous pathways (Tang and Kroemer, 2020). The exogenous pathway is initiated by inhibition of cell membrane transporters, such as cystine/glutamate transporters, or by activation of iron transporters, serum transferrin, and lactotransferrin. The endogenous pathway is activated by blocking intracellular antioxidant enzymes, such as glutathione peroxidase GPX4. All these mechanisms point to a common pathway, namely the formation of more reactive oxygen species (ROS). The ferroptosis pathway is a potential new target in oncology. In particular, cancer cells that are resistant to traditional therapies or have a high propensity to metastasize may be particularly susceptible to ferroptosis (Viswanathan et al., 2017; Tsoi et al., 2018), and this has opened up a new field of targeted therapeutic research.

In our study, 10 FRGs (STEAP3, HSPB1, MAP1LC3A, SOCS1, LOX, CAPG, CP, GDF15, CDKN1A, and CD44) associated with IDH1 status in GBM were identified, and survival analysis suggested that all these genes were of significant risk. Previous studies have suggested that MAP1LC3A is an autophagy-related gene and is a high-risk gene for GBM in risk modeling (Wang et al., 2019). Moreover, MAP1LC3C, which belongs to the same gene family, has significant prognostic and immunotherapeutic value in pan-cancer, especially low-grade gliomas (Zhang et al., 2022). CAPG is expressed at higher levels in glioma tissues than in normal tissues and is significantly associated with prognosis (Fu et al., 2019). SOCS1 is overexpressed in GBM and associated with chemotherapy sensitivity (Ventero et al., 2019), and the abnormal regulation of SOCS1 also enhances the resistance of GBM to ionizing radiation (Zhou et al., 2007). STEAP3 is associated with poor prognosis in GBM (Chen et al., 2021).

Ten key genes were constructed into a complex by GSVA and the GSVA score was calculated in all samples. This method is clearly different from gene signatures in other previous studies (Zhu et al., 2021), in which coefficients of genes were usually obtained from Cox regression analysis. Due to the limited sample size and tumor heterogeneity, we may never know the true

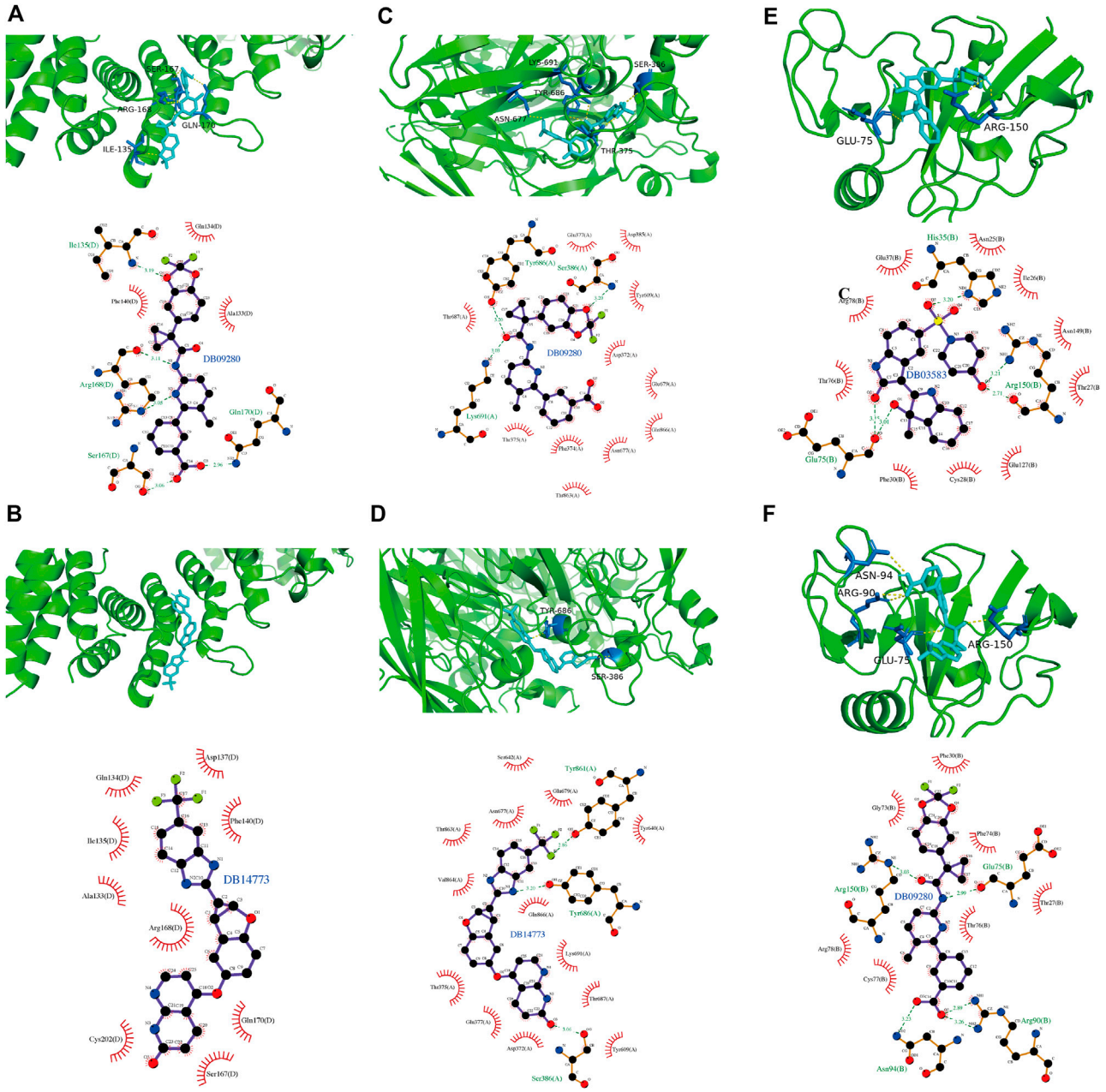

FIGURE 14 | The docking conformation and interaction force analysis of CAPG, CP and CD44 with their docked compounds. Analysis of the docking conformation and interaction forces of CAPG with DB09280 and DB14773 **(A,B)**, of CP with DB09280 and DB14773 **(C,D)** and of CD44 with DB03583 and DB09280 **(E,F)**. Top half: PyMol shows docking conformation and hydrogen bonding with the color symbols of cyan for small molecule, yellow dashed line for hydrogen bonding, and blue for amino acid residues forming hydrogen bond with small molecule. Bottom half: Ligplus force analysis, small molecule in the middle, surrounded by related protein amino acid residues, green dashed line representing for hydrogen bonding formed, green amino acid names representing for amino acid residues forming hydrogen bond.

coefficients of genes (Liu et al., 2020). Therefore, our study had advantages. The GSVA algorithm, a non-parametric, unsupervised method was used to score individual samples based on the key gene set (Hänzelmann et al., 2013), and numerous analysis showed that the GSVA score of the key gene set was an independent prognostic factor for OS and RFS in GBM patients. Based on this prognostic model we have also constructed a nomogram to guide clinicians in predicting the prognosis of patients and the calibration curve shows that this nomogram has a high predictive value.

Our results also revealed that the GSVA model was significantly associated with the level of immune cell infiltration, and the expression of SOCS1, STEAP3, HSPB1, CP, and LOX among the key genes was significantly associated with the level of

infiltration of some immune cells. Neutrophil-triggered ferroptosis has been shown to involve in necrosis in glioblastoma and to predict poor survival (Yee et al., 2020). Our study found that the level of LOX expression was significantly and positively correlated with the level of neutrophil infiltration. In addition, we found that all key genes except for MAP1LC3A showed correlation with immunoinhibitor, immunostimulator and MHC, especially CAPG showed positive and strong correlation with all three factors. Eight key genes were known to be significantly positively correlated with stromal score and immune score by the ESTIMATE algorithm. Thus, these key genes constitute a complex that may be involved in tumor immunity and guide future therapeutic strategies for immunotherapy. Moreover, key genes with higher levels of mutation may be highly expressed as a result of gene amplification as well as affecting patient prognosis and the development and progression of GBM. A nomogram was constructed using the GSVA score to predict the prognosis of patients for clinicians, and the calibration curve showed that this nomogram had a high predictive value. The correlation of each gene expression level with the GBM clinical characteristics (IDH1, gender, and risk level) was analyzed, and GDF15, LOX, and HSPB1 were found to be significantly correlated with the clinical characteristics.

Temozolomide has a high rate of resistance as a chemotherapeutic drug for glioma, and previous studies have shown that the sensitivity of temozolomide to tumor-killing can be increased by exogenous ROS (Yin et al., 2014). It has also been shown that erastin, one of the inducers of ferroptosis, can increase the sensitivity of temozolomide chemotherapy by inhibiting the Xc-amino acid para-transport system to achieve increased ROS and induce ferroptosis (Chen et al., 2015). The results of our Transwell and qPCR experiments combined with an analysis of the available literature led us to conjecture that the drug combination might be more effective than the ferroptosis activitor erastin alone. Moreover, all key genes that we identified in our study suggested a poor prognosis for GBM patients, therefore, we selected three key genes with significant results (CAPG, CP, and CD44) for Virtual Screening and Molecular Docking, and identified three groups of small molecule compounds as potential therapeutic drugs. According to the Drugbank (Wishart et al., 2018), the drug DB09280 we identified, is the FDA-approved and commercialized drug Lumacaftor (Brand names: Orkambi), which is used for the treatment of Cystic Fibrosis (CF) in patients aged 6 years and older. The drug involved CTFR (Cystic fibrosis transmembrane conductance regulator), and it has also been shown that the activation of the CFTR involved in this drug inhibits the proliferation, migration and invasion of GBM cells by suppressing JAK2/STAT3 signaling (Zhong et al., 2019). However, according to our results, the drug may be able to treat GBM through the pathway of CAPG, CP and CD44, and further studies *in vivo* will be needed.

In addition, the functional enrichment analysis showed that the key gene set was significantly involved in the p53 signaling pathway, senescence and autophagy in cancer, and in the negative regulation of protein kinase activity. Previous studies have suggested that the p53 protein and its cellular pathways mediate tumor suppression through an informed, regulated, and integrated response to the environmental perturbations that lead to cell death or maintain cellular homeostasis (Levine, 2020). Inactivation of TP53 (Tumor Protein p53) is the most common mutation in sporadic human cancers because the TP53 gene encodes a transcription factor that is an important barrier to carcinogenesis, which also suggests a strong correlation with p53 function during tumorigenesis and may be associated with the occurrence of the glioma (Kandoth et al., 2013). Autophagy is a lysosomal degradation process that is critical for cellular homeostasis and adaptation to stress. There is growing evidence that autophagy declines with age. The individuals with impaired autophagy are susceptible to age-related diseases, and the stimulation interventions of autophagy tend to promote longevity (Leidal et al., 2018). It is suggested that the key genes may be involved in the onset and development of GBM through these pathways. However, further studies are needed to investigate and validate the functions of these genes.

5 CONCLUSION

In conclusion, our study established a ferroptosis-related prognostic model for GBM patients based on the screened ten key genes by a different modeling method from previous study, the GSVA algorithm. The nomogram was also established to assist clinicians in decision-making. The molecular mechanisms were investigated by several methods including cell biology experiments, functional enrichment analysis, immune cell infiltration analysis, immune-related factors analysis, ESTIMATE and SNV analysis. With the support of these evidences, the key gene set might be involved in the development and onset of GBM. Three groups of potential therapeutic drugs were identified through Virtual Screening and Molecular Docking. These results bring light to the diagnosis and therapy of GBM.

DATA AVAILABILITY STATEMENT

The original contributions presented in the study are included in the article/**Supplementary Material**, further inquiries can be directed to the corresponding authors.

AUTHOR CONTRIBUTIONS

Conceptualization, YB and XZ; methodology, XZ; software, XZ; validation, YB, YW, and SJ; formal analysis, XZ and SJ; investigation, GL, KL, SL, SZ, TL, LL, LR, ST, and NB; resources, XZ and SJ; data curation, XZ; original draft preparation, XZ; review and editing, XZ, YB, and YW; visualization, XZ; supervision, YB and YW; project administration, XZ, YB, and YW; funding acquisition, YB and XS. All authors have read and agreed to the published version of the manuscript.

FUNDING

This study was funded by the Liaoning Provincial Natural Science Foundation (2020-MS-155), China Medical University novel coronavirus pneumonia prevention and control research project (2020-12-11), Shenyang Planning Foundation for Science and Technology (21-173-9-38), the first batch of medical education scientific research project of China Medical University for the 14th Five-Year Plan (YDJK2021011), the Scientific Research Funding Project of Education Department of Liaoning Province (JCZR2020010) and National Science Foundation of China (72074104).

SUPPLEMENTARY MATERIAL

The Supplementary Material for this article can be found online at: https://www.frontiersin.org/articles/10.3389/fphar.2022.898679/full#supplementary-material

REFERENCES

Agnihotri, S., Aldape, K. D., and Zadeh, G. (2014). Isocitrate Dehydrogenase Status and Molecular Subclasses of Glioma and Glioblastoma. *Neurosurg. Focus* 37 (6), E13. doi:10.3171/2014.9.FOCUS14505

Berman, H. M., Westbrook, J., Feng, Z., Gilliland, G., Bhat, T. N., Weissig, H., et al. (2000). The Protein Data Bank. *Nucleic Acids Res.* 28 (1), 235–242. doi:10.1093/nar/28.1.235

Cancer Genome Atlas Research, N., Brat, D. J., Verhaak, R. G., Aldape, K. D., Yung, W. K., Salama, S. R., et al. (2015). Comprehensive, Integrative Genomic Analysis of Diffuse Lower-Grade Gliomas. *N. Engl. J. Med.* 372 (26), 2481–2498. doi:10.1056/NEJMoa1402121

Chai, R. C., Wu, F., Wang, Q. X., Zhang, S., Zhang, K. N., Liu, Y. Q., et al. (2019). m6A RNA Methylation Regulators Contribute to Malignant Progression and Have Clinical Prognostic Impact in Gliomas)A RNA Methylation Regulators Contribute to Malignant Progression and Have Clinical Prognostic Impact in Gliomas. *Aging (Albany NY)* 11 (4), 1204–1225. doi:10.18632/aging.101829

Chen, H., Xu, C., Yu, Q., Zhong, C., Peng, Y., Chen, J., et al. (2021). Comprehensive Landscape of STEAP Family Functions and Prognostic Prediction Value in Glioblastoma. *J. Cel Physiol* 236 (4), 2988–3000. doi:10.1002/jcp.30060

Chen, L., Li, X., Liu, L., Yu, B., Xue, Y., and Liu, Y. (2015). Erastin Sensitizes Glioblastoma Cells to Temozolomide by Restraining xCT and Cystathionine-γ-Lyase Function. *Oncol. Rep.* 33 (3), 1465–1474. doi:10.3892/or.2015.3712

Daisy Precilla, S., Kuduvalli, S. S., and Thirugnanasambandhar Sivasubramanian, A. (2021). Disentangling the Therapeutic Tactics in GBM: From Bench to Bedside and beyond. *Cell Biol Int* 45 (1), 18–53. doi:10.1002/cbin.11484

Dixon, S. J., Lemberg, K. M., Lamprecht, M. R., Skouta, R., Zaitsev, E. M., Gleason, C. E., et al. (2012). Ferroptosis: an Iron-dependent Form of Nonapoptotic Cell Death. *Cell* 149 (5), 1060–1072. doi:10.1016/j.cell.2012.03.042

Eswar, N., Webb, B., Marti-Renom, M. A., Madhusudhan, M. S., Eramian, D., Shen, M. Y., et al. (2007). Comparative Protein Structure Modeling Using MODELLER. *Curr. Protoc. Protein Sci.* **Chapter 2**Unit 2 9. doi:10.1002/0471140864.ps0209s50

Fang, X., Wang, H., Han, D., Xie, E., Yang, X., Wei, J., et al. (2019). Ferroptosis as a Target for protection against Cardiomyopathy. *Proc. Natl. Acad. Sci. U S A.* 116 (7), 2672–2680. doi:10.1073/pnas.1821022116

Fu, Q., Shaya, M., Li, S., Kugeluke, Y., Dilimulati, Y., Liu, B., et al. (2019). Analysis of Clinical Characteristics of Macrophage Capping Protein (CAPG) Gene Expressed in Glioma Based on TCGA Data and Clinical Experiments. *Oncol. Lett.* 18 (2), 1344–1350. doi:10.3892/ol.2019.10396

George, R. E., Sanda, T., Hanna, M., Fröhling, S., Luther, W., Zhang, J., et al. (2008). Activating Mutations in ALK Provide a Therapeutic Target in Neuroblastoma. *Nature* 455 (7215), 975–978. doi:10.1038/nature07397

Goldman, M. J., Craft, B., Hastie, M., Repečka, K., McDade, F., Kamath, A., et al. (2020). Visualizing and Interpreting Cancer Genomics Data via the Xena Platform. *Nat. Biotechnol.* 38 (6), 675–678. doi:10.1038/s41587-020-0546-8

Hänzelmann, S., Castelo, R., and Guinney, J. (2013). GSVA: Gene Set Variation Analysis for Microarray and RNA-Seq Data. *BMC Bioinformatics* 14, 7. doi:10.1186/1471-2105-14-7

Pruim, R., Kaplan, D. T., and Horton, N. J. (2017). The Mosaic Package: Helping Students to 'Think with Data' Using R. *R. J.* 9 (1), 77–102. doi:10.32614/RJ-2017-024

Jiang, T., Mao, Y., Ma, W., Mao, Q., You, Y., Yang, X., et al. (2016). CGCG Clinical Practice Guidelines for the Management of Adult Diffuse Gliomas. *Cancer Lett.* 375 (2), 263–273. doi:10.1016/j.canlet.2016.01.024

Jiang, X., Stockwell, B. R., and Conrad, M. (2021). Ferroptosis: Mechanisms, Biology and Role in Disease. *Nat. Rev. Mol. Cel Biol* 22 (4), 266–282. doi:10.1038/s41580-020-00324-8

Kandoth, C., McLellan, M. D., Vandin, F., Ye, K., Niu, B., Lu, C., et al. (2013). Mutational Landscape and Significance across 12 Major Cancer Types. *Nature* 502 (7471), 333–339. doi:10.1038/nature12634

Leidal, A. M., Levine, B., and Debnath, J. (2018). Autophagy and the Cell Biology of Age-Related Disease. *Nat. Cel Biol* 20 (12), 1338–1348. doi:10.1038/s41556-018-0235-8

Levine, A. J. (2020). p53: 800 Million Years of Evolution and 40 Years of Discovery. *Nat. Rev. Cancer* 20 (8), 471–480. doi:10.1038/s41568-020-0262-1

Liang, J. Y., Wang, D. S., Lin, H. C., Chen, X. X., Yang, H., Zheng, Y., et al. (2020). A Novel Ferroptosis-Related Gene Signature for Overall Survival Prediction in Patients with Hepatocellular Carcinoma. *Int. J. Biol. Sci.* 16 (13), 2430–2441. doi:10.7150/ijbs.45050

Liberzon, A., Birger, C., Thorvaldsdóttir, H., Ghandi, M., Mesirov, J. P., and Tamayo, P. (2015). The Molecular Signatures Database (MSigDB) Hallmark Gene Set Collection. *Cell Syst* 1 (6), 417–425. doi:10.1016/j.cels.2015.12.004

Liu, C., Li, X., Shao, H., and Li, D. (2020). Identification and Validation of Two Lung Adenocarcinoma-Development Characteristic Gene Sets for Diagnosing Lung Adenocarcinoma and Predicting Prognosis. *Front. Genet.* 11, 565206. doi:10.3389/fgene.2020.565206

Louis, D. N., Perry, A., Reifenberger, G., von Deimling, A., Figarella-Branger, D., Cavenee, W. K., et al. (2016). The 2016 World Health Organization Classification of Tumors of the Central Nervous System: a Summary. *Acta Neuropathol.* 131 (6), 803–820. doi:10.1007/s00401-016-1545-1

Mayakonda, A., Lin, D. C., Assenov, Y., Plass, C., and Koeffler, H. P. (2018). Maftools: Efficient and Comprehensive Analysis of Somatic Variants in Cancer. *Genome Res.* 28 (11), 1747–1756. doi:10.1101/gr.239244.118

Norman, P. J., Norberg, S. J., Guethlein, L. A., Nemat-Gorgani, N., Royce, T., Wroblewski, E. E., et al. (2017). Sequences of 95 Human MHC Haplotypes Reveal Extreme Coding Variation in Genes Other Than Highly Polymorphic HLA Class I and II. *Genome Res.* 27 (5), 813–823. doi:10.1101/gr.213538.116

Ricard, D., Idbaih, A., Ducray, F., Lahutte, M., Hoang-Xuan, K., and Delattre, J. Y. (2012). Primary Brain Tumours in Adults. *Lancet* 379 (9830), 1984–1996. doi:10.1016/S0140-6736(11)61346-9

Ritchie, M. E., Phipson, B., Wu, D., Hu, Y., Law, C. W., Shi, W., et al. (2015). Limma powers Differential Expression Analyses for RNA-Sequencing and Microarray Studies. *Nucleic Acids Res.* 43 (7), e47. doi:10.1093/nar/gkv007

Ru, B., Wong, C. N., Tong, Y., Zhong, J. Y., Zhong, S. S. W., Wu, W. C., et al. (2019). TISIDB: an Integrated Repository portal for Tumor-Immune System Interactions. *Bioinformatics* 35 (20), 4200–4202. doi:10.1093/bioinformatics/btz210

Spandidos, A., Wang, X., Wang, H., and Seed, B. (2009). PrimerBank: a Resource of Human and Mouse PCR Primer Pairs for Gene Expression Detection and Quantification. *Nucleic Acids Res.* 38 (Suppl. 1_1), D792–D799. doi:10.1093/nar/gkp1005

Stelzer, G., Rosen, N., Plaschkes, I., Zimmerman, S., Twik, M., Fishilevich, S., et al. (2016). The GeneCards Suite: From Gene Data Mining to Disease Genome Sequence Analyses. *Curr. Protoc. Bioinformatics* 54, 1–33. doi:10.1002/cpbi.5

Stockwell, B. R., Friedmann Angeli, J. P., Bayir, H., Bush, A. I., Conrad, M., Dixon, S. J., et al. (2017). Ferroptosis: A Regulated Cell Death Nexus Linking Metabolism, Redox Biology, and Disease. *Cell* 171 (2), 273–285. doi:10.1016/j.cell.2017.09.021

Tang, D., and Kroemer, G. (2020). Ferroptosis. *Curr. Biol.* 30 (21), R1292–R1297. doi:10.1016/j.cub.2020.09.068

Tsoi, J., Robert, L., Paraiso, K., Galvan, C., Sheu, K. M., Lay, J., et al. (2018). Multi-stage Differentiation Defines Melanoma Subtypes with Differential Vulnerability to Drug-Induced Iron-dependent Oxidative Stress. *Cancer Cell* 33 (5), 890–e5. doi:10.1016/j.ccell.2018.03.017

Uhlén, M., Björling, E., Agaton, C., Szigyarto, C. A., Amini, B., Andersen, E., et al. (2005). A Human Protein Atlas for normal and Cancer Tissues Based on Antibody Proteomics. *Mol. Cel Proteomics* 4 (12), 1920–1932. doi:10.1074/mcp.M500279-MCP200

Ventero, M. P., Fuentes-Baile, M., Quereda, C., Perez-Valeciano, E., Alenda, C., Garcia-Morales, P., et al. (2019). Radiotherapy Resistance Acquisition in Glioblastoma. Role of SOCS1 and SOCS3. *PLoS One* 14 (2), e0212581. doi:10.1371/journal.pone.0212581

Viswanathan, V. S., Ryan, M. J., Dhruv, H. D., Gill, S., Eichhoff, O. M., Seashore-Ludlow, B., et al. (2017). Dependency of a Therapy-Resistant State of Cancer Cells on a Lipid Peroxidase Pathway. *Nature* 547 (7664), 453–457. doi:10.1038/nature23007

Wang, Z., Gao, L., Guo, X., Feng, C., Lian, W., Deng, K., et al. (2019). Development and Validation of a Nomogram with an Autophagy-Related Gene Signature for Predicting Survival in Patients with Glioblastoma. *Aging (Albany NY)* 11 (24), 12246–12269. doi:10.18632/aging.102566

Wickham, H. (2016). *ggplot2: Elegant Graphics for Data Analysis*. New York: Springer-Verlag.

Liaw, A., and Wiener, M. (2002). Classification and Regression by randomForest. *R. News* 2 (3), 18–22.

Wishart, D. S., Feunang, Y. D., Guo, A. C., Lo, E. J., Marcu, A., Grant, J. R., et al. (2018). DrugBank 5.0: a Major Update to the DrugBank Database for 2018. *Nucleic Acids Res.* 46 (D1), D1074–D1082. doi:10.1093/nar/gkx1037

Yan, H., Parsons, D. W., Jin, G., McLendon, R., Rasheed, B. A., Yuan, W., et al. (2009). IDH1 and IDH2 Mutations in Gliomas. *N. Engl. J. Med.* 360 (8), 765–773. doi:10.1056/NEJMoa0808710

Yee, P. P., Wei, Y., Kim, S. Y., Lu, T., Chih, S. Y., Lawson, C., et al. (2020). Neutrophil-induced Ferroptosis Promotes Tumor Necrosis in Glioblastoma Progression. *Nat. Commun.* 11 (1), 5424. doi:10.1038/s41467-020-19193-y

Yin, H., Zhou, Y., Wen, C., Zhou, C., Zhang, W., Hu, X., et al. (2014). Curcumin Sensitizes Glioblastoma to Temozolomide by Simultaneously Generating ROS and Disrupting AKT/mTOR Signaling. *Oncol. Rep.* 32 (4), 1610–1616. doi:10.3892/or.2014.3342

Yoshihara, K., Shahmoradgoli, M., Martínez, E., Vegesna, R., Kim, H., Torres-Garcia, W., et al. (2013). Inferring Tumour Purity and Stromal and Immune Cell Admixture from Expression Data. *Nat. Commun.* 4, 2612. doi:10.1038/ncomms3612

Yu, G., Wang, L. G., Han, Y., and He, Q. Y. (2012). clusterProfiler: an R Package for Comparing Biological Themes Among Gene Clusters. *OMICS* 16 (5), 284–287. doi:10.1089/omi.2011.0118

Zhang, X., Li, K., Zhong, S., Liu, S., Liu, T., Li, L., et al. (2022). Immunotherapeutic Value of MAP1LC3C and its Candidate FDA-Approved Drugs Identified by Pan-Cancer Analysis, Virtual Screening and Sensitivity Analysis. *Front. Pharmacol.* 13, 863856. doi:10.3389/fphar.2022.863856

Zhong, X., Chen, H. Q., Yang, X. L., Wang, Q., Chen, W., and Li, C. (2019). CFTR Activation Suppresses Glioblastoma Cell Proliferation, Migration and Invasion. *Biochem. Biophys. Res. Commun.* 508 (4), 1279–1285. doi:10.1016/j.bbrc.2018.12.080

Zhou, H., Miki, R., Eeva, M., Fike, F. M., Seligson, D., Yang, L., et al. (2007). Reciprocal Regulation of SOCS 1 and SOCS3 Enhances Resistance to Ionizing Radiation in Glioblastoma Multiforme. *Clin. Cancer Res.* 13 (8), 2344–2353. doi:10.1158/1078-0432.CCR-06-2303

Zhou, N., and Bao, J. (2020). FerrDb: a Manually Curated Resource for Regulators and Markers of Ferroptosis and Ferroptosis-Disease Associations. *Database (Oxford)* 2020, baaa021. doi:10.1093/database/baaa021

Zhu, X., Zhou, Y., Ou, Y., Cheng, Z., Han, D., Chu, Z., et al. (2021). Characterization of Ferroptosis Signature to Evaluate the Predict Prognosis and Immunotherapy in Glioblastoma. *Aging (Albany NY)* 13, 17655-17672. doi:10.18632/aging.203257

Zhuo, S., Chen, Z., Yang, Y., Zhang, J., Tang, J., and Yang, K. (2020). Clinical and Biological Significances of a Ferroptosis-Related Gene Signature in Glioma. *Front. Oncol.* 10, 590861. doi:10.3389/fonc.2020.590861

Conflict of Interest: The authors declare that the research was conducted in the absence of any commercial or financial relationships that could be construed as a potential conflict of interest.

Publisher's Note: All claims expressed in this article are solely those of the authors and do not necessarily represent those of their affiliated organizations, or those of the publisher, the editors and the reviewers. Any product that may be evaluated in this article, or claim that may be made by its manufacturer, is not guaranteed or endorsed by the publisher.

frontiers | Frontiers in Oncology

ORIGINAL RESEARCH
published: 09 May 2022
doi: 10.3389/fonc.2022.899402

Andrographolide Inhibits ER-Positive Breast Cancer Growth and Enhances Fulvestrant Efficacy *via* ROS-FOXM1-ER-α Axis

*Tong Xu†, Yanyu Jiang†, Shuying Yuan†, Li Zhang, Xihui Chen, Weili Zhao, Lili Cai, Biying Xiao and Lijun Jia**

Cancer Institute, Longhua Hospital, Shanghai University of Traditional Chinese Medicine, Shanghai, China

Estrogen receptor (ER)-positive breast cancer is the main subtype of breast cancer (BRCA) with high incidence and mortality. Andrographolide (AD), a major active component derived from the traditional Chinese medicine *Andrographis paniculate*, has substantial anti-cancer effect in various tumors. However, the antitumor efficacy and the underlying molecular mechanisms of AD on ER-positive breast cancer are poorly understood. In the present study, we demonstrated that andrographolide (AD) significantly inhibited the growth of ER-positive breast cancer cells. Mechanistically, AD suppressed estrogen receptor 1 (*ESR1*, encodes ER-α) transcription to inhibit tumor growth. Further studies revealed that AD induced ROS production to down-regulate FOXM1-ER-α axis. Conversely, inhibiting ROS production with N-acetylcysteine (NAC) elevated AD-decreased ER-α expression, which could be alleviated by FOXM1 knockdown. In addition, AD in combination with fulvestrant (FUL) synergistically down-regulated ER-α expression to inhibit ER-positive breast cancer both *in vitro* and *in vivo*. These findings collectively indicate that AD suppresses *ESR1* transcription through ROS-FOXM1 axis to inhibit ER-positive breast cancer growth and suggest that AD might be a potential therapeutic agent and fulvestrant sensitizer for ER-positive breast cancer treatment.

Keywords: andrographolide, breast cancer, ROS, ER-α, fulvestrant, bioinformatics analysis

OPEN ACCESS

Edited by:
Zhi Li,
The First Affiliated Hospital of China Medical University, China

Reviewed by:
Lisha Zhou,
Taizhou University, China
Ping Chen,
Zhengzhou University, China

***Correspondence:**
Lijun Jia
ljjia@shutcm.edu.cn

†These authors have contributed equally to this work and share first authorship

Specialty section:
This article was submitted to Pharmacology of Anti-Cancer Drugs, a section of the journal Frontiers in Oncology

Received: *18 March 2022*
Accepted: *13 April 2022*
Published: *09 May 2022*

Citation:
Xu T, Jiang Y, Yuan S, Zhang L, Chen X, Zhao W, Cai L, Xiao B and Jia L (2022) Andrographolide Inhibits ER-Positive Breast Cancer Growth and Enhances Fulvestrant Efficacy via ROS-FOXM1-ER-α Axis. Front. Oncol. 12:899402. doi: 10.3389/fonc.2022.899402

INTRODUCTION

Breast cancer is the most commonly diagnosed cancer among women worldwide, which has surpassed lung cancer as the leading cause of global cancer incidence with 11.7% of all cancer cases in 2020 (1). Based on its receptor status, breast cancer can be classified into estrogen receptor (ER)-positive, progesterone receptor (PR)-positive, human epidermal receptor 2 (HER2)-amplified, and triple-negative breast cancer which is lack of the former three biomarkers (2). Among these types, ER-positive subtype represents approximately 75% of all breast cancer cases (3). Therefore, discovering drugs to target estrogen and its receptors, known as endocrine therapy, is an important research topic for ER-positive breast cancer treatment.

Among several endocrine therapy drugs, fulvestrant, a selective estrogen receptor down-regulator, is the only one approved for postmenopausal women with ER-positive breast cancer who failed to respond to tamoxifen as the first- or second-line treatment (4). Clinical studies have reported that fulvestrant significantly improved patients' progression free survival (PFS) with well tolerated (5, 6). Furthermore, the first-line choice *via* using fulvestrant was associated with greater clinical benefit rate (CBR) than using anastrozole (7). However, the effect of fulvestrant on overall survival (OS) and PFS in ER-positive advanced breast cancer remains to be improved (8, 9).

In recent years, searching for new anti-tumor active substances from natural products of Chinese herbal medicine has become a research hotspot (10). Some natural plant compounds such as paclitaxel and irinotecan have been widely used in breast cancer treatment (11, 12). Andrographlide (AD), one of the major active components of the traditional Chinese medicine *Andrographis paniculate*, has been approved by Food and Drug Administration (FDA) and widely used in clinic to treat inflammatory disease and upper respiratory tract infections (13, 14). In our previous study, we had found that AD induced apoptosis by activating the ATF4-Noxa axis in lung adenocarcinoma cells (15). However, the antitumor efficacy and the underlying molecular mechanisms of AD on ER-positive breast cancer are poorly understood.

In the present study, we demonstrated that AD suppressed *ESR1* transcription through ROS-FOXM1 axis to inhibit the proliferation of ER-positive breast cancer both *in vitro* and *in vivo*. Importantly, we further identified that AD could serve as an effective approach to improve fulvestrant efficacy in ER-positive breast cancer *via* synergistically down-regulating ER-α expression.

MATERIALS AND METHODS

Cell Culture and Reagents

All cell lines used in this study were obtained from the Type Culture Collection of the Chinese Academy of Sciences (Shanghai, China). These cells were cultured in Dulbecco's Modified Eagle's Medium (DMEM, BasalMedia, Shanghai, China) which contains 10% fetal bovine serum (FBS, Biochrom AG, Berlin, Germany) and 1% penicillin–streptomycin solution (BasalMedia, Shanghai, China) at 37°C with 5% CO_2. The cells were exposed to 1 nM β-Estradiol (E2, Sigma-Aldrich, Darmstadt, Germany) and the indicated drugs. Andrographolide (AD) was purchased from Selleck (Houston, Texas, USA). Fulvestrant (FUL) was purchased from MCE (Shanghai, China).

Cell Proliferation Assay

Cells were seeded in ATPlite plates with 3000 cells per well, in triplicate, and cultured overnight. Cells were treated with the indicated drugs for 72 h, followed by the ATPlite luminescence assay (BD Pharmingen, Franklin Lakes, New Jersey, USA), according to the manufacturer's instructions. The combination index (CI) was calculated using CompuSyn software in the combination therapy assay (16). CI<1, = 1, and >1 indicate synergism, additive effect, and antagonism, respectively.

Cell Clonogenic Assay

Cells were seeded in six-well plates (800 cells per well) in triplicate and cultured overnight. Cells were treated with the indicated drugs for 2 weeks. Representative results of three independent experiments with similar trends are presented.

Isolation of Nuclear and Cytoplasmic Extract

Cytoplasmic and nuclear protein extraction were operated according to the Thermo Scientific™ NE-PER™ Nuclear and Cytoplasmic Extraction Reagents (Thermo Fisher Scientific, Waltham, MA, USA).

Cell Protein Extraction and Western Blotting

Cell or tissue lysates were prepared with RIPA lysis buffer (Beyotime, Shanghai, China). 15 μg proteins were loaded per lane. Proteins were transferred to a polyvinylidene fluoride membrane. After blocking with 5% nonfat milk in TBST, the membranes were incubated with the primary antibody as follows ER-α, FOXM1, Cathepsin D, β-tublin, LaminA/C (Cell Signaling Technology, Danvers, MA, USA), ER-β (AbSci, CA, USA), β-actin (HuaBio, Hangzhou, China), C-MYC and PR (Santa Cruz Biotechnology, Santa Cruz, CA, USA), then incubated with secondary antibody. Immune complexes were detected using an ECL Kit (Share Bio, Shanghai, China).

Real-Time Polymerase Chain Reaction Analyses

Ultrapure RNA kit (ComWin Biotech, Beijing, China) was used to isolate total RNA, and 1 μg total RNA was reversed to cDNA by using the PrimerScript reverse transcription reagent kit (Vazyme Biotech, Nanjing, China). Then, the cDNA was quantified with RT-PCR by using the Power SYBR Green PCR MasterMix (Vazyme Biotech, Nanjing, China) on the ABI 7500 thermocycler (Applied Biosystems, Foster City, CA, USA) according to the manufacturer's protocol and instrument manual. The sequences of the primers were as follows:

human *β-actin*: forward 5′-CGTGCGTGACATTAAGGAGAAG-3′,
reverse 5′-AAGGAAGGCTGGAAGAGTGC-3′;
human *ESR1*: forward 5′-GACCGAAGAGGAGGGAGAATG-3′,
reverse 5′-CAACAAGGCACTGACCATCTG-3′;
human *FOXM1*: forward 5′-ACAGCAGAAACGACCGAATC-3′,
reverse 5′-GGCAATGGCACCTTCACC-3′.

Quantifcation of Reactive Oxygen Species

The quantification of reactive oxygen species (ROS) production was monitored by cell permeable ROS indicator 2′,7′-dichlorodihydrofuorescein diacetate (H2-DCFDA) (Sigma-Aldrich, Darmstadt, Germany). The NAC rescue assay was performed as followings: Cells were pre-incubated with 5 mM

NAC for 2 h, then co-incubated with the indicated drugs and assessed for cell viability or ROS production as described above.

Gene Silencing Using Small Interfering RNA

The cells were transfected with siRNA oligonucleotides against the following genes using the Lipofectamine 2000 (Invitrogen, Carlsbad, CA, USA), according to the manufacturer's instructions. All siRNAs were synthesized by GenePharma (Shanghai, China). The sequences of the siRNAs were as follows:

siNC: 5′-UUCUCCGAA CGUGUCACGUTT-3′;
siFOXM1#1: 5′-GCUGGGAUCAAGAUUAUUATT-3′;
siFOXM1#2: 5′-GCCAACCGCUACUUGACAUTT-3′.

Construction of Plasmid

Full-length complementary DNA (cDNA) of ER-α was cloned into the pCDH vector using standard protocols. All constructions were confirmed by DNA sequencing before further applications.

Different Expressed Genes Screening

The raw data of GSE85871, GSE10061 and GSE59732 in the GEO database were analyzed by the interactive web tool, GEO2R (https://www.ncbi.nlm.nih.gov/geo/geo2r/). The GEO2R tool carried out comparisons using the limma R packages from the Bioconductor project. Statistically different expressed genes (DEGs) were defined with $P < 0.01$ and $|\log_2 \text{fold change (FC)}| \geq 0.9$.

KEGG Pathway Enrichment Analysis

KEGG pathway were analyzed using the DAVID online tool (https://david-d.ncifcrf.gov/tools.jsp) at the functional level. $P < 0.05$ was set as the cut-off criterion. The top 10 enriched pathways were figured.

Identification of AD-Associated Genes

The human genes associated with AD were acquired from the BATMAN-TCM (http://bionet.ncpsb.org.cn/batman-tcm/) database. BATMAN-TCM is an online bioinformatics analysis tool specially designed for studying the molecular mechanisms of traditional Chinese medicine (17). Score > 3 was set as the cut-off criterion.

PPI Network Construction

The online database STRING (https://cn.string-db.org/) was used to visualize the PPIs between the statistically DEG-encoded proteins in the resultant dataset (18). We used Cytoscape software (http://www.cytoscape.org/) to visualize the PPI network obtained from the STRING database (19). In addition, the Cytoscape plugin cytoHubba was applied to analyze the hub target genes between AD and ER-positive breast cancer. The target genes were ranked by MCC algorithm.

Transcription Factor Analysis

Transcription factors of identified modules were analyzed by the iRegulon plugin of Cytoscape (20). The iRegulon plugin was set as the default. The top five transcription factors with higher NES were listed.

Tumor Xenograft Growth Assay

Five-week-old female BALB/c athymic nude mice purchased from Lingchang Biological Technology Co., Ltd. (Shanghai, China) were maintained and treated in accordance with established guidelines, and the protocol was approved by the Institutional Animal Care and Use Committee of Longhua hospital, Shanghai University of Traditional Chinese Medicine. All the mice were handled using aseptic procedures and allowed to acclimatize to local conditions for one week before the experimental manipulations. 1×10^7 MCF7 cells with Matrigel (1:1) were injected into the right flank of each mouse. Estradiol cypionate (Selleck, Houston, Texas, USA) (1.5 mg/kg, once a week) was injected subcutaneously into each mouse one day before the injection of MCF7 cells. Mice were randomly divided into 4 groups and treated with 20% 2-hydroxypropyl-β-cyclodextrin (HPBCD), fulvestrant, AD or AD plus fulvestrant with the indicated doses. Tumor xenografts were measured with a caliper every 4 days and tumor volume was calculated as $(\text{Length} \times \text{Width}^2)/2$.

Statistical Analysis

GraphPad prism8 software was used to evaluate the statistical significance of the differences among groups. Unmatched 2-tailed t-test was used to compare the parameters between groups. The level of significance was set at $P < 0.05$. For all tests, three levels of significance (*P < 0.05, **P < 0.01, ***P < 0.001) were used.

RESULTS

AD Inhibits *ESR1* Transcription in ER-Positive Breast Cancer

To determine the cellular responses and explore the target of AD on breast cancer cells, the GSE85871 dataset (21) was adapted to comprehensively uncover the altered pathways between the control and AD-treated group. A total of 404 genes were significantly upregulated and 194 genes were significantly downregulated (**Figure 1A**). KEGG pathway enrichment analysis of these 598 different expressed genes (DEGs) showed that the most disturbed pathway was the "estrogen signaling pathway" (**Figure 1B**).

To further ascertain whether AD affects estrogen signaling pathway in ER-positive breast cancer, we performed an integrative analysis *via* using the BATMAN-TCM database (17) and the GSE59732 dataset (22). In the BATMAN-TCM database, 130 genes were identified as AD targets (**Supplementary Table 1**). In the GSE59732 dataset, 1986 DEGs were identified in ER-positive breast cancer cell lines compared with human mammary epithelial cell lines (**Supplementary Table 2**). Venn analysis of these DEGs and AD targets from BATMAN-TCM database showed that a total of 21 genes served as potential targets of AD in ER-positive breast cancer (**Figure 1C**). Further analysis through STRING database

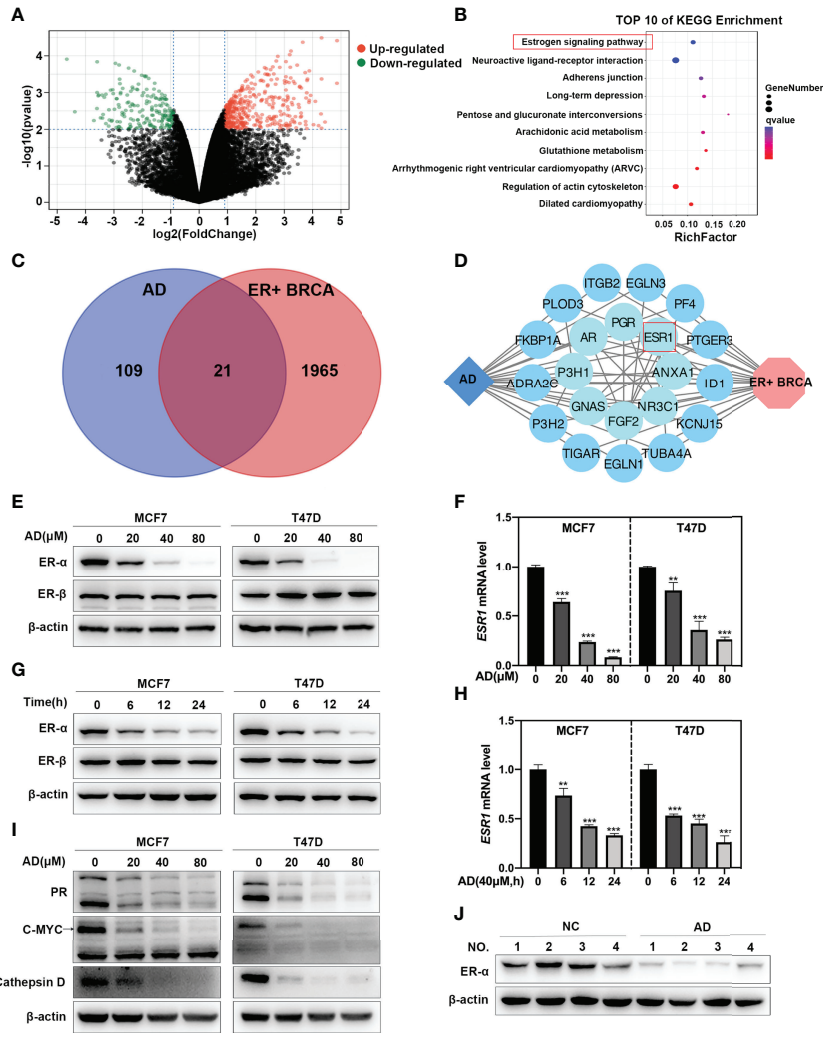

FIGURE 1 | AD inhibits *ESR1* transcription in ER-positive breast cancer. **(A)** Volcano plot showing the DEGs between the control and AD treatment group from the GSE85871 dataset. **(B)** KEGG pathway enrichment analysis for the DEGs and qvalue refers to -$\log_{10}$(pvalue). **(C)** Venn plot revealing the overlapping target genes for AD against ER-positive breast cancer. Blue circle represents AD; red circle represents ER-positive breast cancer. **(D)** Network of target genes for AD against ER-positive breast cancer was built using the STRING database and Cytoscape software. Blue diamond represents AD; red hexagon represents ER-positive breast cancer; blue circles represent target genes of AD in ER-positive breast cancer and were arranged from the inner circle to the outer circle according to the degree of association. **(E)** Cells were treated with 1‰ DMSO or the indicated concentrations of AD for 24 h. Cell protein was extracted and detected by Western blotting with antibodies against ER-α, ER-β and β-actin. **(F)** The mRNA level of *ESR1* was quantified by RT-PCR (normalized to β-actin). **(G)** Cells were treated with AD (40 μM) for 0 h, 6 h, 12 h, 24 h, respectively. Cell protein was extracted and detected by Western blotting with antibodies against ER-α, ER-β and β-actin. **(H)** The mRNA level of *ESR1* was quantified by RT-PCR (normalized to β-actin). **(I)** Cells were treated with 1‰ DMSO or the indicated concentrations of AD for 24 h. Cell protein was extracted and detected by Western blotting with antibodies against PR, C-MYC, Cathepsin D and β-actin. **(J)** Proteins extracted from tumor tissues of mice treated with 20% HPBCD or AD (150 mg/kg) were detected by Western blotting with antibodies against ER-α and β-actin. (Data were presented as mean ± SD. $^{**}P < 0.01$ and $^{***}P < 0.001$).

(18) and Cytoscape software (19) showed that *ESR1*, a critical gene in the "estrogen signaling pathway", was the key target of AD in ER-positive breast cancer (**Figure 1D**).

To verify the above findings, two ER-positive breast cancer cell lines (MCF7 and T47D) were selected to determine the ER-α level after AD treatment. As shown, AD significantly down-regulated the protein and mRNA levels of ER-α in a time- and dose-dependent manner, but did not impact the expression of ER-β in MCF7 and T47D cells (**Figures 1E–H**). Consistently, AD also suppressed the expression levels of ER-α target genes (23, 24), including PR, C-MYC and Cathepsin D (**Figure 1I**). Finally, we investigated the efficacy of AD on ER-α expression *in vivo*, as shown in **Figure 1J**, ER-α was significantly decreased after AD treatment. Taken together, these data collectively indicate that AD inhibits ER-α expression in ER-positive breast cancer both *in vitro and in vivo*.

AD Inhibits Breast Cancer Cell Growth Through Down-Regulating ER-α Expression

Given that ER-α acts as a classical oncogene to promote tumor growth (25), we firstly systematically determined the effect of AD on malignant phenotypes in ER-positive breast cancer cell lines. As shown, AD significantly inhibited the proliferation of MCF7 and T47D, and its IC50 value was 41.8 μM in MCF7 and 46.4 μM in T47D, respectively (**Figures 2A, B**). Furthermore, AD inhibited colony formation of MCF7 and T47D cells in a dose-dependent manner (**Figure 2C**). These findings indicated that AD suppressed the viability of breast cancer cell lines *in vitro*.

To further determine whether AD-induced ER-α inhibition is crucial for tumor malignant phenotypes, we transduced full-length cDNA of human ER-α into MCF7 and T47D cells and evaluated the role of ER-α on AD-treated cells. As shown in **Figures 2D, E**, ER-α overexpression significantly diminished the inhibited effect of AD on cell growth and colony formation in MCF7 and T47D cells. Together, these results indicate that AD suppresses ER-α expression to inhibit the proliferation of ER-positive breast cancer cells.

AD Inhibits *ESR1* Transcription *via* Inducing ROS Production

Previous study reported that ROS could downregulate ER-α expression (26), thus we hypothesized that AD could inhibit ER-α expression through inducing ROS production. Firstly, we detected cellular ROS level through the cell permeable ROS indicator, 2′, 7′-

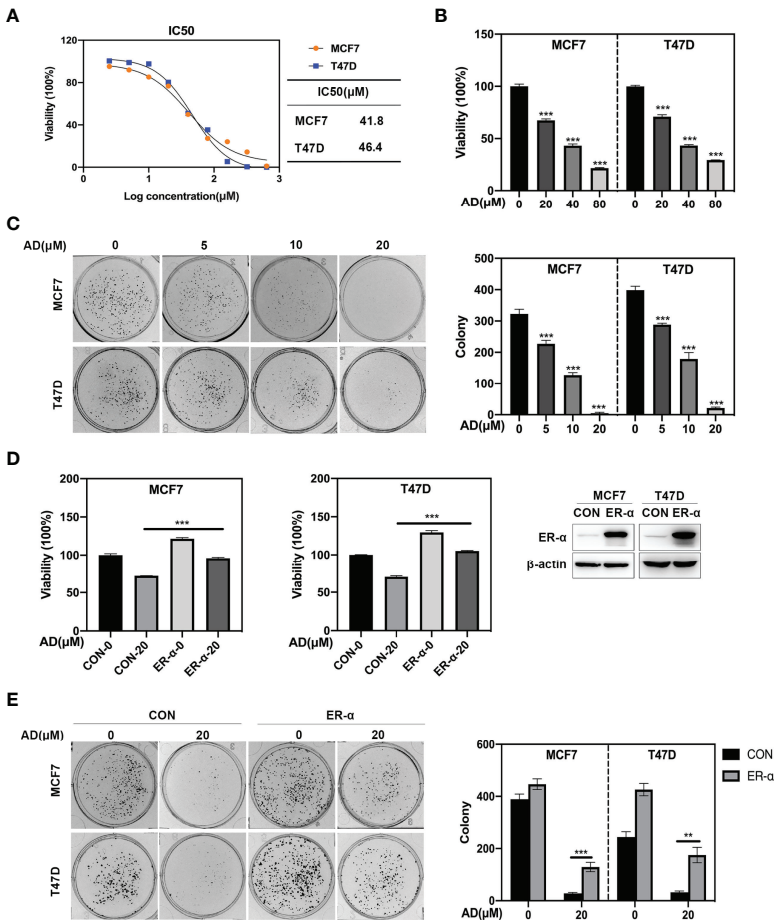

FIGURE 2 | AD inhibits breast cancer cell growth through down-regulating ER-α expression. **(A)** Cells were seeded in ATPlite plates in triplicate, 3000 cells per well, cultured overnight, and treated with 1‰ DMSO or various concentrations of AD (2.5, 5, 10, 20, 40, 80, 160, 320 and 640 μM) for 72 h. The ATPlite luminescence assay was used to determine the half-maximal inhibitory concentrations (IC50) of MCF7 and T47D cells, respectively. **(B)** Cells were seeded in ATPlite plates in triplicate, 3000 cells per well, cultured overnight, and treated with 1‰ DMSO or indicated concentrations of AD for 72 h, followed by the ATPlite luminescence assay. **(C)** Representative images of three independent experiments are shown for the inhibition of colony formation by AD. **(D)** The MCF7 and T47D cells were transduced with either control vector (MCF7/CON and T47D/CON) or human ER-α-expressing lentiviruses (MCF7/ER-α and T47D/ER-α), followed by Western blotting to verify the ER-α expression. These control and ER-α-expressing cells were treated with AD (20 μM) for 72 h, followed by analyzing the cell proliferation rate using the ATPlite luminescence assay. **(E)** The MCF7/CON, MCF7/ER-α and T47D/CON, T47D/ER-α cells were treated with AD (20 μM) for 2 weeks, followed by analyzing the cell colony formation. (Data were presented as mean ± SD. $^{**}P < 0.01$ and $^{***}P < 0.001$).

dichlorodihydrofuorescein diacetate (H2-DCFDA) and found that AD significantly promoted ROS production in MCF7 and T47D cells (**Figure 3A**). Then, we used N-acetylcysteine (NAC), a classical ROS scavenger, to block ROS elevation and found that NAC prevented AD-induced the generation of ROS (**Figure 3B**) and markedly attenuated AD-inhibited ER-α expression both at protein (**Figures 3C, D**) and mRNA levels (**Figures 3E, F**). Furthermore, the proliferation of breast cancer cells increased after NAC treatment in AD-treated group (**Figures 3G, H**). Based on these observations, we concluded that AD induces ROS production to inhibit *ESR1* transcription and cell growth in ER-positive breast cancer cells.

AD Suppresses *ESR1* Transcription *via* ROS-FOXM1 Axis

In order to explore how AD downregulates ER-α *via* inducing ROS production, the GSE10061 dataset (27), a gene expression profiling about H_2O_2 treatment in MCF7 cells was used. In the GSE10061 dataset, 313 DEGs including *ESR1* were identified in the H_2O_2-treated group compared with that in the control group (**Figure 4A**), demonstrating that this dataset was exactly captured the molecular features of ROS-*ESR1* pathway. Given that AD decreased *ESR1* at transcription level, we clustered the altered transcription factors which might regulate *ESR1* transactivation *via* using iRegulon (20). The top five predicted transcription factors with the highest normalized enrichment score (NES) were shown in **Figure 4B**. In these transcription factors, FOXM1 gained the highest NES and could regulate 128 DEGs including *ESR1* (**Figure 4B** and **Supplementary Figure 1A**). Thus, we hypothesized that AD might suppress *ESR1* transcription *via* ROS-FOXM1 axis. To verify this hypothesis, we determined the effect of AD on FOXM1 expression. As shown, we found that AD significantly inhibited FOXM1 expression at protein and mRNA levels in a dose-

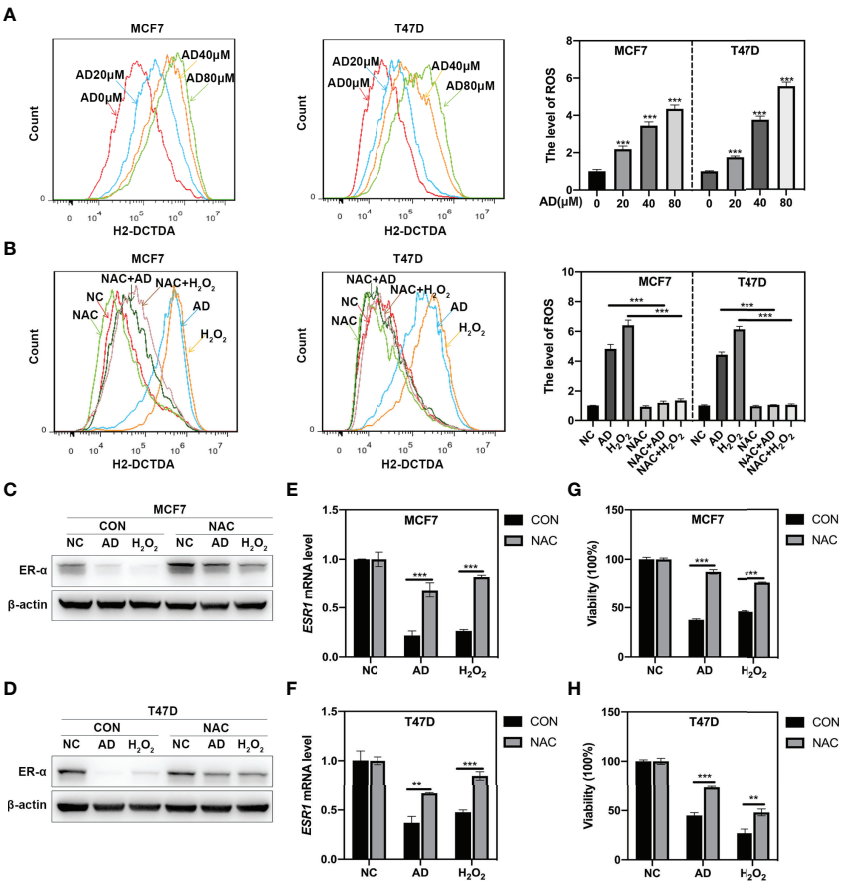

FIGURE 3 | AD inhibits *ESR1* transcription *via* inducing ROS production. **(A)** AD elevated ROS levels in MCF7 and T47D cells. Cells were treated with various concentrations of AD for 24 h. The level of ROS was determined by H2-DCFDA staining and flow cytometry. **(B)** MCF7 and T47D cells were treated with AD (40 μM), H_2O_2 (10 μM), NAC (5 mM) alone or AD+NAC, H_2O_2+NAC for 24 h and subjected to H2-DCFDA staining analysis for determining the levels of ROS. H_2O_2 was used as a positive control. **(C–H)** N-Acetylcysteine (NAC), the classical ROS scavenger, attenuated AD-inhibited the expression of ER-α and cell growth. **(C, D)** MCF7 and T47D cells were treated with AD (40 μM) and/or NAC (5 mM) for 24 h and subjected to Western blotting for the expression of ER-α. H_2O_2 was used as a positive control. **(E, F)** The mRNA level of *ESR1* was quantified by RT-PCR (normalized to β-actin). **(G, H)** The cell proliferation rate was assessed using ATPlite luminescence assay. (Data were presented as mean ± SD. $^{**}P < 0.01$ and $^{***}P < 0.001$).

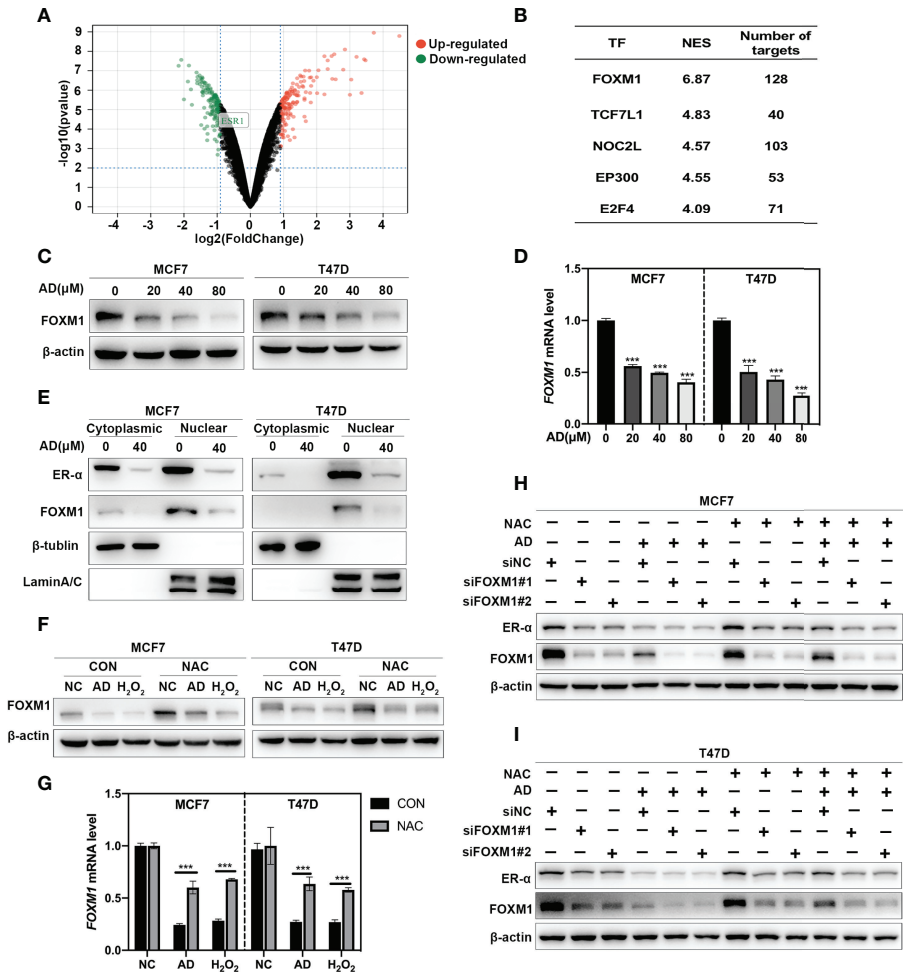

FIGURE 4 | AD suppresses *ESR1* transcription *via* ROS-FOXM1 axis. **(A)** Volcano plot showing the DEGs between the control and H_2O_2 treatment group from the GSE10061 dataset. *ESR1* belonging to the down-regulated genes was highlighted. **(B)** The top five predicted transcription factors regulating the DEGs were listed. **(C)** Cells were treated with 1‰ DMSO or the indicated concentrations of AD for 24 h. Cell protein was extracted and detected by Western blotting with antibodies against FOXM1 and β-actin. **(D)** The mRNA level of *FOXM1* was quantified by RT-PCR (normalized to β-actin). **(E)** MCF7 and T47D cells were treated with 1‰ DMSO or AD (40 μM) for 24 h. Cytoplasmic and nuclear protein extracts were collected as described in the Materials and Methods section and subjected to Western blotting with antibodies against ER-α, FOXM1, β-tublin and LaminA/C. **(F)** NAC attenuated AD-inhibited the expression of FOXM1. MCF7 and T47D cells were treated with AD (40 μM) and/or NAC (5 mM) for 24 h and subjected to Western blotting for the expression of FOXM1. **(G)** The mRNA level of *FOXM1* was quantified by RT-PCR (normalized to β-actin). H_2O_2 was used as a positive control. **(H, I)** MCF7 and T47D cells were transfected with control or FOXM1 siRNA for 48 h, then treated with AD (40 μM) and/or NAC (5 mM) for 24h and subjected to Western blotting for the expression of FOXM1 and ER-α. (Data were presented as mean ± SD. ***$P < 0.001$).

dependent manner (**Figures 4C, D**). Since FOXM1 acts as a transcription factor in the nucleus to regulate *ESR1* transactivation, we detected the expression level of FOXM1 and ER-α in the nucleus upon AD treatment and found that FOXM1 and ER-α were significantly decreased in the nucleus (**Figure 4E**). Next, we used NAC to block ROS production and found that NAC markedly attenuated AD-inhibited FOXM1 expression both at protein and mRNA levels (**Figures 4F, G**). Furthermore, the rescue effect of NAC on AD-suppressed ER-α expression and cell proliferation could be alleviated by FOXM1 knockdown (**Figures 4H, I** and **Supplementary Figure 2**). These results collectively demonstrate that AD suppresses *ESR1* transcription *via* ROS-FOXM1 axis.

AD Synergizes With Fulvestrant to Inhibit ER-α Expression and Breast Cancer Growth

Considering that AD inhibited *ESR1* transcription, we hypothesized that AD might enhance the efficacy of fulvestrant by synergistically inhibiting ER-α expression. As shown in **Figures 5A, B**, the expression of ER-α was synergistically inhibited after AD and fulvestrant combined treatment. To verify whether AD could

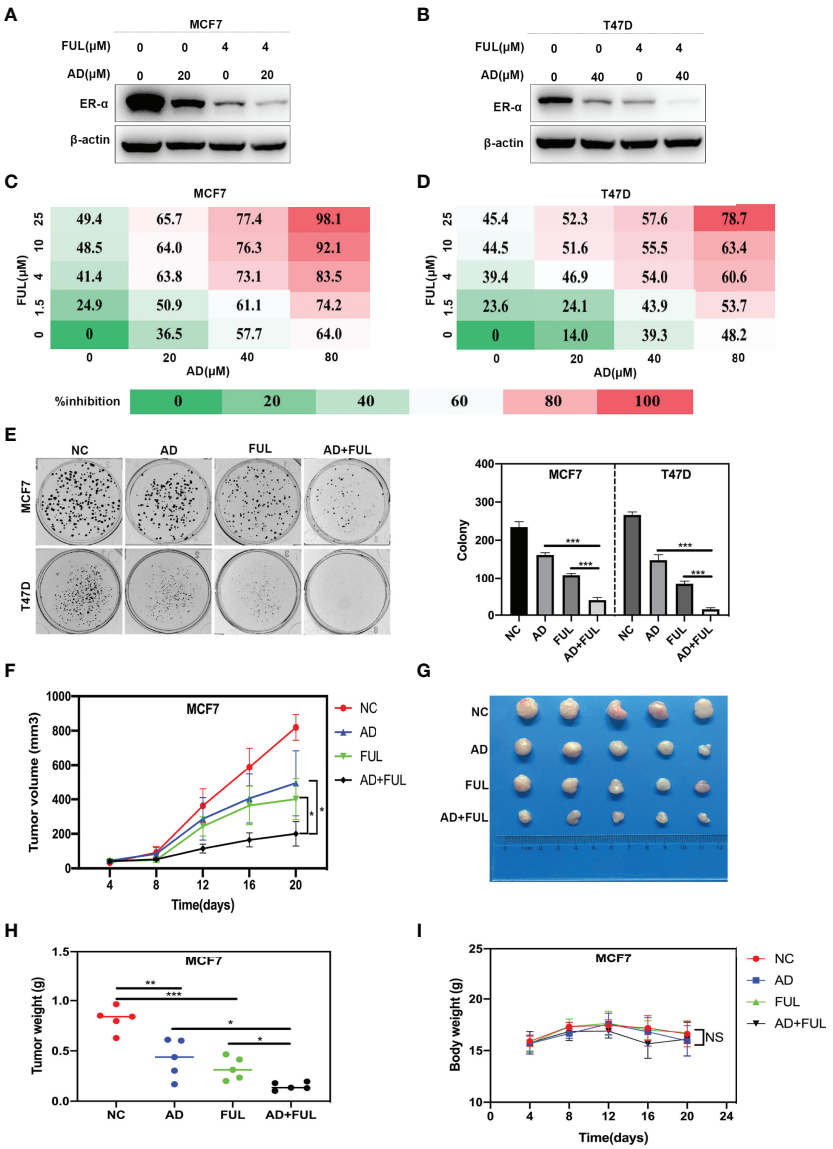

FIGURE 5 | AD synergizes with fulvestrant to inhibit ER-α expression and breast cancer growth. **(A, B)** MCF7 and T47D cells were treated with AD and/or fulvestrant for 24 h and harvested for Western blotting with antibodies against ER-α and β-actin. **(C, D)** MCF7 and T47D cells were treated with escalating doses of either AD or fulvestrant for 72 h, followed by analyzing the cell proliferation rate assessed by ATPlite luminescence assay. Percent inhibition at each dose of drug is presented. **(E)** MCF7 and T47D cells were treated with AD (10 μM) and/or fulvestrant (0.1 μM) for 2 weeks, followed by analyzing the cell colony formation. **(F–I)** Nude mice bearing breast cancer xenografts with MCF7 cells were administered with 20% HPBCD, AD (150 mg/kg per day), fulvestrant (5 mg/mouse administered subcutaneously, once per week) and AD plus fulvestrant. The treatments for the nude mice were carried out on 4 days after MCF7 cells injected and lasted for 16 days. **(F)** Tumor volumes were determined by caliper measurement, and the data was converted to tumor growth curve. **(G)** Images of the tumors in each of the 4 groups at the end of experiment. **(H)** Weight of the tumors in each of the 4 groups was measured with an electronic scale immediately after the tumor was collected. **(I)** The mice weights were recorded every 4 days during the whole experiment. (Data were presented as mean ± SD. *P < 0.05, **P < 0.01, ***P < 0.001, NS denotes not significant.

synergize with fulvestrant to suppress cell growth, MCF7 and T47D cells were treated with AD and fulvestrant alone or in combination with escalating doses. We found that the combination of AD and fulvestrant synergistically suppressed cell proliferation (**Figures 5C, D**), with optimal concentration of AD (80 μM) and FUL (25 μM) for MCF7 and T47D cells (combination index (CI) were 0.02 and 0.4, respectively) (**Supplementary Figures 1B, C**). Moreover, AD synergized with fulvestrant to suppress the colony formation of MCF7 and T47D cells (**Figure 5E**).

Next, we determined whether AD and fulvestrant synergized to suppress ER-positive breast cancer *in vivo*. We found that, compared to AD or fulvestrant treatment alone, the combination

of these two agents further inhibited tumor growth (**Figure 5F**) and reduced tumor volumes (**Figure 5G**) and tumor weight (**Figure 5H**). In addition, there were no obvious treatment-related toxicity, such as body weight loss, in single or combined groups (**Figure 5I**). Taken together, these findings demonstrate that AD synergizes with fulvestrant to inhibit ER-α expression and breast cancer growth.

DISCUSSION

Estrogen receptor (ER)-positive breast cancer is the main subtype of breast cancer with high incidence and mortality, which accounts for about third quarters of all breast cancer patients. In the past few years, achievements have been obtained in the development of novel anti-ER-positive breast cancer strategies and effective drugs (28). Recently, a variety of Chinese herbal extracts and isolated compounds exhibited excellent anti-tumor efficacy in breast cancer cells (29, 30). AD, one of the above compounds, has substantial anti-cancer effect in various tumors by inducing cell cycle arrest, triggering apoptosis or suppressing autophagy (13, 31, 32). In our previous study, we found that AD exhibited a broad-spectrum inhibition of proliferation in lung cancer cells *via* inducing apoptosis (15). In the present study, we found that AD inhibited ER-α expression and the proliferation of ER-positive breast cancer both *in vitro and in vivo*. In terms of mechanisms, AD suppressed *ESR1* transcription *via* inducing ROS production to down-regulate FOXM1.

ER, as one of the most successful molecular target in the history of anti-breast cancer drug discovery, determines the sensitivity and effectiveness of endocrine therapy for breast cancer (33, 34). Therefore, suppressing ER *via* endocrine therapy is recommended as the first-line treatment for ER-positive breast cancer therapy in clinic (35). Fulvestrant, an important endocrine therapy drug, inhibited ER-α expression *via* promoting the proteasomal degradation of ER-α to suppress tumor growth (36). However, the ER-α down-regulated effect of fulvestrant only happened in the nucleus and ER-α was not completely inhibited at clinically feasible dose (37, 38). Therefore, the efficacy of fulvestrant is still limited. In the present study, we found that AD suppressed ER-α expression both in the nucleus and cytoplasm and enhanced the efficacy of fulvestrant to synergistically inhibit ER-positive breast cancer growth.

FOXM1, a potent oncogene, regulates a broad spectrum of normal biological functions, including cell proliferation, cell migration, angiogenesis and cell survival (39). Kwok et al. reported that thiostrepton, a FOXM1 inhibitor, exerted great antitumor effect by inducing cell cycle arrest and caspase-dependent apoptosis in MCF7 cells (40). In addition, FOXM1 and ER-α were closely related in breast cancer (41). FOXM1 was reported to regulate ER-α expression through binding to the two forkhead response elements located at the proximal region of the *ESR1* promoter (23). However, the up-stream of FOXM1-ER-α axis is still unknown. Previous studies reported that ROS could significantly regulate oxidative stress related genes including

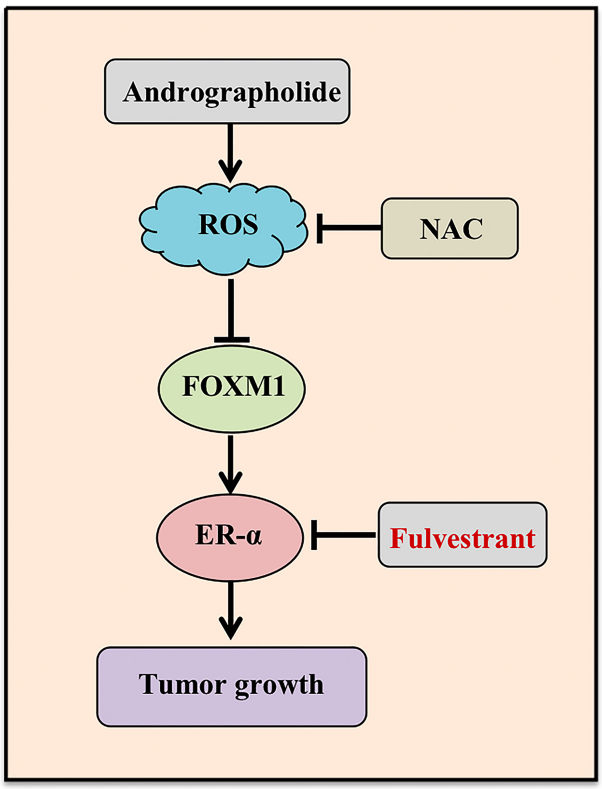

FIGURE 6 | Working model. AD suppressed *ESR1* transcription through ROS-FOXM1 axis and synergized with fulvestrant to inhibit ER-α expression and breast cancer growth.

FOXM1 (42, 43). In the present study, through bioinformatic analysis and experiments, we found that ROS served as an up-stream signal of FOXM1-ER-α axis and down-regulated the expression of FOXM1 at both protein and mRNA levels. Furthermore, pre-treatment with the antioxidant NAC prevented AD-induced generation of ROS and significantly attenuated AD-inhibited FOXM1 expression. Based on these findings, we demonstrated a novel mechanism that AD induced ROS production to down-regulate FOXM1-ER-α axis, thereby inhibiting ER-positive breast cancer growth.

In conclusion, our study highlighted a pivotal role of AD in suppressing the tumor progression of ER-positive breast cancer both *in vitro and in vivo*, and discovered a novel mechanism of AD down-regulating the expression of ER-α in ER-positive breast cancer and enhancing fulvestrant efficacy (**Figure 6**). These findings suggested that AD is a potential therapeutic agent to ameliorate outcomes for breast cancer patients.

DATA AVAILABILITY STATEMENT

The datasets presented in this study can be found in online repositories. The names of the repository/repositories and accession number(s) can be found in the article/**Supplementary Material**.

ETHICS STATEMENT

The animal study was reviewed and approved by Animal Experimental Ethics Committee of Longhua hospital, Shanghai University of Traditional Chinese Medicine.

AUTHOR CONTRIBUTIONS

TX, YJ, and LJ conceived the general framework of this study and designed the experiments. TX, YJ, and SY performed the experiments and drafted the manuscript. LC and LZ provided technical or material support. XC, WZ and BX performed statistical analyses. LJ supervised this study. All authors contributed to the article and approved the submitted version.

FUNDING

This work was supported by the National Natural Science Foundation of China (Grant Nos. 81820108022 and 82003297), Shanghai Frontiers Science Center of Disease and Syndrome Biology of Inflammatory Cancer Transformation (2021KJ03-12), Innovation Program of Shanghai Municipal Education Commission (2019-01-07-00-10-E00056), ChenGuang project supported by Shanghai Municipal Education Commission and Shanghai Education Development Foundation (19CG49).

SUPPLEMENTARY MATERIAL

The Supplementary Material for this article can be found online at: https://www.frontiersin.org/articles/10.3389/fonc.2022.899402/full#supplementary-material

REFERENCES

1. Sung H, Ferlay J, Siegel RL, Laversanne M, Soerjomataram I, Jemal A, et al. Global Cancer Statistics 2020: Globocan Estimates of Incidence and Mortality Worldwide for 36 Cancers in 185 Countries. *CA Cancer J Clin* (2021) 71 (3):209–49. doi: 10.3322/caac.21660
2. Gradishar W, Moran M, Abraham J, Aft R, Agnese D, Allison K, et al. Nccn Guidelines® Insights: Breast Cancer, Version 4.2021. *J Natl Compr Cancer Netw JNCCN* (2021) 19(5):484–93. doi: 10.6004/jnccn.2021.0023
3. Harbeck N, Penault-Llorca F, Cortes J, Gnant M, Houssami N, Poortmans P, et al. Breast Cancer. *Nat Rev Dis Primers* (2019) 5(1):66. doi: 10.1038/s41572-019-0111-2
4. Bross PF, Baird A, Chen G, Jee JM, Lostritto RT, Morse DE, et al. Fulvestrant in Postmenopausal Women With Advanced Breast Cancer. *Clin Cancer Res: Off J Am Assoc Cancer Res* (2003) 9(12):4309–17.
5. Maass N, Ostermann H, Possinger K, Klein P, Tesch H, Mühlenhoff L, et al. Act-Faster, a Prospective Cohort Study Exploring Treatment Patterns With Fulvestrant and Exemestane in Postmenopausal Patients With Advanced Hormone Receptor-Positive Breast Cancer Under Real-Life Conditions in Germany. *Breast Care (Basel Switzerland)* (2019) 14(6):401–8. doi: 10.1159/000493882
6. Robertson J, Bondarenko I, Trishkina E, Dvorkin M, Panasci L, Manikhas A, et al. Fulvestrant 500 Mg Versus Anastrozole 1 Mg for Hormone Receptor-Positive Advanced Breast Cancer (Falcon): An International, Randomised, Double-Blind, Phase 3 Trial. *Lancet (Lond Engl)* (2016) 388(10063):2997–3005. doi: 10.1016/S0140-6736(16)32389-3
7. Robertson JFR, Jiang Z, Di Leo A, Ohno S, Pritchard KI, Ellis M, et al. A Meta-Analysis of Clinical Benefit Rates for Fulvestrant 500 Mg Vs. Alternative Endocrine Therapies for Hormone Receptor-Positive Advanced Breast Cancer. *Breast Cancer (Tokyo Jpn)* (2019) 26(6):703–11. doi: 10.1007/s12282-019-00973-4
8. Slamon D, Neven P, Chia S, Fasching P, De Laurentiis M, Im S, et al. Overall Survival With Ribociclib Plus Fulvestrant in Advanced Breast Cancer. *N Engl J Med* (2020) 382(6):514–24. doi: 10.1056/NEJMoa1911149
9. Albanell J, Martínez M, Ramos M, O'Connor M, de la Cruz-Merino L, Santaballa A, et al. Randomized Phase Ii Study of Fulvestrant Plus Palbociclib or Placebo in Endocrine-Sensitive, Hormone Receptor-Positive/Her2-Advanced Breast Cancer: Geicam/2014-12 (Flipper). *Eur J Cancer (Oxf Engl 1990)* (2021) 161:26–37. doi: 10.1016/j.ejca.2021.11.010
10. Yuan R, Hou Y, Sun W, Yu J, Liu X, Niu Y, et al. Natural Products to Prevent Drug Resistance in Cancer Chemotherapy: A Review. *Ann N Y Acad Sci* (2017) 1401(1):19–27. doi: 10.1111/nyas.13387
11. Abu Samaan TM, Samec M, Liskova A, Kubatka P, Büsselberg D. Paclitaxel's Mechanistic and Clinical Effects on Breast Cancer. *Biomolecules* (2019) 9(12): E789. doi: 10.3390/biom9120789
12. Lorusso V, Latorre A, Giotta F. Chemotherapy Options Beyond the First Line in Her-Negative Metastatic Breast Cancer. *J Oncol* (2020) 2020:9645294. doi: 10.1155/2020/9645294
13. Cheung H, Cheung S, Li J, Cheung C, Lai W, Fong W, et al. Andrographolide Isolated From Andrographis Paniculata Induces Cell Cycle Arrest and Mitochondrial-Mediated Apoptosis in Human Leukemic Hl-60 Cells. *Planta Med* (2005) 71(12):1106–11. doi: 10.1055/s-2005-873128
14. Zou W, Xiao Z, Wen X, Luo J, Chen S, Cheng Z, et al. The Anti-Inflammatory Effect of Andrographis Paniculata (Burm. F.) Nees on Pelvic Inflammatory Disease in Rats Through Down-Regulation of the NF-κB Pathway. *BMC Complement Altern Med* (2016) 16(1):483. doi: 10.1186/s12906-016-1466-5
15. Zhang J, Li C, Zhang L, Heng Y, Xu T, Zhang Y, et al. Andrographolide Induces Noxa-Dependent Apoptosis by Transactivating Atf4 in Human Lung Adenocarcinoma Cells. *Front Pharmacol* (2021) 12:680589. doi: 10.3389/fphar.2021.680589
16. Chou T-C. Drug Combination Studies and Their Synergy Quantification Using the Chou-Talalay Method. *Cancer Res* (2010) 70(2):440–6. doi: 10.1158/0008-5472.CAN-09-1947
17. Tang X, Lu J, Chen H, Zhai L, Zhang Y, Lou H, et al. Underlying Mechanism and Active Ingredients of Tianma Gouteng Acting on Cerebral Infarction as Determined *Via* Network Pharmacology Analysis Combined With Experimental Validation. *Front Pharmacol* (2021) 12:760503. doi: 10.3389/fphar.2021.760503
18. Szklarczyk D, Morris JH, Cook H, Kuhn M, Wyder S, Simonovic M, et al. The String Database in 2017: Quality-Controlled Protein-Protein Association Networks, Made Broadly Accessible. *Nucleic Acids Res* (2017) 45(D1): D362–D8. doi: 10.1093/nar/gkw937
19. Shannon P, Markiel A, Ozier O, Baliga NS, Wang JT, Ramage D, et al. Cytoscape: A Software Environment for Integrated Models of Biomolecular Interaction Networks. *Genome Res* (2003) 13(11):2498–504. doi: 10.1101/gr.1239303
20. Janky RS, Verfaillie A, Imrichová H, Van de Sande B, Standaert L, Christiaens V, et al. Iregulon: From a Gene List to a Gene Regulatory Network Using Large Motif and Track Collections. *PloS Comput Biol* (2014) 10(7):e1003731. doi: 10.1371/journal.pcbi.1003731
21. Lv C, Wu X, Wang X, Su J, Zeng H, Zhao J, et al. The Gene Expression Profiles in Response to 102 Traditional Chinese Medicine (Tcm) Components: A General Template for Research on Tcms. *Sci Rep* (2017) 7(1):352. doi: 10.1038/s41598-017-00535-8
22. Horton J, Siamakpour-Reihani S, Lee C, Zhou Y, Chen W, Geradts J, et al. Fas Death Receptor: A Breast Cancer Subtype-Specific Radiation Response Biomarker and Potential Therapeutic Target. *Radiat Res* (2015) 184(5):456–69. doi: 10.1667/RR14089.1
23. Madureira P, Varshochi R, Constantinidou D, Francis R, Coombes R, Yao K, et al. The Forkhead Box M1 Protein Regulates the Transcription of the

Estrogen Receptor Alpha in Breast Cancer Cells. *J Biol Chem* (2006) 281 (35):25167–76. doi: 10.1074/jbc.M603906200
24. Jia X, Li C, Li L, Liu X, Zhou L, Zhang W, et al. Neddylation Inactivation Facilitates Foxo3a Nuclear Export to Suppress Estrogen Receptor Transcription and Improve Fulvestrant Sensitivity. *Clin Cancer Res an Off J Am Assoc Cancer Res* (2019) 25(12):3658–72. doi: 10.1158/1078-0432.CCR-18-2434
25. Piperigkou Z, Karamanos N. Estrogen Receptor-Mediated Targeting of the Extracellular Matrix Network in Cancer. *Semin Cancer Biol* (2020) 62:116–24. doi: 10.1016/j.semcancer.2019.07.006
26. Tamir S, Izrael S, Vaya J. The Effect of Oxidative Stress on Eralpha and Erbeta Expression. *J Steroid Biochem Mol Biol* (2002) 81(4-5):327–32. doi: 10.1016/S0960-0760(02)00115-2
27. Yau C, Benz CC. Genes Responsive to Both Oxidant Stress and Loss of Estrogen Receptor Function Identify a Poor Prognosis Group of Estrogen Receptor Positive Primary Breast Cancers. *Breast Cancer res: BCR* (2008) 10 (4):R61. doi: 10.1186/bcr2120
28. Singh V, Kumar K, Purohit D, Verma R, Pandey P, Bhatia S, et al. Exploration of Therapeutic Applicability and Different Signaling Mechanism of Various Phytopharmacological Agents for Treatment of Breast Cancer. *Biomed Pharmacother = Biomed Pharmacother* (2021) 139:111584. doi: 10.1016/j.biopha.2021.111584
29. Zhao Y, Liu Y. A Mechanistic Overview of Herbal Medicine and Botanical Compounds to Target Transcriptional Factors in Breast Cancer. *Pharmacol Res* (2018) 130:292–302. doi: 10.1016/j.phrs.2017.12.027
30. Peng Y, Wang Y, Tang N, Sun D, Lan Y, Yu Z, et al. Andrographolide Inhibits Breast Cancer Through Suppressing Cox-2 Expression and Angiogenesis *Via* Inactivation of P300 Signaling and Vegf Pathway. *J Exp Clin Cancer Res CR* (2018) 37(1):248. doi: 10.1186/s13046-018-0926-9
31. Deng Y, Bi R, Guo H, Yang J, Du Y, Wang C, et al. Andrographolide Enhances Trail-Induced Apoptosis *Via* -Mediated Death Receptors Up-Regulation and Suppression of the Nf-Kb Pathway in Bladder Cancer Cells. *Int J Biol Sci* (2019) 15(3):688–700. doi: 10.7150/ijbs.30847
32. Zhou J, Hu S, Tan S, Cao R, Chen Y, Xia D, et al. Andrographolide Sensitizes Cisplatin-Induced Apoptosis *Via* Suppression of Autophagosome-Lysosome Fusion in Human Cancer Cells. *Autophagy* (2012) 8(3):338–49. doi: 10.4161/auto.18721
33. Yersal O, Barutca S. Biological Subtypes of Breast Cancer: Prognostic and Therapeutic Implications. *World J Clin Oncol* (2014) 5(3):412–24. doi: 10.5306/wjco.v5.i3.412
34. Maruthanila VL, Elancheran R, Kunnumakkara AB, Kabilan S, Kotoky J. Recent Development of Targeted Approaches for the Treatment of Breast Cancer. *Breast Cancer (Tokyo Japan)* (2017) 24(2):191–219. doi: 10.1007/s12282-016-0732-1
35. Bonotto M, Gerratana L, Di Maio M, De Angelis C, Cinausero M, Moroso S, et al. Chemotherapy Versus Endocrine Therapy as First-Line Treatment in Patients With Luminal-Like Her2-Negative Metastatic Breast Cancer: A Propensity Score Analysis. *Breast (Edinburgh Scotland)* (2017) 31:114–20. doi: 10.1016/j.breast.2016.10.021
36. Johnston SJ, Cheung KL. Fulvestrant - A Novel Endocrine Therapy for Breast Cancer. *Curr Med Chem* (2010) 17(10):902–14. doi: 10.2174/092986710790820633
37. Ishii Y, Papa L, Bahadur U, Yue Z, Aguirre-Ghiso J, Shioda T, et al. Bortezomib Enhances the Efficacy of Fulvestrant by Amplifying the Aggregation of the Estrogen Receptor, Which Leads to a Proapoptotic Unfolded Protein Response. *Clin Cancer Res an Off J Am Assoc Cancer Res* (2011) 17(8):2292–300. doi: 10.1158/1078-0432.CCR-10-1745
38. Robertson J, Evans A, Henschen S, Kirwan C, Jahan A, Kenny L, et al. A Randomized, Open-Label, Presurgical, Window-Of-Opportunity Study Comparing the Pharmacodynamic Effects of the Novel Oral Serd Azd9496 With Fulvestrant in Patients With Newly Diagnosed Er Her2 Primary Breast Cancer. *Clin Cancer Res an Off J Am Assoc Cancer Res* (2020) 26(16):4242–9. doi: 10.1158/1078-0432.CCR-19-3387
39. Lam EWF, Brosens JJ, Gomes AR, Koo C-Y. Forkhead Box Proteins: Tuning Forks for Transcriptional Harmony. *Nat Rev Cancer* (2013) 13(7):482–95. doi: 10.1038/nrc3539
40. Kwok JMM, Myatt SS, Marson CM, Coombes RC, Constantinidou D, Lam EWF. Thiostrepton Selectively Targets Breast Cancer Cells Through Inhibition of Forkhead Box M1 Expression. *Mol Cancer Ther* (2008) 7 (7):2022–32. doi: 10.1158/1535-7163.MCT-08-0188
41. Millour J, Constantinidou D, Stavropoulou AV, Wilson MSC, Myatt SS, Kwok JMM, et al. Foxm1 Is a Transcriptional Target of Eralpha and Has a Critical Role in Breast Cancer Endocrine Sensitivity and Resistance. *Oncogene* (2010) 29(20):2983–95. doi: 10.1038/onc.2010.47
42. Chua P-J, Yip GW-C, Bay B-H. Cell Cycle Arrest Induced by Hydrogen Peroxide Is Associated With Modulation of Oxidative Stress Related Genes in Breast Cancer Cells. *Exp Biol Med (Maywood NJ)* (2009) 234(9):1086–94. doi: 10.3181/0903-RM-98
43. Leone A, Roca MS, Ciardiello C, Costantini S, Budillon A. Oxidative Stress Gene Expression Profile Correlates With Cancer Patient Poor Prognosis: Identification of Crucial Pathways Might Select Novel Therapeutic Approaches. *Oxid Med Cell Longev* (2017) 2017:2597581. doi: 10.1155/2017/2597581

Conflict of Interest: The authors declare that the research was conducted in the absence of any commercial or financial relationships that could be construed as a potential conflict of interest.

Publisher's Note: All claims expressed in this article are solely those of the authors and do not necessarily represent those of their affiliated organizations, or those of the publisher, the editors and the reviewers. Any product that may be evaluated in this article, or claim that may be made by its manufacturer, is not guaranteed or endorsed by the publisher.

frontiers | Frontiers in Oncology

CASE REPORT
published: 31 May 2022
doi: 10.3389/fonc.2022.861271

Case Report: Afatinib Sensitivity in Rare EGFR E746_L747delinsIP Mutated LUAD With Peritoneal Metastases

Lili Zhang[1,2†], Lu Yang[3†], Binxu Sun[1,2†], Yixiao Deng[3], Jie Yang[3], Dongfang Wu[3] and Fanming Kong[1,2*]*

[1] Department of Oncology, First Teaching Hospital of Tianjin University of Traditional Chinese Medicine, Tianjin, China, [2] National Clinical Research Center for Chinese Medicine Acupuncture and Moxibustion, Tianjin, China, [3] The Genetic Analysis Department, YuceBio Technology Co., Ltd., Shenzhen, China

OPEN ACCESS

Edited by:
Zhi Li,
The First Affiliated Hospital of China Medical University, China

Reviewed by:
Haruhiko Sugimura,
Hamamatsu University School of Medicine, Japan
Junichi Shimizu,
Aichi Cancer Center, Japan

***Correspondence:**
Fanming Kong
kongfanming08@163.com
Dongfang Wu
wudf@yucebio.com

[†]These authors have contributed equally to this work and share first authorship

Specialty section:
This article was submitted to Pharmacology of Anti-Cancer Drugs, a section of the journal Frontiers in Oncology

Received: *24 January 2022*
Accepted: *27 April 2022*
Published: *31 May 2022*

Citation:
Zhang L, Yang L, Sun B, Deng Y, Yang J, Wu D and Kong F (2022) Case Report: Afatinib Sensitivity in Rare EGFR E746_L747delinsIP Mutated LUAD With Peritoneal Metastases. Front. Oncol. 12:861271. doi: 10.3389/fonc.2022.861271

Patients with non-small cell lung cancer harboring the epidermal growth factor receptor (EGFR)-sensitive mutations are known to benefit significantly from EGFR tyrosine kinase inhibitors (TKIs), such as erlotinib, gefitinib, icotinib, or afatinib. However, the efficacy of EGFR-TKIs against rare mutations has not yet been well investigated. Here, we report a female patient with advanced lung adenocarcinoma (LUAD), carrying a rare mutation of *EGFR* Exon19 E746_L747delinsIP, who was administered first-generation EGFR-TKIs as the first-line treatment. The patient continued to progress slowly until peritoneal metastases have occurred. Subsequently, the patient was treated with anlotinib for 5 months until disease progression. Given the finding of the same EGFR rare mutation in peritoneal effusion without other EGFR-TKI resistance mutations, the patient received afatinib with a tremendous response. Our results may be of clinical relevance for patients with LUAD carrying this rare mutation, and these findings warrant further investigation.

Keywords: lung adenocarcinoma, peritoneal carcinomatosis, sensitive, afatinib, EGFR E746_L747delinsIP

INTRODUCTION

Epidermal growth factor receptor (EGFR) tyrosine kinase inhibitor (TKI) targeting therapy has shown promise in the treatment of non-small cell lung cancer (NSCLC) with common *EGFR* mutations, such as L858R and exon 19 deletion (exon 19del) (1). With the rapid development of next-generation sequencing (NGS) technology, many atypical mutations have been identified in *EGFR* exons 18, 19, 20, and 21, respectively, but their sensitivity to TKIs is unclear. In the current study, afatinib, in particular, has demonstrated clinical efficacy in the treatment of some uncommon mutations, compound mutations, and some exon 20 insertions (2, 3).

Previous studies have shown that NSCLC with peritoneal metastases is rare (approximately 2%) (4) and has a poor prognosis with a median overall survival (mOS) of less than 3 months (5). Peritoneal metastases from NSCLC are often complicated by peritoneal effusion. Once malignant ascites occurs, it usually means that patients are in poor physical condition and lose the opportunity for treatment (6). Owing to the lack of experience in treating peritoneal complications, oncologists face a great challenge in the treatment of NSCLC with peritoneal metastases (7). Here, we report the case of a patient carrying *EGFR* E746_L747delinsIP mutated lung adenocarcinoma (LUAD) with

peritoneal metastases that was successfully treated with the second-generation EGFR TKI targeted therapy, afatinib.

CASE PRESENTATION

A 57-year-old Chinese woman without a smoking history or family history of cancer suffered from a cough in January 2020. In April 2020, computed tomography (CT) scans revealed right atelectasis, lung neoplasms, and pleural effusion (**Figure 1A**). Whole-body bone scans and magnetic resonance imaging of the brain revealed no evidence of metastasis. Using immunohistochemistry, the patient was diagnosed with LUAD (stage IV). The E746_L747delinsIP (6.6%) at exon 19 and the S1190F (1.74%) at exon 28 of the *EGFR* were identified in the pleural effusion biopsy specimen by NGS sequencing with a panel covering 525 cancer-related genes. None of the mutations were associated with EGFR-TKI primary resistance. Based on this result, the patient started treatment with gefitinib (250 mg/day) in June 2020; however, no radiological response was observed during treatment. Unfortunately, she experienced slow progressive disease (PD) with increasing lung neoplasms and emerging left pleural effusion in December 2020 (**Figures 1B–D**). The patient was then switched to icotinib in February 2021, because *EGFR* E746_L747delinsIP was misunderstood to be an *EGFR* exon 19 del, which is sensitive to the first-generation of EGFR-TKIs. However, PD was confirmed by CT showing peritoneal metastases in March 2021 (**Figures 1E, F**).

Repetitive NGS analysis using pleural effusion detected *EGFR* E746_L747delinsIP (13.7%) in exon 19 and S1190F (2.95%) in exon 28 with increasing variant allele frequencies (VAF) as per a small, customized panel covering 74 cancer target related genes in Yucebio Technology (**Figure 2**). A timeline illustrating the patient's medical history and therapy is presented in **Figure 1**. The patient was currently exhibiting PD. Some studies have suggested that anlotinib may provide survival benefits to patients with NSCLC with abdominal or pleural effusion (6, 8). Considering that the patient may not tolerate the adverse effects of afatinib, as well as refractory ascites, pleural effusion, and an Eastern Cooperative Oncology Group (ECOG) Performance Status score of 3, she received anlotinib (12 mg/day) in April 2021. During the treatment, the patient's chest symptoms were relieved, and simultaneously, CA125 and CYFRA21-1 showed a decreasing trend, especially CA125 (**Figure 3**); however, the peritoneal effusion with a chylous appearance continued to increase (**Figure 1G2**), requiring drainage of 1000–1500 ml per day. Anlotinib treatment was discontinued in September 2021 because of PD.

Peritoneal effusions were collected for further genetic analysis. As shown in **Figure 1**, *EGFR* E746_L747delinsIP (4.2%) and S1190F (0.88%) were found again without other mutations, indicating that the LUAD metastasized to the peritoneum. Afatinib (40 mg/day) was administered in September 2021. The patient had received afatinib for approximately 3.5 months and achieved a partial response with a significant improvement in ascites and right pleural effusion. The ascites gradually diminished, and

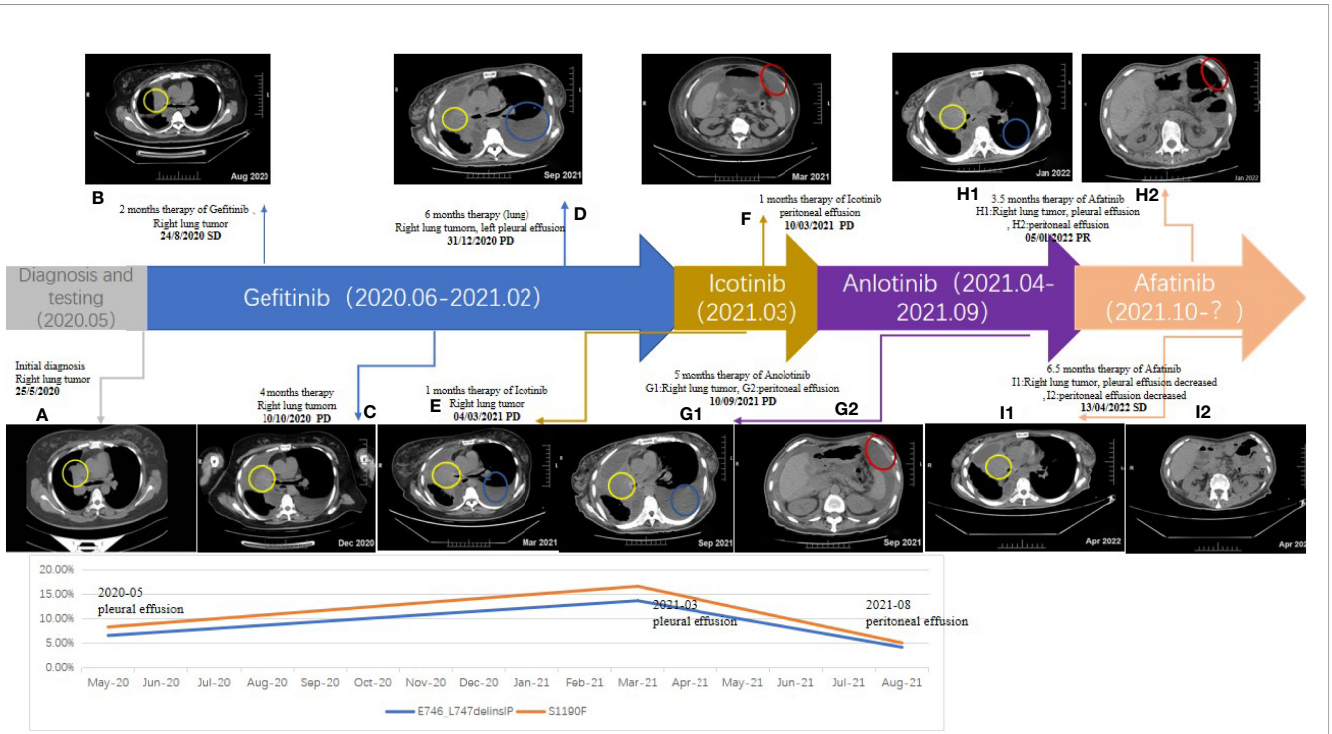

FIGURE 1 | Timeline of the patient: Chest and Abdominal contrast-enhanced CT **(A–F, G1, G2, H1, H2, I1, I2)**; yellow circle: right lung tumor; blue circle: left pleural effusion; red circle: peritoneal effusion.

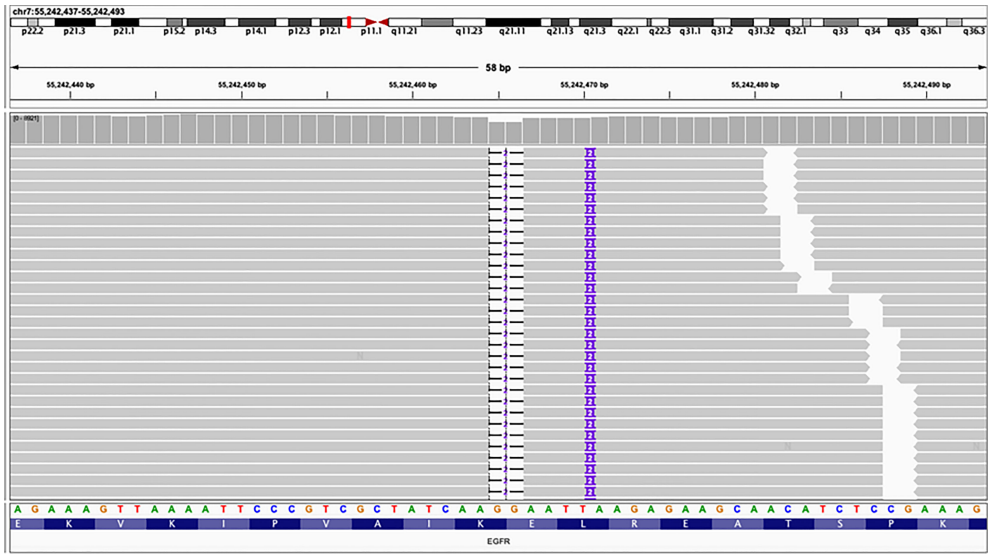

FIGURE 2 | Next-generation sequencing (NGS) panel result showed an epidermal growth factor receptor (EGFR) mutation E746_L747delinsIP *via* simultaneous deletion and insertion of DNA fragments of 2 bp in exon 19.

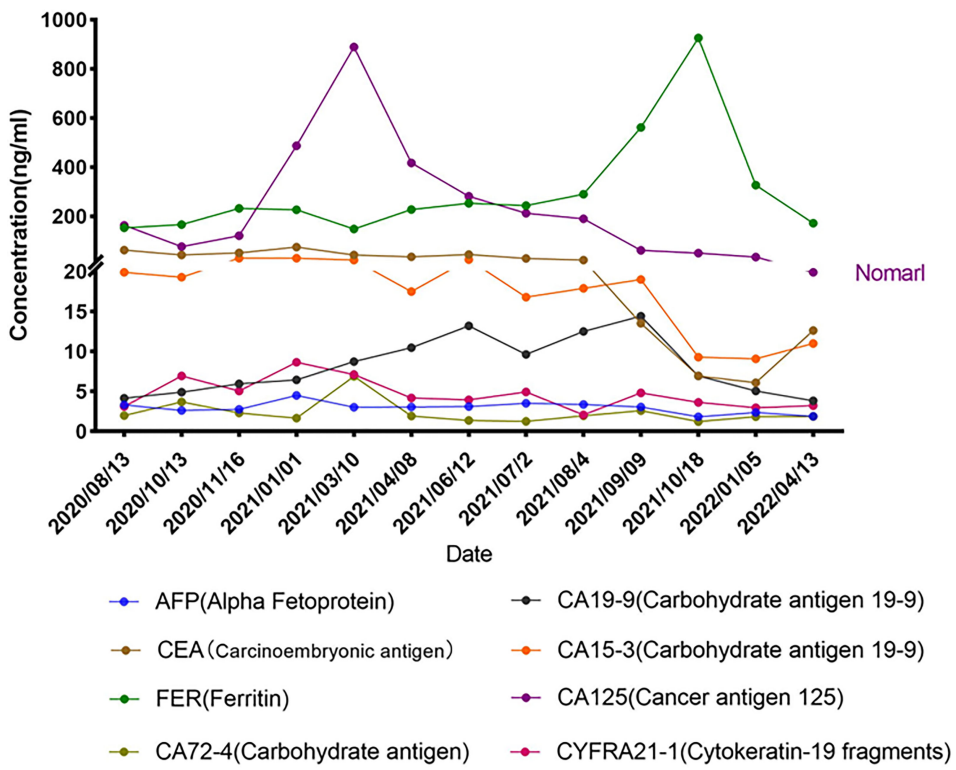

FIGURE 3 | Serum tumor biomarkers during treatment.

only a small amount of ascites was observed within the 1.5 months before the final test (**Figures 1H1, H2**). Serum tumor biomarkers showed a downward trend, especially CA125, decreasing to the average level for the first time (**Figure 3**). The treatment rapidly improved her clinical symptoms, including abdominal distension and appetite, despite the diarrhea. Her general condition improved from 3 to 2 according to the Eastern Cooperative Oncology Group Performance Status score. Since November 2021, the patient has had no further drainage of her ascites or pleural effusion, and the effusion showed a decreasing tendency. Follow-up CT until April 2022 showed that the pulmonary lesions were slightly enlarged, bilateral pulmonary nodules were increased, abdominal nodules continued to be stable, and the curative effect assessment of lesions primarily showed an increasing trend within the stable disease (SD) range (**Figures 1I1, I2**). Furthermore, the serum tumor biomarkers CEA and CYFRA21-1 showed an increase (**Figure 3**). In accordance with the patient's and her family's wishes, we performed a gene test using NGS again to explore if the patient developed drug-resistant mutations.

DISCUSSION

With the increasing popularity of NGS, uncommon *EGFR* mutations have been detected. However, some rare mutations lack clinical efficacy data, leading to the demand for continuous clinical reporting. Our case may be able to illustrate the sensitivity of the rare EGFR E746_L747delinsIP mutation to the efficacy of the first- and the second-generation EGFR-TKIs.

Here, we report the first efficacy data of an NSCLC patient carrying *EGFR* E746_L747delinsIP using the NGS platform. This mutation induces a double amino acid substitution (E746I-L747P) *via* the simultaneous deletion and insertion of two nucleotides at different positions in *EGFR* exon 19 (**Figure 2**). According to the Human Genome Variation Society (HGVS), this mutation is named *EGFR* E746_L747delinsIP (9). We also found a co-mutation *EGFR* S1190F, an uncertain clinically significant mutation, without any functional studies to affect the kinase domain of the EGFR or the efficacy of EGFR-TKIs.

In our case, the patient received gefitinib but continued to progress slowly, and according to the NCCN, it is a viable strategy for limited metastatic NSCLC to continue taking the first-generation EGFR-TKI. Therefore, icotinib was administered. A high frequency of *EGFR* E746_L747delinsIP mutation was found in ascites without other known TKI resistance mutations, indicating that *EGFR* E746_L747delinsIP might be resistant to first-generation TKIs. Pleural and ascites metastases from LUAD are relatively rare in patients with NSCLC. It has an inferior prognosis, with a mOS of approximately 1.3 months in the best supportive care group (7). We detected the same rare EGFR mutations in the patient's pleural fluid and ascites samples. It is plausible that *EGFR* E746_L747delinsIP is sensitive to afatinib owing to its remarkable polyserous effusions and abdominal response.

To date, no actual efficacy data have been reported for patients with NSCLC with *EGFR* E746_L747delinsIP. Koopman et al. (2021) considered it to be comparable to L747P and predicted it to be sensitive to EGFR TKI, and mentioned that *EGFR* E746_L747delinsIP was an uncommon, actionable mutation (10). Additionally, there are still some clinical case reports on L747P and found that the current assessment of L747P efficacy for the first- and third-generation EGFR-TKIs is inconsistent (11–13). Moreover, Coco et al. (2015) reported a similar case in which a patient carrying an *EGFR* E746V-L747P (E746_L747delinsVP) activating mutation caused by four continuous nucleotides (AATT > TTCC) was resistant to gefitinib. He predicted that *EGFR* E746V-L747P was resistant to gefitinib *via* structure prediction (14). The phenomenon presented in our case was similar to that described above. Therefore, we speculate that *EGFR* E746_L747delinsIP is a primary resistance variant for the first-generation EGFR-TKIs.

In addition, most case reports suggest that *EGFR* L747P is sensitive to afatinib *via* the Uncommon *EGFR* Mutations Database. Retrospective studies suggest that afatinib has clinical activity in NSCLC with uncommon *EGFR* mutations (3). A survey conducted by Robichaux et al. (2021) identified L747P as a PACC-class (P-loop and αC-helix compressing) variant, which was thought to be more effective against afatinib than any other TKI classes (15). Combined with the efficacy data of our case in the real world, we suggest that *EGFR* E746_L747delinsIP may be sensitive to afatinib, which is comparable to L747P.

In 2020, a retrospective study found that the NSCLC patients with uncommon *EGFR* exon 19 delins had significantly longer mPFS than those with the common exon 19 del with EGFR-TKI treatment (16). The patients in that study all presented *EGFR* exon19 in-frame deletion, which is unlike the complex variant in our case that did not cause any changes in amino acid length (**Supplementary 1**). *EGFR* exon 19 del at the K745-I759 position increases the kinase activity of EGFR, leading to the downstream pro-survival pathway hyperactivity, and consequently confers *EGFR* oncogenicity, which is sensitive to EGFR-TKIs (17, 18). Thus, the sensitivity of *EGFR* exon 19 rare complex delins mutation, in which the amino acid effect is missense mutations, to EGFR-TKIs warrants further investigation.

Our study had some limitations. First, the first-generation EGFR-TKI resistance mechanism of the *EGFR* E746_L747delinsIP should be supported by additional clinical data and functional studies. Second, large-scale data are required to support the use of afatinib to treat LUAD with *EGFR* E746_L747delinsIP, and a longer follow-up is needed to track the effect of afatinib on *EGFR* E746_L747delinsIP.

In conclusion, our case firstly showed that patients with rare *EGFR* E746_L747delinsIP mutated NSCLC-peritoneal metastases may be sensitive to afatinib and resistant to first-generation gefitinib and icotinib therapies. We suggest that first-generation EGFR-TKIs should be cautiously applied to patients with this *EGFR* exon 19 mutation, which causes amino acid substitution. Clinical trials are needed to develop treatment strategies for NSCLC harboring *EGFR* E746_L747delinsIP, and prospective or clinical studies are required to support these preliminary findings.

DATA AVAILABILITY STATEMENT

The datasets for this article are not publicly available due to concerns regarding participant/patient anonymity. Requests to access the datasets should be directed to the corresponding author.

ETHICS STATEMENT

Ethical review and approval was not required for the study on human participants in accordance with the local legislation and institutional requirements. The patients/participants provided their written informed consent to participate in this study. Written informed consent was obtained from the individual(s) for the publication of any potentially identifiable images or data included in this article.

AUTHOR CONTRIBUTIONS

FK and DW: Conceptualization, Methodology, and Review. LY, LZ, and BS: Data collection and analysis, Writing, and Editing. YD and JY: Literature research. All authors contributed to the article and approved the submitted version.

FUNDING

This work is supported by the National Natural Science Foundation of China (No. 81403220) and Tianjin Health and Family Planning-High Level Talent Selection and Training Project, National Key Research and Development (R&D) Plan (2018YFC1707400).

SUPPLEMENTARY MATERIAL

The Supplementary Material for this article can be found online at: https://www.frontiersin.org/articles/10.3389/fonc.2022.861271/full#supplementary-material

Supplementary 1 | Epidermal growth factor receptor tyrosine kinase inhibitor (EGFR-TKI) efficacy in non-small cell lung cancer (NSCLC) with rare EGFR exon 19 mutation.

REFERENCES

1. Li MM, Datto M, Duncavage EJ, Kulkarni S, Lindeman NI, Roy S, et al. Standards and Guidelines for the Interpretation and Reporting of Sequence Variants in Cancer: A Joint Consensus Recommendation of the Association for Molecular Pathology, American Society of Clinical Oncology, and College of American Pathologists. *J Mol Diagn* (2017) 19(1):4–23. doi: 10.1016/j.jmoldx.2016.10.002
2. Beau-Faller M, Prim N, Ruppert AM, Nanni-Metellus I, Lacave R, Lacroix L, et al. Rare EGFR Exon 18 and Exon 20 Mutations in Non-Small-Cell Lung Cancer on 10 117 Patients: A Multicentre Observational Study by the French ERMETIC-IFCT Network. *Ann Oncol* (2014) 25(1):126–31. doi: 10.1093/annonc/mdt418
3. Yang JC, Schuler M, Popat S, Miura S, Heeke S, Park K, et al. Afatinib for the Treatment of NSCLC Harboring Uncommon EGFR Mutations: A Database of 693 Cases. *J Thorac Oncol* (2020) 15(5):803–15. doi: 10.1016/j.jtho.2019.12.126
4. Lurvink RJ, Rijken A, Bakkers C, Aarts MJ, Kunst PWA, van deBorne BE, et al. Synchronous Peritoneal Metastases From Lung Cancer: Incidence, Associated Factors, Treatment and Survival: A Dutch Population-Based Study. *Clin Exp Metastasis* (2021) 38(3):295–303. doi: 10.1007/s10585-021-10085-z
5. Patil T, Aisner DL, Noonan SA, Bunn PA, Purcell WT, Carr LL, et al. Malignant Pleural Disease is Highly Associated With Subsequent Peritoneal Metastasis in Patients With Stage IV Non-Small Cell Lung Cancer Independent of Oncogene Status. *Lung Cancer* (2016) 96:27–32. doi: 10.1016/j.lungcan.2016.03.007
6. Cao B, Liu Y, Yin W, Li Q, Liang L. [A Single Center, Retrospective Analysis of Prognosis in Non-Small Cell Lung Cancer Patients With Peritoneal Carcinomatosis]. *Zhongguo Fei Ai Za Zhi* (2019) 22(3):143–50. doi: 10.3779/j.issn.1009-3419.2019.03.0
7. Tani T, Nakachi I, Ikemura S, Nukaga S, Ohgino K, Kuroda A, et al. Clinical Characteristics and Therapeutic Outcomes of Metastatic Peritoneal Carcinomatosis in Non-Small-Cell Lung Cancer. *Cancer Manag Res* (2021) 13:7497–503. doi: 10.2147/CMAR.S330103
8. Liu Y, Cheng Y, Wang Q, Li K, Shi J, Wu L, et al. 1787p Effect of Anlotinib in Advanced Small Cell Lung Cancer Patients With Pleural Metastases/Pleural Effusion: A Subgroup Analysis From a Randomized, Double-Blind Phase II Trial (ALTER1202). *Ann Oncol* (2020) 31:S1036. doi: 10.1016/j.annonc.2020.08.1548
9. den Dunnen JT, Dalgleish R, Maglott DR, Hart RK, Greenblatt MS, McGowan-Jordan J, et al. HGVS Recommendations for the Description of Sequence Variants: 2016 Update. *Hum Mutat* (2016) 37(6):564–9. doi: 10.1002/humu.22981
10. Koopman B, Garcia BNC, Kuijpers C, Damhuis RAM, van derWekken AJ, Groen HJM, et al. A Nationwide Study on the Impact of Routine Testing for EGFR Mutations in Advanced NSCLC Reveals Distinct Survival Patterns Based on EGFR Mutation Subclasses. *Cancers (Basel)* (2021) 13(14):3641. doi: 10.3390/cancers13143641
11. Huang J, Wang Y, Zhai Y, Wang J. Non-Small Cell Lung Cancer Harboring a Rare EGFR L747P Mutation Showing Intrinsic Resistance to Both Gefitinib and Osimertinib (AZD9291): A Case Report. *Thorac Cancer* (2018) 9(6):745–9. doi: 10.1111/1759-7714.12637
12. Huang X, Yang Y, Wang P, Wang J, Chen S, Mao X, et al. A Rare EGFR Mutation L747P Conferred Therapeutic Efficacy to Both Ge Fi Tinib and Osimertinib: A Case Report. *Lung Cancer* (2020) 150:9–11. doi: 10.1016/j.lungcan.2020.09.017
13. van der Wekken AJ, Stigt JA, A'T Hart N. A Novel EGFR Mutation in Exon 19 Showed Stable Disease After TKI Treatment. *J Thorac Oncol* (2012) 7(8):e8. doi: 10.1097/JTO.0b013e31825ccae8
14. Coco S, Truini A, Vanni I, Genova C, Rosano C, Dal Bello MG, et al. Uncommon EGFR Exon 19 Mutations Confer Gefitinib Resistance in Advanced Lung Adenocarcinoma. *J Thorac Oncol* (2015) 10(6):e50–2. doi: 10.1097/JTO.0000000000000538
15. Robichaux JP, Le X, Vijayan RSK, Hicks JK, Heeke S, Elamin YY, et al. Structure-Based Classification Predicts Drug Response in EGFR-Mutant NSCLC. *Nature* (2021) 597(7878):732–7. doi: 10.1038/s41586-021-03898-1
16. Peng X, Long X, Liu L, Zeng L, Yang H, Jiang W, et al. Clinical Impact of Uncommon Epidermal Growth Factor Receptor Exon 19 Insertion-Deletion Variants on Epidermal Growth Factor Receptor-Tyrosine Kinase Inhibitor Efficacy in Non-Small-Cell Lung Cancer. *Eur J Cancer* (2020) 141:199–208. doi: 10.1016/j.ejca.2020.10.005
17. Zhang Z, Stiegler AL, Boggon TJ, Kobayashi S, Halmos B. EGFR-Mutated Lung Cancer: A Paradigm of Molecular Oncology. *Oncotarget* (2010) 1(7):497–514. doi: 10.18632/oncotarget.186
18. Rotow J, Bivona TG. Understanding and Targeting Resistance Mechanisms in NSCLC. *Nat Rev Cancer* (2017) 17(11):637–58. doi: 10.1038/nrc.2017.84

Conflict of Interest: Authors LY, YD, JY, and DW were employed by YuceBio Technology Co., Ltd.

The remaining authors declare that the research was conducted in the absence of any commercial or financial relationships that could be construed as a potential conflict of interest.

Publisher's Note: All claims expressed in this article are solely those of the authors and do not necessarily represent those of their affiliated organizations, or those of the publisher, the editors and the reviewers. Any product that may be evaluated in

this article, or claim that may be made by its manufacturer, is not guaranteed or endorsed by the publisher.

frontiers | Frontiers in Pharmacology

ORIGINAL RESEARCH
published: 09 August 2022
doi: 10.3389/fphar.2022.847499

Identification of PARP12 Inhibitors By Virtual Screening and Molecular Dynamics Simulations

Tahani M. Almeleebia[1†], Shahzaib Ahamad[2†], Irfan Ahmad[3], Ahmad Alshehri[4], Ali G. Alkhathami[3], Mohammad Y. Alshahrani[3], Mohammed A. Asiri[3], Amir Saeed[5,6], Jamshaid Ahmad Siddiqui[7], Dharmendra K. Yadav[8] and Mohd Saeed[9]**

[1]Department of Clinical Pharmacy, College of Pharmacy, King Khalid University, Abha, Saudi Arabia, [2]School of Biotechnology, IFTM University, Moradabad, India, [3]Department of Clinical Laboratory Sciences, College of Applied Medical Sciences, King Khalid University, Abha, Saudi Arabia, [4]College of Applied Medical Sciences, Najran University, Najran, Saudi Arabia, [5]Department of Clinical Laboratory Sciences, College of Applied Medical Sciences, University of Hail, Hail, Saudi Arabia, [6]Department of Medical Microbiology, Faculty of Medical Laboratory Sciences, University of Medical Sciences and Technology, Khartoum, Sudan, [7]Department of Transplant Immunology and Immunogenetics, All India Institute of Medical Sciences, New Delhi, India, [8]Department of Pharmacy, Gachon Institute of Pharmaceutical Sciences, College of Pharmacy, Gachon University of Medicine and Science, Incheon, South Korea, [9]Department of Biology, College of Sciences, University of Hail, Hail, Saudi Arabia

OPEN ACCESS

Edited by:
Fengfeng Zhou,
Jilin University, China

Reviewed by:
Debashree Chakraborty,
National Institute of Technology, Karnataka, India
Tugba Taskin-Tok,
University of Gaziantep, Turkey
Sumit Sharma,
Dr. B. R. Ambedkar National Institute of Technology Jalandhar, India

***Correspondence:**
Mohd Saeed
mo.saeed@uoh.edu.sa
Dharmendra K. Yadav
dharmendra30oct@gmail.com

†These authors have contributed equally to this work

Specialty section:
This article was submitted to Pharmacology of Anti-Cancer Drugs, a section of the journal Frontiers in Pharmacology

Received: *02 January 2022*
Accepted: *27 April 2022*
Published: *09 August 2022*

Citation:
Almeleebia TM, Ahamad S, Ahmad I, Alshehri A, Alkhathami AG, Alshahrani MY, Asiri MA, Saeed A, Siddiqui JA, Yadav DK and Saeed M (2022) Identification of PARP12 Inhibitors By Virtual Screening and Molecular Dynamics Simulations. Front. Pharmacol. 13:847499. doi: 10.3389/fphar.2022.847499

Poly [adenosine diphosphate (ADP)-ribose] polymerases (PARPs) are members of a family of 17 enzymes that performs several fundamental cellular processes. Aberrant activity (mutation) in PARP12 has been linked to various diseases including inflammation, cardiovascular disease, and cancer. Herein, a large library of compounds (ZINC-FDA database) has been screened virtually to identify potential PARP12 inhibitor(s). The best compounds were selected on the basis of binding affinity scores and poses. Molecular dynamics (MD) simulation and binding free energy calculation (MMGBSA) were carried out to delineate the stability and dynamics of the resulting complexes. To this end, root means deviations, relative fluctuation, atomic gyration, compactness, covariance, residue-residue contact map, and free energy landscapes were studied. These studies have revealed that compounds ZINC03830332, ZINC03830554, and ZINC03831186 are promising agents against mutated PARP12.

Keywords: PARP12, ZINC-FDA, virtual screening, MMGBSA, MD simulations

1 INTRODUCTION

Poly [adenosine diphosphate (ADP)-ribose] polymerases (PARPs) are the nuclear enzymes that regulate fundamental cellular processes involving protein degradation and gene expression (Kim et al., 2011; Bai and Virag, 2012; Langelier et al., 2018). PARPs use nicotinamide adenine dinucleotide (NAD+) for the process of post-translation that modify substrate proteins with ADP-ribose, a vital process referred to as ADP ribosylation (Carter-O'Connell and Cohen, 2015; Griffiths et al., 2020). The majority of PARP family members are monoPARPs as they catalyze the transfer of mono-ADP-ribose (MAR) onto their substrates (MARylation) (Cohen, 2020). In contrast, polyPARPs attach polymers of poly-ADP-ribose (PAR) onto their substrates (PARylation) (Carter-O'Connell and Cohen, 2015; Lu et al., 2019). PARP1 is a well-known cancer target involved in DNA damage-induced cellular stress/genetic mutation/cytotoxic chemotherapy (Gozgit et al., 2021). There are four drugs readily available on the market, and other drugs are at their late-stage development (Schiewer et al., 2012; Schiewer and Knudsen, 2014; Green et al., 2015; Rudolph et al., 2021). PARP12 is also a

mono-ART of the PARP family, which controls the regulation of cell survival and regrowth (Catara et al., 2017). The function of PARP12 is the mono-ADP-ribosyltransferase that mediates mono-ADP-ribosylation of target proteins, although the molecular mechanism responsible for cell survival is still unclear (Catara et al., 2017; Grimaldi et al., 2020). Recently, PARP12 involvement in intracellular membrane transport at this point deserves much attention and alternative effective strategies (Gozgit et al., 2021). Several studies also suggested that PARP12 is a novel target that reduces breast cancer resistance to genotoxic stress (Ke et al., 2019). Thus, PARP12 is marked as a potential target that must be utilized further to identify and design potential inhibitors/vaccine candidates at the molecular and genetic levels. The authors identify PARP1 potent targets and various computational studies that have been published to utilize the ZINC-FDA library and traditional Chinese medicine (Costantino et al., 2001; Chen et al., 2014; Maksimainen et al., 2021; Sahin and Durdagi, 2021). Similarly, there are other recently published theoretical studies on PARP2 to find novel benzimidazole derivatives (Venugopal and Chakraborty, 2021).

Bioinformatics tools and databases are wonderful approaches to identify the novel drugs and vaccine candidates as an alternative strategy. Taking the lead from here, the current study aimed to utilize the available small-molecule ZINC database, which is a publicly available and accessible database. We used a comprehensive *in silico* approach involving literature mining, virtual screening based molecular docking, pharmacological analysis, and large-scale molecular dynamics (MD) simulations to identify potential PARP12 inhibitors from a pool of ZINC-FDA. We analyzed 3,100 chemically diverse pharmacologically active compounds (Sterling and Irwin, 2015). Based on the comparative analysis of docking scores, binding affinity, and energies, we selected four compounds, namely, ZINC03830332, ZINC03830554, ZINC03831186, and ZINC03831189. Consequently, the compounds were analyzed for ADME/T properties and were potential drug-like candidates. Furthermore, we analyzed the conformational stability of the docked complexes using MD simulations with the help of various parameters such as root mean square deviation (RMSD), root mean square fluctuation (RMSF), radius of gyration (Rg), solvent accessible surface area (SASA), free energy landscapes (FEL), H-bond monitoring, principal component analysis (PCA), and density distribution map (Ahamad et al., 2021b). Based on MD simulation results, two compounds (ZINC03830332 and ZINC03831186) were identified as PARP12 inhibitors.

2 MATERIALS AND METHODS

The work was carried out on a Dell workstation, 256 GB RAM, and NVIDIA graphics card GeForce GTX 1080Ti GDDR5 11 GB. The workstation was installed with several bioinformatics software applications such as GROningen MAchine for Chemical Simulations (GROMACS), XMGrace (GROMACS results analysis), and Schrödinger Molecular Mechanics Generalized Born Surface Area (MMGBSA) and 2D plots. The detailed workflow used in this study is represented in **Figure 1**.

2.1 Protein Preparation and Grid Generation for Docking Studies

The human PARP12 with four-point mutations (Val570, Gly573, His577, and Phe607) has been selected in this study. The PARP12 has a 701 amino acid length, and the crystal structure (PDB = 6V3W) is available with the PARP catalytic domain (496–680 amino acids). To identify the potential surface structural pockets, their shape and volume, internal cavities of the protein, and surface areas, 6V3W was given as the input (Gozgit et al., 2021). The active site and

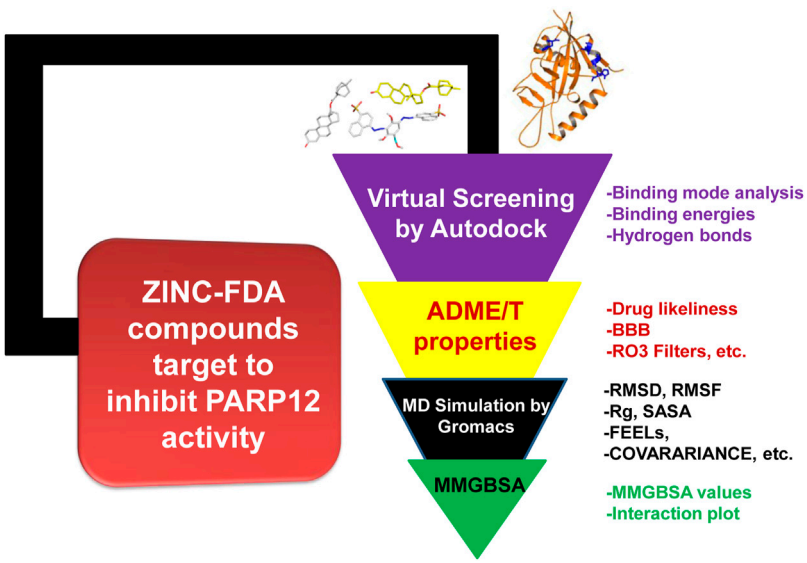

FIGURE 1 | Optimized protocol employed in this work.

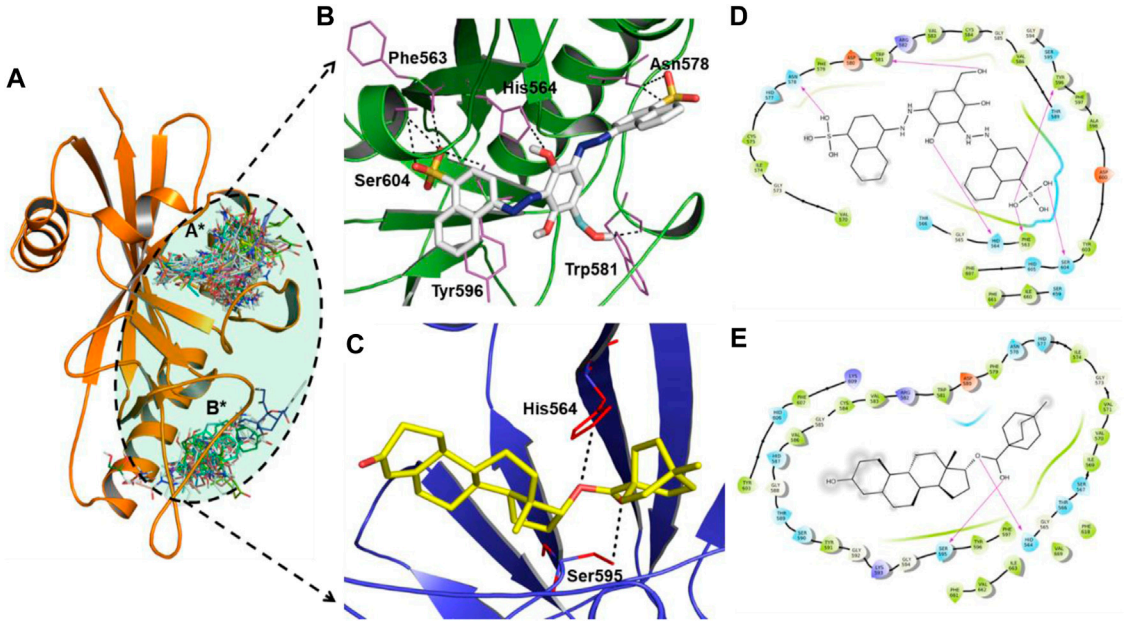

FIGURE 2 | (A) Close-up view of the binding pockets (A* and B* encircled by black dotted lines) of the PARP12 enzyme. H-bond interactions between **(B)** ZINC03830332 (white stick), **(C)** ZINC03831186 (yellow stick), and PARP12 receptor (in green and blue color cartoon models). **(D,E)** 2D plot of the complexes.

the interactive residues were identified using the online tools CASTp and PDBsum and verified using the literature (Laskowski, 2001; Dundas et al., 2006; Gozgit et al., 2021). The ligands (FDA-ZINC compounds) were prepared using AutoDock tools (ADT) by converting the PDB file into a PDBQT format (Huey and Morris, 2008; Ahamad et al., 2019). The crystal structure of PARP12 was prepared by using the ADT protein preparation wizard. Polar hydrogen (H) bonds and missing H-atoms were added while the water molecules and heteroatoms were deleted from the 3D structure. Energy minimization was performed with a default constraint of 0.3 Å root mean square (RMS), and charges were assigned. Finally, the clean structure was saved as a PDBQT file, and docking was performed by AutoDockVina (version 1.1.2) software (Trott and Olson, 2010). The size of the grid box selected was 106 Å × 108 Å × 106 Å, respectively, and generated around the centroid of the compounds and PARP12 complex. Default parameter settings were used during docking. The 3D structure of the docked complexes was analyzed with the help of the PyMOL visualization tool (DeLano, 2002).

2.2 Structure-Based Virtual Screening

The PDBQT formatted ligands (ZINC-FDA compounds) were screened against PARP12. A total of 3,100 molecules were retrieved from the ZINC-FDA database to identify potential PARP12 inhibitors (Sterling and Irwin, 2015). The compounds were ranked on the basis of their binding energy scores and docking interaction poses, and the top four compounds were selected.

2.3 Molecular Dynamics (MD) Simulations

MD simulations were carried out for the best-docked complexes using GROMACS (version 5.18.3) to determine the PARP12 enzyme behavior in the presence of water (Van Der Spoel et al., 2005; Abraham et al., 2015). The topology of PARP12 was created *via* the GROMOS9643a1 force field (Pronk et al., 2013). The PRODRG server was used to generate molecular topologies and coordinate files (Schuttelkopf and van Aalten, 2004). All the systems were solvated using a simple point-charge model (SPC/E) in a cubic box (Mark and Nilsson, 2001). To neutralize the system, 0.15 M counter ions (Na^+ and Cl^-) were added. The energy minimization of all the neutralized systems was performed using the steepest descent and conjugate gradients (50,000 steps for each). The volume (NVT) regulation and pressure (NPT) were run for system equilibration. Steepest descent followed by conjugate gradient algorithms was utilized on enzyme-ligand complexes. The NVT ensemble at a constant temperature of 300 K and the constant pressure of 1 bar was employed. The SHAKE algorithm was used to confine the H-atoms at their equilibrium distances and periodic boundary conditions.

Moreover, the particle mesh Ewald (PME) method was used to define long-range electrostatic forces (Darden et al., 1993; Lee et al., 2016; Wang et al., 2016). The cut-offs for van der Waals and Columbic interactions were 1.0 nm. The LINC algorithm was used to constrain the bonds and angles (Hess et al., 1997). Finally, the production runs were performed for the period of 500 ns The energy, velocity, and trajectory were updated at the time interval of 10 ps The MD simulation analyses were performed, and trajectoris were found by GROMACS utilities and MDTraj-based Python scripts (McGibbon et al., 2015). The Cα-atom deviations of PARP12 and complexes were utilized to calculate using RMSD and RMSF for relative fluctuations of each amino acid. The compactness was measured by Rg, while the SASA was

TABLE 1 | Average RMSD, Rg, SASA, and MMGBSA values of the mutant receptor and complexes. Molecular docking results of four shortlisted ZINC-FDA compounds.

Mutant system and complex	RMSD (nm)	Rg (nm)	SASA (nm^2)	MMGBSA ΔG score (kcal/mol)	Binding score (kcal/mol)	Residues involved in H-bonding	Residues involved in hydrophobic interaction
PARP12	0.43	1.57	101.70	-	-	-	-
ZINC03830332	0.32	1.59	102.17	−135.11	−12.40	Phe563, His564, Asn578, Trp581, Tyr596, and Ser604	Thr566, Val570, Gly573, Ile574, Cys575, His577, Phe579, Asp580, Arg582, Val583, Cys584, Gly585, Val586, Thr589, Gly594, Ser595, Phe597, Ala598, Asp600, Tyr603, His605, Phe607, Ser659, Ile660, and Phe661
ZINC03830554	0.34	1.58	104.02	−39.22	−11.80	Phe563, His564, His577, Asp580, Tyr596, Ser604, and Lys666	Val570, Gly573, Ile574, Val583, Gly565, Phe597, Ala598, Tyr603, and His606
ZINC03831186	0.32	1.59	103.26	−57.63	−11.40	His564 and Ser595	Gly565, Thr566, Ser567, Ile569, Val570, Val571, Gly573, Ile574, His577, Asn578, Phe579, Asp580, Trp581, Arg582, Val583, Cys584, Gly585, Val586, His587, Gly588, Thr589, Gly594, Ser595, Phe597, Ser590, Tyr591, Gly592, Lys593, Gly594, Phe597, Tyr603, His606, Phe607, Lys609, Phe661, Valy662, and Ile663
ZINC03831189	0.37	1.58	103.24	−51.92	−12.11	Gly594 and Ser604	Phe563, His564, Gly565, Thr566, Asn578, Phe579, Asp580, Trp581, Arg582, Val583, Cys584, Gly585, Val586, His587, Thr589, Gly592, Lys593, Ser595, Tyr596 Phe597, Ser590, Tyr591, Gly592, Ala598, Asp600, Ala601, Tyr603, His605, and Phe607

used to know the electrostatic contributions of molecular solvation. PCA is one of the best techniques that help reduce complexity to extract the intensive motions in MD simulation analysis. The matrix was formed for the MD trajectory after excluding rotational and translational movements. So the essential dynamics protocol was implemented to calculate the eigenvectors and eigenvalues and their projections along with the first two principal components (PCs). The diagonalized covariance matrix, eigenvectors, and eigenvalues were identified. The eigenvector of the matrix gives the multidimensional space and the displacement of atoms in the molecule in each direction. This analysis processed the essential subspace built on knowing each atom's movements, which were plotted by Cartesian trajectory coordinates using GROMACS utilities (Ahamad et al., 2021a).

2.4 MMGBSA Calculation

The MMGBSA (ΔG_{bind}) was calculated by the Schrödinger Prime module to compute the ligand binding energies. The prime-MMGBSA was used for rescoring the docked poses.

ΔG is calculated by the following equation:

$$\Delta Gbind = E\_complex\ (minimized) - E\_ligand\ (minimized) - E\_receptor\ (minimized),$$

where ΔG_{bind} specifies the binding free energy, $E_{\_complex}$ is the input for the energy minimization of the protein-ligand complexes, $E_{\_receptor}$ for the free protein, and $E_{\_ligand}$ for free ligands. The sum of molecular mechanical minimized energies including van der Waals interaction, internal energies, electrostatic energies, and solvation free energies were also calculated for the docked conformations.

3 RESULTS

Despite the fact that PARP12 is an intriguing target for treating various ailments, no computational studies on PARP12 have been carried out yet. Based on this notion, we screened 3,100 biologically active molecules from the FDA-approved drug database to find out lead(s) against the PARP12 enzyme. Out of these, four compounds (ZINC03830332, ZINC03830554, ZINC03831186, and ZINC03831189, **Supplementary Figure S1**) were selected on the basis of their docking score and interaction with the receptor. Moreover, the four best hits were analyzed for Lipinski and ADME/T properties. All-atom MD simulations were further performed on the mutant PARP12 and four-drug complexes. The results of the studies are discussed herein.

3.1 Molecular Docking

Molecular docking is a powerful tool for lead discovery and to underpin molecular interactions. **Figure 2A** depicts the binding pockets (A* and B* encircled by black dotted lines) of the PARP12 enzyme and binding poses of the docked ligands. Herein, we have shortlisted four compounds that carried the best binding free

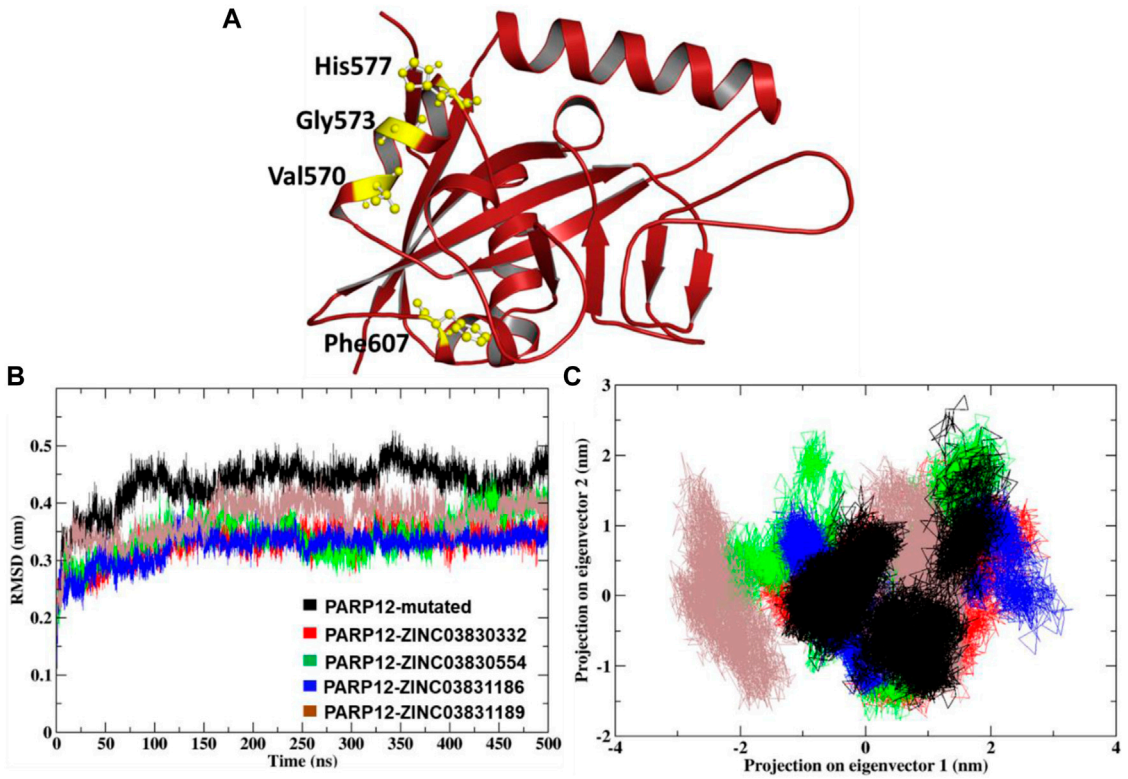

FIGURE 3 | (A) Mutation induced by PARP12 structures, **(B)** comparison of the RMSD plot, and **(C)** dynamic motion of projection in the eigenvector 1 vs. 2 and the plot two generated for the MD complexes showing conformational space of Cα-atoms.

energies, as well as polar and non-polar interactions. Molecular docking allows prediction of the preferred pose and binding orientations of a ligand inside a receptor binding site corresponding to the best energy score. The top-scoring shortlisted four compounds were docked in the A* binding pocket. However, B* binding pocket interaction compounds have fewer binding energies. **Figures 2B,C** and **Supplementary Figure S1** show the molecular interaction between the four hits and receptor. **Table 1** collects the results of the molecular docking study of four shortlisted ZINC-FDA compounds. It is clear from the figures that ligands interacted with the receptor via various polar and non-polar modes (**Figures 2D,E** and **Supplementary Figure S1**). It can be seen that ZINC03830332 formed six H-bonds with Phe563, His564, Asn578, Trp581, Tyr596, and Ser604 residues of the receptor with a docking score of −12.40 kcal/mol. On the other hand, the docking score for the PARP12-ZINC03831186 complex was −11.40 kcal/mol which formed two H-bonds with the receptors His564 and Ser595. The two other ligands ZINC03830554 and ZINC03831189 exhibited relatively higher docking scores (−11.80 kcal/mol and −12.11 kcal/mol, respectively) and interacted *via* seven (Phe563, His564, His577, Asp580, Tyr596, Ser604, and Lys666) and two (Gly594 and Ser604) H-bonds. The 2D plot analyses of PARP12-ligand complexes revealed that the complexes were also stabilized through hydrophobic interactions from nearby residues.

3.2 Physicochemical and ADME/T Studies

The shortlisted best four hits, namely, ZINC03830332, ZINC03830554, ZINC03831186, and ZINC03831189 compounds were used to calculate the pharmacological properties such as MW, dipole, SASA, FOSA, FISA, PISA, WPSA, volume, DonorHB, and AccptHB. We found that all the four molecules obeyed the rule of three (Ro3) (Kö;ster et al., 2011). Preferably, an orally active drug/compound should not cross more than one violation, but various exceptions are available (Lipinski, 2004). Two compounds (ZINC03830332 and ZINC03830554) violated one rule increase in MW, which is still acceptable. The results of the RO3 study revealed that the molecular weight of the compound was in the range of 422–693, with 4–10 H-bond acceptor and 0–14 H-bond donating units. The *in silico* absorption, distribution, metabolism, excretion (ADME), and toxicity (T) are the most widely used techniques in rational drug discovery as it gives a fair idea about the drug candidateship. In this context, we investigated the ADME/T and RO3 properties of the best four hits, and the results are compiled in **Supplementary Table S1**. The QikProp module output data generated for the compounds indicated that the blood–brain barrier (BBB) was in the range of −0.38 to −4.28 with QPlogPo/w between −0.55 and 5.73, QPlogKhsa between −0.63 and 1.14, SASA between 714.08 and 1,083.70, and log *Kp* value ranging from −2.41 to −10.90. Overall, the four hits showed fair enough properties and ability needed for a drug to

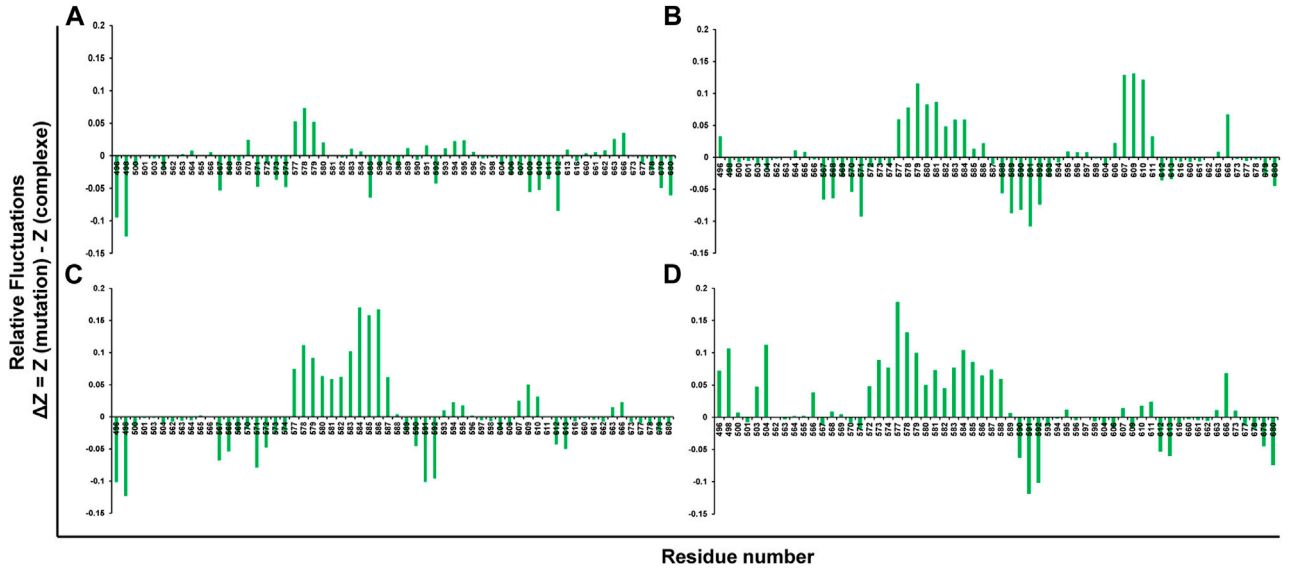

FIGURE 4 | Root mean square fluctuations (RMSFs) of mutant systems of PARP12 and **(A)** ZINC03830332, **(B)** ZINC03830554, **(C)** ZINC03831186, and **(D)** ZINC03831189.

possess (Lee et al., 2003; Lipinski, 2016; Nazarbahjat et al., 2016; Cordeiro and Kachroo, 2020).

3.3 Molecular Dynamics Simulation Analysis

MD simulations have the ability to uncover various dynamic interactions between a ligand and receptor, their interaction mechanism, and stability. MD simulation was carried out at the 0 to 500 nanosecond (ns) time scale for each system with a total of 2,500 ns. The MD simulations of the mutant systems of PARP12 and ZINC03830332, ZINC03830554, ZINC03831186, and ZINC03831189 complexes were utilized to measure the structural changes and parameters such as RMSD, RMSF, Rg, SASA, H-bonds, and Gibbs free energy, i.e., PCA calculation, covariance matrix, and density distribution map. The results of the findings are discussed as follows.

3.3.1 RMS Deviation and Principal Component Analysis

The MD simulation study result dictates the multidimensional data's relative distance to reduce the dimensional space. Atom-positional RMSD value C-alpha (C-α) atoms were calculated for the mutant system and complexes (**Figure 3A**). The MD simulation of mutant PARP12 systems and complexes with ZINC03830332, ZINC03830554, ZINC03831186, and ZINC03831189 compounds provided average RMSD values of ~0.43 nm, ~0.32 nm, ~0.34 nm, ~0.32 nm, and ~0.37 nm, respectively (**Figure 3B**). On the other hand, the mutant system of PARP12 attained equilibrium in 75 ns with a relatively higher average RMSD value due to the mutations in the helix and loop region. However, in the case of complexes, almost all the systems attained equilibrium within 30 ns and the steady-state in all the complexes except ZINC03831189, which possess a slightly greater RMSD value (~ 0.37 nm). Overall, the complexes involving ZINC03830332, ZINC03831186, and ZINC03830554 possessed a stable binding with PARP12.

The 2D projection of trajectories on eigenvectors 1 and 2 is the part of essential dynamics (ED) and reflect an overall expansion of the structural dynamics. The large-scale average motion indicated higher atomic fluctuations, and its flexibility measures the atomic mobility of the mutant and complexes. The eigenvector values of the docked complexes ZINC03830332, ZINC03830554, ZINC03831186, and ZINC03831189 were calculated. We found that the essential subspace for the mutant PARP12 of eigenvector 1 in the range from −1.5 to −2.5 nm, vs. eigenvector 2 in the range from −1.5 to 3 nm of a larger cluster for the mutant PARP12 (**Figure 3C**). Similarly, we extensively investigated the global motion for the complex of the ZINC03830332 compound. We found that the eigenvector 1 in the range from −1.5 nm to −2 nm vs. eigenvector 2 in the range from −1 to 1.5 nm occupied the smallest subspace throughout the MD simulation. However, compounds ZINC03830554 and ZINC03831186 had eigenvector 1 in the range −2 to 2 nm vs. eigenvector 2 in the range −1.5 to 2.5 nm and eigenvector 1 in the range −1 to 3 nm vs. eigenvector 2 in the range −1 to 1 nm, respectively. The compound ZINC03831189 had eigenvector 1 in the range −3 to 1.5 nm vs. eigenvector 2 in the range −1.5 to 2 nm. Out of four complexes, we found a more restricted subspace that leads to well-defined internal motion with ZINC03830332, ZINC03830554, and ZINC03831186 complexes.

The rigid regions and flexibility could be identified by RMSF analysis. The plot's negative drift indicates the increased movement of the Ca atoms of relative fluctuations. It was found that the compound ZINC03830332 showed stable positive amino acid fluctuations at F563-T566, V570, H577-W581, V583-596, Q613, I660-I663, K666, and Y673. A similar trend was found for the other two compounds with a high degree of flexibility (**Figures 4A–D**).

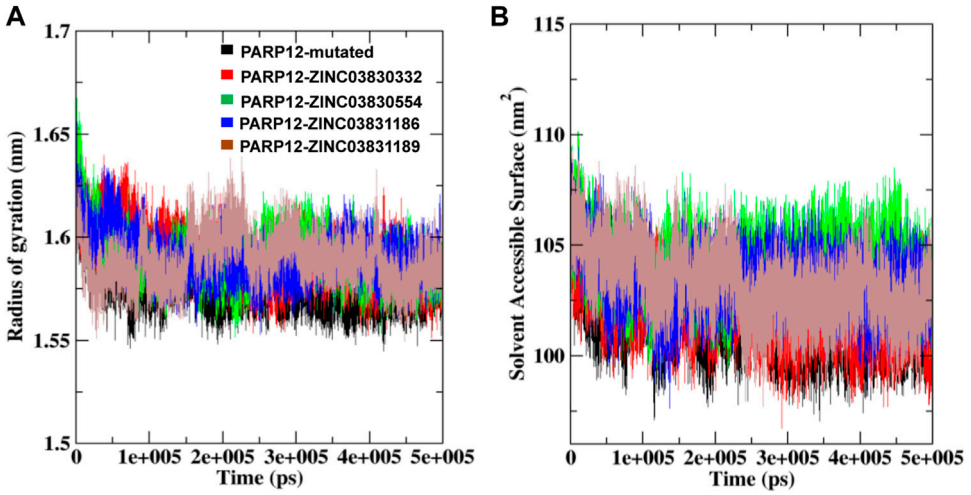

FIGURE 5 | (A) Rg and **(B)** SASA fluctuations per residue variation plot analysis of the mutant system and in the presence of compounds with PARP12 at total simulation time.

To gain more insight into the flexibility, the Rg plot, which measures the mass-weighted RMS distance of a cluster of atoms from their center of mass, was determined. The Rg analysis of C-α atoms of ligand–receptor docked complexes average values was calculated between 0 and 500 ns. **Figure 5A** illustrates the Rg plot, and the results indicated a compact conformation of the complexes, as compared to the native enzyme. For instance, average values ~1.57 nm, ~1.59 nm, ~1.58 nm, ~1.59 nm, and ~1.58 nm were found for PARP12 and ZINC03830332, ZINC03830554, ZINC03831186, and ZINC03831189 complexes, respectively (**Table 1**). Overall, the result suggested mutant expanded conformation while compact conformation for the complexes.

To understand the behavior of the PARP12 mutant system and all the complexes, we also performed a SASA analysis which revealed the PARP12 surface that can be accessed in the solvent (water). The average SASA value of the mutant PARP12, complexes with ZINC03830332, ZINC03830554, ZINC03831186, and ZINC03831189 were found to be 101.70, 102.17, 104.02, 103.26, and 103.24 nm^2, respectively, (**Figure 5B** and **Table 1**).

3.3.2 Hydrogen Bond Vetting

Hydrogen bonding plays a significant role in knowing the complexes' stability. To determine the binding affinity of the selected compounds toward the PARP12 receptor, MD trajectories were analyzed, and an H-bond investigation was carried out to determine the total number of bond formations. The ZINC03830332 and ZINC03830554 formed 0–14 H-bonds consistent for both the compounds' complexes with PARP12 throughout the 500 ns MD simulation. Similarly, the compound ZINC03831186 complex has quite less 0–5 number of H-bonds, whereas ZINC03831189 docked complexes showed H-bonds 0–4 (**supplementary Figures S3A–D**). The intermolecular H-bond examination revealed that the complex containing ZINC03830332 possessed a minimum of fourteen H-bonds during the MD simulation. The number of H-bond interactions also increased in the case of ZINC03830554 during the simulation. Contrarily, complexes containing ZINC03831186 and ZINC03831189 were unable to increase the number of H-bonds; however, both compounds showed consistency in the H-bonds' profile.

3.3.3 Free Energy Landscape Analysis

To monitor the distinct conformation of binding, FEL analysis was performed. The principal components (PCs) dictate the most dominant internal modes of motion of a corresponding system. In the ligand binding or complex formation in MD, through PCA, we found the most probable and dominant conformation changes of the protein during binding. The first PC1 and second PC2 utilized projected eigenvectors generated based on PCA (Stein et al., 2006). The contour map of the FEL derived conformational changes of the mutant system and complexes of PC1 and PC2 eigenvectors (**Figures 6A–E**). The Gibbs free energy landscape shows the global energy minima states (Ali et al., 2019; Ahamad et al., 2021b). The energetically favored PARP12 complex conformation is indicated by dark blue spots, while the unfavorable conformations are indicated by yellow spots. The values of FEL ranged from 0 kJ/mol to 19.1 kJ/mol, 18.2 kJ/mol, 18.2 kJ/mol, 18.1 kJ/mol, and 16.7 kJ/mol for the mutant PARP12 and ZINC03830332, ZINC03831186, ZINC03831189, and ZINC03830554 docked complexes, respectively. The FEL results demonstrated several well-defined energy minima, corresponding to the metastable conformational states. From **Figure 6**, it is clear that the main free energy wells in the global free energy minima area were altered when selected ZINC-FDA compounds were bound with PARP12. The PC analysis of the existing results confirmed that the FEL analysis is complimented to our previous RMSD finding.

The g_covar module by PCA monitors the conformational changes of C-α mutant and complexes. In this analysis, every single atom's collective motion along with directions provides

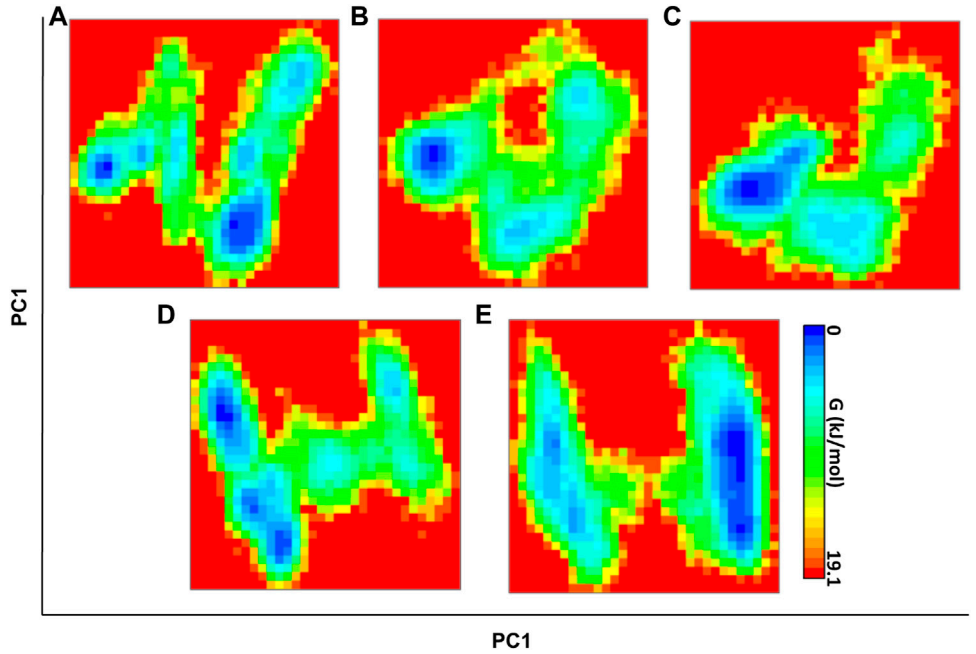

FIGURE 6 | FEL direction of motion and magnitude analysis of the mutant PARP12 **(A)** and complexes with ZINC03830332 **(B)**, ZINC03830554 **(C)**, ZINC03831186, and **(D)** ZINC03831189 **(E)** throughout MD simulations. The color bar denotes the relative free energy value between 0 and 19.1 kcal mol^{-1}.

a covariance matrix that uses atomic motion in Cartesian coordinate space. There are two types of motion: 1) correlated and 2) anticorrelated motion. The covariance matrix is constituted by two intense colors; red-colored region, which means atoms are moving together, and the blue-colored region, which means atoms are moving in the opposite direction. The matrix depicts that the reduction of negative correlation is largely exhibited with the ZINC03830332 complex. The covariance matrix results demonstrated that all the complexes were tolerable atomic displacement of ZINC03830332, ZINC03830554, and ZINC03831186 (**Supplementary Figure S4**). The increment in negative correlation was observed in the case of mutant, while reduction of both negative and positive motion was noted in the case of the ZINC03831189 complex. The overall positional fluctuations on Cα-atoms of all the docked complexes revealed that ZINC03830332, ZINC03830554, and ZINC03831186 were stable with steady atomic displacement and amplitude toward PARP12.

The atomic density distribution was measured using mutant PARP12 and complexes ZINC03830332, ZINC03830554, ZINC03831186, and ZINC03831189 ranging from 1.35 nm^{-3}, 1.89 nm^{-3}, 2.3 nm^{-3}, 1.88 nm^{-3}, and 1.38 nm^{-3}, respectively (**Supplementary Figure S5**). The results showed the stable density area for ZINC03830332, ZINC03830554, ZINC03831186, and ZINC03831189. The density area of each atom of the complexes ZINC03830332, ZINC03830554, and ZINC03831186 was examined to be in stable distribution; the energy wells displayed three compounds signifying the binding at the same binding site and the stabilized PARP12 enzyme.

4 DISCUSSION

Poly [adenosine diphosphate (ADP)-ribose] polymerases (PARPs) are one of the attractive and promising targets to treat several life-threatening diseases including cancer (Kim et al., 2011; Bai and Virág, 2012; Langelier et al., 2018). The present study was undertaken to identify promising lead(s) against the mutated PARP12 enzyme. We carried out an extensive *in silico* study, including virtual screening, drug-likeliness, MD simulations, and MMGBSA analyses. To the best of our knowledge, no computational studies on PARP12 have been carried out before. To this end, virtual screening of the ZINC-FDA dataset of 3,100 compounds was performed.

Molecular docking studies revealed the interaction of the compounds within the active site of receptor via multiple amino acids. For instance, other than H-bonds, the compound ZINC03830332 was also stabilized by Gly564, Thr566, Val570, Gly573, Ile574, Cys575, His577, Phe579, Asp580, Trp581, Arg582, Val583, Cys584, Gly585, Val586, Thr589, Gly594, Ser595, Phe597, Ala598, Asp600, Tyr603, His605, Phe607, Ser659, Ile660, and Phe661 residues. Furthermore, the best four hits (ZINC03830332, ZINC03830554, ZINC03831186, and ZINC03831189) were selected based on their docking score and ADME/T profile used for further studies. The results of the drug-likeness study revealed that the selected compounds obeyed Lipinski's properties very well and have a high propensity to be developed as a drug.

The MD simulation study revealed that mutation in the enzyme altered the enzyme dynamics as revealed by higher fluctuation throughout the MD simulation. However, upon interaction with

the ligand, PARP12 gets stabilized as indicated by smooth fluctuations and showed steady-state throughout the MD simulation. The results of the Rg analysis indicated stable folding behavior of PARP12 after binding with the compounds. The results suggested that the Rg values of complexes with four ZINC-FDA compounds stayed strongly bound to the binding site and maintained stable and enhanced compactness of the PARP12 structure better than the mutant system throughout the MD simulation. The H-bonding profile indicated that compounds ZINC03830332 and ZINC03830554 formed stable complexes throughout the MD simulation. The FEL demonstrated several energy minima corresponding to the metastable conformational states. This analysis observed that the main free energy wells in the global free energy minima area were altered by the ZINC-FDA compounds' complex bound with PARP12.

In addition, SASA study results showed that all the compounds achieved stable hydrophobic contacts, establishing the maximum region of PARP12 complexes accessible to the solvent molecules. The docked complexes exhibited higher average SASA profiles and stability than the native ligands.

5 CONCLUSION

In the present study, we used pharmacoinformatic techniques to identify potential inhibitors of mutant PARP12 receptors. Summarily, we conducted virtual screening, drug-likeliness, MD simulations, and MMGBSA to identify the best lead compounds amongst the ZINC-FDA compound library. Virtual screening–based molecular docking was carried out to select the best compounds capable of binding to the mutant PARP12 binding site, which helped shortlist the four compounds. Furthermore, Lipinski's rule of three and ADME/T properties checked the best four compounds with various parameters to get probable drug candidates. The RMSD, RMSF, H-bonds, essential dynamics, and FEL wells analysis dictated that out of 3,100 compounds, only three ZINC-FDA compounds were the most stable, which perfectly bind to the binding pocket PARP12. Overall, the results indicated that the compounds ZINC03830332, ZINC03830554, and ZINC03831186 were better than others. These promising candidates could be used in the future and should be further explored clinically.

DATA AVAILABILITY STATEMENT

The publicly available datasets were analyzed in this study. These data can be found at: https://zinc.docking.org/.

AUTHOR CONTRIBUTIONS

Conceptualization: TA, MS and DY; data curation: TA, IA, and MS; formal analysis: AA, AGA and DY; funding acquisition: TA and MS; investigation: TA, MS and DY; methodology: TA, MYA and MA; project administration: TA, MS, and DY; resources: TA, MS and DY. Analyzed the data: SA; Writing and corrections: JAS.

FUNDING

This research was funded by the Scientific Research Deanship at King Khalid University and the Ministry of Education in KSA, grant number IFP-KKU-2020/14.

SUPPLEMENTARY MATERIAL

The Supplementary Material for this article can be found online at: https://www.frontiersin.org/articles/10.3389/fphar.2022.847499/full#supplementary-material

REFERENCES

Abraham, M. J., Murtola, T., Schulz, R., Páll, S., Smith, J. C., Hess, B., et al. (2015). GROMACS: High Performance Molecular Simulations through Multi-Level Parallelism from Laptops to Supercomputers. *SoftwareX* 1-2, 19–25. doi:10.1016/j.softx.2015.06.001

Ahamad, S., Hema, K., Kumar, V., and Gupta, D. (2021a). The Structural, Functional, and Dynamic Effect of Tau Tubulin Kinase1 upon a Mutation: A Neuro-Degenerative Hotspot. *J. Cell Biochem.* 122, 1653–1664. doi:10.1002/jcb.30112

Ahamad, S., Islam, A., Ahmad, F., Dwivedi, N., and Hassan, M. I. (2019). 2/3D-QSAR, Molecular Docking and MD Simulation Studies of FtsZ Protein Targeting Benzimidazoles Derivatives. *Comput. Biol. Chem.* 78, 398–413. doi:10.1016/j.compbiolchem.2018.12.017

Ahamad, S., Kanipakam, H., Kumar, V., and Gupta, D. (2021b). A Molecular Journey to Check the Conformational Dynamics of Tau Tubulin Kinase 2 Mutations Associated with Alzheimer's Disease. *RSC Adv.* 11, 1320–1331. doi:10.1039/d0ra07659g

Ali, S., Khan, F. I., Mohammad, T., Lan, D., Hassan, M. I., and Wang, Y. (2019). Identification and Evaluation of Inhibitors of Lipase from Malassezia Restricta Using Virtual High-Throughput Screening and Molecular Dynamics Studies. *Int. J. Mol. Sci.* 20, 884. doi:10.3390/ijms20040884

Bai, P., and Virág, L. (2012). Role of poly(ADP-Ribose) Polymerases in the Regulation of Inflammatory Processes. *FEBS Lett.* 586, 3771–3777. doi:10.1016/j.febslet.2012.09.026

Carter-O'connell, I., and Cohen, M. S. (2015). Identifying Direct Protein Targets of Poly-ADP-Ribose Polymerases (PARPs) Using Engineered PARP Variants-Orthogonal Nicotinamide Adenine Dinucleotide (NAD+) Analog Pairs. *Curr. Protoc. Chem. Biol.* 7, 121–139. doi:10.1002/9780470559277.ch140259

Catara, G., Grimaldi, G., Schembri, L., Spano, D., Turacchio, G., Lo Monte, M., et al. (2017). PARP1-produced Poly-ADP-Ribose Causes the PARP12 Translocation to Stress Granules and Impairment of Golgi Complex Functions. *Sci. Rep.* 7, 14035. doi:10.1038/s41598-017-14156-8

Chen, K.-C., Sun, M.-F., and Chen, C. Y.-C. (2014). in Silico Investigation of Potential PARP-1 Inhibitors from Traditional Chinese Medicine. *Evid. Based Complement. Alternat. Med.* 2014:917605. doi:10.1155/2014/917605

Cohen, M. S. (2020). Interplay between Compartmentalized NAD+ Synthesis and Consumption: a Focus on the PARP Family. *Genes. Dev.* 34, 254–262. doi:10.1101/gad.335109.119

Cordeiro, R., and Kachroo, M. (2020). Synthesis and Biological Evaluation of Anti-tubercular Activity of Schiff Bases of 2-Amino Thiazoles. *Bioorg Med. Chem. Lett.* 30, 127655. doi:10.1016/j.bmcl.2020.127655

Costantino, G., Macchiarulo, A., Camaioni, E., and Pellicciari, R. (2001). Modeling of poly(ADP-Ribose)polymerase (PARP) Inhibitors. Docking of Ligands and

Quantitative Structure-Activity Relationship Analysis. *J. Med. Chem.* 44, 3786–3794. doi:10.1021/jm010116l

Darden, T., York, D., and Pedersen, L. (1993). Particle Mesh Ewald: AnN·Log(N) Method for Ewald Sums in Large Systems. *J. Chem. Phys.* 98, 10089–10092. doi:10.1063/1.464397

Delano, W. L. (2002). Pymol: An open-source molecular graphics tool. CCP4 Newsl. *Protein Crystallogr* 40 (1), 82-92.

Dundas, J., Ouyang, Z., Tseng, J., Binkowski, A., Turpaz, Y., and Liang, J. (2006). CASTp: Computed Atlas of Surface Topography of Proteins with Structural and Topographical Mapping of Functionally Annotated Residues. *Nucleic Acids Res.* 34, W116–W118. doi:10.1093/nar/gkl282

Gozgit, J. M., Vasbinder, M. M., Abo, R. P., Kunii, K., Kuplast-Barr, K. G., Gui, B., et al. (2021a). PARP7 Negatively Regulates the Type I Interferon Response in Cancer Cells and its Inhibition Triggers Antitumor Immunity. *Cancer Cell* 39, 1214–e10. e1210. doi:10.1016/j.ccell.2021.06.018

Green, A. R., Caracappa, D., Benhasouna, A. A., Alshareeda, A., Nolan, C. C., Macmillan, R. D., et al. (2015). Biological and Clinical Significance of PARP1 Protein Expression in Breast Cancer. *Breast Cancer Res. Treat.* 149, 353–362. doi:10.1007/s10549-014-3230-1

Griffiths, H. B. S., Williams, C., King, S. J., and Allison, S. J. (2020). Nicotinamide Adenine Dinucleotide (NAD+): Essential Redox Metabolite, Co-substrate and an Anti-cancer and Anti-ageing Therapeutic Target. *Biochem. Soc. Trans.* 48, 733–744. doi:10.1042/BST20190033

Grimaldi, G., Schembri, L., Monte, M. L., Spano, D., Di Martino, R., Beccari, A. R., et al. (2020). PARP12-catalyzed Mono-ADP-Ribosylation of Golgin-97 Controls the Transport of E-Cadherin. bioRxiv.

Hess, B., Bekker, H., Berendsen, H. J. C., and Fraaije, J. G. E. M. (1997). LINCS: a Linear Constraint Solver for Molecular Simulations. *J. Comput. Chem.* 18, 1463–1472. doi:10.1002/(sici)1096-987x(199709)18:12<1463::aid-jcc4>3.0.co;2-h

Huey, R., and Morris, G. M. (2008). *Using AutoDock 4 with AutoDocktools: A Tutorial*. USA: The Scripps Research Institute. 8, 54–56.

Ke, Y., Wang, C., Zhang, J., Zhong, X., Wang, R., Zeng, X., et al. (2019). The Role of PARPs in Inflammation-And Metabolic-Related Diseases: Molecular Mechanisms and beyond. *Cells* 8. 1047. doi:10.3390/cells8091047

Kim, M. S., An, C. H., Kim, S. S., Yoo, N. J., and Lee, S. H. (2011). Frameshift Mutations of Poly(adenosine Diphosphate-Ribose) Polymerase Genes in Gastric and Colorectal Cancers with Microsatellite Instability. *Hum. Pathol.* 42, 1289–1296. doi:10.1016/j.humpath.2010.11.020

Köster, H., Craan, T., Brass, S., Herhaus, C., Zentgraf, M., Neumann, L., et al. (2011). A Small Nonrule of 3 Compatible Fragment Library Provides High Hit Rate of Endothiapepsin Crystal Structures with Various Fragment Chemotypes. *J. Med. Chem.* 54, 7784–7796. doi:10.1021/jm200642w

Langelier, M. F., Eisemann, T., Riccio, A. A., and Pascal, J. M. (2018). PARP Family Enzymes: Regulation and Catalysis of the poly(ADP-Ribose) Posttranslational Modification. *Curr. Opin. Struct. Biol.* 53, 187–198. doi:10.1016/j.sbi.2018.11.002

Laskowski, R. A. (2001). PDBsum: Summaries and Analyses of PDB Structures. *Nucleic Acids Res.* 29, 221–222. doi:10.1093/nar/29.1.221

Lee, J., Cheng, X., Swails, J. M., Yeom, M. S., Eastman, P. K., Lemkul, J. A., et al. (2016). CHARMM-GUI Input Generator for NAMD, GROMACS, AMBER, OpenMM, and CHARMM/OpenMM Simulations Using the CHARMM36 Additive Force Field. *J. Chem. Theory Comput.* 12, 405–413. doi:10.1021/acs.jctc.5b00935

Lee, S., Lee, I., Kim, H., Chang, G., Chung, J., and No, K. (2003). "The PreADME Approach: Web-Based Program for Rapid Prediction of Physico-Chemical, Drug Absorption and Drug-like Properties. Blackwell Publishing: Boston, MA, USA, 2003; pp. 418–420.

Lipinski, C. A. (2004). Lead- and Drug-like Compounds: the Rule-Of-Five Revolution. *Drug Discov. Today Technol.* 1, 337–341. doi:10.1016/j.ddtec.2004.11.007

Lipinski, C. A. (2016). Rule of Five in 2015 and beyond: Target and Ligand Structural Limitations, Ligand Chemistry Structure and Drug Discovery Project Decisions. *Adv. Drug Deliv. Rev.* 101, 34–41. doi:10.1016/j.addr.2016.04.029

Lu, A. Z., Abo, R., Ren, Y., Gui, B., Mo, J. R., Blackwell, D., et al. (2019). Enabling Drug Discovery for the PARP Protein Family through the Detection of Mono-ADP-Ribosylation. *Biochem. Pharmacol.* 167, 97–106. doi:10.1016/j.bcp.2019.05.007

Maksimainen, M. M., Murthy, S., Sowa, S. T., Galera-Prat, A., Rolina, E., Heiskanen, J. P., et al. (2021). Analogs of TIQ-A as Inhibitors of Human Mono-ADP-Ribosylating PARPs. *Bioorg. Med. Chem.* 52, 116511. doi:10.1016/j.bmc.2021.116511

Mark, P., and Nilsson, L. (2001). Structure and Dynamics of the TIP3P, SPC, and SPC/E Water Models at 298 K. *J. Phys. Chem. A* 105, 9954–9960. doi:10.1021/jp003020w

Mcgibbon, R. T., Beauchamp, K. A., Harrigan, M. P., Klein, C., Swails, J. M., Hernández, C. X., et al. (2015). MDTraj: A Modern Open Library for the Analysis of Molecular Dynamics Trajectories. *Biophys. J.* 109, 1528–1532. doi:10.1016/j.bpj.2015.08.015

Nazarbahjat, N., Ariffin, A., Abdullah, Z., Abdulla, M. A., Shia, J. K. S., and Leong, K. H. (2016). Synthesis, Characterization, Drug-Likeness Properties and Determination of the *In Vitro* Antioxidant and Cytotoxic Activities of New 1,3,4-oxadiazole Derivatives. *Med. Chem. Res.* 25, 2015–2029. doi:10.1007/s00044-016-1660-5

Pronk, S., Páll, S., Schulz, R., Larsson, P., Bjelkmar, P., Apostolov, R., et al. (2013). GROMACS 4.5: a High-Throughput and Highly Parallel Open Source Molecular Simulation Toolkit. *Bioinformatics* 29, 845–854. doi:10.1093/bioinformatics/btt055

Rudolph, J., Roberts, G., and Luger, K. (2021). Histone Parylation Factor 1 Contributes to the Inhibition of PARP1 by Cancer Drugs. *Nat. Commun.* 12, 736. doi:10.1038/s41467-021-20998-8

Sahin, K., and Durdagi, S. (2021). Identifying New Piperazine-Based PARP1 Inhibitors Using Text Mining and Integrated Molecular Modeling Approaches. *J. Biomol. Struct. Dyn.* 39, 681–690. doi:10.1080/07391102.2020.1715262

Schiewer, M. J., Goodwin, J. F., Han, S., Brenner, J. C., Augello, M. A., Dean, J. L., et al. (2012). Dual Roles of PARP-1 Promote Cancer Growth and Progression. *Cancer Discov.* 2, 1134–1149. doi:10.1158/2159-8290.CD-12-0120

Schiewer, M. J., and Knudsen, K. E. (2014). Transcriptional Roles of PARP1 in Cancer. *Mol. Cancer Res.* 12, 1069–1080. doi:10.1158/1541-7786.MCR-13-0672

Schüttelkopf, A. W., and Van Aalten, D. M. (2004). PRODRG: a Tool for High-Throughput Crystallography of Protein-Ligand Complexes. *Acta Crystallogr. D. Biol. Crystallogr.* 60, 1355–1363. doi:10.1107/S0907444904011679

Stein, S. A. M., Loccisano, A. E., Firestine, S. M., and Evanseck, J. D. (2006). Chapter 13 Principal Components Analysis: A Review of its Application on Molecular Dynamics Data. *Annu. Rep. Comput. Chem.* 2, 233–261. doi:10.1016/s1574-1400(06)02013-5

Sterling, T., and Irwin, J. J. (2015). ZINC 15--Ligand Discovery for Everyone. *J. Chem. Inf. Model.* 55, 2324–2337. doi:10.1021/acs.jcim.5b00559

Trott, O., and Olson, A. J. (2010). AutoDock Vina: Improving the Speed and Accuracy of Docking with a New Scoring Function, Efficient Optimization, and Multithreading. *J. Comput. Chem.* 31, 455–461. doi:10.1002/jcc.21334

Van Der Spoel, D., Lindahl, E., Hess, B., Groenhof, G., Mark, A. E., and Berendsen, H. J. (2005). GROMACS: Fast, Flexible, and Free. *J. Comput. Chem.* 26, 1701–1718. doi:10.1002/jcc.20291

Venugopal, P. P., M, S., and Chakraborty, D. (2021). Theoretical Insights into Molecular Mechanism and Energy Criteria of PARP-2 Enzyme Inhibition by Benzimidazole Analogues. *Proteins* 89, 988–1004. doi:10.1002/prot.26077

Wang, H., Nakamura, H., and Fukuda, I. (2016). A Critical Appraisal of the Zero-Multipole Method: Structural, Thermodynamic, Dielectric, and Dynamical Properties of a Water System. *J. Chem. Phys.* 144, 114503. doi:10.1063/1.4943956

Conflict of Interest: The authors declare that the research was conducted in the absence of any commercial or financial relationships that could be construed as a potential conflict of interest.

Publisher's Note: All claims expressed in this article are solely those of the authors and do not necessarily represent those of their affiliated organizations, or those of the publisher, the editors, and the reviewers. Any product that may be evaluated in this article, or claim that may be made by its manufacturer, is not guaranteed or endorsed by the publisher.

frontiers | Frontiers in Pharmacology

TYPE Review
PUBLISHED 23 August 2022
DOI 10.3389/fphar.2022.944147

OPEN ACCESS

EDITED BY
Zhi Li,
The First Affiliated Hospital of China Medical University, China

REVIEWED BY
Pingli Mo,
Xiamen University, China
Justyna Agier,
Medical University of Lodz, Poland

*CORRESPONDENCE
Zunpeng Liu,
zpliu@cmu.edu.cn

SPECIALTY SECTION
This article was submitted to Pharmacology of Anti-Cancer Drugs, a section of the journal Frontiers in Pharmacology

RECEIVED 14 May 2022
ACCEPTED 22 July 2022
PUBLISHED 23 August 2022

CITATION
Lu F, Zhu Y, Zhang G and Liu Z (2022), Renovation as innovation: Repurposing human antibacterial peptide LL-37 for cancer therapy.
Front. Pharmacol. 13:944147.
doi: 10.3389/fphar.2022.944147

Renovation as innovation: Repurposing human antibacterial peptide LL-37 for cancer therapy

Fatai Lu, Yingkang Zhu, Guodong Zhang and Zunpeng Liu*

Department of Orthopedics, The Fourth Affiliated Hospital of China Medical University, Shenyang, China

In many organisms, antimicrobial peptides (AMPs) display wide activities in innate host defense against microbial pathogens. Mammalian AMPs include the cathelicidin and defensin families. LL37 is the only one member of the cathelicidin family of host defense peptides expressed in humans. Since its discovery, it has become clear that they have pleiotropic effects. In addition to its antibacterial properties, many studies have shown that LL37 is also involved in a wide variety of biological activities, including tissue repair, inflammatory responses, hemotaxis, and chemokine induction. Moreover, recent studies suggest that LL37 exhibits the intricate and contradictory effects in promoting or inhibiting tumor growth. Indeed, an increasing amount of evidence suggests that human LL37 including its fragments and analogs shows anticancer effects on many kinds of cancer cell lines, although LL37 is also involved in cancer progression. Focusing on recent information, in this review, we explore and summarize how LL37 contributes to anticancer effect as well as discuss the strategies to enhance delivery of this peptide and selectivity for cancer cells.

KEYWORDS

antimicrobial peptides, cathelicidin (LL37), hCAP18, LL37, cancer, anticancer

Introduction

As the key components of the innate host immune system, antimicrobial peptides (AMPs) have been discovered in almost all life forms, ranging from bacteria to higher mammals, and act as primary defense against a broad spectrum of pathogens (Jafari et al., 2022). Mammalian AMPs include the cathelicidin and defensin families. Cathelicidins possess a highly conserved cathelin-like prosequence and variable carboxyl-terminal sequences that are consistent with the mature AMPs (Johansson et al., 1998). The only member of cathelicidin identified in humans is hCAP18, which is a positively charged antibacterial protein, with a molecular weight of 18 kDa. LL-37 is released as an active domain of hCAP18 through extracellular cleavage mediated by proteinase-3 enzyme (Kuroda et al., 2015a).

A number of studies have reported that LL-37 exerts a diverse range of pleiotropic attributes including antimicrobial activities, immunity, angiogenesis, wound repair, and bone tissue engineering (Tjabringa et al., 2003; Elssner et al., 2004; Bucki et al., 2010;

Pfosser et al., 2010; Ramos et al., 2011; Liu et al., 2018; Mitchell et al., 2022). However, different from its traditional roles, emerging evidence from cancer biology studies suggests that LL-37 might promote or inhibit tumor progression (Ren et al., 2012; Piktel et al., 2016; Chen et al., 2018; Jiang et al., 2020; Chen et al., 2021; Vitale et al., 2021; Kiatsurayanon et al., 2022; Zhang et al., 2022). LL-37 plays an important and complex role in the regulation of different human cancers. These data are beginning to reveal the complex and contradictory functions of LL-37.

In this review, we first introduce the characteristic features of LL-37, focusing on its anticancer effects on various human cancers and the underlying mechanisms involved. Based on the recent studies, we also discuss the therapeutic implications of LL-37 as a potential anticancer drug. We believe that this important peptide will eventually be developed into a new anticancer drug suitable for clinical use in the future.

Characteristics and structure of LL-37

Characteristics of LL-37

Human AMPs include the cathelicidin and defensin families. Different from other animals, there is only one cathelicidin gene in humans (Frohm et al., 1997; Zanetti, 2005). As shown in Figure 1, the single *cathelicidin* gene called *CAMP* located on the human chromosome 3p21.3 encodes the human cationic antimicrobial peptide-18 (hCAP18) which is composed of 170 amino acids (Zanetti, 2004; Dürr et al., 2006). Like most antimicrobial peptides, hCAP18 is also produced as inactive preproproteins. It is a major component of the azurophilic granules of the neutrophils (Cowland et al., 1995; Sørensen et al., 2001) and is primarily produced by bone marrow, keratinocytes of inflamed sites, and cells of the mucosal epithelium (Agerberth et al., 1995; Chen and Fang, 2004; Tjabringa et al., 2005; Wolk et al., 2006). Once cell injury or infection occurs, it can provide a trigger to activate the cell degranulation by stimulating toll-like receptors (TLRs) and/or altering the cytokine (Vandamme et al., 2012). Thereafter, the inactive hCAP18 precursor protein is released from the intracellular environment and then processed by the proteolytic cleavage into the active LL-37 peptide (Zaiou et al., 2003; Fahy and Wewers, 2005; Pazgier et al., 2013).

LL-37 (4.5 kDa) is an active 37-amino acid peptide. The precursor protein pre-hCAP18 (18 kDa) is converted into propeptide hCAP18 (16 kDa) *via* processing of the signaling peptide, and then the active LL-37 peptide is produced from the C-terminus of hCAP18 *via* specific serine proteases, for instance, proteinase 3 (PR3) (Vandamme et al., 2012; Gudmundsson et al., 1996). Its primary sequence is LLGDFFRKSKEKIGKEFKRIVQRIKDFLRNLVPRTES (Gudmundsson et al., 1996). LL-37 is commonly found in mucosal secretion, sweat, semen, urine, breast milk, and plasma (Malm et al., 2000; Murakami et al., 2002; Armogida et al., 2004; Rieg et al., 2005; Berkestedt et al., 2010; Fábián et al., 2012; Babikir et al., 2018).

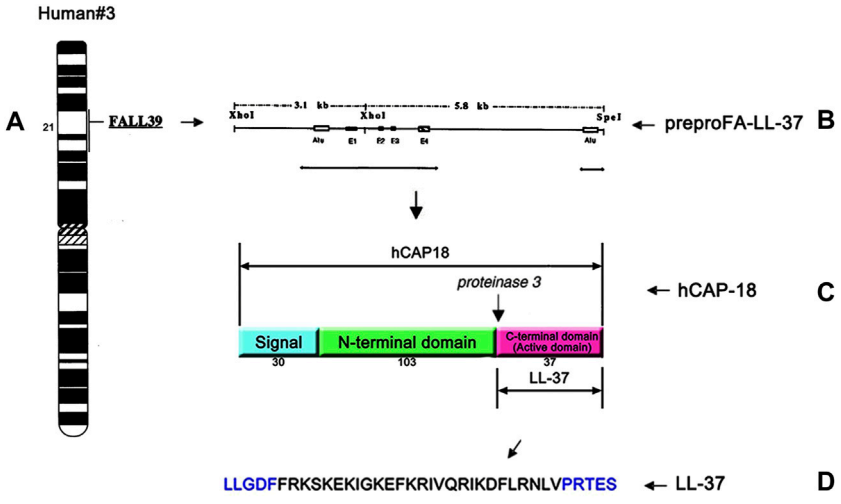

FIGURE 1
Single cathelicidin gene called *CAMP* located on human chromosome 3p21.3 encodes hCAP18 **(A)**, a schematic drawing of cDNA for the complete prepro-LL-37 **(B)**, structure and cleavage sites of hCAP18 **(C)**, and the amino acid sequence of the antibacterial peptide LL-37 **(D)**. The human cathelicidin hCAP18 consists of a signal peptide (30 amino acids), N-terminal domain (103 amino acids), and C-terminal domain (37 amino acids). The C-terminal domain shows various activities as an active domain and is called LL-37.

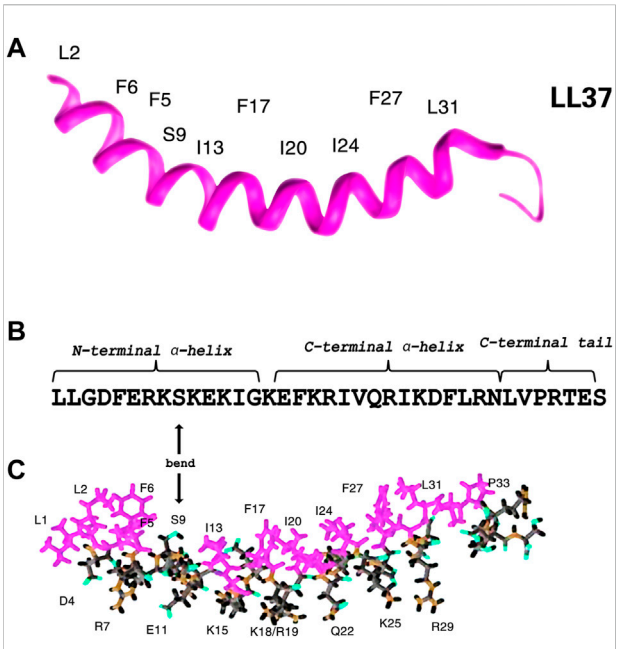

FIGURE 2
Three-dimensional structure of human cathelicidin reveals a helix followed by a C-terminal tail. Note the four phenylalanine side chains lying on the concave surface of the peptide (F6, F5, F17, and F27) **(A)**. Sequence of LL-37. S9 is marked **(B)**. Stick view of the structure of LL-37 with hydrophobic and hydrophilic residues selectively labeled. In both views, hydrophobic amino acids are in purplish red **(C)**. Therefore, it is evident that there is a discontinuation of the hydrophobic surface at S9 rather than the helices (Wang, 2008).

Structure of LL-37

According to previous circular dichroism (CD), Fourier transform infrared (FT-IR) (Tossi et al., 1994; Oren et al., 1999) spectroscopy, and NMR spectroscopy studies (Porcelli et al., 2008; Wang, 2008; Wang et al., 2014), LL-37 possesses a linear cationic α-helical structure which might aid to exert its function. As shown in Figures 2A,B, the α-helical structure spanning residues 2 to 31 with unstructured C-terminal residues 32 to 37 consists of three parts, namely, an N-terminal α-helix with a pair of leucine residues (LL), a C-terminal α-helix, and a disordered C-terminal tail (residues 32–37) (Porcelli et al., 2008; Wang, 2008; Wang et al., 2019). The C-terminal tail is mobile, while the helical region is rigid. LL-37 is bent with a series of hydrophobic side chains, whereas its hydrophobic surface bordered by the positively charged residues is composed of four distinct aromatic phenylalanine side chains that all point in the same direction (Wang, 2008; Vandamme et al., 2012). The amphiphilic peptide with a positive charge and net charge of +6 can facilitate an interaction with the negatively charged molecules or structures, such as bacterial cell walls (Wang, 2008). Similarly, LL-37 also targets and binds to the cancer cells as the anionic phosphoryl serine is exposed on their surface (Wu et al., 2010a). Interestingly, not only antimicrobial but also the anticancer effect is primarily exerted by the C-terminal helix (Li et al., 2006; Falcao et al., 2015). Moreover, the N-terminal helix has been related to hemolytic activity, proteolytic resistance, and chemotaxis, whereas the disordered C-terminal tail is essential for tetramerization (Wang, 2014). The two helices are separated by a bend or break. Furthermore, it has been found that the discontinuation is found on the hydrophobic surface at S9, rather than the helix (Figures 2B,C) (Wang, 2008; Zhang et al., 2021).

How LL-37 can eradicate/affect cancer?

The cytotoxic effects of numerous AMPs on different tumor cell lines have been reported previously (Cheng et al., 2020; Lee et al., 2021; Athira et al., 2022; Jafari et al., 2022; Patil and Kunda, 2022). These AMPs contain several cationic and hydrophobic amino acids and were found to be involved in various anticancer activities. They were thus termed as anticancer peptides (ACPs) (Hoskin and Ramamoorthy, 2008). ACPs can bind and kill the cancer cells through direct or indirect mechanisms (Dennison et al., 2006; Huang et al., 2015).

ACPs exert their biological functions in a diverse manner. These ACPs generally contain positively charged amino acids like lysine and arginine and possess a net positive charge ranging from +1 to +9 at neutral pH (Habes et al., 2019; Chiangjong et al., 2020). Moreover, as AMPs bind with bacterial membranes, ACPs can bind directly with the cancer cell walls due to their cationic and amphipathic nature (Ma et al., 2019). It has been established that different from normal eukaryotic cell membranes which are made of uncharged neutral phospholipids, sphingomyelins, and cholesterol and are neutral in charge (Zachowski, 1993; Doktorova et al., 2020), the surface of the cancer cells is net negatively charged because of increased proportions of anionic phosphatidylserine, heparan, and chondroitin sulfate proteoglycans, O-glycosylated mucins, and sialylated glycoproteins (Warren, 1974; Warren et al., 1979; Utsugi et al., 1991; Zwaal et al., 2005; Calianese and Birge, 2020; Brockhausen and Melamed, 2021; Hassan et al., 2021; Hugonnet et al., 2021). ACPs can selectively recognize cancer cells by electrostatic interactions with the negatively charged phospholipids on the surface. Some ACPs tend to kill cancer cells by causing membrane perturbation; however, some ACPs can penetrate the target cell and disrupt the mitochondrial membrane, thereby resulting in apoptosis (Deslouches and Di, 2017). ACPs bind to the membranes in different models, including carpet model, surface binding non-inserted, and perpendicular to the surface (Quemé-Peña et al., 2021). ACPs can enter the cells through two distinct mechanisms: direct or indirect. The former causes irreparable membrane damage,

followed by the cell lysis, which is non-energy dependent, and the latter can modulate the integrity of the cancer cell membrane by altering some intracellular pathways, thereby resulting in cell death by apoptosis, which is energy dependent (Kumar et al., 2018; Hilchie et al., 2019; Jafari et al., 2022).

One of the best-studied ACPs is LL-37. However, contradictory results have been shown for LL-37 linked to cancers in different models. The existing data indicate that LL-37 can exert a tumorigenic effect in some cancers, including lung cancer, breast cancer, ovarian cancer, melanoma, prostate cancer, liver cancer, and skin squamous cell carcinoma (Coffelt et al., 2009; Cha et al., 2016; Muñoz et al., 2016; Wang et al., 2017; Habes et al., 2019; Jiang et al., 2020; Ding et al., 2021; Zhang et al., 2022). Mechanistically, LL-37 activated Wnt/β-catenin signaling by inducing the phosphorylation of protein kinase B and subsequent phosphorylation of glycogen synthase kinase 3β mediated by the toll-like receptor-4 expressed in lung tumor cells (Ji et al., 2019). Furthermore, LL-37 cooperated with IL-33 to increase the phosphorylation of p38 MAPK and NF-κB p65 pathways and augmented IL-6 and IL-1β secretion, which resulted in the proliferation of lung cancer cells. Sulfated glycoaminoglycans and proteoglycan syndecan-4 increase the binding of LL-37 to the cell surface, which promotes the migration of breast cancer cells. In addition, *via* activating TRPV2 and PI3/Akt signaling, and then inducing recruitment of TRPV2 from intracellular vesicles to the plasma membrane of pseudopodia, LL-37 promotes proliferation and growth of breast cancer cells (Farabaugh et al., 2016). On the contrary, it has also been shown that LL-37 can exert anticancer effects on other cancers, including colon cancer, glioblastoma, hematologic malignancy, gastric cancer, and oral squamous cell carcinoma (Aarbiou et al., 2006; Wu et al., 2010b; Bruns et al., 2015; Prevete et al., 2015; Chen et al., 2020; Porter et al., 2021; Chernov et al., 2022). There is no smoking gun to explain the reported opposite effects on different cancer types. Whether and how LL-37 can affect cancer and metastasis deserves further studies. In the next section, our principal discussion focusses on the potential anticancer mechanisms of LL-37.

The membranolytic mechanisms

LL-37 could directly bind and perturb efficiently zwitterionic PC (phosphatidylcholine) and negatively charged PC/PS (phosphatidylcholine/phosphatidylserine) phospholipid membranes (Juba et al., 2015). The initial interaction with the membrane is primarily brought about by various electrostatic forces, and the correlation between the cationic charge and biological activity is strengthened with the increasing charge until the optimum charge for activity has been reached (Fillion et al., 2015; Juba et al., 2015). The presence of the negatively charged lipids such as anionic phosphatidylserine (PS) in membranes of the cancer cells can also mediate an electrostatic interaction with the cationic peptides (Alvares et al., 2017; Vasquez-Montes et al., 2019). In addition to its high net positive charge (+6) (Figure 3) that can markedly reduce the repulsive forces *via* neutralization by the negative charges, the high affinity of LL-37 for the negatively charged membranes in light of its hydrophobic interactions between the peptide and the membranes has been reported (Oren et al., 1999; Shai, 2002).

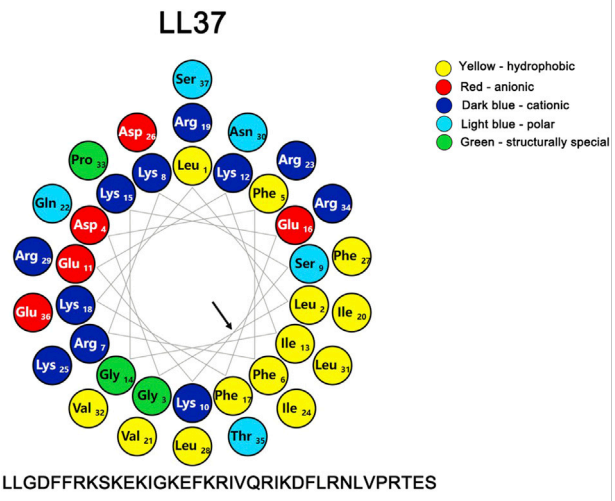

FIGURE 3
Helical wheel representation of LL-37, illustrating the amphipathic and cationic nature of LL-37. The residues are color coded: potentially negatively charged as red, potentially positively charged as dark blue, the hydrophobic residue is in yellow, the polar residues are coded as light blue, and the structurally special residues are coded as green. The helix diagram of the polypeptide was drawn with a Protein ORIGAMI (Reißer et al., 2018) software package. The arrow indicates the hydrophobic surface of the peptide.

A number of studies (Pouny and Shai, 1992; Oren et al., 1999; Ding et al., 2013; Wang, 2015; Lee et al., 2016; Zhao et al., 2018) have shown that, different from other ACPs, the model of action of LL-37 with negatively charged membranes such as the membranes of the cancer cells is a detergent-like effect exhibited through a "carpet-like" mechanism rather than a channel-forming model. In contrast to the channel formation mechanism, when bound to either zwitterionic PC or negatively charged PC/PS, LL-37 can effectively dissociate into monomers, and the hydrophobic N-terminus of LL-37 is buried only slightly in the membrane.

Specifically (Oren et al., 1999; Shai, 2002; Lee et al., 2016; Quemé-Peña et al., 2021), as shown in Figure 4, LL-37 reaches and remains on the negatively charged membranes such as the membranes of cancer cells as oligomers of different sizes; thereafter, a change in the membrane energetics and fluidity causes several local perturbations followed by dissociation into the monomers. Afterward, it is bound to the surface of the membrane, with the hydrophobic surface facing the membrane and the hydrophilic surface facing the solvent.

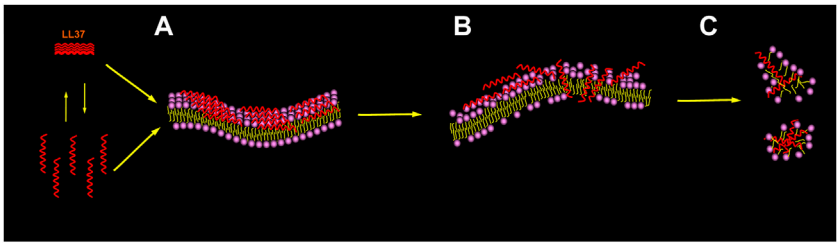

FIGURE 4
Membrane-associated mechanism for the peptide. Picture illustrating the carpet model recommended for membrane permeation. The initial binding to the membrane interface is mediated by the electrostatic interaction. The peptide reaches the membrane in the form of a monomer or oligomer and then binds to the membrane surface **(A)**. When the threshold concentration of peptide monomer is reached, the membrane is penetrated and forms instantaneous pores **(B)**, which also leads to membrane disintegration **(C)**.

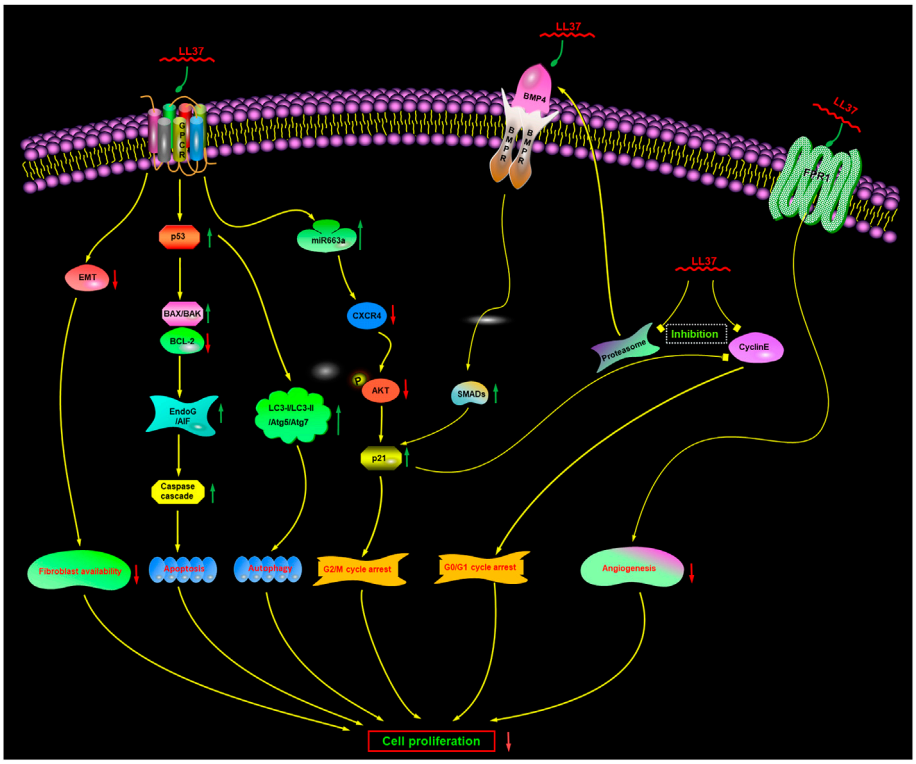

FIGURE 5
Proposed non-membranolytic anticancer mechanism of human cathelicidin LL-37. Inhibition of proteasome activity induces the upregulation of BMP4, which subsequently activates BMP signaling. GPCR, G protein-coupled receptor; CXCR4, CXC chemokine receptor type 4; EndoG, endonuclease G; AIF, apoptosis-inducing factor; FPR1, formyl peptide receptor 1. BMP4, bone morphogenetic protein 4; BMPR, bone morphogenetic protein receptor.

When the threshold concentration is reached, the peptide monomers can easily diffuse into the membrane, cover, and disintegrate it in a detergent-like manner through a "carpet-like" mechanism. The overall outcome can lead to cancer cell death, such as that reported in acute myeloid leukemia cells (Xhindoli et al., 2014), bronchial epithelial cancer cells (Tzitzilis et al., 2020), and human osteosarcoma cells (Bankell et al., 2021a).

The non-membranolytic mechanisms

It was originally thought that membranolytic mechanisms were the only mechanism of action, but there is increasing evidence now to suggest that there may be also additional or complementary non-membranolytic mechanisms (Figure 5), such as a receptor-mediated mechanism.

G protein-coupled receptors

G protein-coupled receptors (GPCRs) are membrane-embedded receptors that can regulate several important biological functions. In some cancer cells (Mader et al., 2009; Ren et al., 2012; Piktel et al., 2016), LL-37 induces characteristic apoptotic cell death in a caspase-independent manner, such as phosphatidylserine externalization and DNA fragmentation, without activation of caspases. One requirement for caspase-independent apoptosis of cancer cells is the altered activity of Bcl-2 and p53. LL-37 has been reported to reduce the level of antiapoptotic Bcl-2 and increase the level of pro-apoptotic Bax/Bak (Mader et al., 2009; Ren et al., 2012; Ren et al., 2013; Chen et al., 2020; Yang et al., 2021). LL-37 can also increase the expression of p53 and p53-upregulated modulator of apoptosis (PUMA) (Ren et al., 2012; Piktel et al., 2016; Chen et al., 2020). PUMA, a direct transcriptional target of p53, is a highly efficient pro-apoptotic protein and acts as a modulator of apoptosis in several cancer cell lines (Han et al., 2001; Yu et al., 2001; Jeffers et al., 2003; Yu et al., 2003; Yu and Zhang, 2003; Roufayel et al., 2022). Another requirement for the caspase-independent apoptosis of cancer cells is the upregulated expression and translocation of apoptosis-inducing factor (AIF) and endonuclease G (EndoG). After treatment with LL-37, the nuclear levels of both AIF and EndoG are prominently increased and translocated from the mitochondria into the nucleus, resulting in cancer cell apoptosis that is caspase-independent but calpain- and AIF-dependent apoptosis and mediated *via* BAX activation (Mader et al., 2009; Ren et al., 2012; Açil et al., 2018; Bankell et al., 2021b).

Nevertheless, interestingly, recent studies have suggested that except in a caspase-independent manner, the cell apoptosis induced by LL-37 can also occur through a caspase-dependent manner (Açil et al., 2018; Chen et al., 2020) *via* the p53-Bcl-2/BAX signaling pathway.

So, a mechanism was inferred that LL-37 can potentially exert its apoptogenic action in a caspase-independent or caspase-dependent manner *via* activating a GPCR-p53-Bax/Bak/Bcl-2 signaling cascade to trigger AIF/EndoG-mediated apoptosis.

Regulation of the proteasome activation *via* bone morphogenetic protein signaling

The bone morphogenetic protein (BMP) signal is an important tumor suppressive pathway involved in the process of tumorigenesis. It is initiated *via* the binding of BMP ligands to BMP receptors, which can then recruit and phosphorylate the downstream Smad1/5/8. Thereafter, the heterodimers are formed by phosphorylated Smads with Smad4, which can translocate into the nucleus as transcription factors to induce the transcription of various genes mediating the biological effects of BMPs (Varga and Wrana, 2005). The proteasome is a multimeric protein complex with proteolytic activity, which can effectively upregulate the level of BMP ligands and stimulate the phosphorylation of Smad1/5/8 (Wu et al., 2008a; Wu et al., 2008b; Zhang et al., 2014).

The anticancer effect of LL-37 has been reported to involve regulation of the proteasome activation *via* modulation of BMP signaling (Rajkumar et al., 2005; Wu et al., 2010b; Wu et al., 2010c). The chymotrypsin-like and caspase-like activities of 20S proteasome have been reported to be significantly inhibited by LL-37. The expression of BMP4 and the phosphorylation of Smad1/5 are upregulated, and then the expression of $p21^{Waf1}$ is subsequently induced at both the protein and mRNA levels (Rajkumar et al., 2005; Wu et al., 2010b). Furthermore, RNA interference which can target BMP receptor II was found to partially block the activation of the BMP signal and the inhibition of cell proliferation induced by LL-37. Moreover, LL-37 can also downregulate the expression level of cyclin E2 (Wu et al., 2010b). Both p21WAF1 and cyclin E2 can regulate the cell cycle progression by affecting the late G1 phase (Bartek and Lukas, 2001). As shown in Figure 5, the alteration of p21 and cyclin E2 expression levels can trigger G0/G1 phase cell cycle arrest and contribute to the antitumor effects of LL-37 (Wu et al., 2010a; Wu et al., 2010b). Furthermore, MG-132, the proteasome inhibitor, can produce similar effects to those of LL-37. It can induce the BMP/p21 cascade to inhibit cell proliferation in the gastric cancer cells. However, the inhibition of cancer cell proliferation could not be blocked by pertussis toxin. These findings clearly suggested that LL-37 could exert its anticancer effects through the activation of BMP signaling *via* a proteasome-dependent mechanism (Wu et al., 2010b).

LL-37 can act as an antitumor immunostimulatory agent on the host immune system

Immune modulation and anticancer activity are the two different faces of the same coin. A recent study has conclusively demonstrated that LL-37 can significantly influence immune responses as an essential component of innate immunity (Yang et al., 2020). Aside from the anticancer activity of LL-37, the immunostimulatory or adjuvant effect has also been used. CpG-oligodeoxynucleotides (CpG-ODNs), a toll-like receptor TLR9 ligand, are employed to enhance the tumor suppressive activity of the host immune cells in immunotherapy (Wu et al., 2010a). It has been shown that LL-37 can markedly enhance the perception of CpG-ODN and then induce the proliferation and activation of the host immune cells, such as natural killer (NK) cells, plasmacytoid dendritic cells, and B lymphocytes. These cells can thereafter induct and maintain antitumor immune responses and mediate tumor destruction (Chuang et al., 2009; Büchau et al., 2010; Hurtado and Peh, 2010).

Furthermore, it has been shown that LL-37 can act and expand OVA-antigen-specific $CD8^+$ T cells in draining the lymph nodes and the tumor microenvironment (Mader et al., 2011a; Singh et al., 2012), which could potentially delay tumor growth. LL-37 can also promote an anticancer immune response *via* inhibiting $CD25^+CD4^+FOXP3^+$T regulatory cells (Mader et al., 2011b). Moreover, some studies have demonstrated that intra-tumoral injections of LL-37 stimulate the innate immune system by acting plasmacytoid dendritic cells, which can in turn mediate tumor destruction (Dolkar et al., 2018). In fact, LL-37 has been utilized in a phase 1 clinical trial for melanoma patients with cutaneous metastases *via* intra-tumoral injections. These findings suggested that LL-37 could be employed as an antitumor immunostimulatory agent and could provide a promising strategy for antitumor immunotherapy.

Strategies to enhance LL-37 delivery and selectivity for cancer cells

Since both anticancer and cytotoxic activities of LL-37 are inhibited in human plasma, the delivery platform and modification strategies might be needed to ensure that LL-37 can reach the tumor microenvironment and promote tumor cell targeting, such as the use of nanoparticles and fusogenic liposomes and the design of peptides (Wang et al., 1998; Hilchie et al., 2019; Wang et al., 2019).

Use of nano-sized drug delivery systems

Application of nano-sized drug delivery systems can serve as a potential strategy to improve the delivery of peptides into host cells (Radaic et al., 2020). Nanoparticles with different structures and materials have been examined previously to facilitate the optimal delivery of anticancer peptides (Marverti et al., 2020; Akkın et al., 2021; Zielińska et al., 2021). In addition to being stable and non-toxic, the nanoparticles must be targetable in order to facilitate directed delivery of drugs to the exact tissues or cells (Hilchie et al., 2019). For instance, it has been reported that LL-37 loaded onto zinc oxide nanoparticles (ZnO NP) significantly suppressed the growth of the human lung cancer model cell line (BEAS-2B) (DeLong et al., 2019). Moreover, LL-37-loaded thermosensitive hydrogel nanoparticles displayed improved antiangiogenesis and antitumor activity (Fan et al., 2015). Moreover, it has been shown that CaP nanoparticles also can protect LL-37 from proteolysis (Tsikourkitoudi et al., 2020). Moreover, as reported in the literature, the anticancer activity of LL-37 improved when loaded onto the magnetic nanoparticles (Niemirowicz et al., 2015; Niemirowicz et al., 2017; Wnorowska et al., 2020).

Liposomes are lipid-based nanoparticles. Hydrophobic or hydrophilic drugs can be directly delivered into the target cancer cells *via* using fusogenic liposomes without the risk of degradation by the endocytic pathway (Malam et al., 2009; Kube et al., 2017). The drawbacks associated with use of liposomes include spontaneous fusion of the liposome membranes, which can cause decreased drug payload concentration and increase off-target toxicity (Monteiro et al., 2018; Akbarian et al., 2020). In order to solve these problems, nanoassemblies have been designed as an effective drug delivery vehicle. The lipid-coated targeted nanoassembly composed of Col@MSN@LL-(LL-37) has proved to be a successful delivery platform (Rathnayake et al., 2020).

These findings suggested that the formulation of LL-37 with nanoparticles could be successfully used as a potential therapeutic strategy to enhance the delivery of LL-37 against cancers.

Modification and alteration of the peptide

Another potential problem associated with LL-37 peptide is that it can be easily degraded by proteolytic enzymes present in the digestive system and blood plasma (Vlieghe et al., 2010). Susceptibility to degradation is primarily dependent on the peptide sequence. However, modification of the peptide and alteration of the sequence, such as the use of D-amino acid, sequence truncation, and modifications of C- and N-terminal, can render it unrecognizable by the various proteolytic enzymes and even influence the selectivity of the cancer cells as a basis for developing alternative cancer treatment approaches (Wang et al., 2019; Tornesello et al., 2020; Trinidad-Calderón et al., 2021). For instance, part of the LL-37 C-terminal domain, peptide sequence: FRKSKEKIGKEFKRIVQRIKDFLRNLV was found to display antiproliferative effects on human squamous cell carcinoma (Okumura et al., 2004). Moreover, a part of LL-37, KR12C: N-KRIVKLIKKWLR-C, could promote apoptosis in human breast cancer cells (Sengupta et al., 2018). The LL-37 fragments and analog peptides, such as FF/CAP18: FRKSKEKIGKFFKRIVQRIFDFLRNLV, with replacements of a glutamic acid residue and a phenylalanine at position 20, exhibited the functions of both inhibiting proliferation and promoting apoptosis in colon cancer (Kuroda et al., 2012; Kuroda et al., 2015b; Kuroda et al., 2017; Hayashi et al., 2018). Interestingly, the residues 17–32 of LL-37, abbreviated as FK-16 (FKRIVQRIKDFLRNLV) were found to induce apoptotic cell death and autophagy in the cancer cells, and these effects were even superior to that of LL-37 (Li et al., 2006; Ren et al., 2013; Zhang et al., 2019). It was observed that these peptides containing amino acid substitutions induce apoptosis in some specific types of cancer cells that have more negatively charged cell membranes than those in the normal cells, largely as compared to the original peptide. Furthermore, the variant of LL-37, obtained by cutting out both the C-terminus coil part and the N-terminus heparan sulfate binding region and

replacing some positively charged amino acids with histidines, was found to display higher affinity and generic tumor selectivity than the original peptide (Capozzi et al., 2018). Specific positional Q and K mutants of LL-37 were observed to have lower hemolytic toxicities and preserved the cell-penetrating ability of human breast cancer cells (Kim et al., 2016).

Combinatorial applications of LL-37

Interestingly, some evidence suggests that combined treatment using LL-37 and chemotherapy drugs can yield better results. For example, combinatorial application of LL-37 and etoposide exhibited significantly better antitumor effects on C6 glioma cells (Chernov et al., 2022). Compared with CpG ODN or LL-37 alone, the combination of LL-37 and CpG-ODN in the treatment of ovarian cancer can produce better antitumor effects and improve survival rates (Chuang et al., 2009). The mechanism can be expressed as the combinational use of LL-37, and CpG-ODN enhances the ability of human B lymphocytes and plasma-like dendritic cells to recognize and bind to CpG oligonucleotide and then leading to the activation of TLR-9 (Hurtado and Peh, 2010). Furthermore, the anticancer efficacy of the LL-37 fragment peptide analog was enhanced *via* linking PLGA conjugate (Mori et al., 2021). Compared with the peptide alone, the conjugate micelles were shown to effectively inhibit tumor cells and increase cell permeability in colon cancer, gastric cancer, hematologic malignancy, and oral squamous cell carcinoma. In addition, when LL37 was genetically fused with M-CSFRJ6-1 in the murine model, the antitumor immune response of the M-CSFRJ6-1 DNA vaccine was also enhanced (An et al., 2005). It suggests a possible use of LL-37 as an immune adjuvant in the gene therapy of some types of diseases, such as leukemia, Hodgkin's disease, and many solid tumors. This practical approach not only enhances the effect of traditional anticancer drugs but also markedly reduces the dosage of peptide and potential cytotoxicity.

Conclusion and future perspectives

Human cathelicidin LL-37 is an interesting peptide, which can display multiple functional roles and has been implicated in numerous diseases. The extensive functions of the peptide provide a scientific basis for analyzing its potential applications. The high interest in the therapeutic potential of this peptide originates from its potency against targeting bacteria. However, there is an increasing amount of evidence about the anticancer effects of LL-37. To date, the poor bioavailability, high production cost, and potential cytotoxicity have effectively limited the therapeutic use of LL-37.

Although a large number of studies have shown that the anticancer effects of LL-37 have potential applications in novel cancer treatment strategies, there remain some major challenges that need to be overcome. Particularly, as described in this review, the sensitivity of LL-37 varies among different cancer types. For instance, in colon cancer, glioblastoma, hematologic malignancy, gastric cancer, and oral squamous cell carcinoma, LL-37 can suppress proliferation and induce autophagy as well as apoptotic cell death *via* both non-membrane-based and membrane-based mechanisms. However, in other types of cancer, such as lung cancer, breast cancer, ovarian cancer, melanoma, prostate cancer, liver cancer, and skin squamous cell carcinoma, it can promote proliferation, migration, and tumorigenesis. To date, there is still no conclusive proof to explain the opposite effects of LL-37 on various cancer types. Furthermore, its selectivity and toxicity are complex. It will be very important to consider the different strategies to enhance both delivery and selectivity of LL-37 for cancer cells.

As a milestone, a phase 1 clinical trial (NCT02225366) with intra-tumoral injections of LL-37 for melanoma patients with cutaneous metastases has been completed and shown significant potency against cancer. We anticipate that research interest in the therapeutic potential of LL-37 will continue to expand, and there will be new discoveries in the near future. These achievements will reignite the hope to develop this important peptide into a novel anticancer drug suitable for clinical use.

Author contributions

Conceptualization: ZL and FL. Data curation: FL and YZ. Formal analysis: YZ. Investigation: FL and YZ. Methodology: ZL and FL. Project administration: FL and YZ. Resources: ZL. Software: FL and YZ. Supervision: ZL. Validation: ZL. Visualization: FL, YZ, and GZ. Writing—original draft: FL and YZ. Writing—review editing: ZL. ZL proposed the concept. FL and YZ wrote the main manuscript text. GZ prepared figures 1–5. All authors reviewed the manuscript.

Conflict of interest

The authors declare that the research was conducted in the absence of any commercial or financial relationships that could be construed as a potential conflict of interest.

The handling editor ZH declared a shared parent affiliation with the authors at the time of review.

Publisher's note

References

Aarbiou, J., Tjabringa, G. S., Verhoosel, R. M., Ninaber, D. K., White, S. R., Peltenburg, L. T., et al. (2006). Mechanisms of cell death induced by the neutrophil antimicrobial peptides alpha-defensins and LL-37. *Inflamm. Res.* 55 (3), 119–127. doi:10.1007/s00011-005-0062-9

Açil, Y., Torz, K., Gülses, A., Wieker, H., Gerle, M., Purcz, N., et al. (2018). An experimental study on antitumoral effects of KI-21-3, a synthetic fragment of antimicrobial peptide LL-37, on oral squamous cell carcinoma. *J. Craniomaxillofac. Surg.* 46 (9), 1586–1592. doi:10.1016/j.jcms.2018.05.048

Agerberth, B., Gunne, H., Odeberg, J., Kogner, P., Boman, H. G., and Gudmundsson, G. H. (1995). FALL-39, a putative human peptide antibiotic, is cysteine-free and expressed in bone marrow and testis. *Proc. Natl. Acad. Sci. U. S. A.* 92 (1), 195–199. doi:10.1073/pnas.92.1.195

Akbarian, A., Ebtekar, M., Pakravan, N., and Hassan, Z. M. (2020). Folate receptor alpha targeted delivery of artemether to breast cancer cells with folate-decorated human serum albumin nanoparticles. *Int. J. Biol. Macromol.* 152, 90–101. doi:10.1016/j.ijbiomac.2020.02.106

Akkın, S., Varan, G., and Bilensoy, E. (2021). A review on cancer immunotherapy and applications of nanotechnology to chemoimmunotherapy of different cancers. *Molecules* 26 (11), 3382. doi:10.3390/molecules26113382

Alvares, D. S., Wilke, N., Ruggiero Neto, J., and Fanani, M. L. (2017). The insertion of Polybia-MP1 peptide into phospholipid monolayers is regulated by its anionic nature and phase state. *Chem. Phys. Lipids* 207, 38–48. doi:10.1016/j.chemphyslip.2017.08.001

An, L. L., Yang, Y. H., Ma, X. T., Lin, Y. M., Li, G., Song, Y. H., et al. (2005). LL-37 enhances adaptive antitumor immune response in a murine model when genetically fused with M-CSFR (J6-1) DNA vaccine. *Leuk. Res.* 29 (5), 535–543. doi:10.1016/j.leukres.2004.11.009

Armogida, S. A., Yannaras, N. M., Melton, A. L., and Srivastava, M. D. (2004). Identification and quantification of innate immune system mediators in human breast milk. *Allergy Asthma Proc.* 25 (5), 297–304.

Athira, P. P., Anooja, V. V., Anju, M. V., Neelima, S., Archana, K., Muhammed Musthafa, S., et al. (2022). A hepatic antimicrobial peptide, hepcidin from Indian major carp, catla catla: Molecular identification and functional characterization. *J. Genet. Eng. Biotechnol.* 20 (1), 49. doi:10.1186/s43141-022-00330-7

Babikir, I. H., Abugroun, E. A., Bilal, N. E., Alghasham, A. A., Abdalla, E. E., and Adam, I. (2018). The impact of cathelicidin, the human antimicrobial peptide LL-37 in urinary tract infections. *BMC Infect. Dis.* 18 (1), 17. doi:10.1186/s12879-017-2901-z

Bankell, E., Dahl, S., Gidlöf, O., Svensson, D., and Nilsson, B. O. (2021a). LL-37-induced caspase-independent apoptosis is associated with plasma membrane permeabilization in human osteoblast-like cells. *Peptides* 135, 170432. doi:10.1016/j.peptides.2020.170432

Bankell, E., Liu, X., Lundqvist, M., Svensson, D., Swärd, K., Sparr, E., et al. (2021b). The antimicrobial peptide LL-37 triggers release of apoptosis-inducing factor and shows direct effects on mitochondria. *Biochem. Biophys. Rep.* 29, 101192. doi:10.1016/j.bbrep.2021.101192

Bartek, J., and Lukas, J. (2001). Pathways governing G1/S transition and their response to DNA damage. *FEBS Lett.* 490 (3), 117–122. doi:10.1016/s0014-5793(01)02114-7

Berkestedt, I., Herwald, H., Ljunggren, L., Nelson, A., and Bodelsson, M. (2010). Elevated plasma levels of antimicrobial polypeptides in patients with severe sepsis. *J. Innate Immun.* 2 (5), 478–482. doi:10.1159/000317036

Brockhausen, I., and Melamed, J. (2021). Mucins as anti-cancer targets: Perspectives of the glycobiologist. *Glycoconj. J.* 38 (4), 459–474. doi:10.1007/s10719-021-09986-8

Bruns, H., Büttner, M., Fabri, M., Mougiakakos, D., Bittenbring, J. T., Hoffmann, M. H., et al. (2015). Vitamin D-dependent induction of cathelicidin in human macrophages results in cytotoxicity against high-grade B cell lymphoma. *Sci. Transl. Med.* 7 (282), 282ra47. doi:10.1126/scitranslmed.aaa3230

Büchau, A. S., Morizane, S., Trowbridge, J., Schauber, J., Kotol, P., Bui, J. D., et al. (2010). The host defense peptide cathelicidin is required for NK cell-mediated suppression of tumor growth. *J. Immunol.* 184 (1), 369–378. doi:10.4049/jimmunol.0902110

Bucki, R., Leszczyńska, K., Namiot, A., and Sokołowski, W. (2010). Cathelicidin LL-37: A multitask antimicrobial peptide. *Arch. Immunol. Ther. Exp.* 58 (1), 15–25. doi:10.1007/s00005-009-0057-2

Calianese, D. C., and Birge, R. B. (2020). Biology of phosphatidylserine (PS): Basic physiology and implications in immunology, infectious disease, and cancer. *Cell Commun. Signal.* 18 (1), 41. doi:10.1186/s12964-020-00543-8

Capozzi, E., Aureli, S., Minicozzi, V., Rossi, G. C., Stellato, F., and Morante, S. (2018). Designing effective anticancer-radiopeptides. A Molecular Dynamics study of their interaction with model tumor and healthy cell membranes. *Biochim. Biophys. Acta. Biomembr.* 1860 (11), 2348–2355. doi:10.1016/j.bbamem.2018.05.021

Cha, H. R., Lee, J. H., Hensel, J. A., Sawant, A. B., Davis, B. H., Lee, C. M., et al. (2016). Prostate cancer-derived cathelicidin-related antimicrobial peptide facilitates macrophage differentiation and polarization of immature myeloid progenitors to protumorigenic macrophages. *Prostate* 76 (7), 624–636. doi:10.1002/pros.23155

Chen, K., Gong, W., Huang, J., Yoshimura, T., and Wang, J. M. (2021). The potentials of short fragments of human anti-microbial peptide LL-37 as a novel therapeutic modality for diseases. *Front. Biosci.* 26 (11), 1362–1372. doi:10.52586/5029

Chen, P. H., and Fang, S. Y. (2004). The expression of human antimicrobial peptide LL-37 in the human nasal mucosa. *Am. J. Rhinol.* 18 (6), 381–385. doi:10.1177/194589240401800608

Chen, X., Ji, S., Si, J., Zhang, X., Wang, X., Guo, Y., et al. (2020). Human cathelicidin antimicrobial peptide suppresses proliferation, migration and invasion of oral carcinoma HSC-3 cells *via* a novel mechanism involving caspase-3 mediated apoptosis. *Mol. Med. Rep.* 22 (6), 5243–5250. doi:10.3892/mmr.2020.11629

Chen, X., Zou, X., Qi, G., Tang, Y., Guo, Y., Si, J., et al. (2018). Roles and mechanisms of human cathelicidin LL-37 in cancer. *Cell. Physiol. biochem.* 47 (3), 1060–1073. doi:10.1159/000490183

Cheng, M. H., Pan, C. Y., Chen, N. F., Yang, S. N., Hsieh, S., Wen, Z. H., et al. (2020). Piscidin-1 induces apoptosis *via* mitochondrial reactive oxygen species-regulated mitochondrial dysfunction in human osteosarcoma cells. *Sci. Rep.* 10 (1), 5045. doi:10.1038/s41598-020-61876-5

Chernov, A. N., Tsapieva, A., Alaverdian, D. A., Filatenkova, T. A., Galimova, E. S., Suvorova, M., et al. (2022). *In vitro* evaluation of the cytotoxic effect of *Streptococcus pyogenes* strains, protegrin PG-1, cathelicidin LL-37, nerve growth factor and chemotherapy on the C6 glioma cell line. *Molecules* 27 (2), 569. doi:10.3390/molecules27020569

Chiangjong, W., Chutipongtanate, S., and Hongeng, S. (2020). Anticancer peptide: Physicochemical property, functional aspect and trend in clinical application (Review). *Int. J. Oncol.* 57 (3), 678–696. doi:10.3892/ijo.2020.5099

Chuang, C. M., Monie, A., Wu, A., Mao, C. P., and Hung, C. F. (2009). Treatment with LL-37 peptide enhances antitumor effects induced by CpG oligodeoxynucleotides against ovarian cancer. *Hum. Gene Ther.* 20 (4), 303–313. doi:10.1089/hum.2008.124

Coffelt, S. B., Marini, F. C., Watson, K., Zwezdaryk, K. J., Dembinski, J. L., LaMarca, H. L., et al. (2009). The pro-inflammatory peptide LL-37 promotes ovarian tumor progression through recruitment of multipotent mesenchymal stromal cells. *Proc. Natl. Acad. Sci. U. S. A.* 106 (10), 3806–3811. doi:10.1073/pnas.0900244106

Cowland, J. B., Johnsen, A. H., and Borregaard, N. (1995). hCAP-18, a cathelin/pro-bactenecin-like protein of human neutrophil specific granules. *FEBS Lett.* 368 (1), 173–176. doi:10.1016/0014-5793(95)00634-l

DeLong, R. K., Comer, J., Mathew, E. N., and Jaberi-Douraki, M. (2019). Comparative molecular immunological activity of physiological metal oxide nanoparticle and its anticancer peptide and RNA complexes. *Nanomater. (Basel)* 9 (12), 1670. doi:10.3390/nano9121670

Dennison, S. R., Whittaker, M., Harris, F., and Phoenix, D. A. (2006). Anticancer alpha-helical peptides and structure/function relationships underpinning their interactions with tumour cell membranes. *Curr. Protein Pept. Sci.* 7 (6), 487–499. doi:10.2174/138920306779025611

Deslouches, B., and Di, Y. P. (2017). Antimicrobial peptides with selective antitumor mechanisms: Prospect for anticancer applications. *Oncotarget* 8 (28), 46635–46651. doi:10.18632/oncotarget.16743

Ding, B., Soblosky, L., Nguyen, K., Geng, J., Yu, X., Ramamoorthy, A., et al. (2013). Physiologically-relevant modes of membrane interactions by the human antimicrobial peptide, LL-37, revealed by SFG experiments. *Sci. Rep.* 3, 1854. doi:10.1038/srep01854

Ding, X., Bian, D., Li, W., Xie, Y., Li, X., Lv, J., et al. (2021). Host defense peptide LL-37 is involved in the regulation of cell proliferation and production of pro-inflammatory cytokines in hepatocellular carcinoma cells. *Amino Acids* 53 (3), 471–484. doi:10.1007/s00726-021-02966-0

Doktorova, M., Symons, J. L., and Levental, I. (2020). Structural and functional consequences of reversible lipid asymmetry in living membranes. *Nat. Chem. Biol.* 16 (12), 1321–1330. doi:10.1038/s41589-020-00688-0

Dolkar, T., Trinidad, C. M., Nelson, K. C., Amaria, R. N., Nagarajan, P., Torres-Cabala, C. A., et al. (2018). Dermatologic toxicity from novel therapy using antimicrobial peptide LL-37 in melanoma: A detailed examination of the clinicopathologic features. *J. Cutan. Pathol.* 45 (7), 539–544. doi:10.1111/cup.13262

Dürr, U. H., Sudheendra, U. S., and Ramamoorthy, A. (2006). LL-37, the only human member of the cathelicidin family of antimicrobial peptides. *Biochim. Biophys. Acta* 1758 (9), 1408–1425. doi:10.1016/j.bbamem.2006.03.030

Elssner, A., Duncan, M., Gavrilin, M., and Wewers, M. D. (2004). A novel P2X7 receptor activator, the human cathelicidin-derived peptide LL37, induces IL-1 beta processing and release. *J. Immunol.* 172 (8), 4987–4994. doi:10.4049/jimmunol.172.8.4987

Fábián, T. K., Hermann, P., Beck, A., Fejérdy, P., and Fábián, G. (2012). Salivary defense proteins: Their network and role in innate and acquired oral immunity. *Int. J. Mol. Sci.* 13 (4), 4295–4320. doi:10.3390/ijms13044295

Fahy, R. J., and Wewers, M. D. (2005). Pulmonary defense and the human cathelicidin hCAP-18/LL-37. *Immunol. Res.* 31 (2), 75–89. doi:10.1385/IR:31:2:075

Falcao, C. B., Pérez-Peinado, C., de la Torre, B. G., Mayol, X., Zamora-Carreras, H., Jiménez, M. Á., et al. (2015). Structural dissection of crotalicidin, a rattlesnake venom cathelicidin, retrieves a fragment with antimicrobial and antitumor activity. *J. Med. Chem.* 58 (21), 8553–8563. doi:10.1021/acs.jmedchem.5b01142

Fan, R., Tong, A., Li, X., Gao, X., Mei, L., Zhou, L., et al. (2015). Enhanced antitumor effects by docetaxel/LL37-loaded thermosensitive hydrogel nanoparticles in peritoneal carcinomatosis of colorectal cancer. *Int. J. Nanomedicine* 10, 7291–7305. doi:10.2147/IJN.S89066

Farabaugh, S. M., Chan, B. T., Cui, X., Dearth, R. K., and Lee, A. V. (2016). Lack of interaction between ErbB2 and insulin receptor substrate signaling in breast cancer. *Cell Commun. Signal.* 14 (1), 25. doi:10.1186/s12964-016-0148-8

Fillion, M., Valois-Paillard, G., Lorin, A., Noël, M., Voyer, N., and Auger, M. (2015). Membrane interactions of synthetic peptides with antimicrobial potential: Effect of electrostatic interactions and amphiphilicity. *Probiotics Antimicrob. Proteins* 7 (1), 66–74. doi:10.1007/s12602-014-9177-z

Frohm, M., Agerberth, B., Ahangari, G., Ståhle-Bäckdahl, M., Lidén, S., Wigzell, H., et al. (1997). The expression of the gene coding for the antibacterial peptide LL-37 is induced in human keratinocytes during inflammatory disorders. *J. Biol. Chem.* 272 (24), 15258–15263. doi:10.1074/jbc.272.24.15258

Gudmundsson, G. H., Agerberth, B., Odeberg, J., Bergman, T., Olsson, B., and Salcedo, R. (1996). The human gene FALL39 and processing of the cathelin precursor to the antibacterial peptide LL-37 in granulocytes. *Eur. J. Biochem.* 238 (2), 325–332. doi:10.1111/j.1432-1033.1996.0325z.x

Habes, C., Weber, G., and Goupille, C. (2019). Sulfated glycoaminoglycans and proteoglycan syndecan-4 are involved in membrane fixation of LL-37 and its pro-migratory effect in breast cancer cells. *Biomolecules* 9 (9), 481. doi:10.3390/biom9090481

Han, J., Flemington, C., Houghton, A. B., Gu, Z., Zambetti, G. P., Lutz, R. J., et al. (2001). Expression of Bbc3, a pro-apoptotic BH3-only gene, is regulated by diverse cell death and survival signals. *Proc. Natl. Acad. Sci. U. S. A.* 98, 11318–11323. doi:10.1073/pnas.201208798

Hassan, N., Greve, B., Espinoza-Sánchez, N. A., and Götte, M. (2021). Cell-surface heparan sulfate proteoglycans as multifunctional integrators of signaling in cancer. *Cell. Signal.* 77, 109822. doi:10.1016/j.cellsig.2020.109822

Hayashi, M., Kuroda, K., Ihara, K., Iwaya, T., and Isogai, E. (2018). Suppressive effect of an analog of the antimicrobial peptide of LL-37 on colon cancer cells *via* exosome-encapsulated miRNAs. *Int. J. Mol. Med.* 42 (6), 3009–3016. doi:10.3892/ijmm.2018.3875

Hilchie, A. L., Hoskin, D. W., and Power Coombs, M. R. (2019). Anticancer activities of natural and synthetic peptides. *Adv. Exp. Med. Biol.* 1117, 131–147. doi:10.1007/978-981-13-3588-4_9

Hoskin, D. W., and Ramamoorthy, A. (2008). Studies on anticancer activities of antimicrobial peptides. *Biochim. Biophys. Acta* 1778 (2), 357–375. doi:10.1016/j.bbamem.2007.11.008

Huang, Y., Feng, Q., Yan, Q., Hao, X., and Chen, Y. (2015). Alpha-helical cationic anticancer peptides: A promising candidate for novel anticancer drugs. *Mini Rev. Med. Chem.* 15 (1), 73–81. doi:10.2174/1389557514666141107120954

Hugonnet, M., Singh, P., Haas, Q., and von Gunten, S. (2021). The distinct roles of sialyltransferases in cancer biology and onco-immunology. *Front. Immunol.* 12, 799861. doi:10.3389/fimmu.2021.799861

Hurtado, P., and Peh, C. A. (2010). LL-37 promotes rapid sensing of CpG oligodeoxynucleotides by B lymphocytes and plasmacytoid dendritic cells. *J. Immunol.* 184 (3), 1425–1435. doi:10.4049/jimmunol.0902305

Jafari, A., Babajani, A., Sarrami Forooshani, R., Yazdani, M., and Rezaei-Tavirani, M. (2022). Clinical applications and anticancer effects of antimicrobial peptides: From bench to bedside. *Front. Oncol.* 12, 819563. doi:10.3389/fonc.2022.819563

Jeffers, J. R., Parganas, E., Lee, Y., Yang, C., Wang, J., Brennan, J., et al. (2003). Puma is an essential mediator of P53-dependent and-independent apoptotic pathways. *Cancer Cell* 4, 321–328. doi:10.1016/s1535-6108(03)00244-7

Ji, P., Zhou, Y., Yang, Y., Wu, J., Zhou, H., Quan, W., et al. (2019). Myeloid cell-derived LL-37 promotes lung cancer growth by activating Wnt/β-catenin signaling. *Theranostics* 9 (8), 2209–2223. doi:10.7150/thno.30726

Jiang, Y., Liao, H., Zhang, X., Cao, S., Hu, X., Yang, Z., et al. (2020). IL-33 synergistically promotes the proliferation of lung cancer cells *in vitro* by inducing antibacterial peptide LL-37 and proinflammatory cytokines in macrophages. *Immunobiology* 225 (6), 152025. doi:10.1016/j.imbio.2020.152025

Johansson, J., Gudmundsson, G. H., Rottenberg, M. E., Berndt, K. D., and Agerberth, B. (1998). Conformation-dependent antibacterial activity of the naturally occurring human peptide LL-37. *J. Biol. Chem.* 273 (6), 3718–3724. doi:10.1074/jbc.273.6.3718

Juba, M. L., Porter, D. K., Williams, E. H., Rodriguez, C. A., Barksdale, S. M., and Bishop, B. M. (2015). Helical cationic antimicrobial peptide length and its impact on membrane disruption. *Biochim. Biophys. Acta* 1848 (5), 1081–1091. doi:10.1016/j.bbamem.2015.01.007

Kiatsurayanon, C., Peng, G., and Niyonsaba, F. (2022). Opposing roles of antimicrobial peptides in skin cancers. *Curr. Pharm. Des.* 28 (3), 248–258. doi:10.2174/1381612827666211021163318

Kim, S., Hyun, S., Lee, Y., Lee, Y., and Yu, J. (2016). Nonhemolytic cell-penetrating peptides: Site specific introduction of glutamine and lysine residues into the α-helical peptide causes deletion of its direct membrane disrupting ability but retention of its cell penetrating ability. *Biomacromolecules* 17 (9), 3007–3015. doi:10.1021/acs.biomac.6b00874

Kube, S., Hersch, N., Naumovska, E., Gensch, T., Hendriks, J., Franzen, A., et al. (2017). Fusogenic liposomes as nanocarriers for the delivery of intracellular proteins. *Langmuir* 33 (4), 1051–1059. doi:10.1021/acs.langmuir.6b04304

Kumar, P., Kizhakkedathu, J. N., and Straus, S. K. (2018). Antimicrobial peptides: Diversity, mechanism of action and strategies to improve the activity and biocompatibility *in vivo*. *Biomolecules* 8 (1), 4. doi:10.3390/biom8010004

Kuroda, K., Fukuda, T., Isogai, H., Okumura, K., Krstic-Demonacos, M., and Isogai, E. (2015b). Antimicrobial peptide FF/CAP18 induces apoptotic cell death in HCT116 colon cancer cells *via* changes in the metabolic profile. *Int. J. Oncol.* 46 (4), 1516–1526. doi:10.3892/ijo.2015.2887

Kuroda, K., Fukuda, T., Krstic-Demonacos, M., Demonacos, C., Okumura, K., Isogai, H., et al. (2017). miR-663a regulates growth of colon cancer cells, after administration of antimicrobial peptides, by targeting CXCR4-p21 pathway. *BMC Cancer* 17 (1), 33. doi:10.1186/s12885-016-3003-9

Kuroda, K., Fukuda, T., Yoneyama, H., Katayama, M., Isogai, H., Okumura, K., et al. (2012). Anti-proliferative effect of an analogue of the LL-37 peptide in the colon cancer derived cell line HCT116 p53+/+ and p53-/-. *Oncol. Rep.* 28 (3), 829–834. doi:10.3892/or.2012.1876

Kuroda, K., Okumura, K., Isogai, H., and Isogai, E. (2015a). The human cathelicidin antimicrobial peptide LL-37 and mimics are potential anticancer drugs. *Front. Oncol.* 5, 144. doi:10.3389/fonc.2015.00144

Lee, R. H., Oh, J. D., Hwang, J. S., Lee, H. K., and Shin, D. (2021). Antitumorigenic effect of insect-derived peptide poecilocorisin-1 in human skin cancer cells through regulation of Sp1 transcription factor. *Sci. Rep.* 11 (1), 18445. doi:10.1038/s41598-021-97581-0

Lee, T. H., Hall, K. N., and Aguilar, M. I. (2016). Antimicrobial peptide structure and mechanism of action: A focus on the role of membrane structure. *Curr. Top. Med. Chem.* 16 (1), 25–39. doi:10.2174/1568026615666150703121700

Li, X., Li, Y., Han, H., Miller, D. W., and Wang, G. (2006). Solution structures of human LL-37 fragments and NMR-based identification of a minimal membrane-targeting antimicrobial and anticancer region. *J. Am. Chem. Soc.* 128 (17), 5776–5785. doi:10.1021/ja0584875

Liu, Z., Yuan, X., Liu, M., Fernandes, G., Zhang, Y., Yang, S., et al. (2018). Antimicrobial peptide combined with BMP2-modified mesenchymal stem cells promotes calvarial repair in an osteolytic model. *Mol. Ther.* 26 (1), 199–207. doi:10.1016/j.ymthe.2017.09.011

Ma, R., Wong, S. W., Ge, L., Shaw, C., Siu, S. W. I., and Kwok, H. F. (2019). *In vitro* and MD simulation study to explore physicochemical parameters for antibacterial peptide to become potent anticancer peptide. *Mol. Ther. Oncolytics* 16, 7–19. doi:10.1016/j.omto.2019.12.001

Mader, J. S., Ewen, C., Hancock, R. E., and Bleackley, R. C. (2011b). The human cathelicidin, LL-37, induces granzyme-mediated apoptosis in regulatory T cells. *J. Immunother.* 34 (3), 229–235. doi:10.1097/CJI.0b013e318207ecdf

Mader, J. S., Marcet-Palacios, M., Hancock, R. E., and Bleackley, R. C. (2011a). The human cathelicidin, LL-37, induces granzyme-mediated apoptosis in cytotoxic T lymphocytes. *Exp. Cell Res.* 317 (4), 531–538. doi:10.1016/j.yexcr.2010.11.015

Mader, J. S., Mookherjee, N., Hancock, R. E., and Bleackley, R. C. (2009). The human host defense peptide LL-37 induces apoptosis in a calpain- and apoptosis-inducing factor-dependent manner involving Bax activity. *Mol. Cancer Res.* 7 (5), 689–702. doi:10.1158/1541-7786.MCR-08-0274

Malam, Y., Loizidou, M., and Seifalian, A. M. (2009). Liposomes and nanoparticles: Nanosized vehicles for drug delivery in cancer. *Trends Pharmacol. Sci.* 30 (11), 592–599. doi:10.1016/j.tips.2009.08.004

Malm, J., Sørensen, O., Persson, T., Frohm-Nilsson, M., Johansson, B., Bjartell, A., et al. (2000). The human cationic antimicrobial protein (hCAP-18) is expressed in the epithelium of human epididymis, is present in seminal plasma at high concentrations, and is attached to spermatozoa. *Infect. Immun.* 68 (7), 4297–4302. doi:10.1128/iai.68.7.4297-4302.2000

Marverti, G., Gozzi, G., Maretti, E., Lauriola, A., Severi, L., Sacchetti, F., et al. (2020). A peptidic thymidylate-synthase inhibitor loaded on pegylated liposomes enhances the antitumour effect of chemotherapy drugs in human ovarian cancer cells. *Int. J. Mol. Sci.* 21 (12), 4452. doi:10.3390/ijms21124452

Mitchell, G., Silvis, M. R., Talkington, K. C., Budzik, J. M., Dodd, C. E., Paluba, J. M., et al. (2022). Ceragenins and antimicrobial peptides kill bacteria through distinct mechanisms. *mBio* 13 (1), e0272621. doi:10.1128/mbio.02726-21

Monteiro, L. O. F., Fernandes, R. S., Oda, C. M. R., Lopes, S. C., Townsend, D. M., Cardoso, V. N., et al. (2018). Paclitaxel-loaded folate-coated long circulating and pH-sensitive liposomes as a potential drug delivery system: A biodistribution study. *Biomed. Pharmacother.* 97, 489–495. doi:10.1016/j.biopha.2017.10.135

Mori, T., Hazekawa, M., Yoshida, M., Nishinakagawa, T., Uchida, T., and Ishibashi, D. (2021). Enhancing the anticancer efficacy of a LL-37 peptide fragment analog using peptide-linked PLGA conjugate micelles in tumor cells. *Int. J. Pharm.* 606, 120891. doi:10.1016/j.ijpharm.2021.120891

Muñoz, M., Craske, M., Severino, P., de Lima, T. M., Labhart, P., Chammas, R., et al. (2016). Antimicrobial peptide LL-37 participates in the transcriptional regulation of melanoma cells. *J. Cancer* 7 (15), 2341–2345. doi:10.7150/jca.16947

Murakami, M., Ohtake, T., Dorschner, R. A., Schittek, B., Garbe, C., and Gallo, R. L. (2002). Cathelicidin anti-microbial peptide expression in sweat, an innate defense system for the skin. *J. Invest. Dermatol.* 119 (5), 1090–1095. doi:10.1046/j.1523-1747.2002.19507.x

Niemirowicz, K., Durnaś, B., Tokajuk, G., Piktel, E., Michalak, G., Gu, X., et al. (2017). Formulation and candidacidal activity of magnetic nanoparticles coated with cathelicidin LL-37 and ceragenin CSA-13. *Sci. Rep.* 7 (1), 4610. doi:10.1038/s41598-017-04653-1

Niemirowicz, K., Prokop, I., Wilczewska, A. Z., Wnorowska, U., Piktel, E., Wątek, M., et al. (2015). Magnetic nanoparticles enhance the anticancer activity of cathelicidin LL-37 peptide against colon cancer cells. *Int. J. Nanomedicine* 10, 3843–3853. doi:10.2147/IJN.S76104

Okumura, K., Itoh, A., Isogai, E., Hirose, K., Hosokawa, Y., Abiko, Y., et al. (2004). C-terminal domain of human CAP18 antimicrobial peptide induces apoptosis in oral squamous cell carcinoma SAS-H1 cells. *Cancer Lett.* 212 (2), 185–194. doi:10.1016/j.canlet.2004.04.006

Oren, Z., Lerman, J. C., Gudmundsson, G. H., Agerberth, B., and Shai, Y. (1999). Structure and organization of the human antimicrobial peptide LL-37 in phospholipid membranes: Relevance to the molecular basis for its non-cell-selective activity. *Biochem. J.* 341 (3), 501–513. doi:10.1042/bj3410501

Patil, S. M., and Kunda, N. K. (2022). Nisin ZP, an antimicrobial peptide, induces cell death and inhibits non-small cell lung cancer (NSCLC) progression *in vitro* in 2D and 3D cell culture. *Pharm. Res.* doi:10.1007/s11095-022-03220-2

Pazgier, M., Ericksen, B., Ling, M., Toth, E., Shi, J., Li, X., et al. (2013). Structural and functional analysis of the pro-domain of human cathelicidin, LL-37. *Biochemistry* 52 (9), 1547–1558. doi:10.1021/bi301008r

Pfosser, A., El-Aouni, C., Pfisterer, I., Dietz, M., Globisch, F., Stachel, G., et al. (2010). NF kappaB activation in embryonic endothelial progenitor cells enhances neovascularization *via* PSGL-1 mediated recruitment: Novel role for LL37. *Stem Cells* 28 (2), 376–385. doi:10.1002/stem.280

Piktel, E., Niemirowicz, K., Wnorowska, U., Wątek, M., Wollny, T., Głuszek, K., et al. (2016). The role of cathelicidin LL-37 in cancer development. *Arch. Immunol. Ther. Exp.* 64 (1), 33–46. doi:10.1007/s00005-015-0359-5

Porcelli, F., Verardi, R., Shi, L., Henzler-Wildman, K. A., Ramamoorthy, A., and Veglia, G. (2008). NMR structure of the cathelicidin-derived human antimicrobial peptide LL-37 in dodecylphosphocholine micelles. *Biochemistry* 47 (20), 5565–5572. doi:10.1021/bi702036s

Porter, R. J., Murray, G. I., Alnabulsi, A., Humphries, M. P., James, J. A., Salto-Tellez, M., et al. (2021). Colonic epithelial cathelicidin (LL-37) expression intensity is associated with progression of colorectal cancer and presence of $CD8^+$ T cell infiltrate. *J. Pathol. Clin. Res.* 7 (5), 495–506. doi:10.1002/cjp2.222

Pouny, Y., and Shai, Y. (1992). Interaction of D-amino acid incorporated analogues of pardaxin with membranes. *Biochemistry* 31 (39), 9482–9490. doi:10.1021/bi00154a022

Prevete, N., Liotti, F., Visciano, C., Marone, G., Melillo, R. M., de Paulis, A., et al. (2015). The formyl peptide receptor 1 exerts a tumor suppressor function in human gastric cancer by inhibiting angiogenesis. *Oncogene* 34 (29), 3826–3838. doi:10.1038/onc.2014.309

Quemé-Peña, M., Juhász, T., Kohut, G., Ricci, M., Singh, P., Szigyártó, I. C., et al. (2021). Membrane association modes of natural anticancer peptides: Mechanistic details on helicity, orientation, and surface coverage. *Int. J. Mol. Sci.* 22 (16), 8613. doi:10.3390/ijms22168613

Radaic, A., de Jesus, M. B., and Kapila, Y. L. (2020). Bacterial anti-microbial peptides and nano-sized drug delivery systems: The state of the art toward improved bacteriocins. *J. Control. Release* 321, 100–118. doi:10.1016/j.jconrel.2020.02.001

Rajkumar, S. V., Richardson, P. G., Hideshima, T., and Anderson, K. C. (2005). Proteasome inhibition as a novel therapeutic target in human cancer. *J. Clin. Oncol.* 23 (3), 630–639. doi:10.1200/JCO.2005.11.030

Ramos, R., Silva, J. P., Rodrigues, A. C., Costa, R., Guardão, L., Schmitt, F., et al. (2011). Wound healing activity of the human antimicrobial peptide LL37. *Peptides* 32, 1469–1476. doi:10.1016/j.peptides.2011.06.005

Rathnayake, K., Patel, U., Pham, C., McAlpin, A., Budisalich, T., and Jayawardena, S. N. (2020). Targeted delivery of antibiotic therapy to inhibit *Pseudomonas aeruginosa* using lipid-coated mesoporous silica core-shell nanoassembly. *ACS Appl. Bio Mat.* 3 (10), 6708–6721. doi:10.1021/acsabm.0c00622

Reißer, S., Prock, S., Heinzmann, H., and Ulrich, A. S. (2018). Protein origami: A program for the creation of 3D paper models of folded peptides. *Biochem. Mol. Biol. Educ.* 46 (4), 403–409. doi:10.1002/bmb.21132

Ren, S. X., Cheng, A. S., To, K. F., Tong, J. H., Li, M. S., Shen, J., et al. (2012). Host immune defense peptide LL-37 activates caspase-independent apoptosis and suppresses colon cancer. *Cancer Res.* 72 (24), 6512–6523. doi:10.1158/0008-5472.CAN-12-2359

Ren, S. X., Shen, J., Cheng, A. S., Lu, L., Chan, R. L., Li, Z. J., et al. (2013). FK-16 derived from the anticancer peptide LL-37 induces caspase-independent apoptosis and autophagic cell death in colon cancer cells. *PLoS One* 8 (5), e63641. doi:10.1371/journal.pone.0063641

Rieg, S., Steffen, H., Seeber, S., Humeny, A., Kalbacher, H., Dietz, K., et al. (2005). Deficiency of dermcidin-derived antimicrobial peptides in sweat of patients with atopic dermatitis correlates with an impaired innate defense of human skin *in vivo*. *J. Immunol.* 174 (12), 8003–8010. doi:10.4049/jimmunol.174.12.8003

Roufayel, R., Younes, K., Al-Sabi, A., and Murshid, N. (2022). BH3-Only proteins noxa and puma are key regulators of induced apoptosis. *Life (Basel)* 12 (2), 256. doi:10.3390/life12020256

Sengupta, P., Banerjee, N., Roychowdhury, T., Dutta, A., Chattopadhyay, S., and Chatterjee, S. (2018). Site-specific amino acid substitution in dodecameric peptides determines the stability and unfolding of c-MYC quadruplex promoting apoptosis in cancer cells. *Nucleic Acids Res.* 46 (19), 9932–9950. doi:10.1093/nar/gky824

Shai, Y. (2002). Mode of action of membrane active antimicrobial peptides. *Biopolymers* 66 (4), 236–248. doi:10.1002/bip.10260

Singh, M., Liu, C., Lou, Y., Gregorio, J., Conrad, C., Hwu, P., et al. (2012). Abstract 1580: LL-37- mediates tumor antigen-specific-T cell expansion and tumor regression. *Cancer Res.* 72, 1580. doi:10.1158/1538-7445.am2012-1580

Sørensen, O. E., Follin, P., Johnsen, A. H., Calafat, J., Tjabringa, G. S., Hiemstra, P. S., et al. (2001). Human cathelicidin, hCAP-18, is processed to the antimicrobial peptide LL-37 by extracellular cleavage with proteinase 3. *Blood* 97 (12), 3951–3959. doi:10.1182/blood.v97.12.3951

Tjabringa, G. S., Aarbiou, J., Ninaber, D. K., Drijfhout, J. W., Sørensen, O. E., Borregaard, N., et al. (2003). The antimicrobial peptide LL-37 activates innate immunity at the airway epithelial surface by transactivation of the epidermal growth factor receptor. *J. Immunol.* 171 (12), 6690–6696. doi:10.4049/jimmunol.171.12.6690

Tjabringa, G. S., Rabe, K. F., and Hiemstra, P. S. (2005). The human cathelicidin LL-37: A multifunctional peptide involved in infection and inflammation in the lung. *Pulm. Pharmacol. Ther.* 18 (5), 321–327. doi:10.1016/j.pupt.2005.01.001

Tornesello, A. L., Borrelli, A., Buonaguro, L., Buonaguro, F. M., and Tornesello, M. L. (2020). Antimicrobial peptides as anticancer agents: Functional properties and biological activities. *Molecules* 25 (12), 2850. doi:10.3390/molecules25122850

Tossi, A., Scocchi, M., Skerlavaj, B., and Gennaro, R. (1994). Identification and characterization of a primary antibacterial domain in CAP18, a lipopolysaccharide binding protein from rabbit leukocytes. *FEBS Lett.* 339 (1-2), 108–112. doi:10.1016/0014-5793(94)80395-1

Trinidad-Calderón, P. A., Varela-Chinchilla, C. D., and García-Lara, S. (2021). Natural peptides inducing cancer cell death: Mechanisms and properties of specific candidates for cancer therapeutics. *Molecules* 26 (24), 7453. doi:10.3390/molecules26247453

Tsikourkitoudi, V., Karlsson, J., Merkl, P., Loh, E., Henriques-Normark, B., and Sotiriou, G. A. (2020). Flame-made calcium phosphate nanoparticles with high drug loading for delivery of biologics. *Molecules* 25 (7), 1747. doi:10.3390/molecules25071747

Tzitzilis, A., Boura-Theodorou, A., Michail, V., Papadopoulos, S., Krikorian, D., Lekka, M. E., et al. (2020). Cationic amphipathic peptide analogs of cathelicidin LL-37 as a probe in the development of antimicrobial/anticancer agents. *J. Pept. Sci.* 26 (7), e3254. doi:10.1002/psc.3254

Utsugi, T., Schroit, A. J., Connor, J., Bucana, C. D., and Fidler, I. J. (1991). Elevated expression of phosphatidylserine in the outer membrane leaflet of human tumor cells and recognition by activated human blood monocytes. *Cancer Res.* 51 (11), 3062–3066.

Vandamme, D., Landuyt, B., Luyten, W., and Schoofs, L. (2012). A comprehensive summary of LL-37, the factotum human cathelicidin peptide. *Cell. Immunol.* 280 (1), 22–35. doi:10.1016/j.cellimm.2012.11.009

Varga, A. C., and Wrana, J. L. (2005). The disparate role of BMP in stem cell biology. *Oncogene* 24 (37), 5713–5721. doi:10.1038/sj.onc.1208919

Vasquez-Montes, V., Gerhart, J., Thévenin, D., and Ladokhin, A. S. (2019). Divalent cations and lipid composition modulate membrane insertion and cancer-targeting action of pHLIP. *J. Mol. Biol.* 431 (24), 5004–5018. doi:10.1016/j.jmb.2019.10.016

Vitale, I., Yamazaki, T., Wennerberg, E., Sveinbjørnsson, B., Rekdal, Ø., Demaria, S., et al. (2021). Targeting cancer heterogeneity with immune responses driven by oncolytic peptides. *Trends Cancer* 7 (6), 557–572. doi:10.1016/j.trecan.2020.12.012

Vlieghe, P., Lisowski, V., Martinez, J., and Khrestchatisky, M. (2010). Synthetic therapeutic peptides: Science and market. *Drug Discov. Today* 15 (1-2), 40–56. doi:10.1016/j.drudis.2009.10.009

Wang, G. (2014). Human antimicrobial peptides and proteins. *Pharm. (Basel)* 7 (5), 545–594. doi:10.3390/ph7050545

Wang, G. (2015). Improved methods for classification, prediction, and design of antimicrobial peptides. *Methods Mol. Biol.* 1268, 43–66. doi:10.1007/978-1-4939-2285-7_3

Wang, G., Mishra, B., Epand, R. F., and Epand, R. M. (2014). High-quality 3D structures shine light on antibacterial, anti-biofilm and antiviral activities of human cathelicidin LL-37 and its fragments. *Biochim. Biophys. Acta* 1838 (9), 2160–2172. doi:10.1016/j.bbamem.2014.01.016

Wang, G., Narayana, J. L., Mishra, B., Zhang, Y., Wang, F., Wang, C., et al. (2019). Design of antimicrobial peptides: Progress made with human cathelicidin LL-37. *Adv. Exp. Med. Biol.* 1117, 215–240. doi:10.1007/978-981-13-3588-4_12

Wang, G. (2008). Structures of human host defense cathelicidin LL-37 and its smallest antimicrobial peptide KR-12 in lipid micelles. *J. Biol. Chem.* 283 (47), 32637–32643. doi:10.1074/jbc.M805533200

Wang, W., Zheng, Y., Jia, J., Li, C., Duan, Q., Li, R., et al. (2017). Antimicrobial peptide LL-37 promotes the viability and invasion of skin squamous cell carcinoma by upregulating YB-1. *Exp. Ther. Med.* 14 (1), 499–506. doi:10.3892/etm.2017.4546

Wang, Y., Agerberth, B., Löthgren, A., Almstedt, A., Johansson, J., and Lothgren, A. (1998). Apolipoprotein A-I binds and inhibits the human antibacterial/cytotoxic peptide LL-37. *J. Biol. Chem.* 273 (50), 33115–33118. doi:10.1074/jbc.273.50.33115

Warren, L., Buck, C. A., and Tuszynski, G. P. (1979). Alterations of membrane glycoproteins in malignant cells. *Dev. Biol. Stand.* 42, 177–182.

Warren, L. (1974). The malignant cell and its membranes. *Am. J. Pathol.* 77 (1), 69–76.

Wnorowska, U., Fiedoruk, K., Piktel, E., Prasad, S. V., Sulik, M., Janion, M., et al. (2020). Nanoantibiotics containing membrane-active human cathelicidin LL-37 or synthetic ceragenins attached to the surface of magnetic nanoparticles as novel and innovative therapeutic tools: Current status and potential future applications. *J. Nanobiotechnology* 18 (1), 3. doi:10.1186/s12951-019-0566-z

Wolk, K., Witte, E., Wallace, E., Döcke, W. D., Kunz, S., Asadullah, K., et al. (2006). IL-22 regulates the expression of genes responsible for antimicrobial defense, cellular differentiation, and mobility in keratinocytes: A potential role in psoriasis. *Eur. J. Immunol.* 36 (5), 1309–1323. doi:10.1002/eji.200535503

Wu, W. K., Cho, C. H., Lee, C. W., Wu, K., Fan, D., Yu, J., et al. (2010c). Proteasome inhibition: A new therapeutic strategy to cancer treatment. *Cancer Lett.* 293 (1), 15–22. doi:10.1016/j.canlet.2009.12.002

Wu, W. K., Sung, J. J., To, K. F., Yu, L., Li, H. T., Li, Z. J., et al. (2010b). The host defense peptide LL-37 activates the tumor-suppressing bone morphogenetic protein signaling *via* inhibition of proteasome in gastric cancer cells. *J. Cell. Physiol.* 223 (1), 178–186. doi:10.1002/jcp.22026

Wu, W. K., Sung, J. J., Wu, Y. C., Li, Z. J., Yu, L., and Cho, C. H. (2008a). Bone morphogenetic protein signalling is required for the anti-mitogenic effect of the proteasome inhibitor MG-132 on colon cancer cells. *Br. J. Pharmacol.* 154 (3), 632–638. doi:10.1038/bjp.2008.115

Wu, W. K., Sung, J. J., Yu, L., and Cho, C. H. (2008b). Proteasome inhibitor MG-132 lowers gastric adenocarcinoma TMK1 cell proliferation *via* bone morphogenetic protein signaling. *Biochem. Biophys. Res. Commun.* 371 (2), 209–214. doi:10.1016/j.bbrc.2008.04.059

Wu, W. K., Wang, G., Coffelt, S. B., Betancourt, A. M., Lee, C. W., Fan, D., et al. (2010a). Emerging roles of the host defense peptide LL-37 in human cancer and its potential therapeutic applications. *Int. J. Cancer* 127 (8), 1741–1747. doi:10.1002/ijc.25489

Xhindoli, D., Pacor, S., Guida, F., Antcheva, N., and Tossi, A. (2014). Native oligomerization determines the mode of action and biological activities of human cathelicidin LL-37. *Biochem. J.* 457 (2), 263–275. doi:10.1042/BJ20131048

Yang, B., Good, D., Mosaiab, T., Liu, W., Ni, G., Kaur, J., et al. (2020). Significance of LL-37 on immunomodulation and disease outcome. *Biomed. Res. Int.* 2020, 8349712. doi:10.1155/2020/8349712

Yang, T., Li, J., Jia, Q., Zhan, S., Zhang, Q., Wang, Y., et al. (2021). Antimicrobial peptide 17BIPHE2 inhibits the proliferation of lung cancer cells *in vitro* and *in vivo* by regulating the ERK signaling pathway. *Oncol. Lett.* 22 (1), 501. doi:10.3892/ol.2021.12762

Yu, J., and Zhang, L. (2003). No PUMA, no death: Implications for p53-dependent apoptosis. *Cancer Cell* 4 (4), 248–249. doi:10.1016/s1535-6108(03)00249-6

Yu, J., Wang, Z., Kinzler, K. W., Vogelstein, B., and Zhang, L. (2003). PUMA mediates the apoptotic response to P53 in colorectal cancer cells. *Proc. Natl. Acad. Sci. U. S. A.* 100, 1931–1936. doi:10.1073/pnas.2627984100

Yu, J., Zhang, L., Hwang, P. M., Kinzler, K. W., and Vogelstein, B. (2001). PUMA induces the rapid apoptosis of colorectal cancer cells. *Mol. Cell* 7, 673–682. doi:10.1016/s1097-2765(01)00213-1

Zachowski, A. (1993). Phospholipids in animal eukaryotic membranes: Transverse asymmetry and movement. *Biochem. J.* 294 (1), 1–14. doi:10.1042/bj2940001

Zaiou, M., Nizet, V., and Gallo, R. L. (2003). Antimicrobial and protease inhibitory functions of the human cathelicidin (hCAP18/LL-37) prosequence. *J. Invest. Dermatol.* 120 (5), 810–816. doi:10.1046/j.1523-1747.2003.12132.x

Zanetti, M. (2004). Cathelicidins, multifunctional peptides of the innate immunity. *J. Leukoc. Biol.* 75 (1), 39–48. doi:10.1189/jlb.0403147

Zanetti, M. (2005). The role of cathelicidins in the innate host defenses of mammals. *Curr. Issues Mol. Biol.* 7 (2), 179–196.

Zhang, H., Zhen, J., Zhang, R., Wanyan, Y., Liu, K., Yuan, X., et al. (2022). Cathelicidin hCAP18/LL-37 promotes cell proliferation and suppresses antitumor activity of 1, 25(OH)2D3 in hepatocellular carcinoma. *Cell Death Discov.* 8 (1), 27. doi:10.1038/s41420-022-00816-w

Zhang, N., Yang, Y., Wang, Z., Yang, J., Chu, X., Liu, J., et al. (2019). Polypeptide-engineered DNA tetrahedrons for targeting treatment of colorectal cancer *via* apoptosis and autophagy. *J. Control. Release* 309, 48–58. doi:10.1016/j.jconrel.2019.07.012

Zhang, Y., Chen, X., Qiao, M., Zhang, B. Q., Wang, N., Zhang, Z., et al. (2014). Bone morphogenetic protein 2 inhibits the proliferation and growth of human colorectal cancer cells. *Oncol. Rep.* 32 (3), 1013–1020. doi:10.3892/or.2014.3308

Zhang, Y., Lakshmaiah Narayana, J., Wu, Q., Dang, X., and Wang, G. (2021). Structure and activity of a selective antibiofilm peptide SK-24 derived from the NMR structure of human cathelicidin LL-37. *Pharm. (Basel)* 14 (12), 1245. doi:10.3390/ph14121245

Zhao, L., Cao, Z., Bian, Y., Hu, G., Wang, J., and Zhou, Y. (2018). Molecular dynamics simulations of human antimicrobial peptide LL-37 in model POPC and POPG lipid bilayers. *Int. J. Mol. Sci.* 19 (4), 1186. doi:10.3390/ijms19041186

Zielińska, A., Szalata, M., Gorczyński, A., Karczewski, J., Eder, P., Severino, P., et al. (2021). Cancer nanopharmaceuticals: Physicochemical characterization and *in vitro*/*in vivo* applications. *Cancers (Basel)* 13 (8), 1896. doi:10.3390/cancers13081896

Zwaal, R. F., Comfurius, P., and Bevers, E. M. (2005). Surface exposure of phosphatidylserine in pathological cells. *Cell. Mol. Life Sci.* 62 (9), 971–988. doi:10.1007/s00018-005-4527-3

frontiers | Frontiers in Pharmacology

TYPE Review
PUBLISHED 24 August 2022
DOI 10.3389/fphar.2022.933655

OPEN ACCESS

EDITED BY
Chi Zhang,
Indiana University Bloomington,
United States

REVIEWED BY
Syed Shams Ul Hassan,
Shanghai Jiao Tong University, China
Jingwen Yan,
Indiana University, Purdue University
Indianapolis, United States

*CORRESPONDENCE
Ying Wu,
wuying@cmu.edu.cn
Yijun Bao,
yjbao@cmu.edu.cn

†These authors have contributed equally to this work and share first authorship

SPECIALTY SECTION
This article was submitted to Pharmacology of Anti-Cancer Drugs, a section of the journal Frontiers in Pharmacology

RECEIVED 01 May 2022
ACCEPTED 19 July 2022
PUBLISHED 24 August 2022

CITATION
Zhong S, Shengyu Liu, Xin Shi, Zhang X, Li K, Liu G, Li L, Tao S, Zheng B, Sheng W, Ye Z, Xing Q, Zhai Q, Ren L, Wu Y and Bao Y (2022), Disulfiram in glioma: Literature review of drug repurposing. *Front. Pharmacol.* 13:933655. doi: 10.3389/fphar.2022.933655

Disulfiram in glioma: Literature review of drug repurposing

Shiyu Zhong[1†], Shengyu Liu[1†], Xin Shi[2,3], Xudong Zhang[1], Kunhang Li[1], Guojun Liu[1], Lishuai Li[1], Shanwei Tao[4], Bowen Zheng[1], Weichen Sheng[1], Ziyin Ye[1], Qichen Xing[1], Qingqing Zhai[5], Lijie Ren[6], Ying Wu[7]* and Yijun Bao[1]*

[1]Department of Neurosurgery, The Fourth Hospital of China Medical University, Huanggu, Shenyang, China, [2]School of Maths and Information Science, Shandong Technology and Business University, Yantai, China, [3]Business School, All Saints Campus, Manchester Metropolitan University, Manchester, United Kingdom, [4]Luoyang Central Hospital Affiliated to Zhengzhou University, Luoyang, China, [5]School of Management, Shanghai University, Shanghai, China, [6]Neurology Department of Shenzhen Second People's Hospital/ First Affiliated Hospital of Shenzhen, University Health Science Center, Shenzhen, China, [7]Department of General Practice, The First Hospital, China Medical University, Shenyang, China

Gliomas are the most common malignant brain tumors. High-grade gliomas, represented by glioblastoma multiforme (GBM), have a poor prognosis and are prone to recurrence. The standard treatment strategy is tumor removal combined with radiotherapy and chemotherapy, such as temozolomide (TMZ). However, even after conventional treatment, they still have a high recurrence rate, resulting in an increasing demand for effective anti-glioma drugs. Drug repurposing is a method of reusing drugs that have already been widely approved for new indication. It has the advantages of reduced research cost, safety, and increased efficiency. Disulfiram (DSF), originally approved for alcohol dependence, has been repurposed for adjuvant chemotherapy in glioma. This article reviews the drug repurposing method and the progress of research on disulfiram reuse for glioma treatment.

KEYWORDS

gliomas, glioblastoma multiforme, disulfiram, drug repurposing, temozolomide

1 Introduction

Glioma is a central nervous system (CNS) tumor and is one of the most common malignant brain tumors (Özcan et al., 2021), accounting for approximately 80% of all brain-related malignancies (Ostrom et al., 2019). According to the World Health Organization (WHO) classification, gliomas are divided into four grades based on their malignancy. Grades I–II are low-grade gliomas (LGGs), whereas grades III–IV are called high-grade gliomas (HGGs) (Özcan et al., 2021). Glioblastomas (GBMs) are WHO grade IV tumors with a high degree of malignancy and a median overall survival of approximately 15–26 months (Seliger and Hau, 2018).

Conventional treatment only modestly prolongs survival (Jakola et al., 2018). The growing demand for effective anticancer drugs has led researchers to search for Food and Drug Administration (FDA)-approved drugs that can be reused as chemotherapeutic agents (McMahon et al., 2020). Drug repurposing, also known as drug repositioning, drug

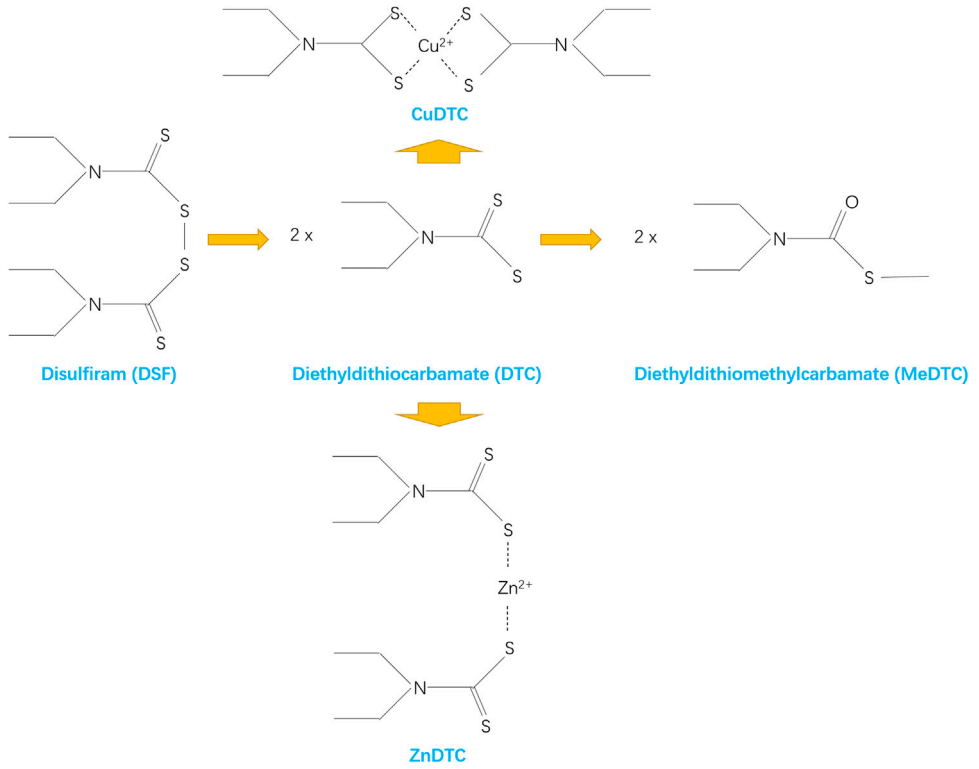

FIGURE 1
Molecular structure of DSF.

reprofiling, drug redirecting, drug rediscovery, and others (Langedijk et al., 2015), is a promising treatment strategy for reusing drugs with known formulations, pharmacokinetics, toxicity, clinical trials, and post-marketing surveillance safety data that offer increased scope for use (Ashburn and Thor, 2004; Turanli et al., 2021).

Disulfiram (DSF), also known as antabuse, is an FDA-approved acetaldehyde dehydrogenase inhibitor (Shirley et al., 2021; Turanli et al., 2021). Figure 1 shows the molecular structure of DSF. It has been used for treating alcohol dependence for the past 70 years with good pharmacokinetic properties, safety, and tolerability owing to the flu-like symptoms that patients experience when consuming alcohol (Seliger and Hau, 2018; Shirley et al., 2021). Preclinical and clinical studies have shown that DSF exhibits broad-spectrum anticancer activity against a variety of cancer types when administered with copper (Cu)-containing supplements (McMahon et al., 2020). Therefore, this review describes the drug repurposing of DSF in gliomas.

2 Chemotherapy for glioma

The standard initial treatment for GBM is extensive neurosurgical resection, followed by postoperative segmental radiotherapy, temozolomide (TMZ) chemotherapy, and combined adjuvant therapy (Jakola et al., 2018; Stylli, 2020). The therapy using some natural and synthetic anti-glioma agents, such as medicinal cannabis or cannabinoids, bipolaris setariae fungi, oncolytic viruses, neurostatin, and fatty acid synthase (FAS) inhibitors, can also help combat gliomas (Anjum et al., 2017). Despite comprehensive strategies, residual GBM cells can develop treatment resistance (TR), resulting in GBM recurrence within a median time of approximately 7 months (Louis et al., 2016; Liu C. C. et al., 2021).

TMZ is a chemotherapeutic agent specifically used for brain cancer and was approved for recurrent mesenchymal astrocytoma in the United States in 1999 and recurrent mesenchymal astrocytoma and glioblastoma in Europe in 2000 (Mutter and Stupp, 2006). However, mitozolomide, the essential compound of TMZ, entered the clinic in 1983 (Newlands et al., 1997) and a phase I trial was completed in 1985 (Newlands et al., 1985), indicating that TMZ was developed over 16 years. A randomized clinical study conducted by Stupp in 2005 showed that adding TMZ to radiotherapy improved the 2-year survival rate of patients with GBM from 10.9% to 27.2% with minimal toxicity (Stupp et al., 2005). Since then, TMZ has been used as the first-line chemotherapeutic agent for gliomas (Stylli, 2020).

However, it is estimated that at least 50% of patients treated with TMZ do not respond to it, exhibiting innate or acquired chemoresistance, which ultimately leads to tumor recurrence (Lee, 2016). Presumably, during the window of chemotherapy with TMZ, most tumor cells are vulnerable and killed and may not have acquired full resistance (Osuka and Van Meir, 2017). Eventually, tumor cells resistant to multiple therapies persist in the brain parenchyma surrounding the tumor cavity and become the basis of tumor regeneration and recurrence (Osuka and Van Meir, 2017).

Given the slow and costly development of new therapies, drug repurposing has become an attractive strategy (Stylli, 2020). For example, a trial on metformin for GBM in 2015 showed that metformin prolonged the survival of patients with glioblastoma and diabetes (Adeberg et al., 2015). However, a pooled analysis questioned this finding and showed that metformin did not prolong survival in patients with GBM (Seliger et al., 2020). Similarly, celecoxib, as an adjuvant to TMZ chemotherapy, has shown good tolerability, but its efficacy in terms of survival benefits for patients remains uncertain (Stockhammer et al., 2010). The classical antimalarial drug, chloroquine, has been found to kill various cancer types, including GBM, through drug repurposing (Weyerhäuser et al., 2018). However, its concentration threshold for killing tumor cells under laboratory conditions is much higher than the clinically tolerable dose; therefore, its clinical value remains unclear (Weyerhäuser et al., 2018).

TMZ has shown great therapeutic value; however, the rate of drug resistance and recurrence of glioma remains reasonably high. Drug repurposing has contributed to the discovery of new therapies, but clinical application remains slow. Thus, there is an urgent need for developing new adjuvant chemotherapeutic agents.

3 Drug repurposing

3.1 Significance of drug repurposing

Drug repurposing can shorten development times by 5–7 years, reduce research investment costs by accounting for less than 10% of new compounds, and avoid risks such as a constant weight of generics (Cha et al., 2018). Moreover, a strict and burdensome regulatory process for new drugs forces developers to explore novel therapeutic uses for existing drugs (Turanli et al., 2021). Drug repurposing provides sufficient assurance regarding the safety, efficacy, and administration route of existing drugs (Parvathaneni et al., 2019; Juárez-López and Schcolnik-Cabrera, 2021; Turanli et al., 2021). Studies have shown that the cost and time to develop DSF as an anticancer drug are reduced by over 40% with an estimated annual cost of approximately $550 with DSF 500 mg per day (Cvek, 2012).

Drug repurposing facilitates the passage of projects and improves development efficiency. Only a minority of drug development projects can obtain FDA approval among newly developed drugs, compared with over 65% of drug repurposing projects (Masoudi-Sobhanzadeh et al., 2019). Recently, drug repurposing projects have accounted for approximately 30% of all newly approved drugs by the FDA (Parvathaneni et al., 2019). Additionally, drug repurposing can allow the revaluation of drugs that failed in the development phase for other uses and the change of application settings for better use (Masoudi-Sobhanzadeh et al., 2019).

3.2 Methods of drug repurposing

As high-throughput screening and computational biology methods advance, accumulated data lay the foundation for new approaches to rational drug repurposing (Turanli et al., 2021). Currently, numerous drug repurposing databases are available, allowing easy access to drug repurposing research, and systematic analysis is now accessible on platforms or screening systems dedicated to identifying repurposable drug candidates (Juárez-López and Schcolnik-Cabrera, 2021).

There are multiple information-gathering methods for drug repurposing. Electronic drug repurposing involves using various public databases to gather information from research, clinical trials, utilization reports, and other published data, and then to identify drug targets and networks of drug-drug interactions with the help of bioinformatics tools and artificial intelligence (Kumar et al., 2019). Text mining methods are used to discover new information by extracting aggregated new information from multiple published resources with the help of a computer, and by obtaining a large amount of data on conceptual relationships in biology from publications (Kumar et al., 2019). Clustering methods are applied to display and discover new drug targets or drug-disease relationships through various modules, groups, or subnetworks using clustering algorithms (Kumar et al., 2019). Propagation methods are based on information transmission from the source node to the network nodes and individual subnetwork nodes to determine the relationship between disease genes and target diseases (Emig et al., 2013). Semantic approaches seek biological entity relationships from medical databases, build semantic networks based on existing ontology networks, develop algorithms to discover the relationships, and extract medical information and image resources for drug reuse (Xue et al., 2018). Biological approaches include using systems and network biology to develop various models for drug reutilization studies that mimic the physiological environment of the target protein and modulate the outcome of its action, particularly targeting multifactorial complex diseases (Pujol et al., 2010). Knowledge-based empirical approaches are methods based on the knowledge of researchers and physicians and their ability, experience, and skills to interpret

observations, with the opportunity for the serendipitous discovery of new drug utilization pathways (Kumar et al., 2019). Experimental methods include target screening, cellular analysis, animal models, and clinical trials (Kumar et al., 2019). These various methods of drug repurposing have been developed to evaluate the clinical efficacy for glioma treatment.

3.3 Database for drug repurposing

Advances in biotechnology, bioinformatics, and histological techniques (proteomics, genomics, metabolomics, etc.) have facilitated the development of several databases in biology, chemistry, medicine, and pharmacology (Kumar et al., 2019).

Basic databases for drug repurposing, such as DrugBank (Wishart et al., 2018), DGIdb (Cotto et al., 2018), and KEGG (Kanehisa et al., 2017), can provide information on drugs, targets, and pathways (Masoudi-Sobhanzadeh et al., 2019; Turanli et al., 2021). Recently, the newly developed DrugR + database based on DrugBank and KEGG provides a new source of information for the single application and reuse of drugs (Masoudi-Sobhanzadeh et al., 2019). The DrugR + database supports not only specialist users with structured query language (SQL) query functions, but also nonspecialist users with different options for targeted functions (Masoudi-Sobhanzadeh et al., 2019). The DrugR + database can also be readjusted to include drug use and provide a list of potential drugs for certain uses (Masoudi-Sobhanzadeh et al., 2019). The DrugR + database has several advantages, such as 1) providing a suitable and simple way to search for and obtain information about drugs with no technical problems, 2) providing information on the reusability of drugs, 3) allowing the selection of different types of research targets to obtain lists of drugs for diseases, and 4) providing up-to-date information on new drugs and the latest research (Masoudi-Sobhanzadeh et al., 2019).

Drug repurposing databases contain news, articles, and results obtained from drug repurposing studies (Masoudi-Sobhanzadeh et al., 2019), such as RepoDB (Brown and Patel, 2017b), Excelra (Arora et al., 2017), Drug Repurposing Hub (DRH) (Corsello et al., 2017), and TTD (Yang et al., 2016). Databases such as PREDICT (Gottlieb et al., 2011) and RepurposeDB (Shameer et al., 2018) summarize similarities between one drug or target and another (Masoudi-Sobhanzadeh et al., 2019). ChemMapper and iDrug Target are databases that assess ligand similarity (Sam and Athri, 2019). Drug target-based databases, such as DMAP (Huang et al., 2015), DrugSig (Wu et al., 2017), DDW (Holland, 2016), PDID, and idTarget (Sam and Athri, 2019), summarize drugs and their various targets, based on which new drug application pathways is proposed (Masoudi-Sobhanzadeh et al., 2019).

There are other databases such as ConnectivityMap (Lamb et al., 2006) for drug-induced gene expression studies, LINCS (Koleti et al., 2018) and GEO (Barrett et al., 2013) for transcriptomic characterization of tumor tissue from patients with cancer, CSNAP (Gaulton et al., 2012) and STITCH (Kuhn et al., 2012) for biological networks, RE:fine drugs (Moosavinasab et al., 2016) and MeSHDD (Brown and Patel, 2017a) linking drugs to disease databases, and PubChem (Wang et al., 2017) for comprehensive chemical and structural information on active ingredient components.

These databases cover an amount of information on drug targets, pathways, characteristics, and recent advances, allowing for exploring potentially efficient drugs.

4 History of drug repurposing of disulfiram

The urgent need for glioma treatment and the application of DSF to cancer through drug repurposing has led to a steady stream of studies in recent years that have shown good results in treating glioma (Huang J. et al., 2016; Huang et al., 2018; Huang et al., 2019; Halatsch et al., 2021). Table 1 shows the information on DSF in the drug repurposing database.

In 1937, factory workers who were regularly exposed to DSF developed flu-like symptoms when they ingested alcohol (Triscott et al., 2015). DSF has been used to treat alcohol dependence since 1947 (Chick, 1999).

In the last 40 years, the anticancer effects of DSF have been discovered *in vitro* and in cancer xenografts (Conticello et al., 2012; Paranjpe et al., 2014). In 2003, Wang et al. suggested the possible clinical use of DSF in rectal cancer using cellular assays (Wang et al., 2003). In 2006, Chen et al. demonstrated through animal testing that DSF promotes selective apoptosis of tumor cells by inhibiting proteasome activity (Chen et al., 2006). In 2009, Iljin et al. systematically investigated the efficacy of most drugs and drug-like molecules already on the market against prostate cancer cells, and ultimately showed that DSF reduced tumor growth, induced metallothionein expression, and reduced DNA replication *in vivo*, indicating its potential as a therapeutic agent for prostate cancer (Iljin et al., 2009).

In 2009, Richard et al. speculated that DSF should be studied as an adjuvant to chemotherapy for glioblastoma based on its effect on acetaldehyde dehydrogenase (ALDH) in glioma (Kast and Belda-Iniesta, 2009), and since then the value of DSF in glioma has been focused. In 2012, Joanna et al. used the database approach for drug repurposing and selected DSF from numerous drugs that inhibit tumor-initiating cells using the Prestwick database (Triscott et al., 2012). They found that DSF inhibited PLK1 expression in GBM cells, suggesting that DSF could be repurposed for the treatment of refractory GBM (Triscott et al., 2012). In 2015, high ALDH1A1 expression was found to be associated with highly aggressive tumor cells and high-grade

TABLE 1 The information on DSF in the drug repurposing database.

Drug repurposing database	Website	Id number	Disease area	Drug repurposing area
RepoDB	http://apps.chiragjpgroup.org/repoDB/	None	Alcoholic Intoxication, Chronic (CUI: C0001973)	GBM/glioma
DRH	www.broadinstitute.org/repurposing	BRD-K32744045	Abstinence from alcohol (neurology/psychiatry)	None
DrugBank	www.drugbank.ca	DB00822	Chronic Alcoholism	GBM/glioma
DGIdb	www.dgidb.org	NSC-25953	Alcohol Deterrents	Cocaine abuse
KEGG	http://www.kegg.jp	D00131	Management of selected chronic alcohol patients	Antiparasitic
LINCS	http://lincsportal.ccs.miami.edu/	LSM-5467	Alcohol dependence	Melanoma
DrugSig	http://biotechlab.fudan.edu.cn/database/drugsig/	BCTD00137	Chronic alcoholism	None
PubChem	https://pubchem.ncbi.nlm.nih.gov	3117	Alcoholism	GBM

gliomas (Chen et al., 2006). ALDH1A1 promoted glioma progression, invasion, and proliferation, and led to poor prognosis (Chen et al., 2006). This finding brought the anti-glioma effects of DSF as an ALDH inhibitor back into the spotlight (Chen et al., 2006). In 2016, Huang et al. conducted the first phase I clinical trial using DSF in combination with TMZ for GBM treatment (Huang J. et al., 2016). In 2017, Karamanakos et al. combined DSF with standard treatment modalities to treat a patient with GBM and ultimately improved his prognosis, thereby confirming the clinical value of DSF (Karamanakos et al., 2017). In 2019, DSF was first reported to preferentially enhance radiosensitivity in GBM cells, particularly in radioresistant cells (Koh et al., 2019). In 2021, Meier et al. demonstrated the therapeutic value of DSF as a repurposed drug for treating gliomas in children (Meier et al., 2021). To date, relevant clinical trials are ongoing (NCT03363659, NCT03151772, NCT02715609, etc.).

5 Clinical practice for disulfiram in glioma

Huang et al. (2016) conducted a phase I clinical trial. Twelve patients newly diagnosed with supratentorial primary GBM were studied using concomitant adjuvant DSF and TMZ chemotherapy after radiotherapy. Patients were divided into two groups and received 500 mg/day or 1000 mg/day of DSF in combination with TMZ chemotherapy. The results showed that the maximum tolerated dose of DSF was 500 mg/day. Although some associated adverse effects, such as fatigue, delirium, ataxia, dizziness, and peripheral motor/sensory neuropathy, existed, these adverse reactions were self-limiting and resolved within 30 days after DSF discontinuation (Huang J. et al., 2016).

In 2018, Huang et al. updated data from a phase I clinical trial. The study population comprised 18 patients newly diagnosed with GBM after standard radiotherapy. DSF was also administered during the chemotherapy phase of TMZ. Seven patients received DSF at 500 mg/day, five patients received DSF at 1000 mg/day, and six patients received DSF/Cu at 500 mg/day. The results showed that a maximum dose of 500 mg/day of DSF was well tolerated with or without combined Cu, while 1000 mg/day was poorly tolerated. Of the patients receiving 500 mg DSF with a combination of Cu per day, one patient suffered from nausea and diarrhea in the first 30 days, which was relieved after the reduction of DSF to 250 mg per day. Additionally, without the combination of Cu, one patient developed delirium after 1.6 months and one developed motor neuropathy after 2.6 months. All adverse reactions resolved rapidly after dose reduction or DSF discontinuation. Notably, a 40-year-old woman in the study who received 500 mg DSF per day discontinued DSF therapy after 2.6 months of treatment due to motor neuropathy. At 33 months after DSF treatment, the patient survived in good health with no signs of tumor recurrence (Huang et al., 2018).

Based on a previous study, Huang et al. conducted a phase II clinical trial in 2019. Twenty-three patients with recurrent TMZ-resistant GBM were enrolled in the study. DSF (80 mg) and Cu gluconate (1.5 mg) were administered orally thrice daily at approximately 4–8 hourly intervals in conjunction with TMZ chemotherapy. The results showed that 14% of the patients achieved clinical benefit over a stabilization period of over 6 months. The most common adverse effects were nausea and vomiting in 17% of patients, followed by dizziness (Huang et al., 2019).

In 2021, Marc et al. conducted a phase Ib/IIa clinical trial using a CUSP9 treatment regimen in combination with TMZ. Ten patients with GBM were included in this study. CUSP9 was gradually added at increasing doses during uninterrupted TMZ

chemotherapy. When all drugs reached the target dose, the drug was maintained until side effects or tumor progression occurred. The results showed that the regimen was safe under clinical, laboratory, and electrocardiographic monitoring and that the side effects were mild and disappeared after discontinuation (Halatsch et al., 2021).

Since 2016, there have been updates on clinical trials using DSF as an adjuvant in the treatment of glioma. Evidence suggests that DSF has great therapeutic potential but with mild side effects; however, clinical studies are still inadequate.

6 Pharmacological mechanism of disulfiram

DSF can act as an anticancer agent through various Cu- and zinc-dependent processes, including the inhibition of nuclear factor kappa B (NF-κB), NPL4, and phosphoglycerol dehydrogenase (Spillier et al., 2019). DSF produces oxidative stress by inhibiting NF-κB activation and superoxide dismutase (SOD) and inducing an increased ratio of oxidized glutathione to its reduced form (Tesson et al., 2017). DSF cytotoxicity is dependent on Cu (Ye et al., 2011). Cu plays a key role in redox reactions and triggers the generation of reactive oxygen species (ROS) in human cells (Liu et al., 2012). Many cancer types, including GBM, have significantly higher intracellular Cu levels than normal tissues, and DSF penetrates and chelates Cu intracellularly (Liu et al., 2012). As DSF cytotoxicity appears to be Cu-dependent, high Cu concentrations in cancer cells produce cytotoxicity through oxidative stress generated by the Fenton reaction (production of Cu ions and hydroxyl radicals) or through inhibiting enzymes that bind Cu to peptide bonds, allowing DSF to specifically target cancer cells and preserve normal tissue (Liu et al., 2012; Tesson et al., 2017).

Approximately 80–95% of the orally administered DSF is absorbed and the unabsorbed portion is excreted (Shirley et al., 2021). In the body, DSF is rapidly metabolized to DTC acid and then rapidly formed as diethylthiocarbamic acid methyl ester (diethyldithiomethylcarbamate, MeDTC) or broken down into carbon disulphide and dimethylamine (Shirley et al., 2021). MeDTC inhibits ALDH and is a strong metal chelate that can form complexes with metal ions (Shirley et al., 2021). DSF is also reduced to DTC in the stomach and forms metal-ion complexes in the gastrointestinal tract (Shirley et al., 2021). DTC metal complexes have a relatively long half-life, are widely distributed throughout the body, and penetrate the blood-brain barrier (BBM) (Shirley et al., 2021). This pharmacological mechanism makes it possible for DSF to kill glioma cells specifically. During DSF treatment, alcohol ingestion leads to acetaldehyde accumulation due to ALDH inhibition, causing the DSF-ethanol reaction (Jørgensen et al., 2011). This reaction manifests as tachypnea, tachycardia, facial flushing, nausea, vomiting, hypotension, and even cardiovascular collapse (Jørgensen et al., 2011).

7 Molecular mechanism of disulfiram against tumor stem cells

7.1 Inhibition of ALDH

DSF has a symmetric structure, and its first metabolic step is reducing the disulfide bond at the center of the molecule to produce two diethyldithiocarbamate (DTC) fractions (Lipsky et al., 2001a). DTC is further converted to its methyl ester and other metabolites (Lipsky et al., 2001a). DTC is a potent ALDH inhibitor, which forms a mixed disulfide bond with the key cysteine near the active site (Lipsky et al., 2001a). DSF significantly alters alcohol metabolism and treats chronic alcohol dependence by irreversibly inhibiting ALDH and causing acetaldehyde accumulation (Jørgensen et al., 2011). ALDH belongs to a family of metabolic enzymes that catalyze the oxidation of aldehydes, a toxic alcohol metabolism product (Lipsky et al., 2001b). ALDH promotes cell survival by protecting DNA from genotoxic damage and providing resistance to a wide range of anticancer drugs (Hothi et al., 2012). Therefore, ALDH inhibition is an effective way to sensitize resistant cell populations to the cytotoxic effects of chemotherapeutic drugs (Hothi et al., 2012). The strong expression of ALDH is a prominent feature of normal and cancer stem cells, including the stem cell subpopulation of glioblastoma (Kast and Belda-Iniesta, 2009). In GBM and other cancers, increased ALDH expression is observed in a small subpopulation of tumor cells with stem cell properties (Rappa et al., 2013). ALDH expression is associated with the anti-apoptotic capacity of glioma stem cells (GSCs) and the protection of DNA against damage by ROS and aldehydes (Kast and Belda-Iniesta, 2009). DSF and its metabolites form mixed disulfide bonds with key cysteines (Cys302) near the active site of ALDH to inactivate it (Paranjpe et al., 2014). With ALDH inhibition, the division of stem cells into non-stem daughter cells is blocked (Kast and Belda-Iniesta, 2009). However, such inhibitory effect of DSF on ALDH does not affect normal neural stem cells or fibroblasts (Choi et al., 2015).

7.2 Induced degradation of mixed lineage leukemia

MLL1 and MLL2 are human homologs of the *Drosophila* epigenetic regulator Trithorax (Trx) (Schuettengruber et al., 2017). MLL1 promotes tumor stem cell characteristics, cell growth, and tumorigenicity in adult glioblastomas (Meier et al., 2021). MLL2 mutations are found in 14% of patients with medulloblastoma (Parsons et al., 2011). Studies have shown that DSF can effectively kill both childhood glioma stem cells at low concentrations and glioma cell lines at slightly higher concentrations by inducing MLL degradation (Meier et al., 2021).

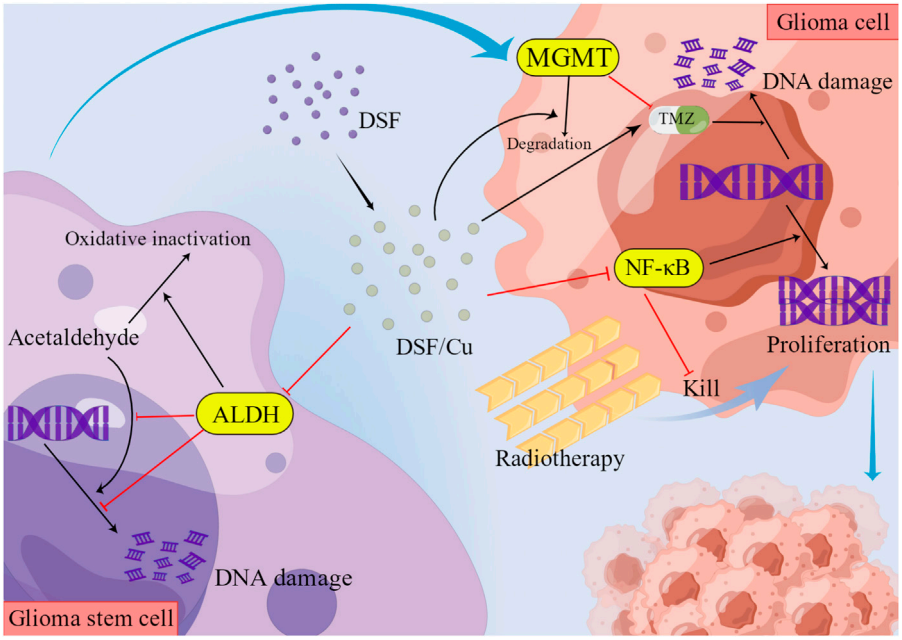

FIGURE 2
Molecular mechanisms of DSF.

7.3 Mediation of increased intracellular ROS production

DSF-mediated cytotoxicity is partially due to increased ROS production. Elevated ROS levels are the major mode of DSF-mediated cell death (Kast et al., 2014). DSF/Cu induces ROS in GBM cell lines, which activates the JNK and p38 pathways, and inhibits NF-κB activity (Liu et al., 2012). DSF/Cu eliminates stem cell-like cell populations in GBM cell lines by modulating the Bcl2 family to trigger the intrinsic apoptotic pathway (Liu et al., 2012). DSF rapidly inhibits superoxide dismutase 1 (SOD1) in murine microglia to induce neurotoxic microglia activation (Dimayuga et al., 2007). ROS production by activated microglia directs redox-sensitive inflammatory signaling and initiates neurotoxic inflammation (Dimayuga et al., 2007). The inhibition of activated microglia might lower the neurological side effects of DSF during the treatment.

8 Molecular mechanism of disulfiram against glioma cells

8.1 Inhibition of MGMT activity

O6-methylguanine-DNA methyltransferase (MGMT) is a DNA repair protein and chemotherapeutic target that is highly expressed in approximately 80% of brain tumors and other cancers (Gerson, 2002). MGMT, as an anti-mutagenic DNA repair protein, can remove mutagenic O6-alkyl groups from guanine and interfere with the cytotoxic effects of alkylating agents to make tumors resistant (Gerson, 2002). The survival of patients with GBM depends on the MGMT promoter methylation status (Koh et al., 2019). Those with methylated MGMT promoter (MGMT meth) had a higher survival rate than those with the wild-type (MGMT wt) (Paranjpe et al., 2014; Koh et al., 2019). Thus, MGMT has become a central determinant of tumor resistance to alkylating agents (Paranjpe et al., 2014). DSF causes MGMT degradation (Srivenugopal et al., 2016) and synergistically inhibits the growth and renewal of TMZ-resistant GBM cells (Triscott et al., 2012). Compared to normal astrocytes, DSF induces a preferential increase in radiosensitivity in GBM cells, causing increased apoptosis and delayed DNA damage repair (Koh et al., 2019). DSF-induced radiosensitization is more pronounced in radioresistant cells, especially drug-resistant GBM cells with wild-type non-methylated MGMT promoters (Koh et al., 2019). In brain tumor cell lines, DSF reduced MGMT activity in a rapid and dose-dependent manner (Paranjpe et al., 2014). Of these, DSF/Cu was approximately five times more potent than DSF in inhibiting MGMT activity in cultured brain tumor cells (Paranjpe et al., 2014). There are no reports about adverse effects on normal neuronal cells caused by this mechanism.

8.2 Inhibition of NF-κB

NF-κB promotes disease progression by increasing tumor cell proliferation, inducing the transcription of anti-apoptotic genes and genes involved in the DNA damage response, and promoting angiogenesis (Voorhees and Orlowski, 2006). NF-κB activation is associated with radioresistance, particularly through inducing anti-apoptotic and antioxidant gene expression (Tesson et al., 2017). DSF is an NF-κB inhibitor, which interferes with TGF-β-induced epithelial-mesenchymal transition in cancer (Han et al., 2015). The blockade of NF-κB activation by DSF reduces tumor volume and cell invasion (Westhoff et al., 2013). The aggressiveness of GBM is associated with the secretion and processing of fibronectin by GBM cells via fibrinogen and matrix metallopeptidases (Mettang et al., 2018). GBM causes reduced intercellular interactions by creating this new extracellular matrix (ECM)-based microenvironment, and generating a stress response that triggers NF-κB activation and enhances cell-matrix adhesion of GBM (Mettang et al., 2018). DSF blockade of NF-κB activation inhibits cell-matrix adhesion between GBM and the brain tissue microenvironment, and reduces tumor volume and cell invasion (Mettang et al., 2018). Other drugs that modulate fibrinogen, metallopeptidases, and fibronectin in the microenvironment of glioma cells might synergistically enhance the anti-invasive effects of DSF.

8.3 Inhibition of proteasome activation

Proteasome activity promotes tumorigenesis by enhancing tumor cell proliferation, down-regulating apoptosis, and promoting angiogenesis (Voorhees and Orlowski, 2006). Therefore, the ubiquitin-proteasome pathway is an important target for cancer therapy (Voorhees and Orlowski, 2006). DSF inhibits proteasome activation (Voorhees and Orlowski, 2006), leading to the accumulation of misfolded proteins and potentially toxic protein aggregates (Hothi et al., 2012), subsequently inducing tumor cell death (Hothi et al., 2012). The DSF activity depends on the presence of Cu ions, and Cu thiocarbamate complexes act as proteasome inhibitors (Hothi et al., 2012). As a potent proteasome inhibitor, DSF/Cu can functionally impair the DNA repair pathways and enhance the effects of DNA alkylating agents and radiation (Lun et al., 2016). DSF/Cu inhibits the chymotrypsin-like proteasome activity in cultured glioma stem cells (GSC), consistent with the inactivation of the ubiquitin-proteasome pathway and subsequent tumor cell death induction (Hothi et al., 2012).

8.4 Downregulation of PLK1 expression

Polo-like kinase 1 (PLK1), which is highly expressed in tumor cells, is a key serine/threonine kinase involved in many important cell cycle functions such as mitotic entry, centrosome maturation, cell cycle progression, and cytoplasmic division (Triscott et al., 2012). As GBM tumors with higher levels of PLK1 expression have a higher incidence and poorer prognosis, PLK1 could be a promising therapeutic target for brain tumors (Triscott et al., 2012). DSF leads to downregulation of cell cycle kinase PLK1 in GBM cells (Triscott et al., 2012).

DSF is involved in the regulation of complicated molecular mechanisms. These molecular mechanisms of DSF are shown in Figure 2.

9 DSF delivery route

The standard dosage following FDA-approved indications for managing chronic alcohol use is 250 mg/day orally, with a maximum dose of 500 mg/day (Ekinci et al., 2019). Additionally, the nasal-brain pathway is considered a safe and effective alternative for direct drug delivery to the CNS (Landis et al., 2012). Administration via the nasal cavity to the CNS bypasses the blood-brain barrier and avoids hepatic first-pass effects (Qu et al., 2021). The clinical application of DSF as an anticancer drug is limited by its poor oral bioavailability and rapid metabolism *in vivo* (Shergill et al., 2016). It has been shown that DSF encapsulation in hydroxypropyl-β-cyclodextrin (HP-β-CD) produces a DSF complex with enhanced solubility (Qu et al., 2021). *In vitro* anti-GBM activity and safety (DSF/HP-β-CD/Cu) can increase the aqueous solubility of DSF by approximately 2,450-fold and may be a promising intranasal agent to treat (Qu et al., 2021). Animal studies have shown that DSF/HP-β-CD/Cu significantly inhibited tumor growth and migration, promoted tumor apoptosis, and prolonged the median survival time in male glioma rats in the intranasal administration group (Qu et al., 2021). Besides oral and nasal-brain access, 1,2-distearoyl-sn-glycero-3-phosphocholine (DSPC)/cholesterol liposomes to prepare DSF as an injectable $Cu(DDC)_2$ formulation are also therapeutically active (Wehbe et al., 2017).

10 Combination therapy of disulfiram

Combinations of two or more drugs with different mechanisms of action, also referred to as combination therapy, is an alternative strategy for improving the success of drug repurposing (Masoudi-Sobhanzadeh et al., 2019). Compared with single-drug therapy, it reduces the incidence/emergence of resistance mechanisms, doses of drugs, and adverse effects, and improves the synergistic effects and success of treatment modalities (Masoudi-Sobhanzadeh et al., 2019). Combination therapy allows simultaneous targeting of multiple therapeutic genes, and is currently the most effective treatment for aggressive tumors, such as GBM (Ghosh et al.,

TABLE 2 The candidate chemicals used in combination with DSF for anticancer therapy.

Combination of drugs	Tumor type	Evidence type	Year and References
Temozolomide (TMZ)	Glioblastoma (GBM)	Clinical trials	Huang et al. (2019)
	Glioblastoma stem cells (GSCs)	Cells	Zirjacks et al. (2021)
Cisplatin	Ovarian *Cancer*	Animals	Bai et al. (2021)
	Head and neck squamous cell carcinoma (HNSCC)	Cells	Yao et al. (2021)
	Mammary cancer	Cells	Yang et al. (2019)
	Prostate adenocarcinoma	Cells	O'Brien et al. (2012)
	Atypical teratoid/rhabdoid tumor (AT/RT)	Animals	Jangra et al. (2020)
	Bladder cancer	Cells	Kita et al. (2019)
	Testicular germ cell tumors	Animals	Schmidtova et al. (2019)
	Esophageal squamous cell carcinoma	Animals	Jivan et al. (2018)
	Metastatic non-small cell lung cancer	Clinical trials	Nechushtan et al. (2015)
	Nasopharyngeal carcinoma (NPC)	Animals	Li et al. (2020)
Auranofin	Pediatric glioma	Cells	Meier et al. (2021)
	Hepatoma	Cells/Animals	Huang et al. (2016a)
	Ovarian cancer	Cells	Papaioannou et al. (2014)
Gemcitabine (dFdC)	Glioblastoma (GBM)	Cells	Tesson et al. (2017)
	Mammary cancer	Animals	Liu et al. (2021a)
	Pancreatic ductal adenocarcinoma (PDAC)	Cells/Animals	Kim et al. (2013)
	Colon cancer	Cells	Guo et al. (2010)
Regorafenib	Glioblastoma (GBM)	Animals	Zhao et al. (2018)
Carbenoxolone	Glioblastoma (GBM)	Animals	Mettang et al. (2018)
CUSP9/ Temozolomide (TMZ)	Glioblastoma stem cells (GSCs)	Cells	Skaga et al. (2019)
Paclitaxel	Mammary cancer	Cells	Liu et al. (2013)
	Lung adenocarcinoma	Animals	Mohammad et al. (2019)
Docetaxel	Mammary cancer	Cells	Swetha et al. (2020)
Doxorubicin	Osteosarcoma	Cells	Mandell et al. (2022)
	Mammary cancer	Cells	Rolle et al. (2020)
	Acute myeloid leukemia (AML)	Cells	Xu et al. (2011)
5-Fluorouracil (5-Fu)	Cervical carcinoma	Cells	Abidin et al. (2020)
	Pancreatic ductal Adenocarcinoma (PDAC)	Animals	Cong et al. (2017)
	Colorectal cancer (CRC)	Cells	Wang et al. (2003)
Arsenic trioxide (ATO)	Pancreatic cancer	Animals	Dinnen et al. (2013)

All references listed in the table are the latest research progress.

2018). Combination therapy of DSF with other modalities holds great promise.

10.1 Disulfiram in combination with metal supplements

Preclinical and clinical studies have shown that DSF has broad-spectrum anticancer activity against a variety of cancer types when combined with Cu-containing supplements, such as Cu gluconate (McMahon et al., 2020). The combination regimen comprised 500 mg of DSF daily plus 50 mg of zinc gluconate or 2 mg of Cu gluconate three times daily (Ekinci et al., 2019). It has been shown that DSF/Cu sulphide (CuS) nanocomplexes (Tf-DSF/CuS) modified with transferrin (Tf) exhibit high cytotoxic effects *in vitro* (Lan et al., 2021). The CuS nanoparticles enable them to accumulate specifically and within tumor tissue by enhancing the permeability and retention (EPR) effect of the tumor tissue (Lan et al., 2021). The metallic nature of the nanoparticles enhanced the drug-loading capacity by forming Cu complexes on the CuS surface (Lan et al., 2021). Additionally, the use of a long-wavelength laser in the near-infrared (700–1000 nm) region activated the photothermal effect of the nanoparticles, resulting in minimal damage to normal tissue from tumor ablation (Lan et al., 2021). Besides Cu, DSF can act through zinc chelation to inhibit the activities of MMP-2 and MMP-9 (Kast and Halatsch, 2012).

10.2 Disulfiram in combination with standard chemotherapy drugs

In vitro cytotoxicity is enhanced by the addition of DSF to standard chemotherapeutic agents (Rappa et al., 2013) such as cisplatin (O'Brien et al., 2012), TMZ (Triscott et al., 2012), paclitaxel (Yip et al., 2011), gemcitabine (Cunningham and Chaiton, 2018), doxorubicin (Budman and Calabro, 2002), cyclophosphamide (Moreb et al., 2012), 5-fluorouracil (Wang et al., 2003), and adriamycin (Xu et al., 2011). The combination regimens for DSF against gliomas are described below.

10.2.1 Disulfiram in combination with temozolomide

The 5-year survival rate of patients with GBM treated with radiation alone was 1.9%, and TMZ, in conjunction with radiation therapy, only increased the rate to 9.8% (Triscott et al., 2015). Additionally, TMZ toxicity is often not well tolerated by patients, and other modalities of TMZ resistance, such as MGMT expression, make it complicated (Triscott et al., 2015).

DSF is highly effective in cases where cells develop TMZ resistance (Triscott et al., 2012). DSF has synergistic activity when combined with TMZ, which is highly effective against TMZ-resistant cells (Lun et al., 2016). In the presence of low Cu doses, DSF significantly enhanced TMZ activity *in vitro* (Lun et al., 2016). *In vivo* studies have confirmed that DSF and Cu have synergistic effects with TMZ and improve survival in mice with *in situ* GBM tumors (Lun et al., 2016).

DSF can be safely used in combination with TMZ, although it causes reversible neurotoxicity (Huang J. et al., 2016). At a maximum tolerated dose (MTD) of 500 mg/day of DSF with TMZ without concomitant Cu administration, slight proteasomal inhibition of peripheral blood cells was observed after 4 weeks, with an average reduction of approximately 5% (Huang J. et al., 2016). A dose-response trend appeared with doubling proteasome inhibition at a dose of 1000 mg/day (Huang J. et al., 2016). The results of a phase II clinical study in 23 patients showed that adding DSF/Cu to TMZ was safe and well tolerated in TMZ-resistant IDH wild-type GBM (Huang et al., 2019).

10.2.2 Disulfiram in combination with cisplatin

DSF enhances cisplatin-induced cytotoxicity by directly damaging DNA (O'Brien et al., 2012). Activating transcription factor 3 (ATF3) exerts a pro-apoptotic effect in response to cisplatin by directly binding to and activating vascular endothelial cells (O'Brien et al., 2012). It has been shown that the combination of cisplatin and DSF plays a synergistic role in inducing ATF3 protein expression and promoting tumor cell death (O'Brien et al., 2012). Adding DSF to the combination regimen of cisplatin and vincristine is well tolerated in antitumor therapy (Nechushtan et al., 2015). A dose of 40 mg DSF, with a half-life of approximately 7 hours, can be administered three times daily to improve its therapeutic effect with minimal side effects (Nechushtan et al., 2015). Significant neurotoxicity has not been reported with this combination therapy, besides fatigue (Nechushtan et al., 2015).

DSF may assist cisplatin in enhancing cytotoxic effects. This strategy appears to be safe, but the *in vivo* efficacy in glioma patients remains unclear.

10.2.3 Disulfiram in combination with auranofin

A study of glioma stem cells in children found that DSF killed glioma stem cells at low concentrations and killed cell lines at slightly higher concentrations (Meier et al., 2021). The addition of auranofin increased DSF efficiency, and the synergistic effect was more pronounced in differentiated cells than in undifferentiated cells (Meier et al., 2021). Auranofin was also used in combination with DSF in the CUSP9 treatment program (Skaga et al., 2019).

10.2.4 Combination with coordinated undermining of survival paths

DSF with aprepitant, auranofin, captopril, celecoxib, itraconazole, minocycline, quetiapine, and sertraline constituted a CUSP9 regimen that was used in combination with TMZ to synergistically disrupt the active survival pathway in GBM, block multiple signaling pathways, and make GBM vulnerable to the cytotoxic effects of TMZ (Skaga et al., 2019). A study of patient-derived glioblastoma stem cell (GSC) cultures from 15 patients with GBM showed that combining CUSP9 with TMZ produced a synergistic effect compared to the single drug (Skaga et al., 2019). CUSP9, combined with TMZ, was more effective than TMZ monotherapy in terms of the clinical plasma concentrations (Skaga et al., 2019). The CUSP9* regimen was generated based on the CUSP9 regimen, comprising DSF in combination with aprepitant, artesunate, auranofin, captopril, celecoxib, itraconazole, sertraline, and ritonavir (Kast et al., 2014). All nine drugs in the CUSP9* regimen were FDA-approved, each inhibiting one or more of the important GBM growth pathways (Kast et al., 2014).

DSF and auranofin have synergistic effect even without the other components of a CUSP9 regimen. All these might be the powerful adjuncts to TMZ chemotherapy. However, the side effects of CUSP9 or CUSP9* regimens combined with multiple agents deserve further clinical study.

10.2.5 Disulfiram in combination with gemcitabine

Gemcitabine (2,2′-difluorodeoxycytidine, dFdC) is a deoxyribonucleic acid analogue that can be used as a single agent or combined with other anticancer drugs (Metro et al., 2010). Gemcitabine is active against a wide range of hematological and solid cancers. It is one of the few classical anticancer drugs that

can pass through the BBB, penetrate the tumor mass, and be effectively converted to its active form in GBM tissue (Metro et al., 2010). However, its use in GBM chemotherapy is limited by the high resistance of GBM cells to dFdCs (Liu et al., 2012). Therefore, it is currently used mainly in combination with radiotherapy as a radiosensitizer for GBM treatment (Liu et al., 2012). DSF can synergistically enhance gemcitabine cytotoxicity and reverse gemcitabine resistance in cancer cell lines through ROS induction and inhibition of the ALDH and NF-κB pathways (Liu et al., 2012; O'Brien et al., 2012). In preclinical studies, DSF and its derivative pyrrolidine dithiocarbamate have been successfully used to enhance gemcitabine efficacy, particularly through NF-κB inhibition and oxidative stress generation (Iljin et al., 2009; Tesson et al., 2017). Increased oxidative stress due to DSF/Cu interactions with glutathione sensitizes cancer cells to gemcitabine treatment (Iljin et al., 2009; Tesson et al., 2017).

10.2.6 Disulfiram in combination with carbenoxolone

Carbenoxolone is mainly used to treat gastric ulcers and other types of inflammation (Connors, 2012) and can play a role in inhibiting tumor cell growth by interfering with intracellular signaling through inhibiting ligand proteins (Zhang et al., 2003). DSF and carbenoxolone inhibit distinct interactions of GBM with the brain tissue microenvironment and stress-induced GBM cell-matrix adhesion with gap junction-mediated intercellular communication (Mettang et al., 2018). Animal experiments have shown that the combined use of DSF, carbenoxolone, and TMZ reduces tumor size in an *in situ* mouse model (Mettang et al., 2018). Tumor-initiating and adherent differentiated cells form gap junctions, and carbenoxolone can block adherent differentiated cells and affect intercellular communication (Mettang et al., 2018). Adherent differentiated cells are more sensitive to DSF treatment, and DSF interferes with cell-matrix adhesion by modulating NF-κB signaling (Mettang et al., 2018).

Table 2 shows the candidate chemicals used in combination with DSF for cancer treatment.

10.3 Disulfiram in combination with radiotherapy

DSF has a radiosensitizing effect on GBM cells (Koh et al., 2019) and enhances the radiosensitivity of AT/RT cell lines by increasing DNA damage, apoptosis, and autophagy (Lee et al., 2017). Combining DSF and Cu enhanced radiosensitivity by inducing cell death or interfering with DNA repair (Liu C. C. et al., 2021).

Thus, the efficacy of both chemotherapy and radiotherapy might be enhanced by DSF.

11 Adverse effects of disulfiram

DSF is a safe and well-tolerated drug, with mild side effects (Shirley et al., 2021). With chronic lymphocytic leukemia and normal lymphocytes (Wickström et al., 2007), invasive cancer and normal endothelial cells (Shian et al., 2003), and glioblastoma and normal astrocytes (Hothi et al., 2012), DSF is selectively toxic and kills human cancer cells (Paranjpe et al., 2014). The ability of different organs to resist endogenous and environmentally derived alkylating agents may be compromised, and this unrepaired DNA damage, particularly in regulatory oncogenes, may manifest as deleterious mutations and promote genomic instability (Paranjpe et al., 2014). DSF combined with Cu has an enhanced role in killing cancer cells; however, Cu-mediated cytotoxicity is also significantly increased in normal cells (Choi et al., 2015). The combined use of Cu and Zn in therapy is potentially dangerous because they are teratogenic and may lead to developmental defects (Choi et al., 2015). High DSF doses are hepatotoxic (Triscott et al., 2015), and rare cases of severe atopic hepatitis may occur, along with a risk of neuropathy; however, these symptoms are reversible after discontinuation (Huang J. et al., 2016). The mechanisms of neurological side effects of DSF remain unclear and may involve free acid radicals, inhibition of certain enzymes, calcium-induced neuronal toxicity, synergistic activity of neurotoxic drugs/chemicals, and other mechanisms (Kulkarni et al., 2013). If ethanol is ingested during DSF treatment, the large amounts of acetaldehyde produced from ethanol can cause severe nausea, headache, vomiting, flushing, and physical discomfort (Kast and Belda-Iniesta, 2009).

DSF is considered a relatively safe treatment since most of its adverse effects resolve after discontinuation. The mechanism of neuropathy caused by DSF still requires further research.

12 Conclusion

Malignant gliomas have a poor prognosis and high recurrence rate, posing a major threat to global public health. Current conventional treatment modalities hardly eradicate gliomas; therefore, new therapeutic approaches are urgently needed. Drug repurposing approaches have provided new research ideas for glioma treatment. This can help the pharmaceutical industry and researchers identify new uses for existing drugs. The expanding research on gliomas through drug repurposing approaches has made DSF a potential adjuvant for glioma treatment. DSF has a good safety profile and is an economical drug that is expected to play a broader role in the future treatment of gliomas. Further epidemiological studies should be performed to investigate the relationship between DSF and the risk to or survival of patients with gliomas. More clinical trials are needed to further refine treatment options for DSF. However, drug repurposing may not yet reach its full potential in the field of glioma, and new therapeutic agents through drug repurposing deserve further exploration.

Author contributions

Conceptualization, YB and SZ; methodology, SZ; critical revision of the manuscript for important intellectual content, YB, YW, and SL; analysis and interpretation of data, XZ and SL; investigation, XS, GL, KL, XZ, LL, LR, ST, QZ, BZ, WS, ZY, and QX; reference collection and data acquisition, SZ and SL; original draft preparation, SZ; review and editing, SZ, YB, and YW; visualization, SZ; supervision, YB and YW; project administration, SZ, SL, YB, and YW; funding acquisition, YB and XS. All authors have read and agreed to the published version of the manuscript.

Funding

This study was funded by Liaoning Provincial Natural Science Foundation (2020-MS-155), China Medical University novel coronavirus pneumonia prevention and control research project (2020-12-11), Shenyang Planning Foundation for Science and Technology (21-173-9-38), the first batch of medical education scientific research project of China Medical University for the 14th Five-Year Plan (YDJK2021011), the Scientific Research Funding Project of Education Department of Liaoning Province (JCZR2020010), National Science Foundation of China (72074104), Immersion Technology and Evaluation Shandong Engineering Research Center (2022), and Immersion Technology and Evaluation Shandong Engineering Research Center (2022). The researchers are grateful for the support of several organizations.

Conflict of interest

The authors declare that the research was conducted in the absence of any commercial or financial relationships that could be construed as a potential conflict of interest.

Publisher's note

References

Abidin, I. Z., Rezoagli, E., Simonassi-Paiva, B., Fehrenbach, G. W., Masterson, K., Pogue, R., et al. (2020). A bilayer vaginal tablet for the localized delivery of disulfiram and 5-fluorouracil to the cervix. *Pharmaceutics* 12, E1185. doi:10.3390/pharmaceutics12121185

Adeberg, S., Bernhardt, D., Ben Harrabi, S., Bostel, T., Mohr, A., Koelsche, C., et al. (2015). Metformin influences progression in diabetic glioblastoma patients. *Strahlenther. Onkol.* 191, 928–935. doi:10.1007/s00066-015-0884-5

Anjum, K., Shagufta, B. I., Abbas, S. Q., Patel, S., Khan, I., Shah, S. A. A., et al. (2017). Current status and future therapeutic perspectives of glioblastoma multiforme (GBM) therapy: A review. *Biomed. Pharmacother.* 92, 681–689. doi:10.1016/j.biopha.2017.05.125

Arora, N., Kacker, P. K. M., and Kacker, P. (2017). *Translational research in drug discovery and development*. Translational Bioinformatics and its Application.

Ashburn, T. T., and Thor, K. B. (2004). Drug repositioning: Identifying and developing new uses for existing drugs. *Nat. Rev. Drug Discov.* 3, 673–683. doi:10.1038/nrd1468

Bai, M. Y., Yu, M. H., Wang, T. T., Chen, S. H., and Wang, Y. C. (2021). Plate-like alginate microparticles with disulfiram-SPIO-coencapsulation: An *in vivo* study for combined therapy on ovarian cancer. *Pharmaceutics* 13, 1348. doi:10.3390/pharmaceutics13091348

Barrett, T., Wilhite, S. E., Ledoux, P., Evangelista, C., Kim, I. F., Tomashevsky, M., et al. (2013). NCBI GEO: Archive for functional genomics data sets--update. *Nucleic Acids Res.* 41, D991–D995. doi:10.1093/nar/gks1193

Brown, A. S., and Patel, C. J. (2017b). A standard database for drug repositioning. *Sci. Data* 4, 170029. doi:10.1038/sdata.2017.29

Brown, A. S., and Patel, C. J. (2017a). MeSHDD: Literature-based drug-drug similarity for drug repositioning. *J. Am. Med. Inf. Assoc.* 24, 614–618. doi:10.1093/jamia/ocw142

Budman, D. R., and Calabro, A. (2002). *In vitro* search for synergy and antagonism: Evaluation of docetaxel combinations in breast cancer cell lines. *Breast Cancer Res. Treat.* 74, 41–46. doi:10.1023/a:1016070230538

Cha, Y., Erez, T., Reynolds, I. J., Kumar, D., Ross, J., Koytiger, G., et al. (2018). Drug repurposing from the perspective of pharmaceutical companies. *Br. J. Pharmacol.* 175, 168–180. doi:10.1111/bph.13798

Chen, D., Cui, Q. C., Yang, H., and Dou, Q. P. (2006). Disulfiram, a clinically used anti-alcoholism drug and copper-binding agent, induces apoptotic cell death in breast cancer cultures and xenografts via inhibition of the proteasome activity. *Cancer Res.* 66, 10425–10433. doi:10.1158/0008-5472.Can-06-2126

Chick, J. (1999). Safety issues concerning the use of disulfiram in treating alcohol dependence. *Drug Saf.* 20, 427–435. doi:10.2165/00002018-199920050-00003

Choi, S. A., Choi, J. W., Wang, K. C., Phi, J. H., Lee, J. Y., Park, K. D., et al. (2015). Disulfiram modulates stemness and metabolism of brain tumor initiating cells in atypical teratoid/rhabdoid tumors. *Neuro. Oncol.* 17, 810–821. doi:10.1093/neuonc/nou305

Cong, J., Wang, Y., Zhang, X., Zhang, N., Liu, L., Soukup, K., et al. (2017). A novel chemoradiation targeting stem and nonstem pancreatic cancer cells by repurposing disulfiram. *Cancer Lett.* 409, 9–19. doi:10.1016/j.canlet.2017.08.028

Connors, B. W. (2012). Tales of a dirty drug: Carbenoxolone, gap junctions, and seizures. *Epilepsy Curr.* 12, 66–68. doi:10.5698/1535-7511-12.2.66

Conticello, C., Martinetti, D., Adamo, L., Buccheri, S., Giuffrida, R., Parrinello, N., et al. (2012). Disulfiram, an old drug with new potential therapeutic uses for human hematological malignancies. *Int. J. Cancer* 131, 2197–2203. doi:10.1002/ijc.27482

Corsello, S. M., Bittker, J. A., Liu, Z., Gould, J., Mccarren, P., Hirschman, J. E., et al. (2017). The drug repurposing hub: A next-generation drug library and information resource. *Nat. Med.* 23, 405–408. doi:10.1038/nm.4306

Cotto, K. C., Wagner, A. H., Feng, Y. Y., Kiwala, S., Coffman, A. C., Spies, G., et al. (2018). DGIdb 3.0: A redesign and expansion of the drug-gene interaction database. *Nucleic Acids Res.* 46, D1068-D1073–d1073. doi:10.1093/nar/gkx1143

Cunningham, J. A., and Chaiton, M. (2018). Has there been an increase in the frequency with which people who drink in a risky fashion receive advice to cut down on their drinking from 1998 to 2015? *Subst. Abus.* 39, 449–451. doi:10.1080/08897077.2018.1449048

Cvek, B. (2012). Nonprofit drugs as the salvation of the world's healthcare systems: The case of antabuse (disulfiram). *Drug Discov. Today* 17, 409–412. doi:10.1016/j.drudis.2011.12.010

Dimayuga, F. O., Wang, C., Clark, J. M., Dimayuga, E. R., Dimayuga, V. M., and Bruce-Keller, A. J. (2007). SOD1 overexpression alters ROS production and reduces neurotoxic inflammatory signaling in microglial cells. *J. Neuroimmunol.* 182, 89–99. doi:10.1016/j.jneuroim.2006.10.003

Dinnen, R. D., Mao, Y., Qiu, W., Cassai, N., Slavkovich, V. N., Nichols, G., et al. (2013). Redirecting apoptosis to aponecrosis induces selective cytotoxicity to pancreatic cancer cells through increased ROS, decline in ATP levels, and VDAC. *Mol. Cancer Ther.* 12, 2792–2803. doi:10.1158/1535-7163.Mct-13-0234

Ekinci, E., Rohondia, S., Khan, R., and Dou, Q. P. (2019). Repurposing disulfiram as an anti-cancer agent: Updated review on literature and patents. *Recent Pat. anticancer. Drug Discov.* 14, 113–132. doi:10.2174/1574892814666190514104035

Emig, D., Ivliev, A., Pustovalova, O., Lancashire, L., Bureeva, S., Nikolsky, Y., et al. (2013). Drug target prediction and repositioning using an integrated network-based approach. *PLoS One* 8, e60618. doi:10.1371/journal.pone.0060618

Gaulton, A., Bellis, L. J., Bento, A. P., Chambers, J., Davies, M., Hersey, A., et al. (2012). ChEMBL: A large-scale bioactivity database for drug discovery. *Nucleic Acids Res.* 40, D1100–D1107. doi:10.1093/nar/gkr777

Gerson, S. L. (2002). Clinical relevance of MGMT in the treatment of cancer. *J. Clin. Oncol.* 20, 2388–2399. doi:10.1200/jco.2002.06.110

Ghosh, D., Nandi, S., and Bhattacharjee, S. (2018). Combination therapy to checkmate glioblastoma: Clinical challenges and advances. *Clin. Transl. Med.* 7, 33. doi:10.1186/s40169-018-0211-8

Gottlieb, A., Stein, G. Y., Ruppin, E., and Sharan, R. (2011). Predict: A method for inferring novel drug indications with application to personalized medicine. *Mol. Syst. Biol.* 7, 496. doi:10.1038/msb.2011.26

Guo, X., Xu, B., Pandey, S., Goessl, E., Brown, J., Armesilla, A. L., et al. (2010). Disulfiram/copper complex inhibiting NFkappaB activity and potentiating cytotoxic effect of gemcitabine on colon and breast cancer cell lines. *Cancer Lett.* 290, 104–113. doi:10.1016/j.canlet.2009.09.002

Halatsch, M. E., Kast, R. E., Karpel-Massler, G., Mayer, B., Zolk, O., Schmitz, B., et al. (2021). A phase ib/IIa trial of 9 repurposed drugs combined with temozolomide for the treatment of recurrent glioblastoma: CUSP9v3. *Neurooncol. Adv.* 3, vdab075. vdab075. doi:10.1093/noajnl/vdab075

Han, D., Wu, G., Chang, C., Zhu, F., Xiao, Y., Li, Q., et al. (2015). Disulfiram inhibits TGF-β-induced epithelial-mesenchymal transition and stem-like features in breast cancer via ERK/NF-κB/Snail pathway. *Oncotarget* 6, 40907–40919. doi:10.18632/oncotarget.5723

Holland, R. (2016). Drug discovery world, drug discovery and development news. *Drug Discov.*

Hothi, P., Martins, T. J., Chen, L., Deleyrolle, L., Yoon, J. G., Reynolds, B., et al. (2012). High-throughput chemical screens identify disulfiram as an inhibitor of human glioblastoma stem cells. *Oncotarget* 3, 1124–1136. doi:10.18632/oncotarget.707

Huang, H., Liao, Y., Liu, N., Hua, X., Cai, J., Yang, C., et al. (2016a). Two clinical drugs deubiquitinase inhibitor auranofin and aldehyde dehydrogenase inhibitor disulfiram trigger synergistic anti-tumor effects *in vitro* and *in vivo*. *Oncotarget* 7, 2796–2808. doi:10.18632/oncotarget.6425

Huang, H., Nguyen, T., Ibrahim, S., Shantharam, S., Yue, Z., and Chen, J. Y. (2015). Dmap: A connectivity map database to enable identification of novel drug repositioning candidates. *BMC Bioinforma.* 16 (13), S4. doi:10.1186/1471-2105-16-s13-s4

Huang, J., Campian, J. L., Gujar, A. D., Tran, D. D., Lockhart, A. C., Dewees, T. A., et al. (2016b). A phase I study to repurpose disulfiram in combination with temozolomide to treat newly diagnosed glioblastoma after chemoradiotherapy. *J. Neurooncol.* 128, 259–266. doi:10.1007/s11060-016-2104-2

Huang, J., Campian, J. L., Gujar, A. D., Tsien, C., Ansstas, G., Tran, D. D., et al. (2018). Final results of a phase I dose-escalation, dose-expansion study of adding disulfiram with or without copper to adjuvant temozolomide for newly diagnosed glioblastoma. *J. Neurooncol.* 138, 105–111. doi:10.1007/s11060-018-2775-y

Huang, J., Chaudhary, R., Cohen, A. L., Fink, K., Goldlust, S., Boockvar, J., et al. (2019). A multicenter phase II study of temozolomide plus disulfiram and copper for recurrent temozolomide-resistant glioblastoma. *J. Neurooncol.* 142, 537–544. doi:10.1007/s11060-019-03125-y

Iljin, K., Ketola, K., Vainio, P., Halonen, P., Kohonen, P., Fey, V., et al. (2009). High-throughput cell-based screening of 4910 known drugs and drug-like small molecules identifies disulfiram as an inhibitor of prostate cancer cell growth. *Clin. Cancer Res.* 15, 6070–6078. doi:10.1158/1078-0432.Ccr-09-1035

Jakola, A. S., Werlenius, K., Mudaisi, M., Hylin, S., Kinhult, S., Bartek, J., JR., et al. (2018). Disulfiram repurposing combined with nutritional copper supplement as add-on to chemotherapy in recurrent glioblastoma (DIRECT): Study protocol for a randomized controlled trial. *F1000Res.* 7, 1797. doi:10.12688/f1000research.16786.1

Jangra, A., Choi, S. A., Yang, J., Koh, E. J., Phi, J. H., Lee, J. Y., et al. (2020). Disulfiram potentiates the anticancer effect of cisplatin in atypical teratoid/rhabdoid tumors (AT/RT). *Cancer Lett.* 486, 38–45. doi:10.1016/j.canlet.2020.05.006

Jivan, R., Peres, J., Damelin, L. H., Wadee, R., Veale, R. B., Prince, S., et al. (2018). Disulfiram with or without metformin inhibits oesophageal squamous cell carcinoma *in vivo*. *Cancer Lett.* 417, 1–10. doi:10.1016/j.canlet.2017.12.026

Jørgensen, C. H., Pedersen, B., and TøNNESEN, H. (2011). The efficacy of disulfiram for the treatment of alcohol use disorder. *Alcohol. Clin. Exp. Res.* 35, 1749–1758. doi:10.1111/j.1530-0277.2011.01523.x

Juárez-López, D., and Schcolnik-Cabrera, A. (2021). Drug repurposing: Considerations to surpass while Re-directing old compounds for new treatments. *Arch. Med. Res.* 52, 243–251. doi:10.1016/j.arcmed.2020.10.021

Kanehisa, M., Furumichi, M., Tanabe, M., Sato, Y., and Morishima, K. (2017). Kegg: New perspectives on genomes, pathways, diseases and drugs. *Nucleic Acids Res.* 45, D353-D361–d361. doi:10.1093/nar/gkw1092

Karamanakos, P. N., Trafalis, D. T., Papachristou, D. J., Panteli, E. S., Papavasilopoulou, M., Karatzas, A., et al. (2017). Evidence for the efficacy of disulfiram and copper combination in glioblastoma multiforme - a propos of a case. *J. buon* 22, 1227–1232.

Kast, R. E., and Belda-Iniesta, C. (2009). Suppressing glioblastoma stem cell function by aldehyde dehydrogenase inhibition with chloramphenicol or disulfiram as a new treatment adjunct: An hypothesis. *Curr. Stem Cell. Res. Ther.* 4, 314–317. doi:10.2174/157488809789649241

Kast, R. E., and Halatsch, M. E. (2012). Matrix metalloproteinase-2 and -9 in glioblastoma: A trio of old drugs-captopril, disulfiram and nelfinavir-are inhibitors with potential as adjunctive treatments in glioblastoma. *Arch. Med. Res.* 43, 243–247. doi:10.1016/j.arcmed.2012.04.005

Kast, R. E., Karpel-Massler, G., and Halatsch, M. E. (2014). CUSP9* treatment protocol for recurrent glioblastoma: Aprepitant, artesunate, auranofin, captopril, celecoxib, disulfiram, itraconazole, ritonavir, sertraline augmenting continuous low dose temozolomide. *Oncotarget* 5, 8052–8082. doi:10.18632/oncotarget.2408

Kim, S. K., Kim, H., Lee, D. H., Kim, T. S., Kim, T., Chung, C., et al. (2013). Reversing the intractable nature of pancreatic cancer by selectively targeting ALDH-high, therapy-resistant cancer cells. *PLoS One* 8, e78130. doi:10.1371/journal.pone.0078130

Kita, Y., Hamada, A., Saito, R., Teramoto, Y., Tanaka, R., Takano, K., et al. (2019). Systematic chemical screening identifies disulfiram as a repurposed drug that enhances sensitivity to cisplatin in bladder cancer: A summary of preclinical studies. *Br. J. Cancer* 121, 1027–1038. doi:10.1038/s41416-019-0609-0

Koh, H. K., Seo, S. Y., Kim, J. H., Kim, H. J., Chie, E. K., Kim, S. K., et al. (2019). Disulfiram, a Re-positioned aldehyde dehydrogenase inhibitor, enhances radiosensitivity of human glioblastoma cells *in vitro*. *Cancer Res. Treat.* 51, 696–705. doi:10.4143/crt.2018.249

Koleti, A., Terryn, R., Stathias, V., Chung, C., Cooper, D. J., Turner, J. P., et al. (2018). Data portal for the library of integrated network-based cellular signatures (LINCS) program: Integrated access to diverse large-scale cellular perturbation response data. *Nucleic Acids Res.* 46, D558-D566–d566. doi:10.1093/nar/gkx1063

Kuhn, M., Szklarczyk, D., Franceschini, A., von Mering, C., Jensen, L. J., and Bork, P. (2012). Stitch 3: Zooming in on protein-chemical interactions. *Nucleic Acids Res.* 40, D876–D880. doi:10.1093/nar/gkr1011

Kulkarni, R. R., Pradeep, A. V., and Bairy, B. K. (2013). Disulfiram-induced combined irreversible anterior ischemic optic neuropathy and reversible peripheral neuropathy: A prospective case report and review of the literature. *J. Neuropsychiatry Clin. Neurosci.* 25, 339–342. doi:10.1176/appi.neuropsych.12120410

Kumar, R., Harilal, S., Gupta, S. V., Jose, J., Thomas Parambi, D. G., Uddin, M. S., et al. (2019). Exploring the new horizons of drug repurposing: A vital tool for turning hard work into smart work. *Eur. J. Med. Chem.* 182, 111602. doi:10.1016/j.ejmech.2019.111602

Lamb, J., Crawford, E. D., Peck, D., Modell, J. W., Blat, I. C., Wrobel, M. J., et al. (2006). The connectivity map: Using gene-expression signatures to connect small molecules, genes, and disease. *Science* 313, 1929–1935. doi:10.1126/science.1132939

Lan, Q. H., du, C. C., Yu, R. J., Zhai, J., Shi, Y., Kou, L., et al. (2021). Disulfiram-loaded copper sulfide nanoparticles for potential anti-glioma therapy. *Int. J. Pharm.* 607, 120978. doi:10.1016/j.ijpharm.2021.120978

Landis, M. S., Boyden, T., and Pegg, S. (2012). Nasal-to-CNS drug delivery: Where are we now and where are we heading? An industrial perspective. *Ther. Deliv.* 3, 195–208. doi:10.4155/tde.11.149

Langedijk, J., Mantel-Teeuwisse, A. K., Slijkerman, D. S., and Schutjens, M. H. (2015). Drug repositioning and repurposing: Terminology and definitions in literature. *Drug Discov. Today* 20, 1027–1034. doi:10.1016/j.drudis.2015.05.001

Lee, S. Y. (2016). Temozolomide resistance in glioblastoma multiforme. *Genes. Dis.* 3, 198–210. doi:10.1016/j.gendis.2016.04.007

Lee, Y. E., Choi, S. A., Kwack, P. A., Kim, H. J., Kim, I. H., Wang, K. C., et al. (2017). Repositioning disulfiram as a radiosensitizer against atypical teratoid/rhabdoid tumor. *Neuro. Oncol.* 19, 1079–1087. doi:10.1093/neuonc/now300

Li, Y., Chen, F., Chen, J., Chan, S., He, Y., Liu, W., et al. (2020). Disulfiram/copper induces antitumor activity against both nasopharyngeal cancer cells and cancer-associated fibroblasts through ROS/MAPK and ferroptosis pathways. *Cancers (Basel)* 12, E138. doi:10.3390/cancers12010138

Lipsky, J. J., Shen, M. L., and Naylor, S. (2001a). *In vivo* inhibition of aldehyde dehydrogenase by disulfiram. *Chem. Biol. Interact.* 130-132, 93–102. doi:10.1016/s0009-2797(00)00225-8

Lipsky, J. J., Shen, M. L., and Naylor, S. (2001b). Overview--*in vitro* inhibition of aldehyde dehydrogenase by disulfiram and metabolites. *Chem. Biol. Interact.* 130-132, 81–91. doi:10.1016/s0009-2797(00)00224-6

Liu, C. C., Wu, C. L., Lin, M. X., Sze, C. I., and Gean, P. W. (2021b). Disulfiram sensitizes a therapeutic-resistant glioblastoma to the TGF-β receptor inhibitor. *Int. J. Mol. Sci.* 22, 10496. doi:10.3390/ijms221910496

Liu, C., Qiang, J., Deng, Q., Xia, J., Deng, L., Zhou, L., et al. (2021a). ALDH1A1 activity in tumor-initiating cells remodels myeloid-derived suppressor cells to promote breast cancer progression. *Cancer Res.* 81, 5919–5934. doi:10.1158/0008-5472.Can-21-1337

Liu, P., Brown, S., Goktug, T., Channathodiyil, P., Kannappan, V., Hugnot, J. P., et al. (2012). Cytotoxic effect of disulfiram/copper on human glioblastoma cell lines and ALDH-positive cancer-stem-like cells. *Br. J. Cancer* 107, 1488–1497. doi:10.1038/bjc.2012.442

Liu, P., Kumar, I. S., Brown, S., Kannappan, V., Tawari, P. E., Tang, J. Z., et al. (2013). Disulfiram targets cancer stem-like cells and reverses resistance and cross-resistance in acquired paclitaxel-resistant triple-negative breast cancer cells. *Br. J. Cancer* 109, 1876–1885. doi:10.1038/bjc.2013.534

Louis, D. N., Perry, A., Reifenberger, G., von Deimling, A., Figarella-Branger, D., Cavenee, W. K., et al. (2016). The 2016 world health organization classification of tumors of the central nervous system: A summary. *Acta Neuropathol.* 131, 803–820. doi:10.1007/s00401-016-1545-1

Lun, X., Wells, J. C., Grinshtein, N., King, J. C., Hao, X., Dang, N. H., et al. (2016). Disulfiram when combined with copper enhances the therapeutic effects of temozolomide for the treatment of glioblastoma. *Clin. Cancer Res.* 22, 3860–3875. doi:10.1158/1078-0432.Ccr-15-1798

Mandell, J. B., Douglas, N., Ukani, V., Beumer, J. H., Guo, J., Payne, J., et al. (2022). ALDH1A1 gene expression and cellular copper levels between low and highly metastatic osteosarcoma provide a case for novel repurposing with disulfiram and copper. *Sarcoma* 2022, 7157507. doi:10.1155/2022/7157507

Masoudi-Sobhanzadeh, Y., Omidi, Y., Amanlou, M., and Masoudi-Nejad, A. (2019). DrugR+: A comprehensive relational database for drug repurposing, combination therapy, and replacement therapy. *Comput. Biol. Med.* 109, 254–262. doi:10.1016/j.compbiomed.2019.05.006

Mcmahon, A., Chen, W., and Li, F. (2020). Old wine in new bottles: Advanced drug delivery systems for disulfiram-based cancer therapy. *J. Control. Release* 319, 352–359. doi:10.1016/j.jconrel.2020.01.001

Meier, S., Cantilena, S., Niklison Chirou, M. V., Anderson, J., Hargrave, D., Salomoni, P., et al. (2021). Alcohol-abuse drug disulfiram targets pediatric glioma via MLL degradation. *Cell. Death Dis.* 12, 785. doi:10.1038/s41419-021-04078-9

Metro, G., Fabi, A., Mirri, M. A., Vidiri, A., Pace, A., Carosi, M., et al. (2010). Phase II study of fixed dose rate gemcitabine as radiosensitizer for newly diagnosed glioblastoma multiforme. *Cancer Chemother. Pharmacol.* 65, 391–397. doi:10.1007/s00280-009-1155-x

Mettang, M., Meyer-Pannwitt, V., Karpel-Massler, G., Zhou, S., Carragher, N. O., FöHR, K. J., et al. (2018). Blocking distinct interactions between glioblastoma cells and their tissue microenvironment: A novel multi-targeted therapeutic approach. *Sci. Rep.* 8, 5527. doi:10.1038/s41598-018-23592-z

Mohammad, I. S., Teng, C., Chaurasiya, B., Yin, L., Wu, C., and He, W. (2019). Drug-delivering-drug approach-based codelivery of paclitaxel and disulfiram for treating multidrug-resistant cancer. *Int. J. Pharm.* 557, 304–313. doi:10.1016/j.ijpharm.2018.12.067

Moosavinasab, S., Patterson, J., Strouse, R., Rastegar-Mojarad, M., Regan, K., Payne, P. R., et al. (2016). *'RE:fine drugs': An interactive dashboard to access drug repurposing opportunities*. Oxford): Database. doi:10.1093/database/baw083

Moreb, J. S., Ucar, D., Han, S., Amory, J. K., Goldstein, A. S., Ostmark, B., et al. (2012). The enzymatic activity of human aldehyde dehydrogenases 1A2 and 2 (ALDH1A2 and ALDH2) is detected by Aldefluor, inhibited by diethylaminobenzaldehyde and has significant effects on cell proliferation and drug resistance. *Chem. Biol. Interact.* 195, 52–60. doi:10.1016/j.cbi.2011.10.007

Mutter, N., and Stupp, R. (2006). Temozolomide: A milestone in neuro-oncology and beyond? *Expert Rev. Anticancer Ther.* 6, 1187–1204. doi:10.1586/14737140.6.8.1187

Nechushtan, H., Hamamreh, Y., Nidal, S., Gotfried, M., Baron, A., Shalev, Y. I., et al. (2015). A phase IIb trial assessing the addition of disulfiram to chemotherapy for the treatment of metastatic non-small cell lung cancer. *Oncologist* 20, 366–367. doi:10.1634/theoncologist.2014-0424

Newlands, E. S., Blackledge, G., Slack, J. A., Goddard, C., Brindley, C. J., Holden, L., et al. (1985). Phase I clinical trial of mitozolomide. *Cancer Treat. Rep.* 69, 801–805.

Newlands, E. S., Stevens, M. F., Wedge, S. R., Wheelhouse, R. T., and Brock, C. (1997). Temozolomide: A review of its discovery, chemical properties, pre-clinical development and clinical trials. *Cancer Treat. Rev.* 23, 35–61. doi:10.1016/s0305-7372(97)90019-0

O'brien, A., Barber, J. E., Reid, S., Niknejad, N., and Dimitroulakos, J. (2012). Enhancement of cisplatin cytotoxicity by disulfiram involves activating transcription factor 3. *Anticancer Res.* 32, 2679–2688.

Ostrom, Q. T., Cioffi, G., Gittleman, H., Patil, N., Waite, K., Kruchko, C., et al. (2019). CBTRUS statistical report: Primary brain and other central nervous system tumors diagnosed in the United States in 2012-2016. *Neuro. Oncol.* 21, v1–v100. doi:10.1093/neuonc/noz150

Osuka, S., and Van Meir, E. G. (2017). Overcoming therapeutic resistance in glioblastoma: The way forward. *J. Clin. Investig.* 127, 415–426. doi:10.1172/jci89587

Özcan, H., Emiroğlu, B. G., Sabuncuoğlu, H., Özdoğan, S., Soyer, A., and SAYGı, T. (2021). A comparative study for glioma classification using deep convolutional neural networks. *Math. Biosci. Eng.* 18, 1550–1572. doi:10.3934/mbe.2021080

Papaioannou, M., Mylonas, I., Kast, R. E., and BRüNING, A. (2014). Disulfiram/copper causes redox-related proteotoxicity and concomitant heat shock response in ovarian cancer cells that is augmented by auranofin-mediated thioredoxin inhibition. *Oncoscience* 1, 21–29. doi:10.18632/oncoscience.5

Paranjpe, A., Zhang, R., Ali-Osman, F., Bobustuc, G. C., and Srivenugopal, K. S. (2014). Disulfiram is a direct and potent inhibitor of human O6-methylguanine-DNA methyltransferase (MGMT) in brain tumor cells and mouse brain and markedly increases the alkylating DNA damage. *Carcinogenesis* 35, 692–702. doi:10.1093/carcin/bgt366

Parsons, D. W., Li, M., Zhang, X., Jones, S., Leary, R. J., Lin, J. C., et al. (2011). The genetic landscape of the childhood cancer medulloblastoma. *Science* 331, 435–439. doi:10.1126/science.1198056

Parvathaneni, V., Kulkarni, N. S., Muth, A., and Gupta, V. (2019). Drug repurposing: A promising tool to accelerate the drug discovery process. *Drug Discov. Today* 24, 2076–2085. doi:10.1016/j.drudis.2019.06.014

Pujol, A., Mosca, R., FARRéS, J., and Aloy, P. (2010). Unveiling the role of network and systems biology in drug discovery. *Trends Pharmacol. Sci.* 31, 115–123. doi:10.1016/j.tips.2009.11.006

Qu, Y., Sun, X., Ma, L., Li, C., Xu, Z., Ma, W., et al. (2021). Therapeutic effect of disulfiram inclusion complex embedded in hydroxypropyl-β-cyclodextrin on intracranial glioma-bearing male rats via intranasal route. *Eur. J. Pharm. Sci.* 156, 105590. doi:10.1016/j.ejps.2020.105590

Rappa, F., Cappello, F., Halatsch, M. E., Scheuerle, A., and Kast, R. E. (2013). Aldehyde dehydrogenase and HSP90 co-localize in human glioblastoma biopsy cells. *Biochimie* 95, 782–786. doi:10.1016/j.biochi.2012.11.007

Rolle, F., Bincoletto, V., Gazzano, E., Rolando, B., Lollo, G., Stella, B., et al. (2020). Coencapsulation of disulfiram and doxorubicin in liposomes strongly reverses multidrug resistance in breast cancer cells. *Int. J. Pharm.* 580, 119191. doi:10.1016/j.ijpharm.2020.119191

Sam, E., and Athri, P. (2019). Web-based drug repurposing tools: A survey. *Brief. Bioinform.* 20, 299–316. doi:10.1093/bib/bbx125

Schmidtova, S., Kalavska, K., Gercakova, K., Cierna, Z., Miklikova, S., Smolkova, B., et al. (2019). *Disulfiram Overcomes Cisplatin Resistance in Human Embryonal Carcinoma Cells*, 11. doi:10.3390/cancers11091224*Cancers (Basel)*

Schuettengruber, B., Bourbon, H. M., di Croce, L., and Cavalli, G. (2017). Genome regulation by polycomb and Trithorax: 70 Years and counting. *Cell.* 171, 34–57. doi:10.1016/j.cell.2017.08.002

Seliger, C., Genbrugge, E., Gorlia, T., Chinot, O., Stupp, R., Nabors, B., et al. (2020). Use of metformin and outcome of patients with newly diagnosed glioblastoma: Pooled analysis. *Int. J. Cancer* 146, 803–809. doi:10.1002/ijc.32337

Seliger, C., and Hau, P. (2018). Drug repurposing of metabolic agents in malignant glioma. *Int. J. Mol. Sci.* 19, E2768. doi:10.3390/ijms19092768

Shameer, K., Glicksberg, B. S., Hodos, R., Johnson, K. W., Badgeley, M. A., Readhead, B., et al. (2018). Systematic analyses of drugs and disease indications in RepurposeDB reveal pharmacological, biological and epidemiological factors influencing drug repositioning. *Brief. Bioinform.* 19, 656–678. doi:10.1093/bib/bbw136

Shergill, M., Patel, M., Khan, S., Bashir, A., and Mcconville, C. (2016). Development and characterisation of sustained release solid dispersion oral

tablets containing the poorly water soluble drug disulfiram. *Int. J. Pharm.* 497, 3–11. doi:10.1016/j.ijpharm.2015.11.029

Shian, S. G., Kao, Y. R., Wu, F. Y., and Wu, C. W. (2003). Inhibition of invasion and angiogenesis by zinc-chelating agent disulfiram. *Mol. Pharmacol.* 64, 1076–1084. doi:10.1124/mol.64.5.1076

Shirley, D. A., Sharma, I., Warren, C. A., and Moonah, S. (2021). Drug repurposing of the alcohol abuse medication disulfiram as an anti-parasitic agent. *Front. Cell. Infect. Microbiol.* 11, 633194. doi:10.3389/fcimb.2021.633194

Skaga, E., Skaga, I., Grieg, Z., Sandberg, C. J., Langmoen, I. A., and Vik-Mo, E. O. (2019). The efficacy of a coordinated pharmacological blockade in glioblastoma stem cells with nine repurposed drugs using the CUSP9 strategy. *J. Cancer Res. Clin. Oncol.* 145, 1495–1507. doi:10.1007/s00432-019-02920-4

Spillier, Q., Vertommen, D., Ravez, S., Marteau, R., THéMANS, Q., Corbet, C., et al. (2019). Anti-alcohol abuse drug disulfiram inhibits human PHGDH via disruption of its active tetrameric form through a specific cysteine oxidation. *Sci. Rep.* 9, 4737. doi:10.1038/s41598-019-41187-0

Srivenugopal, K. S., Rawat, A., Niture, S. K., Paranjpe, A., Velu, C., Venugopal, S. N., et al. (2016). Posttranslational regulation of O(6)-methylguanine-DNA methyltransferase (MGMT) and new opportunities for treatment of brain cancers. *Mini Rev. Med. Chem.* 16, 455–464. doi:10.2174/1389557515666150722101046

Stockhammer, F., Misch, M., Koch, A., Czabanka, M., Plotkin, M., Blechschmidt, C., et al. (2010). Continuous low-dose temozolomide and celecoxib in recurrent glioblastoma. *J. Neurooncol.* 100, 407–415. doi:10.1007/s11060-010-0192-y

Stupp, R., Mason, W. P., van Den Bent, M. J., Weller, M., Fisher, B., Taphoorn, M. J., et al. (2005). Radiotherapy plus concomitant and adjuvant temozolomide for glioblastoma. *N. Engl. J. Med.* 352, 987–996. doi:10.1056/NEJMoa043330

Stylli, S. S. (2020). Novel treatment strategies for glioblastoma. *Cancers (Basel)* 12, E2883. doi:10.3390/cancers12102883

Swetha, K. L., Sharma, S., Chowdhury, R., and Roy, A. (2020). Disulfiram potentiates docetaxel cytotoxicity in breast cancer cells through enhanced ROS and autophagy. *Pharmacol. Rep.* 72, 1749–1765. doi:10.1007/s43440-020-00122-1

Tesson, M., Anselmi, G., Bell, C., and Mairs, R. (2017). Cell cycle specific radiosensitisation by the disulfiram and copper complex. *Oncotarget* 8, 65900–65916. doi:10.18632/oncotarget.19539

Triscott, J., Lee, C., Hu, K., Fotovati, A., Berns, R., Pambid, M., et al. (2012). Disulfiram, a drug widely used to control alcoholism, suppresses the self-renewal of glioblastoma and over-rides resistance to temozolomide. *Oncotarget* 3, 1112–1123. doi:10.18632/oncotarget.604

Triscott, J., Rose Pambid, M., and Dunn, S. E. (2015). Concise review: Bullseye: Targeting cancer stem cells to improve the treatment of gliomas by repurposing disulfiram. *Stem Cells* 33, 1042–1046. doi:10.1002/stem.1956

Turanli, B., Altay, O., BORéN, J., Turkez, H., Nielsen, J., Uhlen, M., et al. (2021). Systems biology based drug repositioning for development of cancer therapy. *Semin. Cancer Biol.* 68, 47–58. doi:10.1016/j.semcancer.2019.09.020

Voorhees, P. M., and Orlowski, R. Z. (2006). The proteasome and proteasome inhibitors in cancer therapy. *Annu. Rev. Pharmacol. Toxicol.* 46, 189–213. doi:10.1146/annurev.pharmtox.46.120604.141300

Wang, W., Mcleod, H. L., and Cassidy, J. (2003). Disulfiram-mediated inhibition of NF-kappaB activity enhances cytotoxicity of 5-fluorouracil in human colorectal cancer cell lines. *Int. J. Cancer* 104, 504–511. doi:10.1002/ijc.10972

Wang, Y., Bryant, S. H., Cheng, T., Wang, J., Gindulyte, A., Shoemaker, B. A., et al. (2017). PubChem BioAssay: 2017 update. *Nucleic Acids Res.* 45, D955-D963–d963. doi:10.1093/nar/gkw1118

Wehbe, M., Anantha, M., Shi, M., Leung, A. W., Dragowska, W. H., Sanche, L., et al. (2017). Development and optimization of an injectable formulation of copper diethyldithiocarbamate, an active anticancer agent. *Int. J. Nanomedicine* 12, 4129–4146. doi:10.2147/ijn.S137347

Westhoff, M. A., Zhou, S., Nonnenmacher, L., Karpel-Massler, G., Jennewein, C., Schneider, M., et al. (2013). Inhibition of NF-κB signaling ablates the invasive phenotype of glioblastoma. *Mol. Cancer Res.* 11, 1611–1623. doi:10.1158/1541-7786.Mcr-13-0435-t

Weyerhäuser, P., Kantelhardt, S. R., and Kim, E. L. (2018). Re-Purposing chloroquine for glioblastoma: Potential merits and confounding variables. *Front. Oncol.* 8, 335. doi:10.3389/fonc.2018.00335

Wickström, M., Danielsson, K., Rickardson, L., Gullbo, J., Nygren, P., Isaksson, A., et al. (2007). Pharmacological profiling of disulfiram using human tumor cell lines and human tumor cells from patients. *Biochem. Pharmacol.* 73, 25–33. doi:10.1016/j.bcp.2006.08.016

Wishart, D. S., Feunang, Y. D., Guo, A. C., Lo, E. J., Marcu, A., Grant, J. R., et al. (2018). DrugBank 5.0: A major update to the DrugBank database for 2018. *Nucleic Acids Res.* 46, D1074-D1082–d1082. doi:10.1093/nar/gkx1037

Wu, H., Huang, J., Zhong, Y., and Huang, Q. (2017). DrugSig: A resource for computational drug repositioning utilizing gene expression signatures. *PLoS One* 12, e0177743. doi:10.1371/journal.pone.0177743

Xu, B., Shi, P., Fombon, I. S., Zhang, Y., Huang, F., Wang, W., et al. (2011). Disulfiram/copper complex activated JNK/c-jun pathway and sensitized cytotoxicity of doxorubicin in doxorubicin resistant leukemia HL60 cells. *Blood Cells Mol. Dis.* 47, 264–269. doi:10.1016/j.bcmd.2011.08.004

Xue, H., Li, J., Xie, H., and Wang, Y. (2018). Review of drug repositioning approaches and resources. *Int. J. Biol. Sci.* 14, 1232–1244. doi:10.7150/ijbs.24612

Yang, H., Qin, C., Li, Y. H., Tao, L., Zhou, J., Yu, C. Y., et al. (2016). Therapeutic target database update 2016: Enriched resource for bench to clinical drug target and targeted pathway information. *Nucleic Acids Res.* 44, D1069–D1074. doi:10.1093/nar/gkv1230

Yang, Z., Guo, F., Albers, A. E., Sehouli, J., and Kaufmann, A. M. (2019). Disulfiram modulates ROS accumulation and overcomes synergistically cisplatin resistance in breast cancer cell lines. *Biomed. Pharmacother.* 113, 108727. doi:10.1016/j.biopha.2019.108727

Yao, W., Qian, X., Ochsenreither, S., Soldano, F., Deleo, A. B., Sudhoff, H., et al. (2021). Disulfiram acts as a potent radio-chemo sensitizer in head and neck squamous cell carcinoma cell lines and transplanted xenografts. *Cells* 10, 517. doi:10.3390/cells10030517

Ye, X. Q., Li, Q., Wang, G. H., Sun, F. F., Huang, G. J., Bian, X. W., et al. (2011). Mitochondrial and energy metabolism-related properties as novel indicators of lung cancer stem cells. *Int. J. Cancer* 129, 820–831. doi:10.1002/ijc.25944

Yip, N. C., Fombon, I. S., Liu, P., Brown, S., Kannappan, V., Armesilla, A. L., et al. (2011). Disulfiram modulated ROS-MAPK and NFκB pathways and targeted breast cancer cells with cancer stem cell-like properties. *Br. J. Cancer* 104, 1564–1574. doi:10.1038/bjc.2011.126

Zhang, Y. W., Kaneda, M., and Morita, I. (2003). The gap junction-independent tumor-suppressing effect of connexin 43. *J. Biol. Chem.* 278, 44852–44856. doi:10.1074/jbc.M305072200

Zhao, P., Wang, Y., Kang, X., Wu, A., Yin, W., Tang, Y., et al. (2018). Dual-targeting biomimetic delivery for anti-glioma activity via remodeling the tumor microenvironment and directing macrophage-mediated immunotherapy. *Chem. Sci.* 9, 2674–2689. doi:10.1039/c7sc04853j

Zirjacks, L., Stransky, N., Klumpp, L., Prause, L., Eckert, F., Zips, D., et al. (2021). Repurposing disulfiram for targeting of glioblastoma stem cells: An *in vitro* study. *Biomolecules* 11, 1561. doi:10.3390/biom11111561

Frontiers in Oncology

Advances knowledge of carcinogenesis and tumor progression for better treatment and management

The third most-cited oncology journal, which highlights research in carcinogenesis and tumor progression, bridging the gap between basic research and applications to imrpove diagnosis, therapeutics and management strategies.

Discover the latest Research Topics

See more →

Frontiers

Avenue du Tribunal-Fédéral 34
1005 Lausanne, Switzerland
frontiersin.org

Contact us

+41 (0)21 510 17 00
frontiersin.org/about/contact